Design and validation of pressure vessels for optimized payload in subsea applications

Tomás Figueiredo Marques

Masters Final Thesis

Advisor in CEiiA: Eng.º Marcos Guilherme Moreira
Advisor in FEUP: Prof. José Ferreira Duarte

U.PORTO
FEUP FACULDADE DE ENGENHARIA
UNIVERSIDADE DO PORTO

Mechanical Engineering Master's Degree

February 2021

Overhead the albatross
Hangs motionless upon the air
And deep beneath the rolling waves
In labyrinths of coral caves

The echo of a distant time
Comes willowing across the sand
And everything is green and submarine

And no one showed us to the land
And no one knows the where's or why's
But something stirs, and something tries
And starts to climb toward the light

- Gilmour, Waters, Wright, Mason

This page was intentionally left blank

Abstract

Design and validation of pressure vessels for optimized payload in subsea applications

Humanity has a long history of symbiotic relationship with our seas and oceans, mutually for transportation, commerce, prospection, investigation and defence. However, more than 80% of our ocean remain unexplored. The past decades saw the development of unmanned submersible equipment, with AUVs, ROVs and Landers becoming the norm in sea exploration.

A common component of most submersibles are pressure vessels, structural components whose main function is to withstand the demanding hydrostatic pressure conditions while remaining watertight to protect the sensitive inner payload from water and pressure damage. Most pressure vessels have a circular cylindrical shell configuration, justified by the balance between structural integrity and internal volume this vessel provides. However, these shells are associated with a considerable waste of useful volume since the curvature of the shell is incompatible with the typically prismatic internal payload. Another challenge is the susceptibility to buckling failure, which can occur prior to failure by yielding. Stiffeners can be used to increase structural stability, but the resulting weight increase can be challenging, as vessels are ideally designed to be as light as possible.

Both these problems result from the limitations of cylindrical shells, but alternative configurations could provide valid trade-offs for pressure vessel design. These concepts can either adopt a noncircular cross-section, which is better suited for the internal payload, or a shell with external thickness variation, so to emulate the effect of stiffeners and its increase of stability without increasing the weight of the vessel.

This thesis proposes the behaviour study of these alternative concepts so to compare them to a standard cylindrical shell designed accordingly to market standards. This analysis concluded that relevant trade-offs of increasing either the internal useful volume or the buckling strength can be achieved with these concepts, which can be useful in future subsea applications. The analysis considers numerical methods with analytical methods to validate FEA parameters.

Keywords: Pressure Vessel; External Hydrostatic Pressure; Shell Thickness Variation; Noncircular Cross Section, Shell Buckling; Subsea Applications.

This page was intentionally left blank

Resumo

Projeção e validação de reservatórios de pressão otimizados para carga útil em aplicações submarinas

A história da humanidade está marcada por uma longa relação com os nossos mares e oceanos, desde transporte e comércio, a investigação e defesa. No entanto, mais de 80% dos nossos oceanos continuam por explorar. Nas últimas décadas viu-se o desenvolvimento de equipamento submersível não-tripulado, com AUVs, *ROVs* e *Landers* a tornaram-se prática comum na exploração submarina.

Um componente estrutural usado na maioria do equipamento submersível é o reservatório de pressão, cuja principal função é resistir à exigente pressão hidrostática sem perder a estanquidade, de forma a proteger a sensível carga útil interna de danos causados por água ou pressão. A maioria dos reservatórios de pressão têm uma configuração cilindrica devido ao balanço entre integridade estrutural e volume interno característicos. No entanto, associada a esta geometria existe uma considerável perda de volume interno devido à incompatibilidade entre a curvatura do perfil e a carga, que geralmente é de configuração prismática. Outro desafio vem da susceptabilidade a falha por instabilidade, ou *buckling*, podendo ocorrer antes da tensão-limite de elasticidade do material. Reforços da estrutura do reservatório podem ser usados para aumentar a estabilidade estrutural, mas o aumento de peso é outro desafio dado que estes são projetados para serem leves.

Configurações alternativas à geometria cilíndrica podem apresentar compromissos de projeto relevantes. Como conceitos, pode ser adotado um perfil não-circular de forma a tornar o volume interno mais compatível com a carga útil, ou uma geometria com variações de espessura de forma a assemelhar o aumento de estabilidade com reforços de casca sem aumentar o peso total.

Na presente tese é feita a análise estrutural de diferentes conceitos de reservatórios de pressão, de forma a comparar estes com um reservatório típico projetado de acordo com os semelhantes usados no mercado. Esta análise conclui que compromissos de interesse ao utilizador podem ser conseguidos através destes conceitos, quer através do aumento do volúme útil, quer pelo aumento da resistência ao *buckling*, ambos cenários úteis para aplicações submarinas. Esta análise usa métodos numéricos, bem como métodos analíticos para validar os parâmetros de análise por elementos finitos.

Palavras-chave: Vaso Pressão; Pressão Hidrostática Externa; Variação de Espessura de Casca; Perfil de Secção Não-Circular; Instabilidade de Casca; Aplicações Submarinas

This page was intentionally left blank

Special Thanks

There is way too much to be grateful to translate in a few words.

In the first place, I would like to express the deepest of gratitude to CEiiA and all their staff, for providing the ideal workplace to someone striving for a challenge in a motivating environment. A very special thank you goes to my advisor at CEiiA, Marcos Moreira, whose continuous support, wisdom and availability helped me navigate through these troubled times we all are facing. A final credit goes to Miguel, for being an unexpected new buddy in a social distancing year.

To Professor José Ferreira Duarte, for the all the guidance, recommendations and positive support, and especially for helping me accept all of the things we cannot change.

A big thank you to Zé, Diogo, Mota, Ju and Joana for being the oldest and truest friends I could have ever asked for. To Morais, João, Sofia, Verdade, Sucena, Bia, Chico, Bruno, Henriques, Simão and Lombo for filling my years of college with the most unforgettable stories I can't ever talk about. To Leo, Nuno, Bia, Mari, Zé and Bá for standing with me in the most difficult year of my life, and for making it one of the best ones yet. A very special thank you to Patrick and Magui, for always being there to provide me with shelter, in more ways than one.

To Bea, for making me happy by letting me make her happier.

And my final and largest sympathy goes to my mother, father, brother, godmother and grandparents. Thank you for teaching me what the world is and what role I can play in it. Thank you for treading this path that I am proud to follow.

To all my family and friends. To all my leaders and teams. To FEUP and to AIESEC, to Porto and to Coura. In the longing of all goodbyes, I will carry these secrets with me, for all my life.

This page was intentionally left blank

Index

This page was intentionally left blank

Nomenclature

Abbreviations

ASME	American Society of Mechanical Engineers
ASV	Autonomous Surface Vehicle
ATV	Axial Thickness Variation
AUV	Autonomous Underwater Vehicle
CAE	Computer-Aided Engineering
CDD	Collapse Diving Depth
CDP	Collapse Diving Pressure
CFRP	Carbon Fibre Reinforced Polymer
Config.	Configuration
CPU	Central Processing Unit
CS	Cross Section
DoF	Degree of Freedom
DTMB	David Taylor Model Basin
EEZ	Economic Exclusive Zone
EN	European Norm
FEA	Finite Element Analysis
FEM	Finite Element Method
GRP	Glass Reinforced Plastic
H-ROV	Hybrid Remotely Operated Vehicle
ISO	International Standardization Organization
LNG	Liquified Natural Gas
Mat.	Material
MIT	Massachusetts Institute of Technology
MMC	Metal Matrix Composite
MS	Margin of Safety
NCS	Noncircular Cross Section
NDD	Nominal Diving Depth
NDP	Nominal Diving Pressure

NLQS	Non-Linear Quasi Static
NOAA	National Oceanic and Atmospheric Administration
PKD	Plastic Knockdown Factor
POM	Polyoxymethylene
PV	Pressure Vessel
PVC	Polyvinyl Chloride
ROV	Remotely Operated Vehicle
RTV	Radial Thickness Variation
SCC	Standard Circular Cylindrical
SCF	Standard Circular Filleted
SF	Safety Factor
SPC	Single Point Constraint
Spec.	Specifications
TDD	Test Diving Depth
TDP	Test Diving Pressure
UWT	Underwater Technology
VM	Von Mises

Scandinavian Symbols

⌀ Diameter

Greek symbols

Δ	differential
ε	strain.
θ	rotational displacement
λ'	thinness ratio for general instability
λ_c	Windenburg's thinness ratio
ν	Poisson's ratio
ρ	volumetric mass density
σ	stress
τ	in-plane shear stress

Roman Symbols

b	radial stiffener width
B	buoyant force, i.e. weight of displaced fluid
C_O	O-ring compression
C	elasticity matrix of the material,
D	diameter
d	radial stiffener height
D_0	flexural rigidity of the shell
E	Young's Modulus
F	force
g	gravitational acceleration
h	height of the liquid column
I_{xx}	second moment of inertia
J	deviatoric invariant,
K	stiffness matrix
L	length
L_b	length between adjacent bulkheads
L_s	cross section straight side length
n	number of circumferential lobes
Nw	number of sinusoidal waves,
P	pressure
R	internal radius
R_O	O-ring reduction
R_f	fillet radius,
S	deviatoric stress
S_O	O-ring stretch
t	shell thickness
u	nodal displacements
V	volume
w	radial deflection
W	weight
W_0	deviation of the external surface from the external radius of a perfect cylinder
W_A	sinusoidal amplitude from the external surface of the cylinder,
X_0	out-of-circularity imperfection in the x-axis direction
Y_0	out-of-circularity imperfection in the y-axis direction

Subscripts

x, y, z	cartesian components.
f	displaced fluid
fr	frame component
m	mean value
disp	displaced fluid
cr	critical
c	centroid of a typical ring-shell combination
C	Cauchy
ext	external
int	internal
VM	Von Mises
y	yield
u	ultimate
real	experimental value
G	geometric
ref	reference

Superscripts

-1	indicates the inverse of a matrix
T	indicates the transpose of a matrix

List of Figures

This page was intentionally left blank

List of Tables

This page was intentionally left blank

1. Introduction

1.1 Motivation

The ocean plays a key part in the balance of the modern world, both as a regulatory system for driving weather, maintaining global temperatures and supporting all ecosystems, both directly and indirectly. It is also one of the major backbones of ancient and modern civilizations, used for transportation, commerce, sustenance, and exploration. The history of ocean exploration is as old as the history of humanity, and for centuries it played a major role in the geopolitical intricacies of mankind's progress, and it is easy to understand why. Most oceans present a rich biodiversity, especially on the continental shelf, which means sustenance for early civilizations, but in an age before roads and cars, it meant easy transportation of goods and culture. For centuries, the oceans have attracted our common curiosity. The history or folklore of human exploration inspired some of the greater stories, from Homer's Odyssey to Camões The Lusiads, and a strong naval presence was, and still is, a key to the success of global interventionism of countries. History proves that naval power equals real power, and it is no surprise that the world's most powerful empires for a given period had the strongest navy, like Portugal and Spain's Age of Discoveries, Britain Imperialism and currently, the United States as the superpower of the world, which withholds the largest and strongest sovereign navy.

However, and despite the long history, more than 80% of our ocean remains *"uncharted, unobserved, and unexplored"* [1]. Beneath the surface, the body of water extends to depths difficult to grasp. The oceans have an estimated average depth of about 3 688 meters, 7 times more than the publicly known average maximum depth of military submarines [2]. At this depth, the pressure reaches 38 MPa, the equivalent of 387 kg weighing on every cm^2. Past 200 meters underwater and even the sunlight has difficulty penetrating the body of fluid, making most of the ocean pitch black and the temperature hovering around freezing [3]. Adding the salt water's corrosive action and the difficulty to track and navigate underwater, it becomes clear why deep-sea exploration is so often compared to the exploration of outer space [4]. It is a vast, inhospitable region and the deeper one goes, the more extreme the environment gets.

Despite the challenges, there are huge incentives to keep exploring the depths. As the NOAA Office of Ocean Exploration and Research puts it, "*unlocking the mysteries of deep-sea ecosystems can reveal new sources for medical drugs, food, energy resources, and other products. (...) [it] can help predict earthquakes and tsunamis and help us understand how we are affecting and being affected by changes in Earth's environment*" [5]. Major examples of emerging opportunities in the deep-sea are mining for seabed minerals or collecting marine organisms for pharmaceutical and industrial applications - bioprospecting. New industries will likely appear as a consequence of human activity in the environment, and it has been discussed the possibility of CO_2 storage in the deep seabed, to remove it from the atmosphere [6]. According to recent researches, the global market for deep sea mining alone is expected to grow from 650 million USD in 2020 to 15.3 billion USD by 2030 [7], and that is only one of the many applications that will have an increased demand as technological developments make deep sea industries more viable.

These incentives are also clear for Portugal, a country with a long history of sea exploration. As defined by the United Nations, costal countries hold an Exclusive Economic Zone (EEZ), which gives the sovereign state special rights regarding the exploration and use of resources [8]. Currently the Portuguese EEZ has 1.72 million km^2, the third largest in the EU. By international law, the EEZ should not extend over the 200 nautical miles from the coastline, but a UN committee has been analysing a project proposed in 2017 to more than double this territory, giving the Portuguese nation sovereignty over 4 million km^2 of ocean territory [9] - *Figure 1.1*. This evaluation is still on-going, as the complex project presents plans for the exploration of fish, algae, minerals and other resources, the prospecting for renewable and non-renewable energy sources, the exploration and mapping of the ocean, the surveillance and military activity in the zone, as well as the environment impact on the habitat and its biodiversity. If approved, the Portuguese government will commit with a long-term plan to sustainably explore the vast territory for resources and new opportunities. But to do so, a considerable investment in data collection from the deep sea will be needed to access the viability of future projects [9] [10].

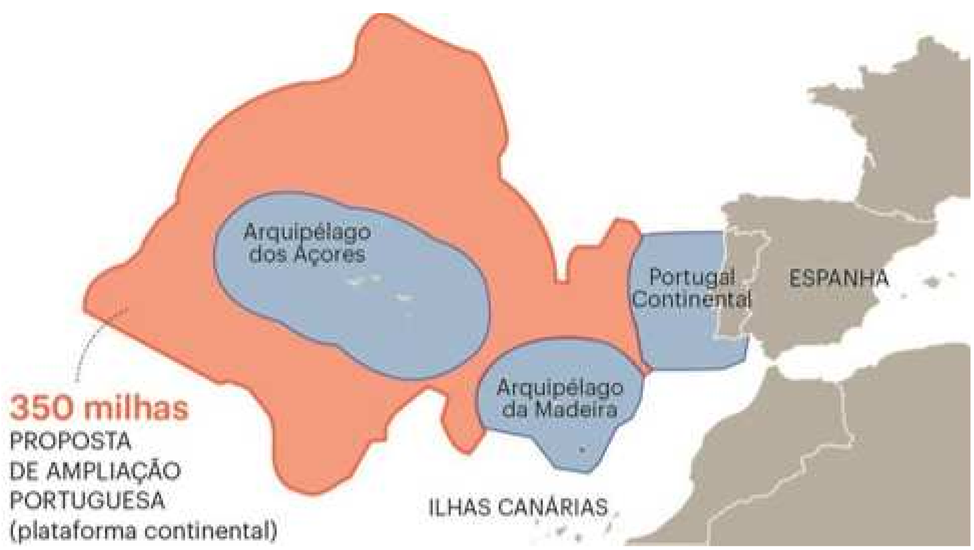

Figure 1.1 Map with the current EEZ of Portugal in blue, and the outer limits of the extended continental platform proposed by Portugal in orange [10].

1.2 Problem Definition & Objectives

To explore and operate on the deep sea, the water pressure is the main barrier that needs to come in mind on vehicle and equipment design, as different components need to be adapted to sustain the hydrostatic pressure for a given depth while remaining watertight to protect the inner payload. Since several components such as electrical components, batteries and sensors are neither watertight or pressure resistant without being purposefully developed to behave as so, most deepwater submersibles employ some form of pressure resistance system with specific conditions depending on the type of submersible considered [11] [12].

The most common pressure resistant systems are watertight pressure vessels or pressure housings. These vessels often have cylindrical or spherical shapes, but such shapes leave a considerable space unoccupied. So, the design of alternative vessel shapes with more internal useful volume can have a major impact on the operating conditions of submersible vehicles and equipment.

The main objectives proposed at the beginning of this thesis research were:

- To investigate the current state of art of pressure vessels in the market;
- To establish a standard pressure vessel configuration based on the market;
- Investigate on other geometric iterations of pressure vessel main body shapes;
- Model and analyse vessels with optimizing the internal useful volume as the main goal and improving structural integrity as the second goal, for a nominal depth of 1 500 m;
- Analyse these geometries and compare then with the standard pressure vessel.

1.3 Project Entities Presentation

1.3.1 CEiiA - Centro de Engenharia e Desenvolvimento de Produto

CEiiA is a centre of engineering and product development operating in Matosinhos, Portugal. It is currently one of the 10 largest R&D investors in Portugal and an international reference, both in sustainable mobility and aeronautical structural engineering [13]. Currently, it designs, develops and operates innovative products in the mobility industries. It has the mission of positioning Portugal as an international reference as a development force in the conception of innovative products and services, always with a focus in sustainability. One of the main areas of operations is the UDPS – Development of Products and Services, which aggregates scientific, engineering, and technological skills to develop a concept from new business models to the development and test of new product or services concepts. This area is divided into four main sectors of operation within CEiiA: Automotive, Urban Mobility, Aeronautics, and Ocean and Space [14]. Regarding the Ocean and Space, CEiiA manages the OceanTech program, which develops, produces, and operates a new generation of sea robotic systems and vehicles to further take advantage of the sea economy.

Several projects were developed in recent years, with highlight to the MEDUSA Deep Sea, an Autonomous Underwater Vehicle – AUV developed for a nominal depth of 3 000 m to conduct scientific missions in the national waters [15] [16]; the Subsea Fish Cage, a program that developed a new offshore structure for salmon aquaculture, which client is Jerónimo Martins S.A. [14] [17]; the EASER project, aimed to develop a new concept of an Autonomous Surface Vehicle – ASV, able to conduct missions of bathymetric analysis in lakes, rivers, reservoirs and seashore [18]; TAGs, the project to create a system of towed tagging devices develop to act as a nonintrusive, timed transmitter capable of collecting data from a diversity of animal behaviour and habitat parameters, such as manta rays and sharks [19].

The current thesis was developed as a program of *Academia CEiiA* research intern project.

Figure 1.2 CEiiA – Centro de Engenharia e Desenvolvimento de Produto logo.

1.3.2 FEUP – Faculdade de Engenharia da Universidade do Porto

Founded in 1911, University of Porto is one of the most prestigious universities in Portugal, ranked among the 300 best in the world according to QS World University Rankings of 2018 [20]. FEUP is its faculty of engineering and one of the largest, widely recognized by its excellence in education and academic research. All its engineering courses are recognized by ENAEE - European Network for Accreditation of Engineering Education, with the attribution of the EUR-ACE quality mark, making the community of FEUP recognized and respected among its European peers.

Figure 1.3 Faculdade de Engenharia da Universidade do Porto logo.

1.4 Thesis Outline

The present thesis is divided into 5 chapters. The present chapter serves as a first contextualization to the reader, where the motivation, problem and objectives presented to the author are described.

Chapter two provides the bibliographical review on pressure vessels. This includes a thorough description of what pressure vessels are, their common shapes and applications, and what operation conditions are usually considered. Then, the failure mechanisms of like-structures is discussed, together with analytical formulations for each type of failure. Then, a summarization of several design considerations is presented to allow for a streamlined design of stiffened and unstiffened shells, together with the presentation of more alternative design concepts described in the consulted bibliography.

Chapter three starts by reviewing the case study presented as the main objective to the thesis author and is followed by a summarization of the conducted market analysis, together with what main conclusions were derived from it. Using these conclusions, the product specifications were determined following a needs-metrics model and benchmark study to select the final metrics ideal and range values. These values were later used as the main guidelines on the development of a market-standard unstiffened cylindrical shell, to what all developed vessels would be compared to. Finally, a conceptual design approach was adopted, and using a morphological matrix, several design options were defined and selected for further study.

In Chapter four, all vessel concepts were dimensioned, modelled and tested via a numerical Finite Element Analysis – FEA, which parameters were determined via an iterative process to approach these results to the estimations via analytical methods. Then, the parallel development of 4 pressure vessel concepts took place. These were first studied using a simplified shell analysis which accelerated the development process time and were followed by a detailed vessel assemble modelling and analysis. The chapter concludes with a side-by-side comparison of all product concepts with the market-reference vessel, together with the final product specifications, which were refined throughout the thesis development.

Chapter five closes the thesis, and its main conclusions are presented, recalling the significant results trade-offs that were considered throughout its development, and future works thought by the author are presented as suggestions of future development.

This page was intentionally left blank

2. Bibliographical Review

To better understand the span of the research to be conducted, the first step is to review pressure vessel for deep-sea applications development, their main characteristics and design solutions, and the failure mechanisms in play. It was also reviewed the numerical method characteristics to be considered for pressure vessel behaviour simulation.

2.1 Pressure Vessels

The exploration of the deep sea takes place on the final frontier of the continental slope. The descent that marks the passage of the continental shelf to the abyssal plain raises the depth of the ocean from 100 to 3 200 meters, and pressure increases approximately by 30 times during this descent [21]. Any device that operates in this region needs to cope with the extreme conditions caused by rising hydrostatic pressure with increasing depth.

The two approaches to protect a submerged system are the pressure tolerant system design and the pressure hull system design - *Figure 2.1*. The first is the most common [12], and requires a pressure-tight encasing to protect the payload which cannot withstand the pressure. It remains watertight, so when submerged, a pressure differential appears with the hull shell acting as boundary condition. On the other hand, in a pressure tolerant system, every component can withstand pressure [22]. To do so, the components are surrounded by an electrically neutral, incompressible medium that distributes pressure so no pressure gradients appear [23]. Pressure transmission can use a liquid, usually oil, or a solid medium [12].

A pressure vessel, also called pressure housing, is a type of pressure hull system. It differs from the pressure hull more in terms of nomenclature since the latter is usually attributed to the encasing of manned submersibles like submarines or bathyscaphes [24]. Such hulls have different design requirements and dimensions to accommodate a self-regulating environment with life-supporting systems to make the vehicle habitable. On the other hand, a pressure vessel simply protects the inner payload of a submersed vehicle or equipment that is unsuited to deal with the hydrostatic pressure: circuit boards, sensors, connectors, and batteries.

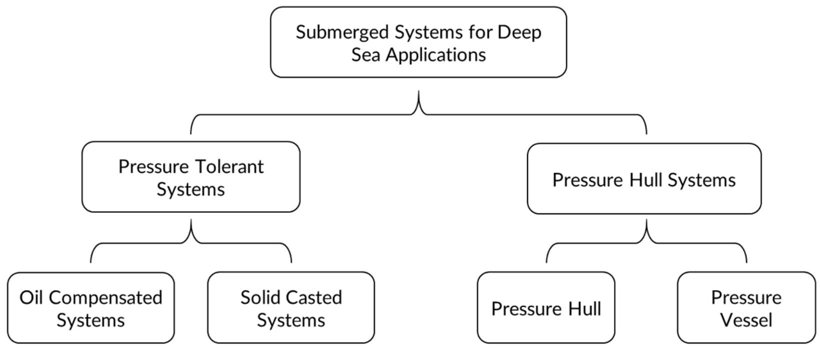

Figure 2.1 Schematics of the different solutions for submerged systems. Adapted from [23].

A common nomenclature misconception arises from the broader meaning of "pressure vessel". According with the American Society of Mechanical Engineers - ASME, pressure vessels are defined as *"containers for the containment of pressure, either internal or external [...] with an operating pressure of over 15 psi"* [25]. However, a vessel under internal pressure, where forces are mostly of tensile, is quite different from one under external pressure, where the forces are mostly of compressive. Different pressure nature means different failure modes are playing a part, and vessels subjected to external pressure are reported to collapse at a considerably lower pressure than what would be required cause failure if subjected to matching internal pressure conditions [25]. The internal pressure vessel finds more applications across multiple sectors than external ones. Since this thesis interest is exclusively on pressure vessels designed for external hydrostatic pressure loads, the nomenclature "pressure vessel" will refer exclusively to this condition.

2.1.1 Pressure vessel common shapes

Pressure vessels can take various shapes - *Figure 2.2*. The ideal shape is of a perfectly spherical shell [26], since by having spherical symmetry, the applied stress will be evenly distributed, partially neutralizing the tangential forces. Plus, out of all closed surface geometries, the sphere will be the one with the minimal surface-area-to-volume ratio, meaning mathematically the applied force will always be the lowest [27]. However, there is more to pressure vessel design than structural efficiency: perfectly built spheres are not only difficult to manufacture, but are of an unpractical shape, since it is usually unsuited for submersible equipment and the useful volume is considerably small [26].

The most common shape is the cylindrical shell. A cylinder's shape has better internal arrangements, lighter exostructures and lower fabrication costs [24]. Manufacturing is less prone to the appearance of geometric imperfections than spherical shells, and more importantly, the useful volume is greatly increased, and the shape is better suited for the submersible equipment. Still, these geometries report a considerable waste of volume since part of it is incompatible with the internal payload, which usually takes a parallelepiped or cuboid shape. Most cylinders are used up to 6 000m, the limit of the abyssal zone [24]. However, cylindrical pressure vessels using ceramic shells were used in the Challenger Deep, reaching 11 000m [28].

Cylindrical vessels are usually classified as thin shells. This can be determined by *Formula (2.1)*, which relates the ratio between R_m, the mean radius of the shell, and t, the shell thickness [29].

$$\begin{aligned} thin\ shells&: \frac{R_m}{t} > 10 \\ thick\ shells&: \frac{R_m}{t} \leq 10 \end{aligned} \tag{2.1}$$

Another solution is the elliptical profile shell, also referred as the hemispherical dome shape. It has a more moderate weight displacement ratio than the cylinder shape, and a higher useful volume than the sphere. However, this shape is quite expensive to build. This shape, along with the cone construction, is usually adapted to act as the end section of a cylindrical shape of a vessel [26].

Figure 2.2 Pressure vessel major configuration examples: sphere pressure vessel on the left; cylindrical pressure vessel on the centre [30]; ellipse section pressure vessel on the right [26].

The following table, developed by MIT as an introduction to their ATLANTIS II development program, which compiles the advantages and disadvantages of the shapes stated above [31]. Despite being developed in the scope of manned submersibles, the validity remains for all geometries of pressure vessels.

Table 2.1. Advantages and disadvantages of pressure vessel shapes. Adapted from [31]

Shape	Advantages	Disadvantages
Sphere	**1.** Most favourable weight to displacement ratio; **2.** Thru-hull penetrations easily made; **3.** Analytical stress analyses are more accurate and less complex.	**1.** Difficult and inefficient interior arrangements; **2.** Large hydrodynamic drag.
Ellipse	**1.** Moderate weight to displacement ratio; **2.** More efficient interior arrangements than in sphere; **3.** Thru-hull penetrations easily incorporated.	**1.** Expensive to construct; **2.** Difficult to perform accurate structural analysis.
Cylinder	**1.** Inexpensive to construct; **2.** More efficient interior arrangements than in ellipse **3.** Low hydrodynamic drag	**1.** Least efficient weight to displacement ratio; **2.** Interior frames required to increase strength.

2.1.2 Subsea applications of pressure vessels

The principal function of pressure vessels is to protect sensitive components like batteries, sensors, processing unit and onboard computers. They are usually integrated into more complex submersible equipment, which can be manoeuvrable when submerged, or simply placed on the seabed to monitor its surroundings. Some of the more common applications are:

- **Autonomous Underwater Vehicle (AUV)** – Unmanned underwater autonomous robots, AUVs can operate independently - *Figure 2.3 (a)*. These vehicles are previously programmed to fulfil a mission, which can range from data and survey monitoring to sea exploring. Since there are no tethered connections, an AUV is unable to transmit data, and rather stores it onboard to be collected when the AUV ascends. They also carry specialized batteries to provide power, and alternative solutions like fuel cells and solar panels are also a possibility, despite not as common [32]. AUVs can range in size and weight, depending on the conditions of the mission, and larger AUVs are usually needed for deeper missions. Common applications of AUVs are ocean-based research, like bathymetric mapping, environmental information recording, deep sea and geologic formations exploration, and others [32]. Compared to other submersibles, AUVs are highly flexible, and can both explore waters too shallow for boats or go deeper than a tethered vehicle could. They are usually modular and highly customizable, and some can operate for long mission periods. Despite expensive, they are cheap when compared to equipment able to fulfil similar operations with a high degree of autonomy and flexibility [32].

- **Remotely Operated Vehicle (ROV)** – ROVs are highly manoeuvrable vehicles that are tethered via a group of cables that connect it to a surface ship, where it is controlled and manoeuvred by an operator - *Figure 2.3 (b)*. These cables also power the vehicle, so no batteries are used. They can conduct more operations that an AUV since mechanical arms can be controlled in real-time [33]. They are commonly used for industrial purposes like oil rig maintenance, pipeline inspection, and search and rescue military operations, but also for scientific missions [33]. Compared to other submersibles, ROVs are usually slower and heavier due to their less hydrodynamic shape, and partly due to the tether drag in the water. For missions where this is a major problem, another class of ROV, called hybrid ROV (H-ROV) is also an option. Like AUVs, these are battery-powered, but controlled via an ultra-thin fibre-optic tether, which greatly reduces water drag [34].

- **Landers** – Landers are instrument carrier systems able to operate autonomously, and are used to study the deep seabed surface, where stay to perform pre-programmed analysis and operations - *Figure 2.3 (c)*. Landers are usually a simple metallic structure where equipment is attached. They are weighted down with high density cylinders, and when it's time to ascend, an acoustic signal triggers the cylinders to drop, making the lander positively buoyant [34]. Landers can perform autonomously a series of functions and in situ experiments and are usually deployed for longer periods. They are extremely useful to accurately measure phenomena that require constant survey during a long time. Like the AUVs, only when retrieved it will be possible to analyse the data collected, which is stored in hard drives [34] [35].

• **Deep-Sea Crawlers** – a remotely operated vehicle, the deep-sea crawler is most suited for applications in the seabed surface - *Figure 2.3 (d)*. Similarly to the ROV, it has a tether connection for both power and manoeuvrability. It is a universal device carrier with multiple sensors, usually used for long term missions, up to one year. Its modular design makes it easy to adapt a crawler for a given task. It's usually smaller than the rest of the vehicles described above [34].

• **Other applications** – Besides the main applications above, some equipment require pressure vessels as well. Manned submersibles usually employ pressure vessels exterior to the main pressure hull, to support additional functionalities [24]. Other examples are seafloor observatories, a combination of different measurement equipment covering an area of several square kilometres and time spans of several months [36]. Another example are recent tests by big tech companies to move data farms underwater. This way, the external ocean temperature acts as coolant, considerably reducing operating costs. Microsoft's Project Natick [37] deployed a data centre 35 meters underwater back in 2018, and successfully validated the performance and reliability of their servers for a two-year span. Other companies are expected to follow and further develop this concept [38].

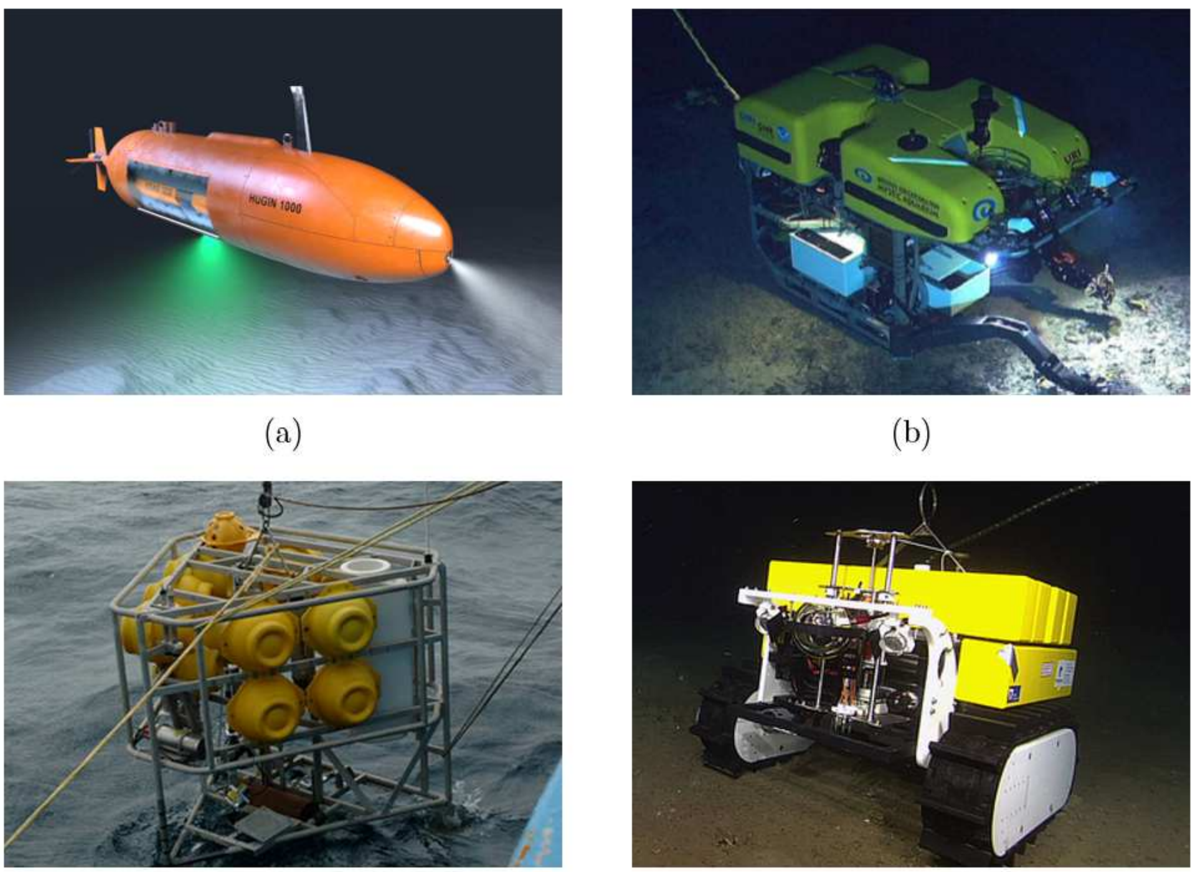

(a) (b)

(c) (d)

Figure 2.3 Common applications of pressure vessels: (a) Autonomous Underwater Vehicle [39]; (b) Remotely Operated Vehicle [40]; (c) Benthic Lander [41]; (d) Deep sea Crawler [42].

2.1.3 Operation conditions

Pressure vessels analysis does not consider the fluid dynamics of the boundary environment since the vessel is usually built to fit inside a casing exostructure of the submersible equipment. This exostructure is water permeable, meaning all components that are not inside the pressure vessel must be pressure tolerant [12] - *Figure 2.4*. So, to simplify the analysis, the vessel is considered to be always in a hydrostatic pressure system.

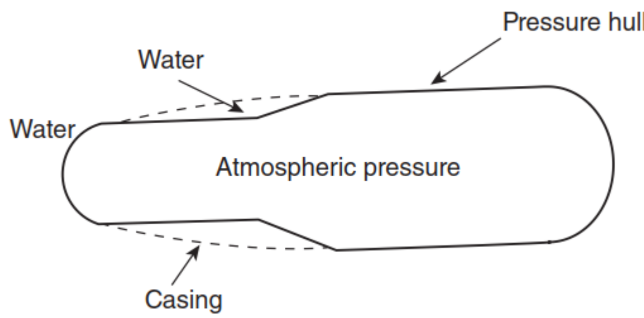

Figure 2.4 A pressure hull with an exostructure casing. Adapted from [26].

Considering the fluid incompressible, the main force is the external pressure. On a cylinder shell, it results as a combination of both a radial force, applied to the curved surface area, and an axial force, acting on both cylinder base areas. This pressure can be simply estimated by considering the fluid incompressible. In such conditions, the pressure, P, is a function of the fluid density, ρ_f, the earth's gravity, g, and the height of the above water column, h - *Formula (2.2)*.

$$P = \rho_f \, g \, h \tag{2.2}$$

Pressure is a function of depth, so equipment is always limited by the limits of the operating pressure it was designed for. For example, military submarines usually dive between 300-450 meters, the limit of the continental shelf. Offshore submersibles, mainly used for research, exploration or seabed prospect range from shallow waters to the abyssal plain, about 5 km deep. Then, research submersibles used to explore the vast depths of ocean trenches - *Figure 2.5*.

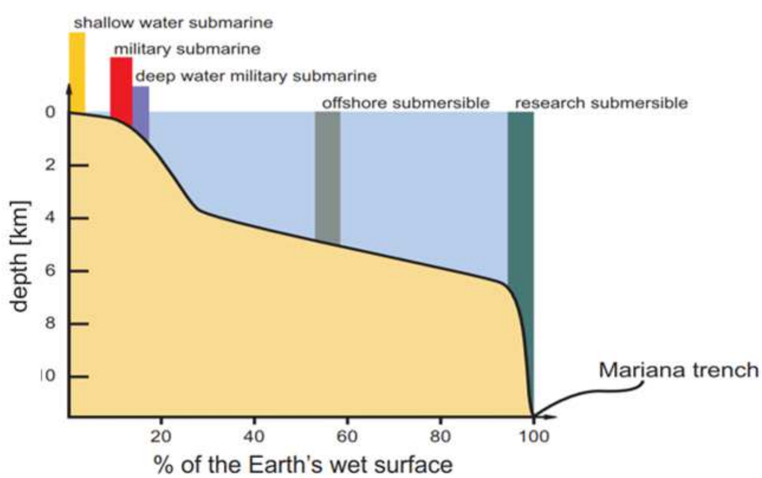

Figure 2.5. Curve of the Earth's wet surface with various submersible depth ranges [43].

The fluid density of saltwater is, on average, 1.028 g cm^{-3} at the surface [44]. Although water is usually regarded as incompressible, it compresses under extreme pressure, which leads to a linear increase in density, observed in *Table 2.2*.

Table 2.2. Seawater density variation with depth. Adapted from [44]

Depth [m]	**Pressure [MPa]**	**Density [g/cm³]**
0	0.101	1.02813
1000	10.13	1.03285
2000	20.35	1.03747
4000	41.06	1.04640
6000	62.09	1.05495
8000	83.44	1.06315

Another condition of high importance is vessel buoyancy. Submersible vehicles and equipment have tight demands regarding weight since its manoeuvrability depends on it. They are usually designed to be positively buoyant so in case of malfunction, it can submerge to be retrieved [26]. So, buoyancy needs to be balanced with the weight of the overall equipment [45]. Syntactic foams are used to increase uplift force, but since the pressure vessel is a considerably heavy component, it must be dimensioned with care. It is typical for pressure vessels to be designed to be neutrally buoyant [24], but they usually have more buoyancy to compensate for the internal payload weight.

Regarding the upward force of the vessel itself, buoyancy must be balanced with the weight. Self-sustaining buoyancy is a usual prerequisite of the design, which means the weight of the vessel equals the weight of its fluid displacement. If this weight-to-displacement ratio [46] is equal to or smaller than the unity, the structure will float; otherwise, it sinks – *Formula (2.3)*

$$\frac{W}{B} = \frac{\rho \, g \, V_{vessel}}{\rho_f \, g \, V_{disp}} \tag{2.3}$$

Where:

W = Weight of the vessel
B = Weight of displaced fluid
ρ = vessel density
ρ_f = fluid density
g = gravitational acceleration
V = volume of the vessel
V_{disp} = volume of displaced fluid

And finally, the net upward force is given by Archimedes' principle:

$$\Delta = W_f - W \tag{2.4}$$

2.2 Failure Mechanisms

A pressure vessel can be understood as a shell structure under external forces, which reflects on compressive strains applied on the shell surface. One of the failure modes which governs design procedures of like structures is related with a sudden loss of stability, where the vessel can no longer hold its shape and suddenly collapses to a shape with less internal volume [47], under a constant load [45]. This failure is defined as buckling.

For static analysis of perfect cylindrical shells, there are two behaviours to consider: Bifurcation buckling, also known as purely elastic buckling, is associated with deformations that are orthogonal to the pre-buckling deformations taking place; And "snap-through" buckling, or limit-point buckling, characterized by deformations that follow the pre-buckling ones. Referring to *Figure 2.6,* "snap-through" buckling would occur at point A, while bifurcation buckling starts at point B.

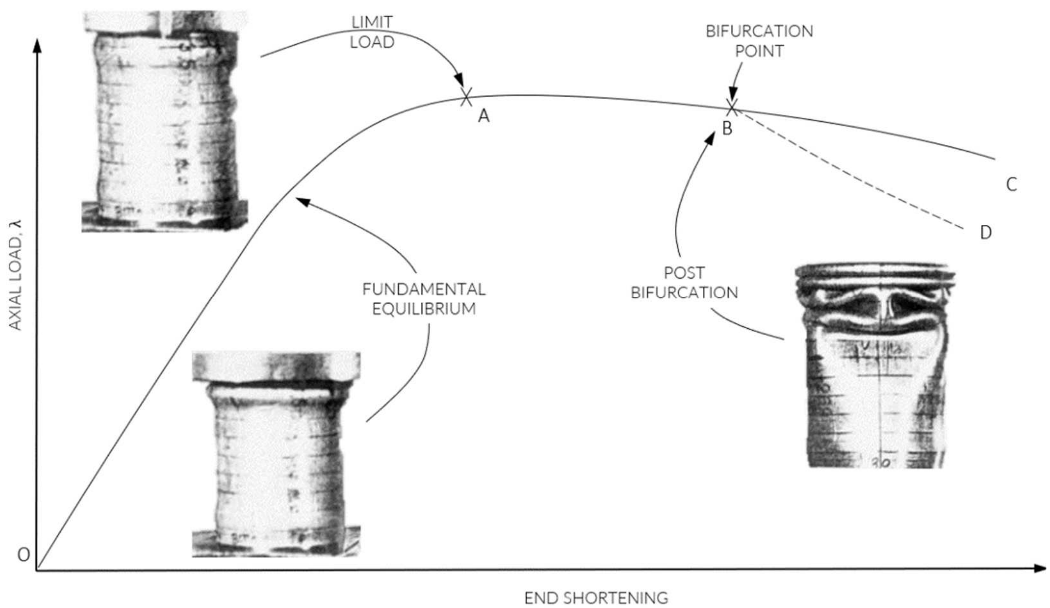

Figure 2.6. The Load-displacement curve of a cylinder shell test piece under axial load [48].

As a starting point to understand buckling, consider a perfect cylindrical shell purely under axial compression - *Figure 2.6*: Following O-A, the cylinder deforms axisymmetrically until a maximum load at point A is reached. If the load is not relived, the cylindrical shell will fail and start to deform plastically, following either the path A-B-C, which results in pure axisymmetric deformation, or the path A-B-D, where bifurcation buckling appears [26] [48]. Bifurcation is sudden and difficult to predict since it can appear at any point of the equilibrium path. This example is rather unusual, since the bifurcation point appears after the collapse point. It is far more common for buckling to occur at a lower load [48]. In *Figure 2.7.* this situation is represented with bifurcation occurring below the yield limit. The equilibrium path O-A-C corresponds to pure axisymmetric deformation, while the B-D path would result in rapidly growing non-axisymmetric deformations.

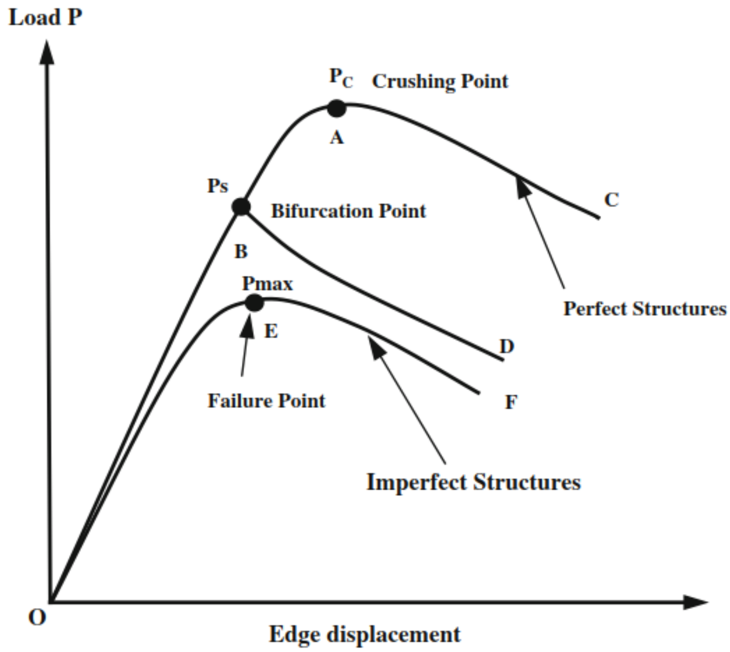

Figure 2.7. Load-deflection curves of perfect and imperfect structures, showing yield limit and predicted bifurcation points. Adapted from [49].

Figure 2.7 also displays the curve O-E-F, showing how a real structure with unavoidable imperfections would behave. Here, failure occurs in point E, at lower pressure than the theoretical critical buckling point [48], and the structure would start failing at a fraction of the pressure it would be required to cause axisymmetric yield [26]. This shows that true bifurcation buckling does not take place in real structures. However, this analytical model is still useful since it leads to a good approximation of real failure [48], but the use of adequate safety factors is required.

It is concluded that buckling is difficult to predict and can either occur at a fraction of the pressure it would take to cause yielding, or it may not appear at all. To understand why, imperfection sensitivity must be considered. This sensitivity means the shell can deform if any incidental disturbance takes place, even if the compressive stress is below the tensile compressive strength of the material [26]. Multiple factors can act as disturbances, which are more than often hard to predict and control, meaning all structures acting under compression will have a sensitivity that must be considered [26]. It is due to this sensitivity that a real shell will always buckle at a lower pressure than the theoretical prediction. This makes buckling highly nonlinear: the change of the output is not proportional to the change of the input.

Overall, the imperfections prone to cause instability are [50]:

i. initial geometric imperfections, such as axisymmetric imperfections, linear buckling mode shape imperfection, and out-of-circularity of the cylinder shell;
ii. related to boundary conditions and load perturbations;
iii. influenced by pre-buckling deformation;
iv. eccentricities and nonuniformities of applied load and length;
v. presence of material discontinuity such as cracks on the shell structure.

The concept of buckling for a thin-walled cylinder shell under axial load was introduced. Shells under hydrostatic pressure are quite similar but buckling can now occur in two different ways: axial buckling, if the structure starts to yield as described in *Figure 2.6*, or radial buckling, if the structure fails by buckling of the walls. Windenburg [51] analysed the influence of basic geometry in the deformation of perfect cylinder shells under hydrostatic pressure, and concluded that the deformation depends largely on the length-diameter and thickness-diameter ratios:

- A short, thick-walled vessel is prone to fail by stress reaching the yield point − Axisymmetric yield;
- A long, thin-walled vessel is prone to fail by buckling for stresses below yielding – Lobar buckling;
- A stiffened vessel is prone to fail by buckling if the added rings are not suited – General instability.

These failure modes are represented in stiffened cylindrical shell in *Figure 2.8*:

(a) (b) (c) (d)

Figure 2.8. Thin Cylinder shell structure with internal ring stiffeners: (a) pre-deformed shell; (b) axisymmetric yielding; (c) lobar buckling; (d) general instability. Adapted from [52].

Axisymmetric yielding happens when the shell evolves in the equilibrium path until it implodes inelastically inwards, keeping its circular cross-section while collapsing [26] [48]. If the cylinder is radial stiffened, this failure mode appears both between stiffeners and at the inner surface of the shell, leading to an accordion-type of pleat - *Figure 2.8 (b)* [24] [52].

Lobar buckling, also referred to as local or shell instability, is triggered by imperfections and by result, the critical buckling pressure of a structure P_{cr}, is only a fraction of what would require to reach yielding limit from bulk stress [26]. The structure starts to collapse around its circumference in the form of several irregular circumferential waves or lobes [26]. This failure mode is mostly a function of radial pressure, so long, thin-walled shells are more prone to this failure [53] [46].

One way to improve lobar buckling resistance is to stiffen the shell. However, lobar buckling can still take place if the shell is weaker than the stiffeners - *Figure 2.8 (c)*. In this case, inward and outward lobes appear between stiffeners which may develop around the cylinder periphery [24].

General instability occurs when the ring-stiffeners added to the cylinder are not strong. This can cause the entire ring-shell arrangement to collapse bodily [54]. The deformation is characterized by inward and outward lobes, but the lobes are fewer - *Figure 2.8 (d)* [24].

2.2.1 Axisymmetric yield of cylindrical shells

Yielding can be explained as deformation past the material yield strength, when the deformation is no longer linear and reversible, and becomes plastic, i.e. nonlinear and non-reversible. This phenomenon is defined for a given material by its characteristic stress-strain curve at the point at which the curve stops progressing linearly. To prevent axisymmetric yield, the calculated stress must always be below the material yield strength. A simple but reliable approach of the yield pressure of a thin-walled cylindrical shell is to use the so-called "boiler formula" [45], which is derived from the membrane stresses for an infinite length cylinder to calculate the circumferential and longitudinal stresses, σ_θ and σ_L respectively - *Formula (2.5).*

$$\begin{aligned} \sigma_\theta &= circumferential\ stress = \frac{P\, R_{ext}}{t} \\ \sigma_L &= longitudinal\ stress = \frac{P\, R_{ext}}{2t} \end{aligned} \tag{2.5}$$

Where:

P = external hydrostatic pressure
R_{ext} = external radius
t = shell thickness of the cylinder cross-section

To predict actual structural failure, yield criterions, which define the allowable state of stress for a material, are used. Structures have a principal plane of stress, defined by the geometry and material used. By using yield criterions, combinations of principal stresses are used to predict when yielding is likely to occur. A Yield criterion can be imagined as curves in a stress space: if stress reaches the curves' contour, yielding occurs [55]. Different criterions can be used, and their accuracy is highly dependent of the material. For metallic, isotropic structures, the Von Mises yield criterion is the most commonly used. It is based on distortion energy theory, which states that energy is associated with the material shape deformations. The Von Mises stress, $\sigma_{VM,}$ is defined by:

$$\sigma_{VM} = \sqrt{3 J_2} \tag{2.6}$$

$$|S - \lambda I| = \lambda^3 - J_1\lambda^2 + J_2\lambda - J_3 = 0 \tag{2.7}$$

$$S = \sigma_C - \frac{1}{3} tr(\sigma) \tag{2.8}$$

Where J_2, the second invariant of the deviatoric stresses, can be determined with *Formula (2.7)*, where I is the identity tensor, J_n the n-th deviatoric invariant, S the deviatoric stress tensor defined in *Formula (2.8)* and σ_C the Cauchy stress tensor. *Formula (2.6)* can be further developed, so it describes stress in tensor element space in *Formula (2.9)*. It is most commonly used with stress tensors projected in the principal stress space - *Formula (2.10).*

$$\sigma_{VM} = \sqrt{\frac{(\sigma_{11} - \sigma_{22})^2 + (\sigma_{22} - \sigma_{33})^2 + (\sigma_{33} - \sigma_{11})^2 + 6({\sigma_{12}}^2 + {\sigma_{23}}^2 + {\sigma_{31}}^2)}{2}} \tag{2.9}$$

$$\sigma_{VM} = \sqrt{\frac{(\sigma_1 - \sigma_2)^2 + (\sigma_2 - \sigma_3)^2 + (\sigma_3 - \sigma_1)^2}{2}} \tag{2.10}$$

2.2.2 Lobar buckling of cylindrical shells

Lobar buckling of a structure is a phenomenon associated with a sudden loss of stability across the shell, which can occur for a lower pressure than what it would require the vessel to yield. This is defined as critical buckling pressure, P_{cr}. For an infinitely long circular cylinder under uniform radial pressure, the critical buckling pressure is given by *Equation (2.11)* [26].

$$P_{cr} = \frac{E}{4(1-\nu^2)}\left(\frac{t}{R_m}\right)^3 \tag{2.11}$$

Where:

P_{cr} = critical buckling pressure
t = shell thickness of the cylinder cross-section
R_m = mean radius of the shell
E = Young's modulus
ν = Poisson's ratio

This equation is valid for perfect long, thin tubes [51]. To determine a more accurate equation for real shells, Von Mises [56] approached the derivation of the critical buckling pressure of a thin-walled cylindrical shell, simply supported at its ends and subjected to the combined action of uniform lateral and axial pressure by direct solution of the equilibrium equations. According to Windenburg [51], it was the most accurate instability formula for a cylindrical shell under hydrostatic pressure:

$$P_{cr} = \frac{E\left(\frac{t}{R}\right)}{\left[n^2 - 1 + \frac{1}{2}\left(\frac{\pi R}{L}\right)^2\right]} \times \left[\frac{1}{12}\left[\left(n^2 + \left(\frac{\pi R}{L}\right)^2\right)^2 - 2\mu_1 n^2 + \mu_2\right]\frac{t^2}{R^2(1-\nu^2)} + \frac{1}{\left(\left(\frac{nL}{\pi R}\right)^2 + 1\right)^2}\right] \tag{2.12}$$

Where:

L = length
R = internal radius
n = number of circumferential waves or lobes into which the vessel buckles - *Figure 2.9*
$\mu_1 = 1 + \frac{\alpha}{2}\left(3 + \nu + \alpha(1-\nu^2)\right)$
$\mu_2 = 1 + \alpha(1+\nu) - \alpha^2\left[\nu(1+2\nu) + (1-\nu^2)(1-\alpha\nu)\left(1 + \alpha\frac{(1+\nu)}{(1-\nu)}\right)\right]$
$\alpha = \dfrac{1}{n^2\left(\frac{2L}{\pi D}\right)^2 + 1}$

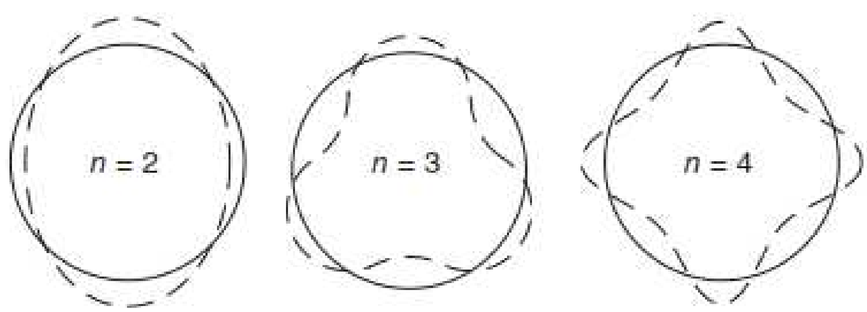

Figure 2.9. Circumferential lobes detected for buckling modes [26].

Lobar buckling is marked by the appearance of lobes across the shell - *Figure 2.9*. These are defined as the characteristic post-buckling deformation mode shapes, and to which the structure will deform to is also a function of material and geometric properties. So, the critical buckling pressure is calculated for different values of n and solved to minimize P_{cr}. The value of n that matches the minimum value of P_{cr} is referred as the buckling eigenmode [26], and translates to the number of lobes that appear when the structure buckles.

Von Mises formula became the standard at the time [57]. Von Mises also developed an approximation that simplifies the calculation by partially neglecting terms of the equation, resulting on an acceptable average deviation of 1.5% [51]: the Von Mises Simplified Formula - *Formula (2.13)*.

$$P_{cr} = \frac{E\left(\frac{t}{R}\right)}{\left[n^2 + \frac{1}{2}\left(\frac{\pi R}{L}\right)^2\right]} \times \left[\frac{1}{\left[n^2\left(\frac{L}{\pi R}\right)^2 + 1\right]^2} + \frac{t^2}{12R^2(1-\nu^2)}\left[n^2 + \left(\frac{\pi R}{L}\right)^2\right]^2\right] \tag{2.13}$$

It should be noted that not only Von Mises was conducting a meaningful study on the buckling behaviour of cylindrical shells under hydrostatic pressure. Takagawa [58] and Flugge [59] also approached these results with similar solutions also derived from the Equilibrium Equations, as well as Donnell [60] who derived the same solution through the Minimum Energy Equations.

A simpler version of the Von Mises formula was developed by Windenburg and Trilling [51], and is independent of the buckling mode n. Known as the David Taylor Model Basin (DTMB) formula, *Formula (2.14)* simplifies considerably the buckling pressure calculation.

$$P_{cr} = \frac{2.42\,E}{(1-\nu^2)^{3/4}} \times \left[\frac{\left(\frac{t}{2R}\right)^{5/2}}{\frac{L}{2R} - 0.45\left(\frac{t}{2R}\right)^{1/2}}\right] \tag{2.14}$$

Kendrick [61] proposed a slight modification to Von Mises simplified formula, which gained popularity and has been incorporated into several pressure hull design codes [57] – *Formula (2.15)*

$$P_{cr} = \frac{E\left(\frac{t}{R}\right)}{\left[n^2 - 1 + \frac{1}{2}\left(\frac{\pi R}{L}\right)^2\right]} \times \left[\frac{1}{\left[n^2\left(\frac{L}{\pi R}\right)^2 + 1\right]^2} + \frac{t^2}{12R^2(1-\nu^2)}\left[n^2 - 1 + \left(\frac{\pi R}{L}\right)^2\right]^2\right] \tag{2.15}$$

All of these formulations consider the same set of assumptions to be mathematically valid [51]:

i. The shell is purely under uniform hydrostatic pressure;
ii. The material of the shell is homogeneous, isotropic, and behaves linear elastically;
iii. The boundary conditions are of a simply supported shell at both ends;
iv. The length of the considered shell is shorter than the critical length, L_{cr}, given by:

$$L_{cr} = \left(\frac{16\pi\sqrt{3}}{27}\sqrt[4]{1-\nu^2}\right)\sqrt{R/h} \tag{2.16}$$

All these methods were found being employed in several papers to analytically determine the buckling pressure. However, they not only provide slightly different estimations from one another, but are estimated for perfect shells, and real structures are expected to buckle at a considerably lower pressure. Ross et al. [62] compared the predictions of analytical formulas, experimental results, and numerical analysis of P_{cr} for a similar aluminium alloy Al 6082-T6 cylinder tubes - *Figure 2.10.*

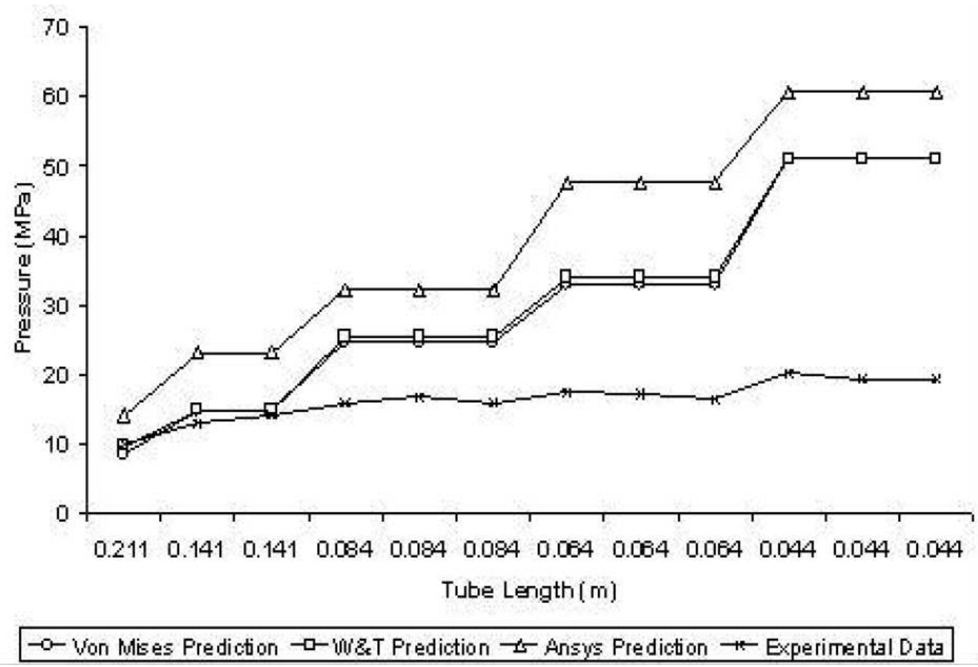

Figure 2.10. Predicted buckling pressure as a function of the tube length for an Al 6082-T6 tube with D_m = 25 mm, t = 1.7 mm [62].

Here, it is possible to notice both a slight variation on the predicted buckling pressure when utilizing either the Von Mises or the Windenburg & Trilling (W&T) formula, but also the discrepancy between theoretical and experimental results. Ross concluded to be due to geometrical imperfections, or initial out-of-circularity for this case, which was particularly noticeable for shorter tubes [62]. Also relevant is how the numerical prediction using the ANSYS software was considerably higher than both the theoretical predictions and the experimental data.

Windenburg and Trilling [51] defined a thinness ratio, λ_c, which allows the comparison in behaviour of cylinders with different lengths, internal radius, shell thickness and the elastic properties of a material – Young Modulus, E, and yield strength, σ_y:

$$\lambda_c = \left[\frac{\left(\frac{L}{2R}\right)^2}{\left(\frac{t}{2R}\right)^3}\right]^{\frac{1}{4}} \left(\frac{\sigma_y}{E}\right)^{\frac{1}{2}} \tag{2.17}$$

Using this ratio, it is possible to predict which failure modes the shell may be susceptible to. The shell is most likely to fail due to axisymmetric yielding when $\lambda_c < 0.8$, due to plastic instability when $0.8 < \lambda_c < 1.2$ and elastic instability is possible whenever $\lambda_c > 1.2$ [51].

2.2.3 General instability of cylindrical shells

If the rings on a stiffened pressure vessel are relatively weak in comparison to the shell, which can happen due to the rings lacking sufficient cross-sectional area or inertia, each ring may "follow" the deforming shell during collapse [63]. This failure mode is known as general instability, which was first identified by Tokugawa in 1929 [64]. He analysed stiffened cylinders considering the elastic instability of an isolated ring, with no supports from bulkheads, and interpreted that a considerable width of shell buckled together with the ring stiffener [26].

$$P_{cr} = \frac{E\left(\frac{t}{R}\right)}{\left[n^2 - 1 + 0.5\left(\frac{\pi R}{L}\right)^2\right]} \times \left[\frac{1}{\left[n^2\left(\frac{L}{\pi R}\right)^2 + 1\right]^2} + \frac{t^2}{12R^2(1-\nu)^2}\left[n^2 - 1 + \left(\frac{\pi R}{L}\right)^2\right]^2\right] \tag{2.18}$$

Years later, Bryant [65] corroborated this conclusion and expanded this research with an approximate formula for the general instability of ring-stiffened circular cylinders considering the pressure for a frame component, P_{fr}, and a pressure for a shell component, P_s [26]:

$$P_{cr} = P_{fr} + P_s$$

$$P_{cr} = \frac{(n^2-1)EI_{xx}}{{R_m}^3 L_f} + \frac{Et}{R}\left[\frac{\mu^4}{\left(n^2 - 1 + \frac{\mu^2}{2}\right)(n^2+\mu^2)^2}\right] \tag{2.19}$$

Where:

P_{cr} = buckling pressure
t = shell thickness of cylinder cross-section
R_m = mean radius of cylindrical shell
E = Young's modulus
n = number of circumferential waves or lobes;
$\mu = \pi R/L_b$;
I_{xx} = second moment of inertia of a ring-stiffener and the effective width of the shell;
L_f = inter-frame spacing length;
L_b = length between adjacent and bulkheads.

The above formula is no longer commonly used since with the advances of digital computer technology, there is no longer the need to use approximate formulas [26]. Kendrick developed a series of differential equations to calculate the total strain energy and potential of a cylindrical, stiffened pressure vessel, which solving using the Rayleigh-Ritz method allowed to calculate the critical buckling pressure of stiffened vessels due to general instability [26]. These equations are not displayed here, since the scope of this thesis is not heavily influenced on analysis of stiffened cylindrical shells.

2.3 Design methods of pressure vessels

The first step on pressure vessel design is to outline the general mission characteristics. Since its main purpose is to sustain pressure while remaining watertight, every individual vessel is built accordingly for its operating depth. The dimensions of the inner payload also needs to be considered, as well as the internal volume compatibility and the resulting uplift net force. And finally, the structure or equipment with will greatly influence its overall shape. As Allmendinger [24] states, the design of submersibles can be divided into two main groups: the pressure vessel design and the exostructure, or casing, design. Each group has its own demands, but an interrelationship is present, and the design of one influences the other [24]. However, stand-alone pressure vessels which dimensions are universally adaptable are usually commercialized.

Several design procedures are compatible for pressure vessel design, but the most common is the hierarchical design approach [45]. It begins by considering a classical analytical buckling analysis. Then, either more rigorous analytical method, or simplified numerical analysis are used, since the goal is to use relatively simple analysis to perform parametric studies of the design variables to define all nominal dimensions. Finally, the structural integrity of a detailed model is determined using more complex nonlinear numerical analysis, together with reliable safety factors. This way, the effect of different design variables can be studied at a fast pace, which leads to an adequate final design which can be later analysed in a more detailed fashion.

On the following chapters, the design variables, charts and safety factor recommendations for unstiffened and stiffened pressure vessels will be presented, as well as some more alternative concepts in pressure vessel design than these typical shells.

2.3.1 Design of unstiffened pressure vessels

Unstiffened pressure vessels design is a fairly documented field of study since they follow the geometry of simple, cylindrical straight shells. Several variables influence structural integrity - *Figure 2.11*. Cylinders are defined by 3 geometric variables: internal diameter, vessel length and shell thickness. Buckling typically occurs in structures where at least one of its dimensions is much smaller than the others: when instability starts, deformation will follow exclusively the direction of the large dimensions. In the case of a cylinder shell, the thickness is this smaller dimension, meaning it must be determined as a function of the vessel diameter, length, and applied load. Since the nominal load increases with depth, the wall thickness must as well increase. Eventually, the wall thickness gets so great that the vessel buoyancy can no longer withstand its weight [53]. Finding this trade-off between wall thickness and weight is one of the greatest challenges in pressure vessel dimensioning. To determine the hull thickness, both analytical and numerical methods are used, each checking for both shell stress and critical bucking pressure.

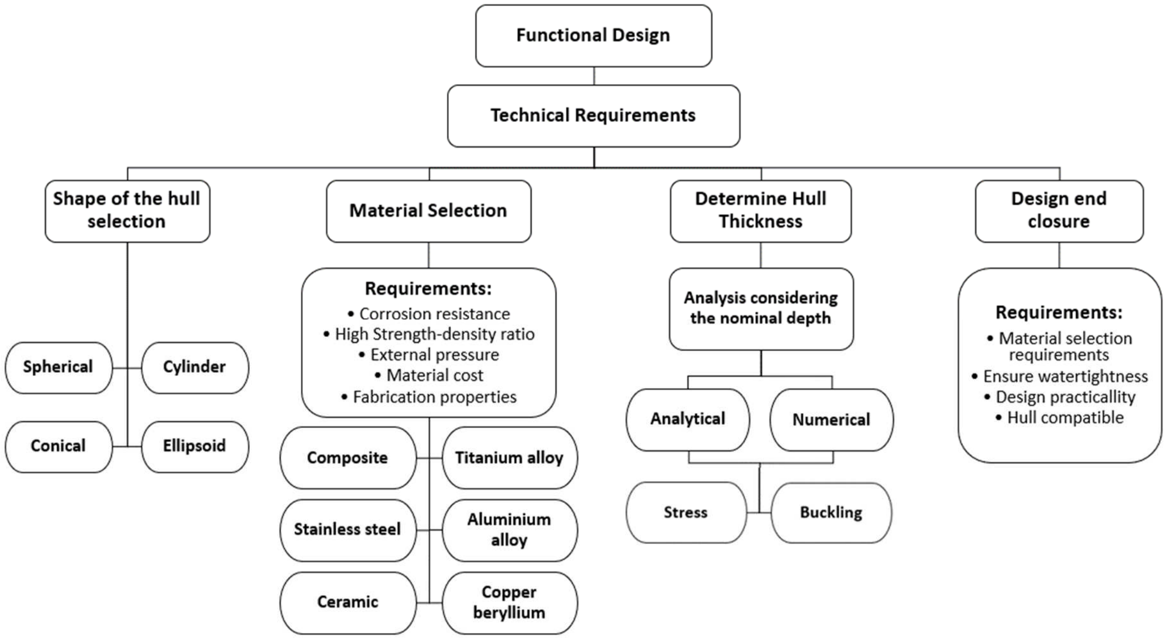

Figure 2.11. Schematic representation of design variables in pressure vessel functional design.

As previously stated, the real critical buckling pressure is lower than classical buckling predictions. The most common design method to account for this gap is to calculate the buckling pressure for an equivalent perfect shell using the equations presented in the previous chapter. Then, the critical pressure of the real shell is taken by applying a Knock-Down Factor (PKD) to the classical buckling load. This is an empirically derived factor, which relates the geometric and material properties of the shell with classical-experimental ratios previously studied to correlate the experimental pressure, P_{cr}, with a more accurate estimation, P_{real}.

$$PKD = \frac{P_{cr}}{P_{real}} \tag{2.20}$$

Ross [26] plotted a design chart for lobar buckling of accurately machined cylinders under hydrostatic pressure - *Figure 2.12*. Shell studies made by Sturm, Reynolds, Seleim, Roorda, Kimber and Ross et al. [26] are plotted to relate the Windenburg thinness ratio, λ – *Formula (2.17)*, with the PKD [51] [26]. This provides an easy way to determine the real cylinder bearable pressure.

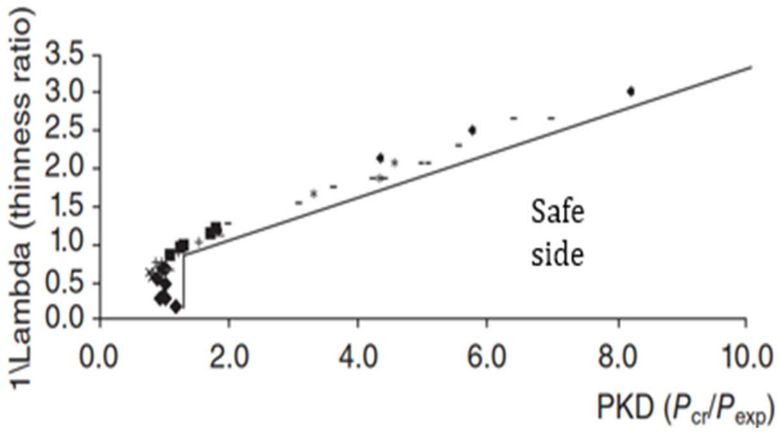

Figure 2.12. Design chart for lobar buckling of machined circular cylinders [26].

According to Ross [26], the best approach to design these vessels is to consider a geometry that eliminates the risk of failure by instability by applying an adequate safety factor when calculating shell thickness. This way, any failure will likely be caused by axisymmetric yield, a far more predictable failure mode and easier to determine both via analytical and numerical approach, and that does not depend as much of geometric or material imperfections.

Safety factors are usually defined by regulatory entities or societies. One of such societies is DNV GL. In "Rules for Classification – Underwater Technology (UWT)" [66], the *"loads to be considered for the design of submersibles, unmanned underwater vehicles and underwater working machines"* are described. Three design loads are defined as requirements to test in design:

- **Design pressure:** the pressure to which a pressure vessel is designed for;
- **Nominal diving pressure - NDP:** the pressure for unrestricted operation of the submersible or working machine, to which corresponds a maximum nominal diving depth
- **Test diving pressure – TDP:** the diving pressure to which the vessel is exposed when testing for the equipment strength, tightness, and function. Is the pressure range at which no yielding will occur, so the vessel can still operate fully.
- **Collapse diving pressure – CDP:** the pressure at which hull collapse is reported without considering creeping behaviour. Is the pressure range at which yielding occurs but without tensile failure being reported, meaning watertightness is still verified.

Three load cases as defined, each one correspondent to one of the pressures defined above. The NDP load case is determined by operational loads, which are simply determined for the design pressure. TDP load case applies the safety factor S1 to determine the correspondent Test Diving Pressure. CDP load case applies the safety factor S2 to determine the correspondent Collapse Diving Pressure. This safety factor also serves to account for the following uncertainties:

i. influences which cannot be covered by the calculation procedure;
ii. negative influences during operation (corrosion, unobserved buckling, alternating stressing);
iii. time-dependent characteristics of the material;
vi. influences as consequence of manufacturing mistakes (material failures, inaccuracies, residual stresses);

A safety factor intends to provide a safeguard from failure. It refers to a ratio between the load that would result in failure and the imposed nominal load. DNV GL provides the minimum safety factors that must be verified as a function of the Nominal Diving Pressure, NDP, for unmanned submersible systems - *Table 2.3:*

Table 2.3. Safety factors of unmanned systems: TDP and CDP in function of NDP [66]

NDP [MPa]	**0.5**	**1**	**2**	**3**	**4**	**5**	**6 ≤ NDP ≤ 400**	**≥ 400**
S1 = TDP / NDP test diving pressure/ nominal diving pressure	1.50	1.30	1.20	1.20	1.20	1.20	1.20	1.10
S2= CDP / NDP collapse diving pressure/ nominal diving pressure	2.20	1.90	1.80	1.75	1.70	1.65	1.60	1.50

2.3.2 Design of stiffened pressure vessels

As previous stated, a way to increase structural stability is to add radial stiffeners to the walls of the vessel. Ring-stiffeners can be internal or external, but according to Ross [26], internal ones are more efficient than externals since, with the same cross-section dimensions, an internal ring would weigh less than an equivalent, external one. However, internal rings decrease the internal useful volume, something of major importance when designing payload-carrying vessels.

The failure mode of a particular ring-shell geometry will depend on several variables: Shell-thickness-to-radius ratio, ring-spacing-to-shell-radius ratio, ring cross-sectional-area-to-shell-cross-sectional-area ratio, materials properties and geometric or material imperfections [43] make these structures far more difficult to analytically study than their unstiffened counterparts, and usually, differential equations are needed to estimate shell failure. However, failure modes are identical to the ones previously presented - *Figure 2.13*.

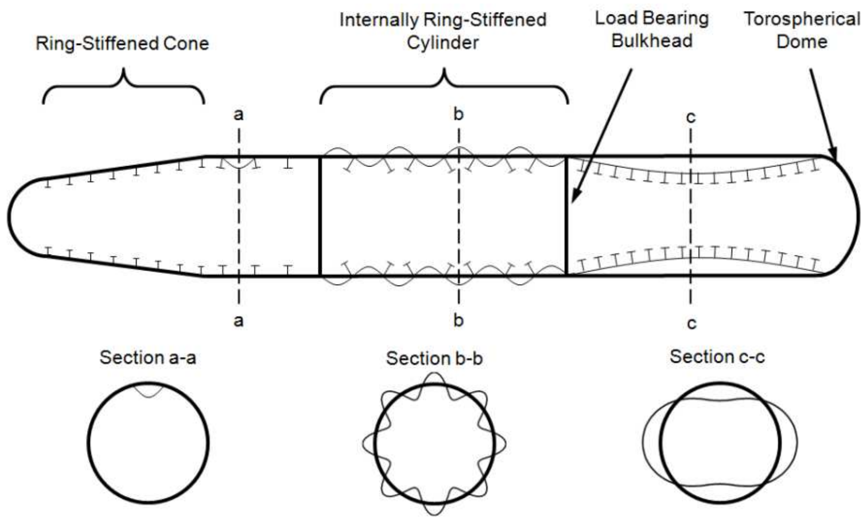

Figure 2.13. Pressure hull structure with: axisymmetric yield interframe collapse on the left (section a-a); interframe lobar buckling on the middle (section b-b); general instability on the right (section c-c) [57].

The main goal of adding stiffeners is to strengthen the hull and prevent buckling. So, a well-designed stiffened hull aims to report axisymmetric yield interframe collapse as its failure mode - *Figure 2.13 section a-a* [43]. It is an accordion-type pleat around the circumference between adjacent rings, and it can occur in more than one bay. Differential equations are typically used [26], but the most reliable was developed by Salerno and Pulos – *Formula (2.21)* [67] [63]:

$$D_0 \frac{d^4 w}{dx^4} + \frac{P_{cr} R}{2} \frac{d^2 w}{dx^2} + \frac{Et}{R^2} w = P_{cr} \left(1 - \frac{\nu}{2}\right) \tag{2.21}$$

Where:

P_{cr} = critical buckling pressure
R = internal radius
E = Young's modulus
w = radial deflection (positive inwards)
D_0 = flexural rigidity of the shell; $D_0 = Et^3/12(1-\nu^2)$

The 2nd failure mode is lobar buckling - *Figure 2.13 section b-b.* This failure mode happens between adjacent rings, resulting in the appearance of lobes around the circumference of the shell [26]. Naturally, with more stiffeners, L_f decreases, which increases P_{cr}. A simple approximation to calculate the critical buckling pressure is to use *Formula (2.14)* from *Chapter 0,* and substitute the length of the vessel, L, with the inter-frame spacing length, L_f.

The 3rd failure mode is general instability - *Figure 2.13 section c-c.* As stated in *Chapter 2.2.3*, both the structure and rings can fail if the rings are not strong enough. *Formula (2.19)* determines the critical buckling pressure for general instability. Ross [54] plotted a design chart, similar to the one in *Chapter 2.3.1*, to determine the PKD for general instability of a perfect ring-stiffened cylinder - *Figure 2.14*. This considers a different thinness ratio, λ', better suited for stiffened shells [26].

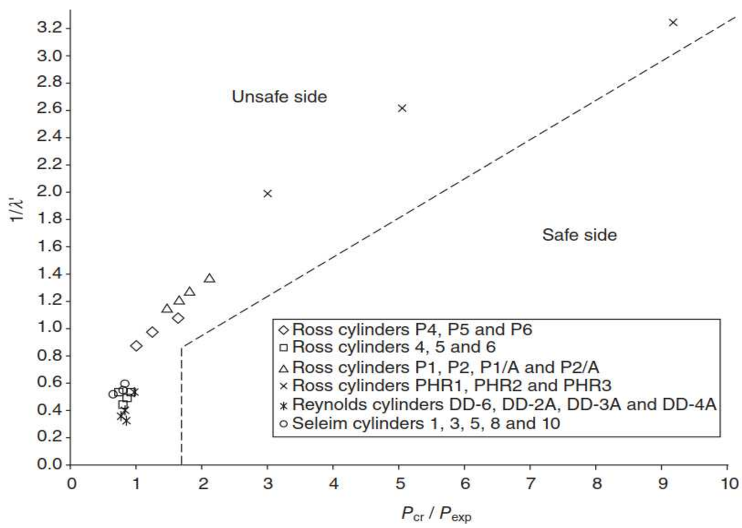

Figure 2.14. Design chart for general instability of ring-stiffened circular cylinders [26].

$$\lambda' = \left[\frac{\left(\frac{L_b}{D_c}\right)^2}{\left(\frac{t'}{D_c}\right)^3}\right]^{\frac{1}{4}} \left(\frac{\sigma_y}{E}\right)^{\frac{1}{2}} \tag{2.22}$$

Where:

L_b = length between adjacent and bulkheads.
D_c = diameter of the centroid of a typical ring-shell combination
t' = equivalent shell thickness
σ_y = material yield strength
E = Young's Modulus

Despite its usefulness, Ross emphasized that more experimental data is required to validate the chart, as well as models with different geometries, especially since only precisely made machine-stiffened models with little out-of-circularity, were used [26].

2.3.3 Alternative design concepts

The objective of the present thesis is to research alternative geometric concepts of pressure vessels that are different from the typical cylindrical shell. So, the bibliographical review also focused on searching for unconventional vessel configurations. These not as tested or validated like the shells discussed previously and are mostly found in proof-of-concept theoretical papers, still with few practical applications. Some of these concepts are displayed in *Figure 2.15.*

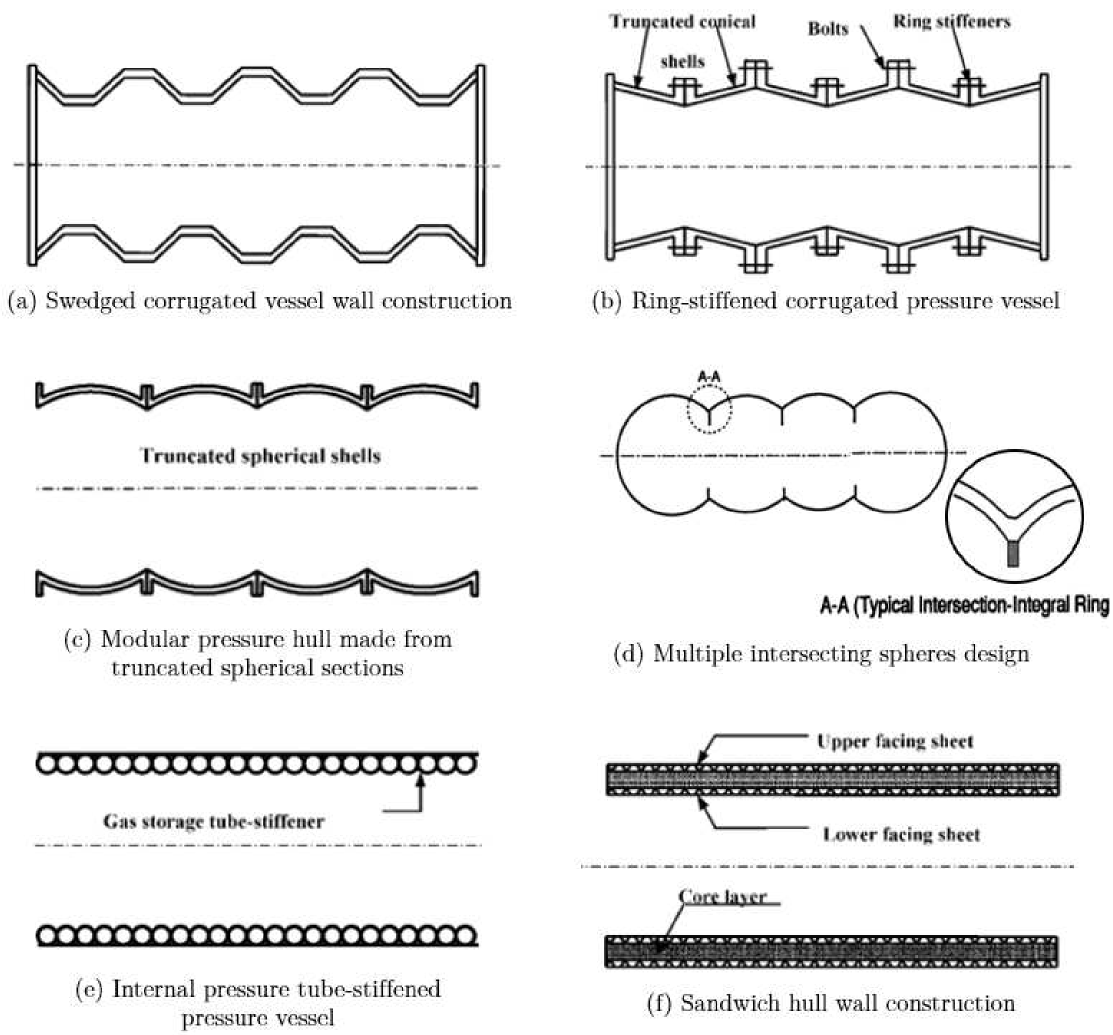

Figure 2.15. Various wall structures utilized for pressure hulls. (a), (b) adapted from [26]; (c), (e), (f) adapted from [68]; (d) adapted from [24].

In 1987, Ross [58] presented an alternative to the ring-stiffened cylinder, where the stiffeners are replaced by a 'swedged' configuration - *Figure 2.15 (a).* These vessels can be seen as repetitive pattern of 3 regions along the axial direction: a "plateau", where the shell thickness is at its largest; a "valley", where is at its smallest; and a "slope" transition zone, where thickness increases linearly (*note:* this nomenclature was adopted in the present thesis for easiness of exposition). Ross reports this geometry helps to distribute stress across the shell while contradicting the buckling deformed mode shape, which in turn increases the buckling pressure.

The manufacture of a swedged vessel can be adapted if constructed from truncated ring-stiffened conical shells - *Figure 2.15 (b)*, and since the conical shells modules can be machined, manufacture of smaller modules may help to reduce the initial out-of-circularity seen in cylindrical models [26]. Smith et al. [69] proposed a similar method of construction but for composite structures: glass, carbon fibres or metal matrix composites.

Another structure proposed by Ross [26] suggests to replace ring stiffeners with circumferential tubes, which are submitted to an internal pressure - *Figure 2.15 (e).* In this configuration, the vessel is in a state of initial tension caused by the tubes internal pressure, so buckling resistance can be even higher. Ross also suggests that this pressure could be controlled and increase linearly with depth, making the vessel responsive to external pressure conditions. However, this is purely a hypothetical solution with no empirical or numerical experimentation [26].

A fairly studied configuration is the multiple intersecting spheres design solution. This shape has the structural advantages of a single sphere, and the improved useful volume of a cylinder. There are two approaches to their design. The first is seen in *Figure 2.15 (c)*, where the vessel is put together via modular spherical sections, similar to the solution Ross presented with his truncated ring-stiffened conical shells [70]. Another concept involves a set of spheres which are reinforced with rings at their intersections, as seen in *Figure 2.15 (d).* These reinforcing rings can be made of a material that is stronger than the main body material, further increasing structural stability [24].

Another fairly studied configuration is the sandwich hull design - *Figure 2.15 (f).* A sandwich structure usually consists of a compliant core material between two strong and stiff layers. They are used to increase bulk and flexural strength without adding significant weight, meaning pressure vessels made of this material can be stronger and lighter than their metallic counterparts. The cores can be of metal foams, composite foams or honeycomb structures [43] [71].

Other studies with alternative geometries were found. Jasion et al. [72] studied the influence in buckling resistance of a family of barrelled shells of revolution of constant mass but with different meridional radius of curvature - *Figure 2.16.* As the parametric models take a more barrelled shape, the buckling resistance is expected to increase. These results were confirmed via a numerical analysis for a family of 6 barrelled shapes under load, as displayed in *Figure 2.16.*

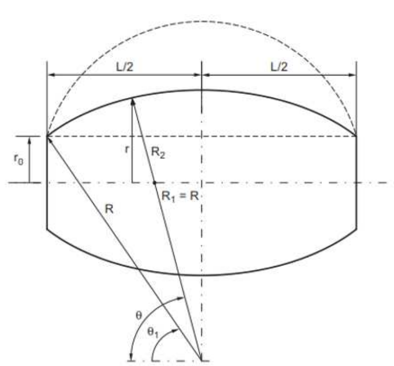

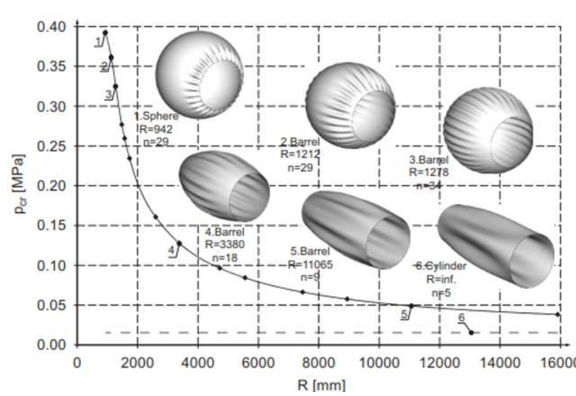

Figure 2.16. Geometry of a barrelled shell, with R as the meridional radius of curvature on the left; Influence of R on the critical buckling load on the right. Adapted from [72].

Siqueira et al. [73] proposed an innovative concept by using sliding stiffeners that are part of an inner, movable structure placed inside the vessel where the payload is accommodated - *Figure 2.17*. These stiffeners are not welded, so no residual stress will contribute to a decrease of buckling strength, and the fabrication of the vessel is simplified. Moreover, it was reported that the buckling resistance increased when compared to an equivalent ring-stiffened shell.

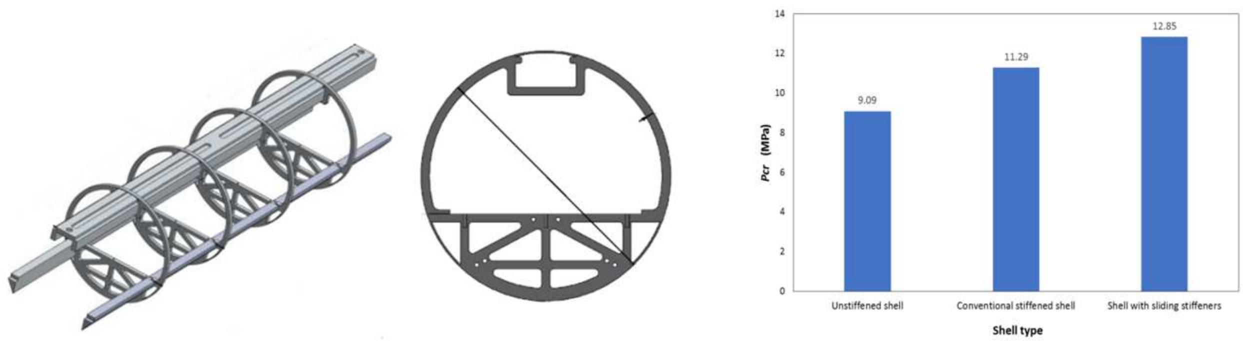

Figure 2.17. Sliding stiffeners solution: schematic view of the structure on the left; FEM-derived critical pressures comparison on the right. Adapted from [73].

Tsouvalis et al. [74] analysed the effect of geometric imperfections purposefully designed to increase the buckling strength of laminated composite shells. This study considered the influence of two types of imperfections: Type 1 imperfections had a constant thickness, but changed the ovality of the cross-section, while Type 2 imperfections had a sinusoidal cross-section thickness variation. These imperfections were small compared to shell thickness, but when introduced in a precise way, buckling strength increased without affecting the vessel weight. This study concludes that these imperfections can affect the deformation mode shape the shell will follow, which increases strength.

2.3.4 Material selection

Proper material selection plays a key part in the structural integrity. Given the trade-off between wall thickness and weight increase, materials with high strength-to-density ratios are usually the more valid choice [26]. However, it is the mission parameters, especially the nominal depth, that largely define what material should be selected. In short, pressure vessel materials must have the following characteristics to be suitable for all operation conditions [26]:

- **i.** Resistance to corrosion;
- **ii.** High strength-to-density ratio;
- **iii.** Cost of material;
- **iv.** Pressure hull design;
- **v.** Fabrication properties: ensure manufacture is compatible material and design;
- **vi.** Susceptibility to temperature and fire protection.
- **vii.** Operating life span of material.

The level of importance of these requirements will depend on the mission parameters but some are always mandatory [20], like corrosion resistance for saltwater conditions. The corrosion rate of oxidizing metals in the marine environment is mostly governed by the oxygen content of the seawater through the outer layers of rust and marine organisms, and depends on the seawater conditions [24]. Corrosion can lead to a form of localized failure known as stress corrosion cracking, which effects drastically worsen when the material is also under the combined stress. This can be triggered by variables such as alloy composition, stress, corrosive environment, temperature and deploy time.

There are several options for material selection. Mild steel is cheap and easy to weld, and an overall good choice if the pressure vessel is not required to dive to great depths. For marine applications, there are some classes of stainless steel typically used - *Table 2.4*. High tensile steels are an option for greater depths, but their strength-to-density ratio may be a problem - *Table 2.5*. Aluminium alloys are a good alternative, since they have a better strength-to-density ratio and are easy to manufacture, but for greater depths, they become too weak to be employed -*Table 2.6*. The most common choice for deep dives is titanium, which mechanical properties are superior to high tensile steels while having a far lower density - *Table 2.7*.

Table 2.4. Mechanical properties for stainless steels [26]

Material	Density [g/cm³]	Young's M. [GPa]	Yield strength [MPa]	Tensile strength [MPa]	σ/ρ ratio
304 (A2)	8.0	193	215	505	26.9
316L	8.0	193	235	560	31.3
316 (A4)	8.0	193	250	565	29.4

Table 2.5. Mechanical properties for high tensile steels [26]

Material	Density [g/cm³]	Young's M [GPa]	Yield strength [MPa]	Tensile strength [MPa]	σ/ρ ratio
HY80	7.8	207	550	-	70.5
HY100	7.8	207	690	-	88.5
HY130	7.8	207	890	-	114.1
HY180	7.8	207	1240	-	159.0

Table 2.6. Mechanical properties for aluminium alloys [26]

Material	Density [g/cm³]	Young's M. [GPa]	Yield strength [MPa]	Tensile strength [MPa]	σ/ρ ratio
5086-H116	2.8	70	207	290	77.8
5456	2.8	70	230	320	86.5
6061-T6	2.8	70	276	310	102.2
7075-T6	2.8	70	503	572	176.2

Table 2.7. Mechanical properties for titanium alloys [26]

Material	Density [g/cm³]	Young's M. [GPa]	Yield strength [MPa]	Tensile strength [MPa]	σ/ρ ratio
Ti 6-4	4.5	113	880	950	198.6
Ti 6-2-1-1	4.5	113	724	869	163.4
Ti 6-4 STOA	4.5	113	830	870	187.4
C.P. Grade 2	4.5	113	276	345	62.3

Besides metallic alloys, polymeric materials like PVC and cast acrylic are commonly used for shallow depths where the pressure is low. Composites like GRP find applications for more demanding conditions since they have a high strength-to-density ratio, and metal matrix composites may be suited for vessels operating in the deep sea, but their cost is high, and manufacture is difficult, so further development is still required [26] - *Table 2.8.* Ceramics were also used successfully in high demanding missions. They are known to be brittle, but their high compressive strength is suited for structures under external pressure that need to be light. However, production is difficult due to tensile stresses which tend to multiply when there are penetrations or geometric imperfections on the ceramic hull, which can dangerously decrease buckling strength [58].

Table 2.8. Mechanical properties for polymers and high strength composites [26]

Material	Specific density [g/cm³]	Young's modulus [GPa]	Yield Strength [MPa]	Fibre volume fraction
GRP epoxy/S-glass filament wound	2.1	50	1000	0.67
CFRP epoxy/HS UD	1.7	210	1200	0.67
MMC 6061 Al/SiC fibre	2.7	140	3000	0.5
MMC 6061 Al/alumina fibre	3.1	190	3100	0.5

2.4 Structural Numerical Analysis

A key part of product development is to test the concept under operating conditions. There are three ways to conduct this approach: Experimental analysis, where functional prototypes are subject to full or scalable load conditions; Numerical methods, where approximation algorithms are used to create numerical solutions for complex multivariable problems; and analytical methods, the classical approach that uses symbolic manipulation to obtain exact solutions to a given problem. All methods play a part in product development of complex concepts. Usually, analytical analyses are used as a first approach to the problem. Then, numerical analyses simulate the behaviour of an equivalent structure under multiple work conditions, and finally, experimental analysis validates these interpolations with real-life behaviour of a mechanism or structure. In this research, only numerical and analytic methods are employed.

2.4.1 The Finite Element Method

One of the most significant step forwards in engineering problem solving was the development of numerical methods in the mid-20th century. The growth in computing power increased both the speed and accuracy of computed mathematical models far too complex to be solved by analytical methods. Complexity could now be reduced to mathematical models defined by the governing equations, assumptions, and constraints. For a structural analysis and validation, the most widely used method is the Finite Element Method, FEM, in which a structure is divided into a finite set of elements of different size and shape that adapts to the boundary surfaces and internal configurations of the structure it is based upon. These elements are defined by their geometric vertices, or nodes, capable of moving in any direction, as long as the boundary conditions defined by the model are respected. At its core, the FEM considers the nodal equilibrium equation as the relation of an applied force, F, with the nodal displacement, u, via the stiffness matrix, K [75]:

$$K\,u = F \tag{2.23}$$

This equilibrium equation is at the core of the finite element method and can be adapted for different types of Finite Element Analysis - FEA. By defining a complex structure with a finite set of elements, the application of this equation to all elements allows to determine a solution for virtually any geometry. This is an approximation, and its accuracy will depend on the considered simplifications such as the analysis parameters, element size and shape, and boundary conditions. Given the resourcefulness of FEM, the CAE-driven design process is standard in most engineering industries - *Figure 2.18*. Simulation is now a tool that simultaneously saves time and reduces costs.

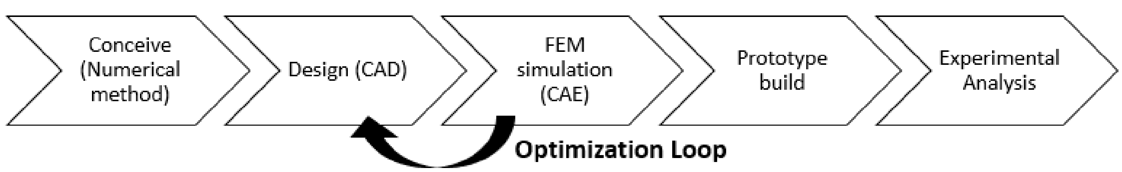

Figure 2.18. The CAE-Driven design process. Adapted from [75].

Computer-Aided Engineering – CAE is the set technologies that use computing powered analysis to conduct accurate simulations of mechanisms, structures, or phenomena, and different analysis types are available for a wide spectrum of engineering applications. The first step in FEA is to create a model that defines the governing properties of the structure with a number of discrete sets, converting a continuous system with infinite degrees of freedom in an approximate system defined by a finite set of elements. This creates a mathematical model equivalent to the real problem that describes the essential governing rules for the analysis by simplifying or eliminating everything else.

Meshing a model requires to decide which element type is going to be used - *Figure 2.19*, and it will mostly depend on the geometry in hands. 1D elements represent a geometry with one dimension much larger than the other two: tubes, shafts, pipes, beams, lattice structures, etc. 2D elements are used when the geometry has two dimensions larger than the third: thin shells, plaques etc. This group includes tria (three nodes) and quad (four nodes) elements [75]. 3D elements are used for geometries more complex, that cannot be defined by the above methods. The elements can be tetrahedral, hexahedral or pentahedral. Hexas are usually used for larger geometries, and due to their geometry are easier to control, resulting in a more organized mesh [75]. Tetras are more suited for smaller geometries, and are used to automate the meshing process, which saves work time. Increasing the level of discretization results in a more accurate analysis, but it also increases the computing power needed, so both the size and type of element must be chosen considering the resulting processing time for the software to converge towards a solution [75]. A common practice is to perform a mesh convergence study, where similar models are meshed with consecutive smaller elements to determine at which discretization level a convergence of results is verified. This finds the perfect trade-off between efficiency and reliability for all future analysis.

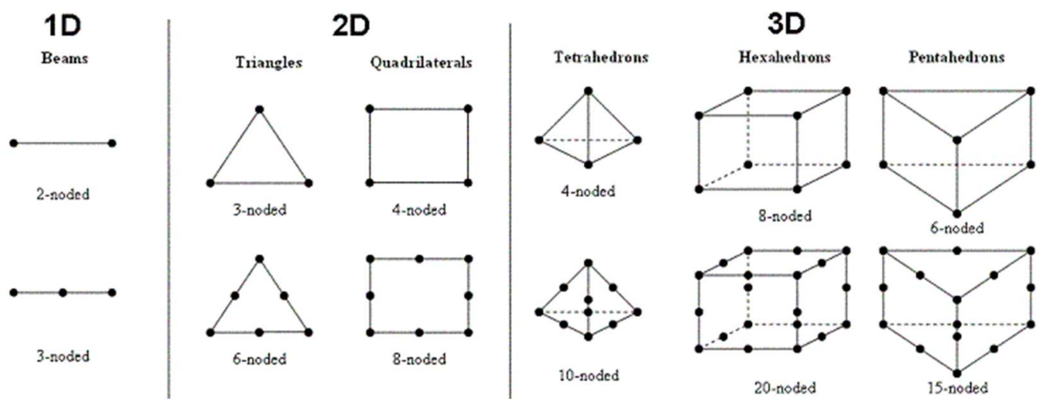

Figure 2.19. Simplified representation of the possible element geometries [76].

2.4.2 Pressure vessel finite element analysis

There are 4 analysis types used in pressure vessel simulation:

- **Linear static analysis:** Solves to determine the stress associated with small displacement deformations of a structure in the elastic region. Considering the stress response of a structure, after the displacements at the nodal points of all of the elements are determined, the stresses, ε, can be inferred by using the constitutive relations for the material - Hooke's law. *Formula (2.24)* relates the strains and displacements linearly for a given elasticity matrix of the material, C [75]:

$$\sigma = C\ \varepsilon \tag{2.24}$$

After crossing the yield point, the material would follow a nonlinear path, but linear solvers will continue to follow a straight line. This analysis is valid for simplified shells under hydrostatic load, where contact-related nonlinearities are not present.

• **Nonlinear quasi-static analysis:** NLQS analysis uses small deformation theory, quite similar to the linear static analysis. However, it accounts for certain sources of nonlinearities, like contact interfaces, gap elements and material nonlinearities, making this analysis suited to test detailed models with different components in contact. Since the displacements are small, this analysis also considers the elements in the contact region will not change direction or orientation due to their components' deformation throughout the simulation.

• **Linear buckling analysis:** Also called eigenvalue buckling analysis, it is used to find the theoretical buckling strength of a perfect elastic structure by determining the critical load of bifurcation buckling through the eigenvalue problem-solving method [72]. A linear buckling analysis starts by solving a linear static analysis under a reference level of loading, P_{ref}. This will determine the stresses which are needed to form the geometric stiffness matrix K_G. Then, the buckling loads can be solved as an eigenvalue problem, described in *Equation (2.25)*.

$$[K - \lambda K_G]x = 0 \tag{2.25}$$

K is the stiffness matrix of the structure and λ is the multiplier to the reference loading, P_{ref}. As a solution, this equation determines n eigenvalues λ, where n is the number of degrees of freedom, and x as the eigenvector corresponding to the eigenvalue. This eigenvalue problem is solved for a small number of the lowest eigenvalues, and the lowest eigenvalue, λ_{cr}, is associated with the buckling failure mode. So, multiplying the lowest eigenvalue by the static analysis reference load:

$$P_{cr} = \lambda_{cr}\, P_{ref} \tag{2.26}$$

However, linear buckling solution does not consider imperfections or nonlinearities that greatly reduce the buckling resistance of a structure. So, after determining the buckling critical pressure of a perfect shell, reduction factors need to be employed to determine the real critical load – PKD.

• **Nonlinear buckling analysis:** This is a more accurate approach to predict buckling but is also more CPU-demanding. It finds the first limit point, i.e. the maximum load before it becomes unstable, which is achieved by gradually increasing the load to determine when instability spreads. Initial imperfections such as plastic behaviour, contacts, gaps or large displacement of post-buckled modes are accounted for. The possible nonlinearities are described below. For vessels, nonlinearities are usually geometrical, but material nonlinearities are also considered if the shell is thick [73].

i. **Geometric nonlinearity:** The stiffness matrix is considered as a function of displacement and is re-calculated after a certain predefined displacement, and typically used to analyse large displacement plastic deformations
ii. **Material nonlinearity:** related to the inelastic stress-displacement material behaviour past the elastic limit, where this curve is no longer linear.
iii. **Contact nonlinearity:** In contact analysis, the stiffness matrix also changes as a function of displacement, since it will depend on the interactions of the contact surfaces.

3. Design Methodology

Throughout this chapter, the design methodology followed in pressure vessel development is presented. Firstly, the case study proposed for the development of the present thesis is defined. Then, a market analysis used to identify competitive product designs and geometries is presented. From these market trends, the customer needs were set, and together with a selected competitive benchmarking study, the product specifications of a market standard vessel were defined. Finally, all the different concepts were discretized and compared via a morphological matrix, and the most appropriate were selected within the scope of the present thesis.

3.1 Definition of the case study

The case study proposed as the outline of this thesis was to study the shape and geometry of pressure vessels to optimize the internal useful volume. This is defined as the volume which can practically be used to store the mission payload or auxiliary equipment, typically batteries, sensors, board computers or other equipment. Currently, most pressure vessels are cylindrical, where a considerable amount of its internal useful volume is wasted, since the components that fit inside are of cuboid or parallelepipedal shapes, which are not compatible with a curved shell. Hence, the goal is to study alternative geometric configurations that either increase the internal useful volume or result in a structure that is more stable for the failure modes in play in like structures - **Table 3.1**.

So, the goal is to investigate the possible existence of trade-offs across different design solutions, with little restraints of production costs. The only defined constraint was the nominal depth, set to 1 500 m. In order to compare these concepts to the ones seen in the market, a pressure vessel following the market trends must also be defined. It was also the goal that research and design should be done without direct access to the methodologies currently being used in CEiiA, since part of the interest in this thesis outline would be to perform and independent research.

Table 3.1. Proposed case study outline characterization

Nominal Depth	Case study	Optimization main goal	Optimization 2nd goal
1 500 m	To study alternative vessel configurations for the main body	Internal useful volume	Structural integrity

3.2 Market research & analysis

The ultimate objective of any product is its ultimate role in the marketplace, ideally as a strong competitor to all other options. In any phase of design should a product be developed independently of the current state of art, and a strong grasp of the consumer and manufacturer reality are strong assets throughout the entire design process [77]. So, a market analysis was the first step to better grasp the product to be developed.

The main goals of this research were to:

i. Understand the current trends in pressure vessel design
ii. Study how depth influences the dimensions and material choice for a cylindrical vessel
iii. Define all the different design choices in pressure vessel design.

On a first step, the goal was simply to understand the manufacturers' design choices and check for similar solutions already being developed. It was decided to not include custom-built vessels, like the one developed for the Nereus submersible [28], since as a project-specific product, they may not reflect overall market trends. Most of the information was obtained in publicly available catalogues, but some manufacturers were directly contacted for further information. Part of this analysis was organized by the manufacturing company, and can be consulted in full on *Appendix A*.

Some useful insights and trends of the pressure vessel market were observed:

- All of the vessels' shape was cylindrical;
- Pressure vessel material and configuration change with the increase of depth, and manufacturers work with similar materials for a given nominal depth;
- Overall, the diameter-to-length ratio tended to drop with the increase of depth
- Most of the models did not employ the use of stiffeners.
- Some manufacturers have standardized dimensions for pressure vessels, while others work on specific projects according to client specifications;
- Most of the manufacturers with standardized models have different sizes for the same depth, allowing for some adaptation;
- Standardized vessels have a shallower operating depth, while manufacturers of personalized vessels usually state that the developed vessel can reach higher depths;
- Several cap attachments are available and can be customized for a given vessel to achieve the necessary mission requirements;
- Most of the manufacturers did not give information on the shell thickness
- Prices vary widely, from ~100€ to ~16 000€, but overall, they increase with the operating depth

This proved to be an efficient way to get some market insight. From the analysis, it was clear that for a given depth, vessels from competing manufacturers were similar, so to facilitate the better label these trends, vessels were divided according to the respective operating depth in four groups: 100 – 450 m; 700 – 2 000 m; 3 000 – 4 000 m; > 6 000 m.

3.2.1 Group 1: 100 – 450 meters depth

This group is made of mostly composite vessels, which are adequate for the considered depth, and are cheaper and easier to produce - *Table 3.2*. The price varies widely since each manufacturer considers different ranges of dimensions. *PREVCO* [78] models have 3 classes defined by the internal diameter, and each has 3 length options. The depth ranges between 70 – 100 m. *BLUE ROBOTICS* [79] has 3 vessels classes, also defined by the internal diameter. The depth ranges between 100 and 450 m. *2' Series* vessels present a decrease of maximum depth with the increase of length, while *3' Series* and *4' Series* maintain these dimensions constant. The material can either be cast acrylic or aluminium alloy, which considerably changes the nominal depth. *OMNI INSTRUMENTS* [30], like the other two, has 2 classes of vessels defined by the internal diameter, while the length can vary between 100 and 700 mm. All models have a flat cap, but *BLUE ROBOTICS* also has glass dome caps as an option. All solutions use an axially tapped bolted solution to attach the cap to the main body - *Figure 3.1*.

Table 3.2. Properties chart of pressure vessels from Group 1

Group 1: 100 - 450 m

Company	Model	D int [mm]	Length [mm]	D/L ratio	Depth [m]	Cap/closure configuration	Vessel Material	Price [€]
PREVCO [78]	P5	133	305	0.44	100	Flat / Axially tapped bolted	PVC	1 535
			457	0.29	100			1 553
			610	0.22	100			1 583
	P7	187	305	0.61	100	Flat / Axially tapped bolted	PVC	1 683
			457	0.41	90			1 710
			610	0.31	70			1830
	P9	235	305	0.77	100	Flat / Axially tapped bolted	PVC	2 282
			457	0.51	100			2 339
			610	0.39	70			2607
BLUE ROBOTICS [79]	2' Series	50	100	0.50	450	Flat or dome/ Axially tapped bolted	Cast acrylic	82
			150	0.33	250			86
			300	0.17	150			91
	3' Series	76	222	0.34	150	Flat or dome/ Axially bolted	Cast acrylic	32
					400		Al 6061-T6	110
	4' Series	101	298	0.34	100	Flat or dome/ Axially bolted	Cast acrylic	60
					400		Al 6061-T6	166
OMNI INSTRU-MENTS [30]	Al 300 #1	100	100	1.00	300	Flat / Stress rod OR axially tapped bolted	6000 series	860
			200	0.50				920
			300	0.33				980
			500	0.20				1130
			700	0.14				1180
	Al 300 #2	160	100	1.60	300	Flat / Stress rod OR axially tapped bolted	6000 series	1200
			200	0.80				1260
			300	0.53				1320
			500	0.32				1470
			700	0.23				1520

Figure 3.1. Examples of vessels from Group 1: PREVCO P5 model on the left [78]; BLUE ROBOTICS *2' Series* model on the middle [79]; OMNI INSTRUMENTS Al 300 #2 model on the right [30].

For each vessel, the diameter-to-length ratio, D/L, was calculated. By conducting the standard aggregation functions to this range of data, it is possible to select the overall dimensions that would better fit the typical pressure vessel for this depth - *Table 3.3*. It must be referred that these values can be misleading but can also help correlate geometric influences if used carefully.

Table 3.3. Vessel dimensions' aggregation functions - Group 1

	Max	**Min**	**Median**	**Average**
Int. Diameter	235	50	117	130
Length	700	100	300	339
D/L ratio	1.60	0.14	0.34	0.47

3.2.2 Group 2: 700 – 2 000 meters depth

Group 2 of pressure vessels was set for depths between 700 – 1100 m. This depth is characteristic for missions on the upper half of the continental slope, where the pressure starts to demand stronger materials, but still not as demanding as the lower half of the continental slope - *Table 3.4*. Aluminium alloys are widely used. *PREVCO* [78] models come in 3 classes for this depth and are organized by the characteristic internal diameter. Depth ranges from 700 m to 1 100 m, and an aluminium alloy Al6061-T6 is used. *BLUE ROBOTICS* [79] *2' Series* also appear in this group, but instead of acrylic they use a 6000 series aluminium. Models vary only in length, and the price is considerably cheaper than the remaining of the manufacturers, and the equipment is smaller. *DEVELOGIC* [80] models are quite small, and one of the few examples found using composite materials. Their vessels have the same internal diameter, with two lengths available, and both are built to resist up to 750 meters. Finally, *IMPACT SUBSEA* [81] vessel stands as an example of the typical dimensions they develop, since this manufacturer's focus is customized by demand vessels. This is also the vessel highest depth vessel, up to 2 000 m, and uses an aluminium alloy 7075-T6, an aluminium alloy commonly used for more demanding structural applications. All models use a flat cap configuration, and most use a bolted connection, either through-bolted, or axially/radially tapped bolted, but *DEVELOGIC* uses a threaded cap solution - *Figure 3.2*. The same aggregation functions previously presented were applied to this group as well - *Table 3.5*.

Table 3.4. Properties chart of pressure vessels from Group 2

Group 2: 700 – 2 000 m								
Company	**Model**	**D int [mm]**	**Length [mm]**	**D/L ratio**	**Depth [m]**	**Cap/closure configuration**	**Vessel Material**	**Price [€]**
PREVCO [78]	A1010	133	609	0.40	1000	Flat / Through bolted	Al 6061-T6	6538
	A1207	299	457 609	0.65 0.49	700 700	Flat / Through bolted	Al 6061-T6	7590 9188
	A811	198	305 457 609	0.49 0.32 0.24	1100 1100 1100	Flat / Through bolted	Al 6061-T6	3805 4037 5264
BLUE ROBOTICS [79]	2' Series	50	100 150 300	0.50 0.33 0.17	950 950 950	Flat or dome/ Axially tapped bolted	Al 6000 series	100 106 121
DEVELOGIC [80]	SW standard	87	230	0.38	750	Flat or dome/ Threaded cap	Fibre-reinforced POM	-
	SW extended		500	0.17				-
IMPACT SUBSEA [81]	ISP2	150	385	0.39	2000	Flat / Radially tapped bolted	Al 7075-T6	-

Figure 3.2. Examples of vessels from Group 2 of manufacturers: *PREVCO* A811 on the left [78]; *DEVELOGIC* SW standard on the middle [80]; *IMPACT SUBSEA* ISP2 on the right [81].

Table 3.5. Vessel dimensions' aggregation functions - Group 2

	Max	**Min**	**Median**	**Average**
Int. Diameter	299	50	174	172
Length	609	100	421	393
D/L ratio	0.65	0.17	0.38	0.38

3.2.3 Group 3: 3 000 – 4 000 meters depth

Group 3 was set for depths between 3 000 and 4 000 meters, characteristic for the lower half of the continental slope. These vessels are fabricated mostly in titanium or steel alloys. *SUBSEA RANGER* [82] models are built to go up to 3 000 m, and the D/L ratio is approximately constant for all models. *OMNI INSTRUMENTS* [30] vessels come in 2 classes according to nominal depth and equal vessel dimensions. IMPACT SUBSEA [81] is the only using an aluminium alloy, but its dimensions are considerably smaller. Most vessels, expect ISP1, use axial bolted connections.

Table 3.6. Properties chart of pressure vessels from Group 3

Group 3: 3 000 – 4 000 m								
Company	**Model**	**D int [mm]**	**Length [mm]**	**D/L ratio**	**Depth [m]**	**Cap/closure configuration**	**Vessel Material**	**Price [€]**
SUBSEA RANGER [82]	PH-Ti 3000	100	500	0.20	3 000	Flat / Through bolted	Ti-6AL-4V	6251
		120	600	0.20	3 000			8271
		140	800	0.18	3 000			9988
		160	800	0.20	3 000			11485
		180	1000	0.18	3 000			12634
		200	1000	0.20	3 000			15255
OMNI INSTRU-MENTS [30]	Subsea Al 3000	75	225	0.33	3 000	Flat / Axially tapped bolted	316L Stainless steel	883
		85	120	0.71	3 000			883
		200	350	0.57	3 000			4220
	Subsea Al 4000	75	225	0.33	4 000	Flat / Axially tapped bolted	316L Stainless steel	1128
		85	120	0.71	4 000			1128
		200	350	0.57	4 000			4466
IMPACT SUBSEA [81]	ISP1	65	400	0.16	3 000	Flat / Vessel threaded	Al 7075-T6	-

Figure 3.3. Examples of vessels from Group 3 of manufacturers: *SUBSEA RANGER* PH-Ti-3000 on the left [82]; *OMNI INSTRUMENTS* Al 3000 on the middle [30]; *IMPACT SUBSEA* ISP1 on the right [81].

Table 3.7. Vessel dimensions' aggregation functions - Group 3

	Max	**Min**	**Median**	**Average**
Int. Diameter	200	65	120	130
Length	1000	120	400	499
D/L ratio	0.71	0.16	0.20	0.35

3.2.4 Group 4: > 6 000 meters depth

Group 4 of was set for depths of above 6 000 meters. This depth is reserved for sea trenches. All models used titanium alloys. All *SUBSEA RANGER* [82] vessels have the same maximum threshold of 6 000 m, and approximately the same D/L ratio. *DEVELOGIC* [80] models are identical to the ones described in group 2 but are now titanium-built. K.U.M. UMWELT [83] pressure vessels are custom-built with dimensions within 25 - 335 mm of internal diameter, and 100 - 1000 mm of length. Most vessels use axially bolted connections, except *DEVELOGIC* threaded vessels.

Table 3.8. Properties chart of pressure vessels from Group 4

Group 4: > 6 000 m								
Company	**Model**	**D int [mm]**	**Length [mm]**	**D/L ratio**	**Depth [m]**	**Cap/closure configuration**	**Vessel Material**	**Price [€]**
SUBSEA RANGER [82]	PH-Ti 6000	100	500	0.20	6 000	Flat / Through bolted	Ti-6AL-4V	6564
		120	600	0.20	6 000			8685
		140	800	0.18	6 000			10487
		160	800	0.20	6 000			11011
		180	1000	0.18	6 000			13265
		200	1000	0.20	6 000			16018
	PH-Ti 11 000	60	300	0.20	11 000	Flat / Through bolted	Ti-6AL-4V	4356
		80	400	0.20	11 000			5663
		100	500	0.20	11 000			6893
DEVE-LOGIC	DW standard	87	230	0.38	6 000	Flat / Vessel threaded	Titanium	-
	DW extended		500	0.17	6 000			-
K.U.M. UMWELT [83]	Minimum	25	100	0.25	6 000	Flat / Axially tapped bolted	Ti-6AL-4V	-
	Maximum	335	1000	0.34	6 000			-

Figure 3.4. Examples of vessels from Group 4 of manufacturers: *SUBSEA RANGER* PH-Ti-11000 on the left [82]; *DEVELOGIC* DW Standard on the middle [80]; *K.U.M. UMWELT* model on the right [83].

Table 3.9. Vessel dimensions' aggregation functions - Group 4

	Max	**Min**	**Median**	**Average**
Int. Diameter	335	25	130	145
Length	1000	100	600	639
D/L ratio	0.38	0.17	0.20	0.23

3.2.5 Market analysis conclusions

This analysis came to some relevant conclusions regarding the influence depth has in pressure vessel design. It was also extremely useful to review different concept configurations and how each plays with one another, which will be further explored in future chapters. The main conclusions regarding the proposed analysis objectives are as follows:

- Almost all manufacturers use unstiffened cylindrical shells as the vessel main body. This means that a pressure vessel modelled to follow the design constraints derived from the market will also follow this configuration;

- It confirmed the validity of the current case study, since there is a clear gap in the market, and an alternative concept with valid trade-offs may satisfy customer needs currently not being met;

- Comparing the different groups, one of the main difference that defines each one is the typical material choice, where more resistant materials are used when the depth increases. There are also differences regarding the closure configuration, and generally, vessels with larger diameters use axially bolted connections, either through bolted or axially tapped.

- When analysing vessel dimensioning discretized by manufacturer, a considerable number of them have several vessel sizes available for the same depth, indicating that customers are demanding in terms of vessel dimensions. However, without access to the sales numbers for each pressure vessel it is impossible to estimate customer demand for each offered geometric dimensioning;

- In *Table 3.10*, the aggregate functions of each group are once again presented. The maximum and minimum dimensions are rather constant, but these are mostly marked by a few vessels that are usually group outliers, and the D/L ratio appears to decrease with depth. This shows that a large range of dimensions are available, and pressure vessels of all dimensions can be useful for different mission parameters. Naturally, smaller vessels will only be useful for specific payload, while larger vessels are more in line with the applications described in *Chapter 2.1.2*.

Table 3.10. Aggregation functions of main geometric dimensions

	Group 1			**Group 2**			**Group 3**			**Group 4**		
	D	**L**	**D/L**	**D**	**L**	**D/L**	**D**	**L**	**D/L**	**D**	**L**	**D/L**
Max	235	700	1.60	299	609	0.65	200	1000	0.71	335	1000	0.38
Min	50	100	0.14	50	100	0.17	65	120	0.16	25	100	0.17
Median	117	300	0.34	174	421	0.38	120	400	0.20	130	600	0.20
Average	130	339	0.47	172	393	0.38	130	499	0.35	145	639.1	0.34

It should be noted that aggregation functions are not the most reliable way to study vessel dimensions, especially when these vessels were not discretized by the function they were designed for. This is simply a first approach to vessel dimensioning, which can be useful to correlate geometric influences with the corresponding depth, but it must be analysed with care.

3.3 Product Specifications

Product specifications are an important stage of the concept development process - *Figure 3.5*. These are a set of characteristics specific for a given product, filtered accordingly to known technical limitations [84]. Product specifications are usually adapted throughout the product development, right until the final iterations, and should be quantifiable whenever it is possible. They are defined from a set of customer needs, which are market-defined guidelines that evaluate the customer interest in the final product. These needs are translated into quantifiable design requirements known as metrics, which when put together define the target specifications of the product. Then, similar solutions found in the market are evaluated and compared accordingly to these metrics via a competitive benchmark study, from which the ideal and marginal values for each metric are set. These act as basic guidelines for future product developments, but must be adapted and refined, making trade-offs when necessary, which is why the final specifications are only set after concept generation, where different iterations are compared. The design process is never straight-forward, but from accurate product specifications, it becomes more streamlined [24].

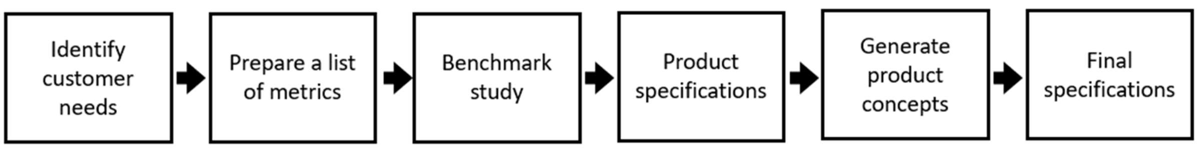

Figure 3.5. Schematic representation of the concept development process [77]

3.3.1 Customer Needs

The customer needs were determined from the analysis in *Chapter 3.2* together with insight from several papers [24] [26] [46] [52] [85] [86] and are displayed in *Table 3.11*. The main purpose of these vessels is to properly secure the payload while under pressure. So, the needs with a higher level of importance are to sustain the structural integrity at nominal depth, while remaining watertight throughout the mission. The second level of importance is related with needs that the user considers critical, such as providing enough internal space and resisting the corrosion effect of salt water, so the equipment can be used on all environments. The third level of importance considers the features that can give an edge advantage when selecting between competitive vessels: the overall cost, and ensuring the vessel is capable of sustaining its own weight. The final two levels are more "nice-to-have" features than "must-have" ones. The fourth level is mostly connected with accessibility, such as the easiness to attach the vessel to the equipment exostructure, easiness to carry or open the pressure vessel, and the possibility of customization of the payload interface by allowing the use of different caps. On the fifth level, the needs were purely aesthetic.

Table 3.11. Customer needs table for pressure vessel design

#	Customer Needs	Importance
1	Sustains the structural integrity for the desired depth	5
2	Remains watertight for the desired depth	5
3	Provides enough internal space for the desired payload	4
4	Is not affected by the corrosive salinity	4
5	Is relatively cheap	3
6	Provides enough buoyancy to sustain its own weight	3
7	Is easily attached to the exostructure	2
8	Is easy to open and to access the inner payload	2
9	Allows for customization of the payload interface	2
10	Is aesthetically appealing	1

3.3.2 Target specifications

Target specifications are defined by a set of engineering metrics, which are measures of quantitative nature that translate the customer needs into precise and quantifiable values [87]. To set target specifications, each customer need is correlated to one or more metric. The needs' order of importance also plays a major role, since they translate into the metrics' order of importance. Firstly, a needs-metrics matrix is created, where the interrelationships between the various customer needs are visually displayed, as well as which needs are connected to each metrics – *Table 3.12*

The first defined metrics relate to geometric dimensioning since these affect multiple needs with high priorities. Vessel weight is connected with the buoyancy and the easiness to use, and material properties are important for both the structural integrity, buoyancy calculations and resistance to seawater corrosion. To ensure watertightness, the main body-cap attachment needs to be considered, so bolt dimensioning metrics were introduced. Finally, the cost of material and manufacture are considered, as well as the surface configuration, related with aesthetics and easiness of attachment.

Some customer needs are not fully defined by these metrics, such as the easiness to use or the aesthetic appeal. To convert these needs in well-defined metrics, marketing studies that reflect a target group's opinion that represent the general market are needed. These needs will still be considered by trying to identify how the typical user would perceive the product concept. However, this approach is subjective to the author's perception of the product, and while personal subjectivity was avoided, any conclusions should be interpreted with that in mind.

For easiness of consultation, the data in the needs-metric matrix was re-organized as a table with the metrics in highlight. These are the product's target specifications - *Table 3.13*. These are a first iteration, and throughout the product development, it is expected for them to change to better represent the product in development.

Table 3.12. Needs-metrics matrix for pressure vessel design

Need \ Metric		1 Internal diameter	2 Length	3 Useful volume	4 Shell thickness	5 Cap thickness	6 Stiffener config	7 Vessel weight	8 Material properties	9 Number of bolts	10 Bolt diameter	11 Bolt pretension	12 Material cost	13 Manufacture cost	14 Surface config
1	Structural integrity	x	x		x	x	x		x						
2	Watertightness					x				x	x	x			
3	Internal space	x	x	x											
4	Corrosion resistance								x						
5	Product cost												x	x	
6	Buoyancy			x	x	x	x	x	x						
7	Attachability		x												x
8	Easiness to use							x							
9	Cap customization					x									
10	Aesthetic appeal														x

Table 3.13. Target specifications for pressure vessel design

#	#need	Metric	Importance	Units
1	1,3	Internal diameter	5	mm
2	1,3,7	Length	5	mm
3	3,6	Useful volume	4	mm^3
4	1,6	Shell thickness	5	mm
5	1,2,6,9	Cap thickness	3	mm
6	1,6	Stiffener configuration	3	-
7	6,8	Total weight of the vessel	3	kg
8	1	Material yield strength	5	MPa
8	1,2	Material ultimate strength	5	MPa
8	4	Material corrosion resistance	4	-
8	6	Material density	4	kg/m^3
9	2	Number of bolts	2	unit
10	2	Bolt diameter	2	mm
11	2	Bolt pretension	2	kN.
12	5	Material cost	2	€
13	5	Manufacture cost	2	€
14	7,10	Surface configuration	1	-

3.3.3 Competitive benchmarking

To define the ideal value for each metric, a competitive benchmark study was conducted. Benchmarking is a process where different solutions are objectively measured and compared to come up with a concept which elevates the best features of each individual product. The market study described in *Chapter 3.2* served to compare different manufacturers' configurations and geometries, but as concluded, these dimensions can be largely different, depending on the vessel final application and mission payload. Focusing on the product development interest of CEiiA, the vessel is to be compatible with the submersible equipment previously described in *Chapter 2.1.2*: AUVs, ROVs, Landers and deep-sea crawlers.

To select an adequate pool of products for competitive benchmarking analysis, several papers describing the design of pressure vessels specific for similar equipment were consulted. The goal of this review is to confirm the typical dimensions of a vessel for these specific applications. Madhavan et al. [86] describes the design and analysis of an optimized pressure vessel for general undersea applications in the 200 m depth range; Freitas et al. [85] proposes a design methodology for pressure vessels, using as reference one used in the AUV *Pirajuba*, developed in the Polytechnic School of University of São Paulo; Meschini et al. [52] describes the design methods in the conception of a pressure vessel, based on the one used in AUV *FeelHippo*, designed in the Department of Industrial Engineering of the University of Florence; Singh H. et al. [88] characterize the *SeaBED* AUV, a low-cost vehicle designed for high resolution optical and acoustic sensing designed for up to 2 000 m; Rahim K. et al. [89] presented a conceptual design of a pressure hull to use in an underwater pole inspection system; Harrington J. et al. [90] describes the pressure vessels designed to operate an inexpensive ROV developed in Lake Superior State University - LSSU. In *Table 3.14*, the general dimensions of these vessels is described.

Table 3.14. General dimensions of vessels described in bibliographical review

Concept study	Application	Depth [m]	Diam. [mm]	Length [mm]
Concept pressure vessel [86]	Theoretical study	200	180 (ext)	550 (ext)
Pirajuba AUV [85]	AUV	100	188	1 200 (ext)
FeelHippo AUV [52]	AUV	30	215	272
Seabed AUV [88]	AUV	2 000	300 (ext)	700 (ext)
Concept pressure vessel [89]	Pole inspection system	200	125	245
LSSU ROV [90]	ROV	90	175	355

The internal diameter of these models ranges between 105 - 300 mm with an average of 194 mm, and the length ranges between 245 - 1 100 mm, with an average value of 520 mm. Some of the length dimensions were estimated, since papers only provided the external vessel length. A selection of vessels compatible with these typical dimensions were chosen for competitive benchmarking. Naturally, these vessels must also operate in depths close to the nominal depth of 1 500 m. Two vessels discussed in the previous market analysis were the *PREVCO* A811 and *IMPACT SUBSEA* ISP2 vessels, which are the ones closer to the average dimensions and nominal depth.

The vessel used in Seabed AUV [88] was also selected. It is important to note that none of these solutions are designed specifically for the proposed nominal depth, so any comparisons will need to keep that in mind. All vessels are displayed in *Figure 3.6*. They all have an unstiffened cylindrical shell configuration and are purposefully built for electronics housing.

(a) (b) (c)

Figure 3.6. The 3 pressure vessels used for benchmarking analysis: (a) PREVCO A811 vessel [78]; (b) IMPACT SUBSEA ISP2 vessel [81] ; (d) Seabed AUV, vessel highlighted [88].

A competitive benchmarking chart based on the table of metrics previously defined is displayed in *Table 3.15*. The geometric dimensions of these three models are approximately the same, and even the diameter-length ratio is similar, respectively 0.43, 0.39 and 0.34. Regarding material choice, all vessels use aluminium alloys. Both 6061-T6 and 7075-T6 alloys are commonly used in pressure vessels, but the mechanical properties of the latter are considerably better. It is worth noting that the A811 model has a higher thickness, despite the nominal depth being 900 m shorter than the ISP2 model, which is explained by its larger dimensions and the use of a weaker aluminium alloy.

Vessel configuration is also interesting to compare. The A811 uses a large flange with through-bolted connections. On one side, this acts as a bulkhead, giving radial stability to the vessel when under compression, but a larger cap area means axial pressure will also increase. On the other hand the ISP2 has no flange and the cap diameter is the same as the main body external diameter. Both examples have flat end caps, which was the most common choice in the market research, but *SEABED* vessel uses hemispherical end caps. These allow to significantly save weight on cap thickness, while increasing the internal volume, but this volume is not useful given its shell curvature, and the cap will also occupy more volume inside the submersible.

Watertightness is assured with bolt placement, pretensioning, and O-rings. A811 uses two equally distanced radial O-rings, while the ISP2 pressure vessel uses only one radial O-ring. These models also differ in bolt configuration. PREVCO places ten bolts axially, while IMPACT SUBSEA uses six radially. No information was found for SEABED pressure vessel, but similar solutions utilizing a hemispherical cap were consulted, and these are usually bolted axially to an auxiliary metal flange, which also holds radial O-ring grooves, and is inserted on the vessel opening.

Table 3.15. Competitive benchmarking for the proposed pressure vessel

#	# need	Metric	Imp	Units	1 PREVCO A811	2 ISP2	3 SEABED AUV
1	1,3	Internal diameter	5	mm	198	150	170
2	1,3,7	Internal Length	5	mm	457	385	500
3	3,6	Useful volume	4	cm^3	14 071.4	6803.5	11 349.0
4	1,6	Shell thickness	5	mm	14.75	12	-
5	1,2,6,9	Cap thickness	3	mm	19.5	13	-
6	1,6	Stiffener configuration	3	-	none	none	none
7	6,8	Total weight of the vessel	3	kg	18	16.5	-
8	1	Selected material	5	-	Al 6061-T6	Al 7075-T6	Al 7075-T6
8	1	Mat. yield strength	5	MPa	276	503	503
8	1,2	Mat. ultimate strength	5	MPa	310	572	572
8	4	Mat. corrosion resistance	4	-	yes	yes	yes
8	6	Material density	4	kg m^{-3}	2.8	2.8	2.8
9	2	No. bolts per cap	2	unit	10	6	-
10	2	Bolt diameter	2	mm	M8	M6	-
11	2	Bolt pretension	2	kN	-	-	-
12,13	5	Market Cost	2	€	4 037	3 000	-
14	7,10	Surface configuration	1	-	cylindrical, unstiffened	Cylindrical, unstiffened	Cylindrical, unstiffened

3.3.4 Selected product specifications

Following the competitive benchmarking, the metric values for the product in hand can finally be set. Two types of values are useful at this stage: set values are defined when the product must follow specific dimensions, and marginal values are used when a margin of iteration is required throughout the design process. It was decided to fix the internal dimensions of the vessel, so the internal volume remains constant for all models. This is a needed requirement to make future comparisons possible. The material must also be the same for all concepts, for the same reason of validity in comparison. The product specifications are displayed in *Table 3.16*.

By defining constraints which are, to a certain degree, independent of future design iterations, it is possible to conduct a comparative study to determine if different geometric solutions are valid when comparing to traditional designs. However, these values followed a benchmark study considering only pressure vessels with unstiffened cylindrical shells, so the set and margin values are considerably more relevant when designing a similar configuration. This way, a pressure vessel designed following these product specifications can be considered as a representative vessel of current market trends and dimensions.

Table 3.16. Defined product specifications for the proposed pressure vessel

#	#need	Metric	Imp	Set values	Marginal Values		Units
					Min	Max	
1	1,3	Internal diameter	5	200	-	-	mm
2	1,3,7	Length	5	500	-	-	mm
3	3,6	Useful volume	4	15 707	-	-	cm^3
4	1,6	Shell thickness	5	-	6	14	mm
5	1,2,6,9	Cap thickness	3	-	6	14	mm
6	1,6	Stiffener configuration	3	none	-	-	-
7	6,8	Total weight of the vessel	3	-	≤ total buoyancy		N
8	1	Selected material	5	Al 7075-T6	-	-	MPa
8	1	Material yield strength	5	503	-	-	MPa
8	1	Material ultimate strength	5	572	-	-	MPa
8	4	Material corrosion resistance	4	yes	-	-	-
8	6	Material density	4	2.8	-	-	kg/m^3
9	2	Number of bolts/cap	2	-	8	10	unit
10	2	Bolt diameter	2	-	M6	M8	mm
11	2	Bolt pretension	2	-	5 000	15 000	N
12,13	5	Total cost	2	-	-	4 500	€
14	7,10	Surface configuration	1	cylindrical	-	-	-

The internal diameter was set to 200 mm, approximately the same seen in PREVCO A811 model, and the internal length was set to 500 mm. These gives a D/L ratio of 0.4, which is close to the ISP2 ratio. So, the overall dimensions are reasonably consistent with real pressure vessels. The useful volume is 15 707 cm^3, which is slightly larger than A811 model. As for the material, the aluminium alloy 7075-T6 was preliminarily selected, since it was used for both pressure vessels with higher nominal depth. As previously stated, the material choice of the A811 model most likely influenced the shell thickness, which would be even larger for the considered nominal depth, consequently increasing the weight. Also regarding weight, it was decided to define it as a function of the predicted buoyancy of the vessel, so that the vessel is at least neutrally buoyant. The remaining metrics are dependent on the structural integrity and/or watertightness of the pressure vessel and need to be determined according to the values presently set. These are the shell and cap thickness, the configuration of bolts. Manufacture cost is an estimation based on the price mark of the consulted vessels. These values were critically discussed with the responsible team in CEiiA and validated to continue the development.

3.4 Concept generation

In engineering design, the selection of the possible configurations of a given product is not always a linear procedure, and more often than not, different configurations carry both strengths and weaknesses which may need to be balanced with other design choices. So, and without taking credit from the final design itself, the concept generation process that is followed throughout the development phase is one of the most significant factors affecting the concept quality [87]. This process aims to identify the best possible concepts for a given description of requirements [84]. There are systematic design processes which when utilized improve the chances of finding good design solutions with consistency. In the scope of the present thesis, the conceptual design procedure was considered [84] - *Figure 3.7*.

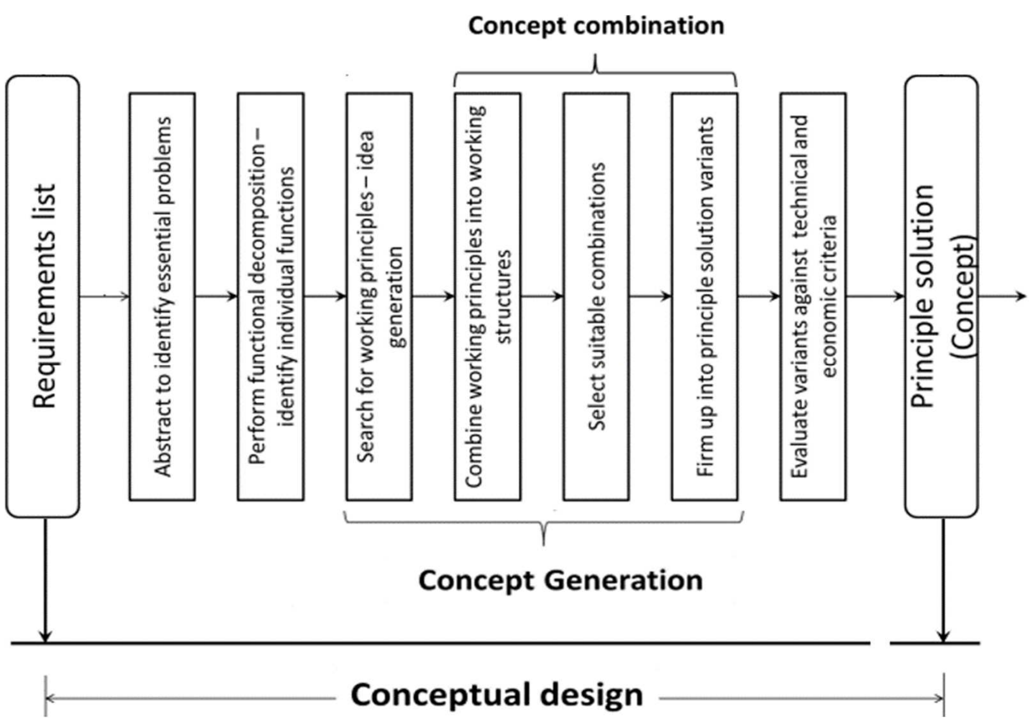

Figure 3.7. Concept generation in the baseline design process. Adapted from [84].

The first step is to determine a list of requirements from an abstracted perspective. This was made in the previous chapter, where the metrics were determined from a customer standpoint, allowing to abstract from the design process and to consider exclusively what users are most concerned with. Then, the functionality is decomposed to identify smaller, individual functions that sub-systems must perform to fulfil the functionality of the system. Then comes the concept generation itself, which can be divided in two distinct phases: the generation of ideas that fulfil specific functional requirements of the system (idea generation), and the combination of means to generate system-level concepts (concept combination). Then it comes down to comparing all different concept solutions to decide which one is better suited for its application [84].

3.4.1 Morphological matrix

There are several tools to facilitate the process of concept generation [91]. One of the most widely used tools is the morphological matrix, which employs the principle of morphological thinking, a systematic full-factorial combination of all possible combinations of fragments that can constitute a system [84]. This way, it is possible to explore the complete set of relationships within a problem, given that it can be decomposed in constituent sub-systems. A morphological matrix is simply a visual tool that, for each design function, associates different solutions that can be employed to fulfil that function.

In *Table 3.17* the morphological matrix is presented. From analysing the market solutions and technical papers, as well as considering theoretical concepts, all the possible design choices were reduced to 9 functions, which were divided into three main groups: material selection (material, raw material source); main body concept (main body shape, structural stiffeners, flange configuration, number of openings, internal pressure); and cap concept (end cap shape, attachment solution, end cap closing, O-ring definition). Some of these solutions are already employed in the market, while others are lacking practical application, and others are solutions most commonly found in other applications of pressure casing systems, like submersible manned hulls. However, all were considered to conduct a thorough concept generation process. On the following chapters, the solutions for each group will be explored, to decide which concepts will be further explored and analysed.

Table 3.17. Morphological matrix for pressure vessel design

Morphological Matrix							
Properties	**1**	**2**	**3**	**4**	**5**	**6**	**7**
Material	Metallic				Composite		Ceramic
	Stainless Steel	Aluminium	Titanium	Copper Beryllium	PVC	Cast acrylic	
Raw material source	Solid round	Extruded tube	Tube w/ welded flanges	Corrugated vessel	Rolled & welded	Injection moulded	Sandwich hull
Main body Shape	Cylinder	Cylinder w/ thickness var	Noncircular cross-section	Sphere	Ellipse	Conical	Jointed spheres
Structural stiffeners	None	Internal Radial stiffeners	External Radial stiffeners	Bulkheads	Axial stiffeners	Sliding Stiffeners	
Flange configuration	Flange vessel	No-flange vessel	Filleted flange vessel				
End cap shape	Solid flat	Holed flat	Solid dome	Holed dome			
End cap closure	Through bolted	Radially tapped bolted	Axially tapped bolted	Threaded vessel tube	Threaded end cap	Stress rod	
Number of openings	Single-ended	Dual-ended					
Sealing configuration	Single face seal	Single radial seal	Single face + radial seal	Dual face seal	Dual radial seal		
Internal pressure	Vacuum	Atmospheric pressure					

3.4.2 Material selection

Previously introduced in *Chapter 2.3.4*, material selection is mainly a function of the nominal depth, and materials with high strength-to-density ratio are usually preferred. It was decided to consider the same material for the caps and the vessel, thus reducing a variable of decision, since the main focus of this thesis is the geometrical configuration of the vessel itself.

• **Material:** Composite materials do not have enough compressive strength to withstand larger nominal depths, and usually operate within the continental shelf to a maximum depth of approximately 300 meters. On the other hand, ceramics are only considered when the extreme compressive strength compensates the cost of manufacture. So, it is safe to assume that for 1 500 m, the vessel will be metallic. While selecting the product specifications it was stated that an aluminium alloy 7075-T6 was preliminarily selected. However, this selection must be validated in future studies by comparing the strength and weight of vessels built with different materials.

• **Raw material source**: This function defines how the pressure vessel is to be manufactured. Injection moulding will not be considered for metallic alloys. Welding is common for manned submersibles, but no example using welded shells was found for pressure vessels. As for the corrugated design, although possible to assemble via a system of fasteners (see *Figure 2.15 -b)*, it results in patterned sections of varying inner radius, which makes part of the internal volume difficult to use, a problem also seen in vessels of spherical or elliptical shapes. So, the selected solutions are the solid round and extruded tube. Extrusion results in different mechanical properties, so after determining the appropriate material, the yield and ultimate strength of the selected alloy must be inferred. Following the preliminarily selected aluminium alloy Al7075-T6, the mechanical properties of this alloy for various configurations of extruded tubes and profiles as defined in the 2016 European Standard EN 755-2 are displayed in *Table 3.18* [92].

Table 3.18. Mechanical properties of Al7075-T6 extruded tubes and profiles [92]

Manufacture process	**Shell thickness [mm]**	**Young's Modulus [GPa]**	**Yield strength [MPa]**	**Tensile strength [MPa]**
Extruded tube	≤ 5	70	485	540
	$5 < t < 10$		505	560
	$10 < t \leq 50$		495	560
Extruded profile	$t \leq 25$	70	460	530
	$25 < t \leq 50$		470	540

3.4.3 Main body concept selection

Defining the main body concepts are of distinct importance given the outline of this thesis: both the main goal to increase the useful volume, and the second goal to increase the structural integrity are mostly dependent on the main body geometry and configuration. So, the design features of this chapter heavily influenced the final concepts.

• **Main body shape:** The unstiffened cylindrical shell was the first concept selected from analysis. This configuration follows the conventional market concept, and so, designing a vessel that emulates their behaviour is an important step to have a standard of comparison with more alternative concepts. These are also fairly studied, with both analytical methods and experimental safety factors previously presented in *Chapter 2.3.1.* So, the Standard Circular Cylinder – SCC vessel was selected - *Figure 3.8 (a).*

Sphere, ellipse, and conic-based shapes are not typically used since, despite better compressive structural behaviour, they have less internal useful volume. The jointed spheres design suffers the same problem of the corrugated vessel: despite increasing the volume, it cannot be used since components do not fit inside the inner configuration of the walls.

In *Chapter 2.3.3,* the paper presented by Tsouvalis et al. [74] defends that small geometric imperfections when purposefully introduced may have a positive effect on the buckling resistance, as long as these are introduced in a way that impedes the development of the predicted mode shape, meaning the buckling pressure may increase with no weight modification. So, the Radial Thickness Variation – RTV vessel was selected as the first alternative concept - *Figure 3.8 (b).*

It was stated that Ross's [93] proposed corrugated vessel is not suited from a useful volume optimization standpoint. However, it is stated that this configuration considerably increases the buckling strength. A similar configuration inspired by this design was thought to result in a similar increase without changing the weight. Quite simply, the external surface can be defined by a repeating sinusoidal pattern, but with a constant internal diameter. This concept, defined as the Axial Thickness Variation – ATV vessel was also selected - *Figure 3.8 (c).*

The final proposed solution is a noncircular cross-section pressure vessel. A geometric limitation of conventional cylindrical shells is the low volume efficiency. A square-shaped cross-section would, for the same internal volume of a conventional cylinder, have a larger useful volume. In fact, for the same set of design constraints, this is the only option to increase the usefulness of the volume without changing its absolute value. However, a squared cross-section would have the largest surface-area-to-volume ratio of all the considered models, and large bending stresses are expected to accumulate in the corner edges. Nonetheless, it is the best option for the main optimization goal, and so the Noncircular Cross Section – NCS vessel is the final selected concept - *Figure 3.8 (d).*

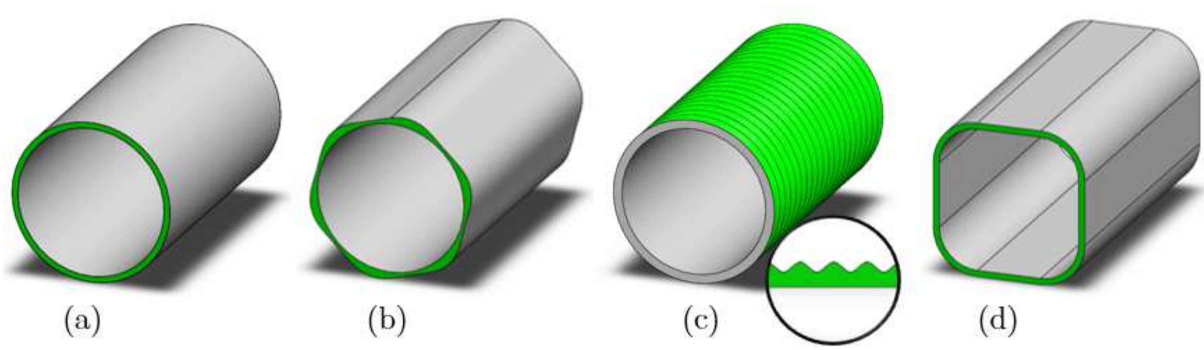

Figure 3.8. Visual examples of main body shape configurations proposed to develop: (a) SCC model; (b) RTV model; (c) ATV model; (d) NCS model.

• **Structural stiffeners:** As stated in *Chapter 2.3.2*, stiffeners may be internal or external, but despite internal ones being more efficient, it comes at the cost of internal volume. Even elegant solutions like the sliding stiffeners seen in *Chapter 2.3.3*, have this problem, since inner components still need to be broke down and dimensioned accordingly to each section. Bulkheads are even worse since it requires the sectioning of a vessel - *Figure 3.9 (a)*. For these reasons, only external stiffeners will be considered. These can be radial ring stiffeners - *Figure 3.9 (b)*, which are used to prevent lobar buckling, or axial stiffeners - *Figure 3.9 (c),* which do not prevent buckling, but may help reduce axisymmetric yield, especially in the case of vessels with large frontal area sections. Axial stiffeners also have a manufacturing advantage, since these stiffeners can be included in the extrusion profile cross-section of aluminium alloys.

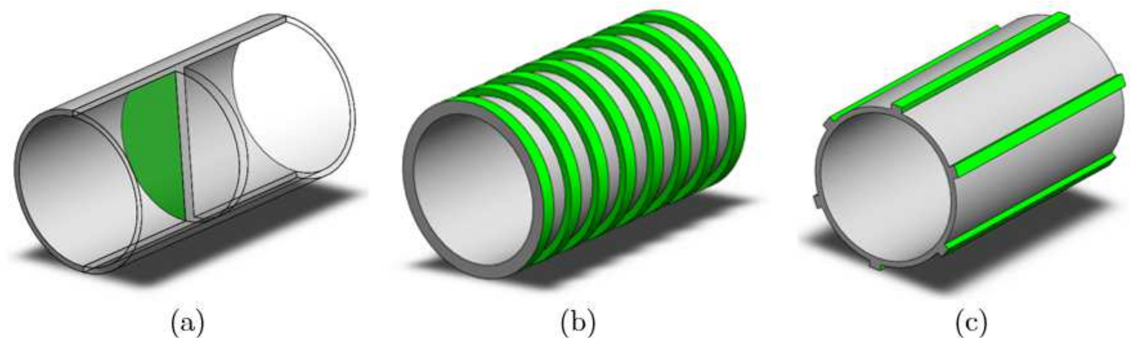

Figure 3.9. Structural stiffener configurations selected for pressure vessel design study: (a) internal bulkhead; (b) external radial stiffener configuration; (c) external axial stiffener configuration.

• **Flange configuration**: A flange - *Figure 3.10 (c)* increases the rigidity of the structure while helping to distribute stresses between the cap and the vessel through a larger area. On the other hand, the larger lateral area increases the axial force, as well as the vessel weight. If a model is built without a flange - *Figure 3.10 (a)*, it can largely increase the cap-vessel stress, and requires the use of either radially tapped bolts or threaded end caps, which are closure solutions away from ideal for the considered depth. Yet another solution found in manufacturers by-demand is the filleted flange vessel - *Figure 3.10 (b)*, which increases the shell thickness at the end of the vessel to allow for an axially tapped bolt closure solution. All solutions have their advantages and disadvantages, so it was decided to properly compare all concepts. However, since the flange model is a more prevalent solution in the market, it is to be integrated as the standard in the SCC vessel.

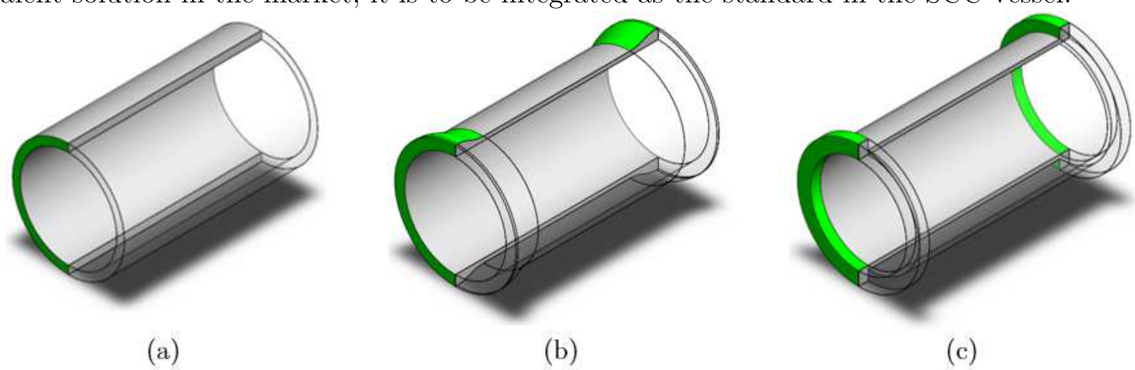

Figure 3.10. Flange configurations selected for pressure vessel design study: (a) No-flange vessel; (b) filleted flange vessel; (c) flange vessel.

• **Number of openings:** a pressure vessel can either be accessible on both sides or only one. Typically, single-ended models are used for small payload applications, while dual-ended models are used when multiple payload applications demand high accessibility. Since this is the case for most of AUV and ROV applications, only dual-ended pressure vessels were considered.

• **Internal pressure:** It can either be left at atmospheric pressure or in a vacuum by pumping out the air. Given the close to freezing temperatures felt at 1 500 m, the presence of air inside results in condensation on the inner walls, which may damage electronics with humidity damage. So, a possible solution is to create a vacuum to the vessel.

3.4.4 Cap concept selection

The end cap concept selection refers to all the design functions that affect the cap design. However, end caps do not have a large influence on the optimization goal, so concepts were simply selected to better reflect the market trends.

• **End cap shape:** This design function defines if the cap is flat - *Figure 3.11 (a)-(b)* or dome-shaped - *Figure 3.11 (c)*. Domes are best from a structural standpoint, since due to the lack of meridional curvature, flat plates have to resist the effects of pressure in flexure [26]. However, domes occupy volume that is not payload compatible. They also greatly reduce the number of connector interfaces that can be placed which is probably why most of the market vessels use flat plates. Since flat end caps are more widely used and compatible with all main body concepts, they were selected.

The solid or holed option refers to the payload accessibility via pressure tolerant connectors. Typically, pressure vessels have at least one cap with connector accessibility, being either power or data cables. The number, size and placement of connector holes are usually up to the consumer to decide, and as stated in the market research, cap customization is a common feature. Since it is not relevant to design connectors, the solid cap was selected for analysis simplification.

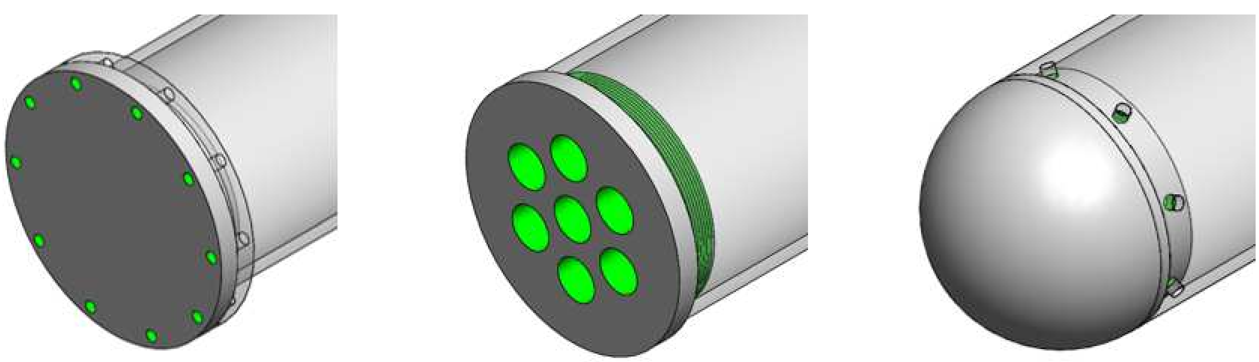

(a) (b) (c)

Figure 3.11. Vessel cap concepts of shape and closure: (a) solid flat plate with through bolted attachment; (b) solid holed plate with threaded tube attachment; (c) solid dome with axially tapped bolted attachment.

• **End cap attachment:** This design function defines how the cap is attached to the main body. The threaded vessel tube - *Figure 3.11 (b),* and threaded end cap are similar, only differing in which of the components act as the male or female thread. These solutions were seen mostly for composite vessels with small diameters, and so both were discarded. The stress rod solution connects the two end caps via a rod, compressing the caps to the vessel flange. This solution can only be used in flange models, and it reduces stresses in the flange. However, a rod is more complicated and expensive than screw bolts, and only one vessel appears to use this solution.

Through bolted, axially tapped and radially tapped solutions use bolts to secure the cap to the vessel. The first uses nuts to tighten the cap to the vessel flange - *Figure 3.11 (a)*, while the latter uses threaded blind holes where bolts that attach the cap are fastened - *Figure 3.11 (c)*. Axial and radial refers to which direction the bolts are attached, and both examples are displayed in the figure above. All these solutions are simple, cheap, and widely used for the considered nominal depth, and so the most adequate solution will be selected to better suit the flange configuration.

• **Sealing configuration:** This design function defines how the vessel will remain its watertightness. O-rings are used for this purpose, and their selection needs to be considered when designing the cap, where inner grooves are machined. Radial seals - *Figure 3.12 (b),* compress both the outside and inside diameter, while face seals - *Figure 3.12 (a)* squeeze both the top and bottom of the sealing system's cross-sections. Both are suited for static applications, but radial seals tend to be preferred for cap and plug applications, except in the case of noncircular cross-sections, where face seals are usually preferred. This design function can consider a single or dual configuration of O-rings, but it is widely preferred to always have two O-rings to create watertightness redundancy, so the failure of the first will not necessarily result in internal payload water damage. When considering a dual seal, another option is having a single radial + single face seal - *Figure 3.12 (c).*

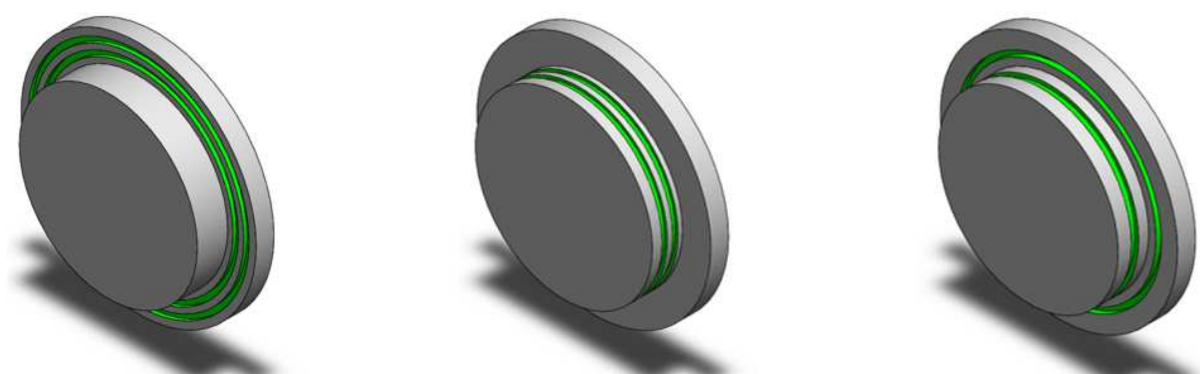

(a) (b) (c)

Figure 3.12. Vessel cap sealing configurations discussed above:
(a) dual face seal; (b) dual radial seal; (c) single face seal + single radial seal.

3.4.5 Concept combination

In previous chapters, the different design functions were introduced, described, and selected. It was decided to consider 4 sets, or "families", of vessels, divided by their main body shape: The SCC, RTV, ATV and NCS families of pressure vessels. To understand the trade-offs these concepts offer, they need to be compared to a market-standard vessel operating in similar conditions. So, the previously defined product specifications are to be considered when designing the SCC family, which is also of unstiffened cylindrical configuration. The NCS family is the only designed to achieve the main optimization goal of increasing the internal useful volume, while the ATV and RTV families are designed for the second optimization goal of increasing the structural integrity, more specifically the buckling strength of these shells.

Combining the different design functions, the product concepts are generated in the following tables. The SCC family will compare de different flange solutions, to which the more adequate end cap closure was considered - *Table 3.19.* ATV and RTV family of vessels are identical in all design functions, expecting the characteristic main body shape - *Table 3.20.* The NCS family is expected to require stiffeners to increase the rigidity of its non-circular profile, so both axial and radial stiffeners are to be analysed - *Table 3.21.* Some of the design functions are common for all vessels: Functions like material, end cap shape, number of openings and internal pressure were previously justified and reduced to a single solution to consider for all models, even though the material selection still must be confirmed in future calculations.

Table 3.19. Design functions of the SCC family of pressure vessels

Main body shape	Structural stiffeners	Flange configuration	End cap closure	Sealing configuration
Circular cylindrical	None	Flange No-flange Filleted flange	Through-bolted Radially tapped Axially tapped	Dual radial

Table 3.20. Design functions of the RTV and ATV families of vessels

Main body shape	Structural stiffeners	Flange configuration	End cap closure	Sealing configuration
Radial thickness var Axial thickness var	None	Flange	Through-bolted	Dual radial

Table 3.21. Design functions of the NCS family of pressure vessels

Main body shape	Structural stiffeners	Flange configuration	End cap closure	Sealing configuration
Noncircular cross-section	Radial stiffeners Axial stiffeners	Flange No-flange	Through-bolted Axially tapped	Face + radial

This page was intentionally left blank

4. Pressure Vessel Design & Analysis

Throughout this chapter, the design solutions discussed in previous ones will be tested via numerical analysis for the mission parameters and compared to one another. Firstly, a Standard Circular Cylindrical vessel - SCC was designed accordingly to the product specifications previously presented, to serve as the market-reference standard. Then, each of the other solutions were studied progressively, starting with the Radial Thickness Variation vessel – RTV, followed by the Axial Thickness Variation vessel – ATV, and finally the Noncircular Cross Section vessel – NCS. Each of these vessels was developed according to a pre-defined methodology that is presented below.

4.1 Analysis methodology

To define the analysis methodology to follow, several papers were consulted. Some regarding the development of pressure vessels for various mission parameters [52] [73] [85] [86] [94], and some regarding the development of pressure vessels concepts with a parametric study approach [49] [72] [74] [93] [95] [96]. It was decided to start with a proper validation of the numerical analysis by comparing results with the analytical prediction. This calculation was only performed for unstiffened cylindrical shells, since it is the only concept in study with reliable analytical formulations. So, the SCC vessel will be used as a reference-market standard for future comparisons, but also to validate the considered analysis methodology. A result deviation threshold of 5% was considered [45]. The procedure schematic for the validation of analysis is described below in *Figure 4.1 (a)*.

After validating the analysis parameters and defining the SCC vessel, the remaining family of vessels were modelled and analysed. Each family was analysed separately, but the methodology of hierarchical design approach is used in all. Since detailed models' analysis is more time consuming both in model definition and analysis processing, it was decided to start by considering a parametric study using simplified shells. These provide good estimations to shell stress and buckling pressure and are considerably faster to model and analyse. A parametric study was considered to compare the influence of small changes in design, similar to what was described by Tsouvalis et al. [74], Jasion et al. [72] and Prabu et al. [49].

So, every detailed model analysis starts by modelling several simplified shells with slightly different geometric dimensions. After a simplified shell analysis, these results are compared with each other and with the unstiffened cylindrical shell. If they show promising results, the best shell geometry is selected, and a detailed vessel is modelled and assembled. If not, the family of vessels is discarded from future analysis. Finally, a detailed model considering element contact interfaces, inertia relief parameters, nonlinearities and bolt pretensioning is analysed. If this vessel is an improvement of the optimization goals proposed in the case study, the vessel is validated. If not, its geometric design functions are adapted in function of the results and a new iteration is created. The procedure schematic is displayed in *Figure 4.1 (b)*. Stress analysis will not consider any post-processing averaging method since the case study aims to determine a conservative approach to this first iteration of the proposed geometries, with future works focused on optimization.

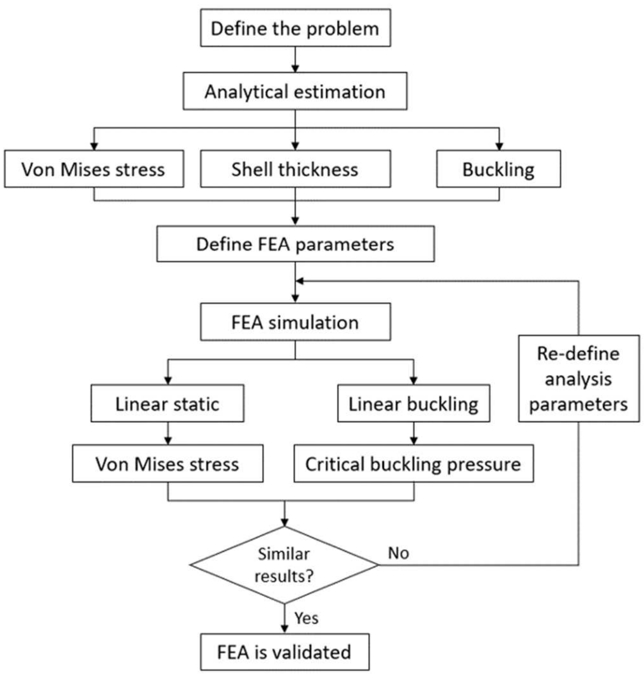

(a)

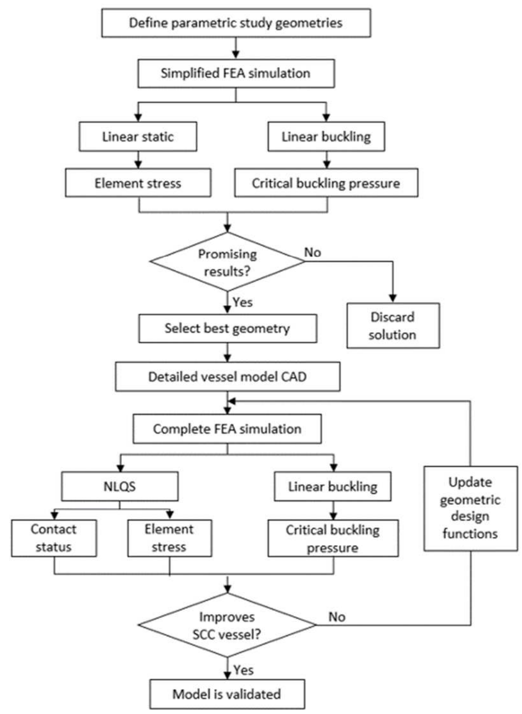

(b)

Figure 4.1. procedure schematics defining the methodology of analysis used: (a) procedure of FEA simulation validation; (b) procedure of vessel design and optimization.

All FEA were performed using *Altair Hyperworks*. *Altair Hyperworks* is a commercially available CAE software widely used in the engineering industry. It has a vast catalogue of tools and solvers suited for most of the simulations required in complex problems. Its features include an advanced mesh modelling software, *HyperMesh*, with several optimization algorithms for 2D and 3D meshing; a rendering and visualisation software, *HyperView*, which provides high-resolution representations and renders of models and analysis; and several solvers suited for different kinds of FEM analysis, such as *OptiStruct*, the recommended solver for the implicit small displacement analysis considered in the present thesis.

4.2 SCC - Standard Circular Cylindrical Vessel Design

The SCC family of pressure vessels are defined as unstiffened, cylindrical shells with a circular cross-section. This was the geometry most commonly found, and the conducted benchmark study consisted only in models with this geometric configuration. So, SCC models are to be dimensioned following the product specifications presented in *Chapter 3.3.4*. To determine the optimized specifications within margin values, both analytical and numerical methods were used. Then, a simplified geometry analysis for stress behaviour across the shell was used to validate further studies. A detailed model was built according to the previously studied configurations for the flange and cap design, and finally, this vessel was checked for structural integrity and further optimized considering other flange configurations.

4.2.1 Shell thickness calculation

The analytical formulations discussed in *Chapter 2.2* are considered good estimates for critical buckling pressure of an unstiffened, perfectly circular cylindrical shell. However, some of these formulations are more conservative than others, which affects the predicted thickness. To compare this influence, 4 formulas were selected:

- The Von Mises complete equation – *Formula (2.12)*
- The Von Mises simplified equation – *Formula (2.13)*
- The David Taylor Model Basin (DTMB) equation – *Formula (2.14)*
- The Kendrick equation – *Formula (2.15)*

These equations predict the critical buckling pressure for the same set of variables. These are the elastic properties of the material: Young's modulus, E, and Poisson coefficient, ν; The geometric properties of the shell: Mean radius, R, length, L, and shell thickness, h; And n, the number of lobes that appear when bucking occurs. It must also be noted that these formulations are only valid if the vessel length is shorter than the critical length, L_{cr}, defined in *Formula (2.17)*.

The geometric dimensions defined previously in *Chapter 3.3.4* are R = 100 mm; L = 500 mm. The preliminary selected material was an aluminium alloy 7075-T6: E = 71.7 GPa; σ_y = 503 MPa; ν = 0.33. Hydrostatic pressure at 1 500 m is the Nominal Diving Pressure, NDP, which was linearly interpolated from the values in *Table 2.2*, ρ_f=1.03516 g/cm^3, NDP = 15.22 MPa. The shell thickness at which the structure is predicted to buckle was determined via an iterative process by solving the above equations so that the objective formula, $P_{cr,}$ was equal to 15.22 MPa by changing the independent variable, t. The calculated results are displayed in *Table 4.1*.

Table 4.1. Calculated shell thickness using different analytical equations

Equation	Pressure [MPa]	Shell thickness [mm]
Von Mises (complete)	NDP = 15.22	6.462
Von Mises (simplified)		6.236
DTMB		6.685
Kendrick		6.451
Mean value	-	6.458

Using the shell thickness mean value to determine the critical length, L_{cr} = 1388.1 mm, proving $L<L_{cr}$ and thus validating the above equations. All equations resulted in a buckling mode shape n=3. It shows that the critical buckling pressure obtained using the DTMB equation is the most conservative, since it estimates the thickest shell, while the least conservative is the Von Mises simplified equation. The Von Mises complete equation and the Kendrick equation provide very similar results, which is in agreement with the consulted bibliography [73]. From these results, it was decided to use the DTMB solution. It was decided to be conservative in this first iteration, in order to have room for later model optimization. So, the shell thickness at NDP is h_{NDP} = 6.7 mm.

The calculations above considered a 7075-T6 aluminium alloy. This was a preliminary selection based on the market research, so to confirm it as the most adequate material, other materials were analysed. Since a paramount property is the yield-to-density ratio [26], both the stresses and weight of the shell were compared The shell circumferential and longitudinal stresses were determined using the "boiler equation" - *Formula (2.5)*, and the equivalent Von Mises stress for a shell structure in a stress plane state were determined using *Formula (4.1)*. In this formula, it was assumed that radial and face shear stresses are negligible compared to the inner surface stress [85]. The predicted shell thickness using the DTMB formula, the analytical Von Mises stress and cylinder weight for a set of materials, are displayed in *Table 4.2*.

$$\sigma_{VM} = \sqrt{\sigma_\theta{}^2 - \sigma_\theta\sigma_L + \sigma_L{}^2} \tag{4.1}$$

Table 4.2. Calculated shell thickness considering different materials

Material	Alloy	DTMB thickness [mm]	Von Mises stress [MPa]	Weight [kg]
Aluminium	5086-H116	6.7	209.6	5.80
	5456-H111	6.7	208.8	5.82
	6061-T6	6.8	206.5	5.98
	7075-T6	6.7	210.4	6.10
High Tensile Steel	HY80 HY130	4.4	311.5	11.07
Stainless Steel	304 (A2) 316 (A4)	4.5	304.9	11.61
Titanium	6Al-4V	5.5	251.5	7.91

Starting with the aluminium alloy, all these shells have approximately the same thickness and stress. However, the stress is above the yield strength of the 5086 alloy, $\sigma_y = 207$ MPa, and quite close to the yield strength of the 5456 alloy, $\sigma_y = 230$ MPa, so the 5000 series alloys are most likely to fail. The high-tensile steel and stainless-steel shells have similar thickness and stress. However, the yield strength of the stainless-steel alloys is below this expected stress, making their also usage unfeasible. The titanium alloy 6Al-4V presents the best mechanical properties, $\sigma_y = 880$ MPa, and the resulting Margin of Safety at NDP is the highest, MS = 2.50. Comparing weight results, the aluminium alloy shells are in advantage: high tensile steels are twice as heavy, and the 6Al-4V titanium shell is about 30% heavier. So, since 6061-T6 and 7075-T6 aluminium alloys are both structurally safe for the mission parameters and the ones with the highest strength-to-density ratio, they are the obvious choice. To determine which is better suited, the DNV GL safety factors [66] were considered - *Table 2.3*. Analysing at the Collapse Diving Pressure – CDP = 24.35 MPa, the predicted stress of the 6061-T6 alloy is $\sigma_{CDP} = 277$ MPa. With an ultimate strength $\sigma_u = 310$ MPa, the margin of safety at CDP is MS = 0.12. On the other hand, the 7075-T6 alloy reports a predicted stress of $\sigma_{CDP} = 282$ MPa, $\sigma_u = 503$ MPa, which results in a margin of safety at CDP of MS = 0.78. Since some of the alternative concepts are expected to result in larger stress accumulations, for sake of valid geometric comparisons, the stronger 7075-T6 alloy was selected thus validating the preliminary selection made when determining the product specifications.

4.2.2 Simplified shell FEA and validation

Analytical procedures used in the previous chapter are good tools to estimate shell thickness and stress in a simple, perfect shell. However, analytical formula are not compatible for a detailed pressure vessel, and instead numerical method-based analysis are required. To validate all future Finite Element Analyses - FEA, a simplified shell, equivalent to the one predicted using analytical formulas, was modelled, and both results were compared.

Before modelling the simplified shell, the thickness must be re-calculated for load safety factors: Despite the previous analytical calculations at the Nominal Diving Depth – NDP = 1500 m, uncertainties which cannot be covered by analytical methods, like manufacturing mistakes or operating pressure fluctuations, must be accounted for. This thesis considers the DNV GL [66] safety factors for unmanned UWT systems, described in *Table 2.3*. For pressures between 6 and 40 MPa, the safety factor for the Test Diving Pressure – TDP is S1 = 1.2, and the safety factor at the Collapse Diving Pressure – CDP is S2 = 1.6. So, using the DTMB equation, the correspondent shell thickness is 7.2 mm for the TDP, and 8.1 mm for the CDP - *Table 4.3*. DNV GL states that the safety factor S2 is the one covering both for material, manufacturing and FEA procedure uncertainties [60]. This is also in agreement with the recommendation that vessels should be over-dimensioned, so that axisymmetric yield is the failure mode most likely to take place [26]. So, a correspondent shell thickness of 8.1 mm, given for CDP = 24.35 MPa was considered, and reasonably rounded to 8 mm.

Table 4.3. Calculated thickness using the DTMB equation for various depths

Equation	Diving pressure [MPa]	Shell thickness [mm]	Von Mises stress [MPa]	Weight [kg]
DTMB	NDP = 15.22	6.7	210.4	6.10
	TDP = NDP × 1.2 = 18.26	7.2	235.7	6.59
	CDP = NDP × 1.6 = 24.35	8.1	281.9	7.34

The Windenburg thinness ratio, λ_c [51] was checked for $t = 8$ mm to predict failure mode. As previously stated, the shell is most likely to fail due to axisymmetric yielding when $\lambda_c < 0.8$, and if $\lambda_c > 1.2$, the shell can fail due to elastic instability. With *Formula* (2.17), this ratio is $\lambda_c = 1.50$, so even with a conservative shell, failure due to lobar buckling is still possible. It was calculated that for this geometry, the shell would have to be over 18 mm thick for Windenburg's ratio to predict axisymmetric yielding as the only failure mode likely to occur.

Two types of analysis were conducted to evaluate the structural behaviour of the shells: a linear static analysis to determine the displacements, strains, and stress load functions on the model; and a linear buckling analysis to estimate the critical buckling pressure. The material was modelled having an isotropic, linear elastic behaviour. The shell was constructed in Hypermesh with PSHELL [97], a 4-node quad shell element, since 2D elements are usually more reliable [75]. It was considered that these models were capped at both ends by flat plates with high stiffness. This can be assumed since the end of the cylinder will be supported by a solid end cap [51] [96]. To simulate this behaviour, the shell was modelled considering one-dimensional rigid body elements RBE2 [97] at each cylinder base, connecting the edge nodes (dependent nodes) to an auxiliary central node (independent node), so the motion of the independent node is transferred to the dependent ones - *Figure 4.2 (a)*. These elements do not deform as they are defined to be infinitely rigid, so the circular shape is kept [75]. Three in-plane Single Point Constraints – SPCs, were used in a way that axial displacements were not affected: The left side of the tube was fully constrained, while the left side was constrained only along Y and Z directions. Loading is equivalent to NDP and imposed as lateral pressure on the shell external surface, and compressive axial load on the rigid body independent node - *Figure 4.2 (b)*.

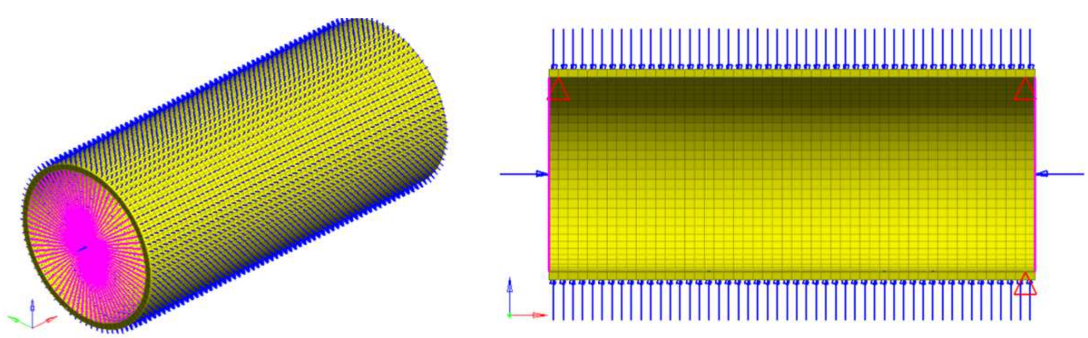

(a) (b)

Figure 4.2. Cylindrical shell designed in Hypermesh: (a) isometric view, with rigid elements (in pink); (b) section view with radial pressure, the equivalent axial load and the SPCs (in red).

To determine the mesh size, a convergence study was conducted. The model was auto meshed with consecutive smaller mesh sizes, from 17 mm to 4 mm, increasing the number of elements from 1 046 to 19 752, a ~20x increase. Plotting this data concludes that element stress converges for a mesh size of 6 mm - *Figure 4.3*, while the buckling pressure converges at 5 mm - *Figure 4.4*.

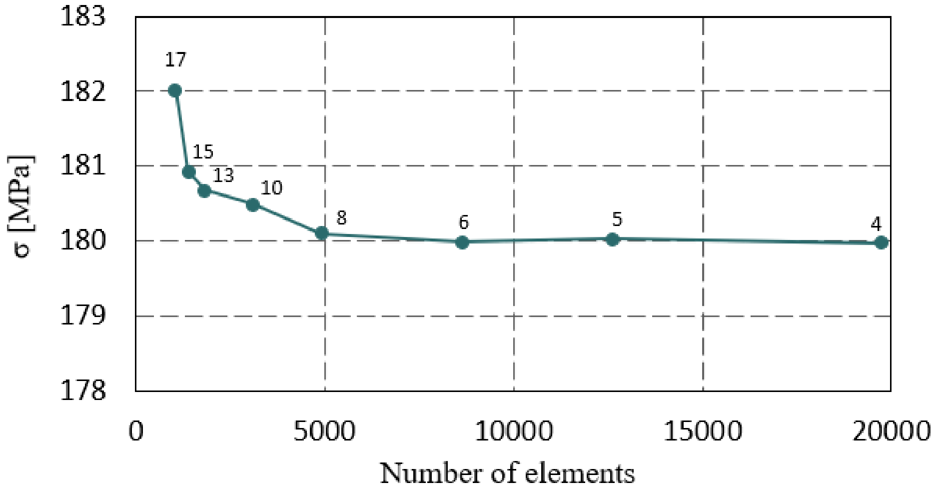

Figure 4.3. Convergence analysis of 2D-shell meshed models: NDP Von Mises stress.

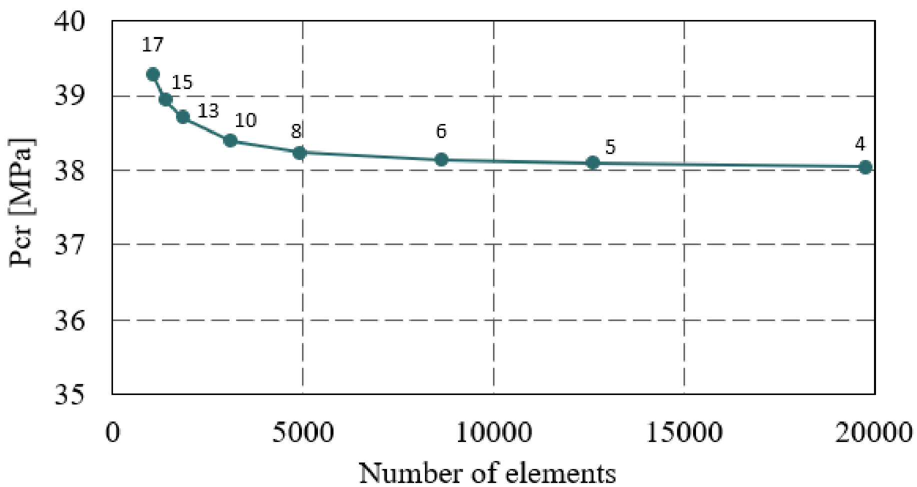

Figure 4.4. Convergence analysis of 2D-shell meshed models: Critical buckling pressure.

Finally, it is possible to compare the FEA results with those calculated in the analytical formulations above - *Table 4.4*. For the 3 load collectors, the Von Mises stress was respectively 1.1%, 1.4% and 2.2% higher than the analytical estimation, an acceptable deviation that validates the FEA. It is important to note that the FEA predicts higher stress results, which makes it more conservative. On the other hand, the estimated buckling pressure was 56.3% higher than the analytical prediction. This gap is quite similar to the gap reported by Ross et al. [62], where the predicted buckling pressure using ANSYS was higher than the theoretical pressure using the Von Mises and DTMB formulas, seen previously in *Figure 2.10*. This is expected due to the considered boundary conditions of the simulation, which underestimate the buckling effects. The verified mode shape was n=3, which is in agreement with the analytical predicament - *Figure 4.5 (b)*.

Table 4.4. Analytical and numerical results of Von Mises stress (VM) and buckling pressure

Pressure [MPa]	t [mm]	VM (analytical) [MPa]	VM (FEM) [MPa]	n	P_{cr} (FEM) [MPa]
NDP = 15.22		178.0	180.0		
TDP = 18.26	8.0	213.5	216.0	3	38.10
CDP = 24.35		281.9	288.0		

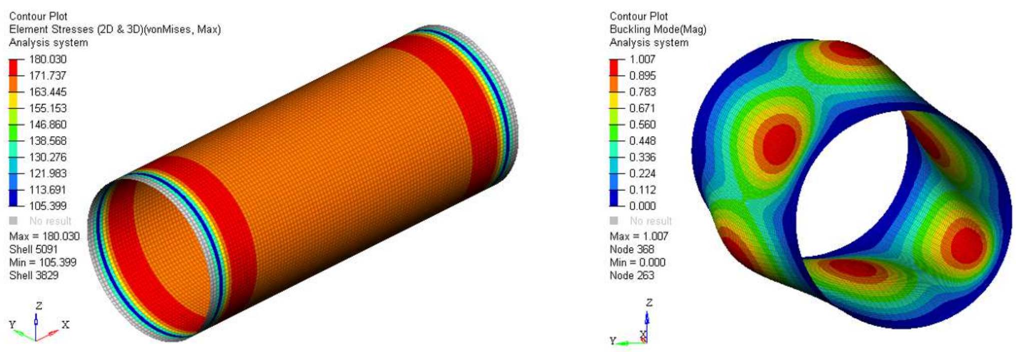

Figure 4.5. Cylinder shell with 2D-shell elements – FEA results: (a) NDP Von Mises stress analysis; (b) First buckling mode, n=3 (deformation multiplier of 30.0).

As stated before, geometric imperfections cause the real buckling pressure of a shell to be lower than numerical estimations. Ross [26] defined a design chart, previously referred in *Figure 2.12*, which correlates the predicted Plastic Knock-Down factor (PKD), with the Windenburg thinness ratio, λ_c, allowing to estimate the real buckling pressure of a shell. Using *Formula (2.17),* it comes that $\lambda_c = 1.49$, to which it corresponds a PKD = 1.2, and consequently, $P_{real} = 18.73$ MPa. Since NDP = 15.22 MPa, there is a safety factor of 1.23, which was considered acceptable for this study.

Despite 2D shell elements being more reliable for static analysis of thin-walled cylinders, it is impossible to model detailed vessels with only shell elements. So, shells modelled with 2D and 3D elements are to be compared to check for discrepancies. The same model was built using PSOLID 3D CTRETRA elements. A convergence study similar to previous one concludes that convergence occurs for a mesh size of 2.5 mm for both shell stress and buckling pressure – *Figure 4.6*.

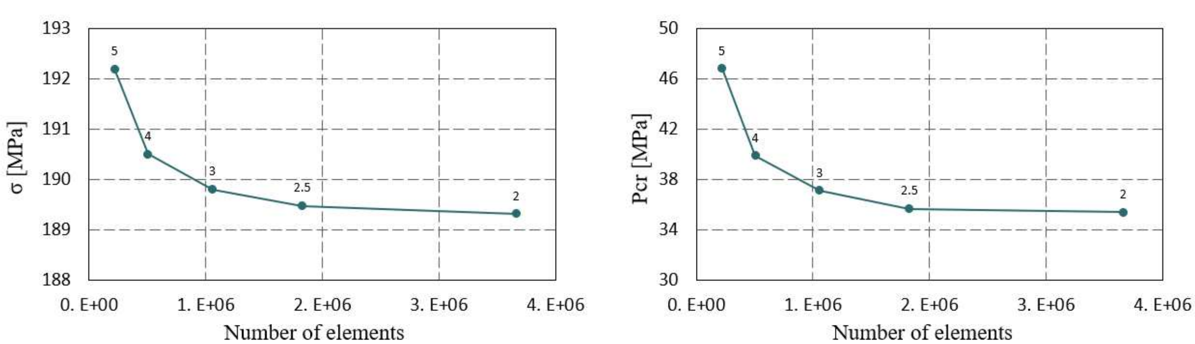

Figure 4.6. Convergence analysis of 3D-solid meshed models: Von Mises stress at NDP on the left; Critical buckling pressure on the right

The results were similar to the 2D shell elements - *Table 4.5*. P_{cr} = 35.4 MPa, a 7.0% decrease of the 2D PSHELL analysis, and $\boldsymbol{\sigma}_{VM}$ = 189.3 MPa, a 5.1% increase. Despite buckling presenting a larger deviation, even above the 5% threshold considered for this thesis, it was already reported that 2D elements buckling pressure is way above the theoretical result. Since this predicted buckling is actually lower, it was accepted that it predicts critical pressure more conservatively. The maximum stress is closely within the 5% deviation threshold, so both values were validated, and analysis congruency is confirmed. However, it must be stated that a mesh size of 2.5 mm is not suitable since the CPU time increased up to 43 minutes, ~25x the 2D-shell analysis. Since detailed models will demand more computing power, the mesh size for 3D-solid elements was fixed at 4 mm - *Figure 4.7*.

Table 4.5. FEA results comparison between 2D-shell and 3D-solid elements (Von Mises stress)

Element type	#elements	CPU time [s]	NDP Stress [MPa]	TDP Stress [MPa]	CDP Stress [MPa]	P_{cr} [MPa]
2D	19 752	105	180.0	216.0	288.0	38.10
3D	1 828 274	2 637	189.5	227.4	303.2	35.39

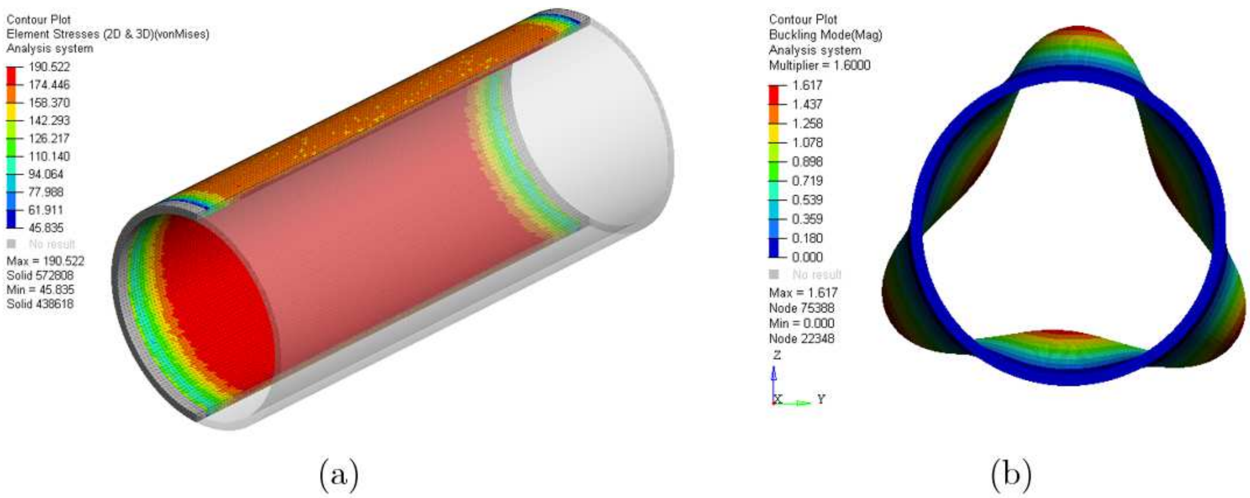

Figure 4.7. Cylinder shell FEM with 3D-solid elements (mesh size = 4 mm) – FEA results: (a) CDP Von Mises stress; (b) First buckling mode n=3 (deformation multiplier of 30.0).

4.2.3 SCC detailed model design

Following the previous chapter conclusions, a detailed vessel with a main body, closing end caps, and fastening components is to be assembled. Starting with the main body, it will have a flange configuration as concluded in *Chapter 3.4*. The principal geometric dimensions were already defined as R = 100 mm, L = 500 mm, t = 8.0 mm. The internal length, L, will be the distance between the inner faces of the caps, so these must be dimensioned to determine their inner length, which together with the flange thickness will define the total external length of the main body.

In *Chapter 3.4.4*, the selected cap design functions are of a flat plate with a through-bolted closure configuration. For the sealing solution, it was decided to use a dual radial seal configuration, which is better suited for this application. End cap design requires the use of standardized components, so its dimensioning must reflect the nominal dimensions of these components.

The first component to design is the O-ring and its housing groove. For a piston-sealing radial installation, the O-Ring internal diameter, d_1 must be equal to or smaller than the groove diameter of the slot, d_3. This causes a stretch of the O-ring, recommended to be 2 - 8%, for static applications. The stretch, S_O, is calculated with *Formula (4.2)*:

$$S_O = \left(\frac{d_3 - d_1}{d_1}\right) \times 100\ [\%] \tag{4.2}$$

This stretch results in a reduction of the O-ring cross-section, making it no longer circular. This percentage reduction, R_O, can be determined with *Formula (4.3)* [98]:

$$R_O = 0.01 + 1.06 \cdot S_O - 0.1 \cdot {S_O}^2 \tag{4.3}$$

Another important factor is the compression, C_O, of the O-ring in the groove. It achieves the sealing capability of the O-Ring, while compensating for usage wear. *Figure 4.8* displays a graph showing the permissible range of initial compression as a function of the cross-section.

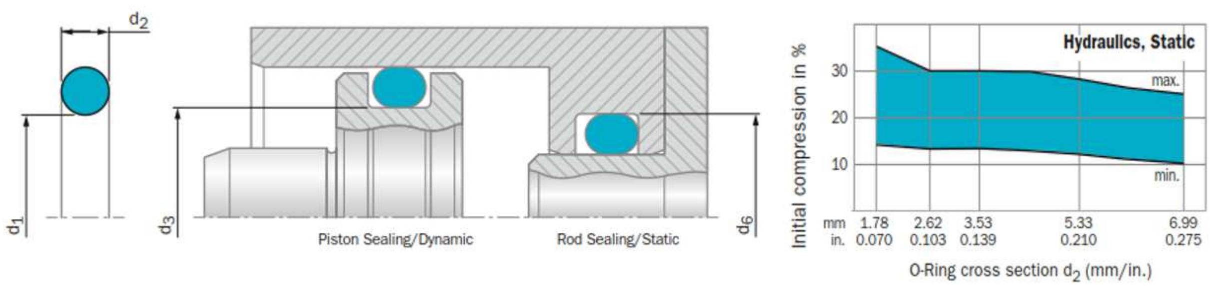

Figure 4.8. Dimensioning for a radial seal application: On the left, O-ring and radial groove dimensions; On the right: Permissible range of initial compression as a function of the cross-section. Adapted from [98].

For static applications, and an considering an applied pressure between 10 and 40 MPa, *Trelleborg* recommends a back-up ring [98]. Back-up rings do not have any sealing functionalities but are used to protect and support the O-ring when installed in a groove, something important when the applied pressure is quite high.

Component designing also needs to consider O-ring installation. To prevent damage during installation, it cannot pass over live edges of bores. So, lead-in chamfers and/or rounded are used. *Trelleborg* recommends a chamfer angle between 15º-20º, and lead-in lengths designed considering the O-ring cross-section - *Table 4.6*.

As for the material, Acrylonitrile-Butadiene Rubber, or Nitrile Rubber (NBR - ISO1629) was selected since it is adequate for the mission parameters, while one of the cheapest elastomers. In general, O-rings made of this material show good mechanical properties [98].

Table 4.6. Lead-in chamfers length as a function of the angle and O-ring cross-section. Adapted from [98]

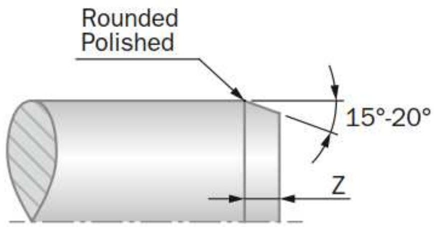

Lead-in chamfer length L_Z 15º	20º	O-Ring cross-section (d_2)
1.1	0.9	≤ 1.80
1.5	1.1	≤ 2.65
1.8	1.4	≤ 3.55
2.7	2.1	≤ 5.35

The O-Ring ORAR00367 (ISO 3601-1) was selected from *Trelleborg Sealing Solutions* 2016 catalogue, with inner diameter, d_1, and cross-section diameter, d_2 defined in *Table 4.7*.

Table 4.7. Metric dimensions of the selected O-ring, Trelleborg [98]

Part No.	Size code ISO 3601-1	d_1 [mm]	d_2 [mm]
ORAR00366	366	183.52 ± 1.42	5.33 ± 0.13

The groove needs to accommodate both the O-ring and the back-up ring. *Trelleborg* recommends a back-up concave ring type (BB), which concave shape has a large contact surface, making it suitable for static, high-pressure applications. The dimensional stability also improves the sealing force, as well as the service life - *Figure 4.9*. Since the applied pressure is unidirectional, only one ring is necessary. The backup ring BBP80B367 was selected - *Table 4.8*.

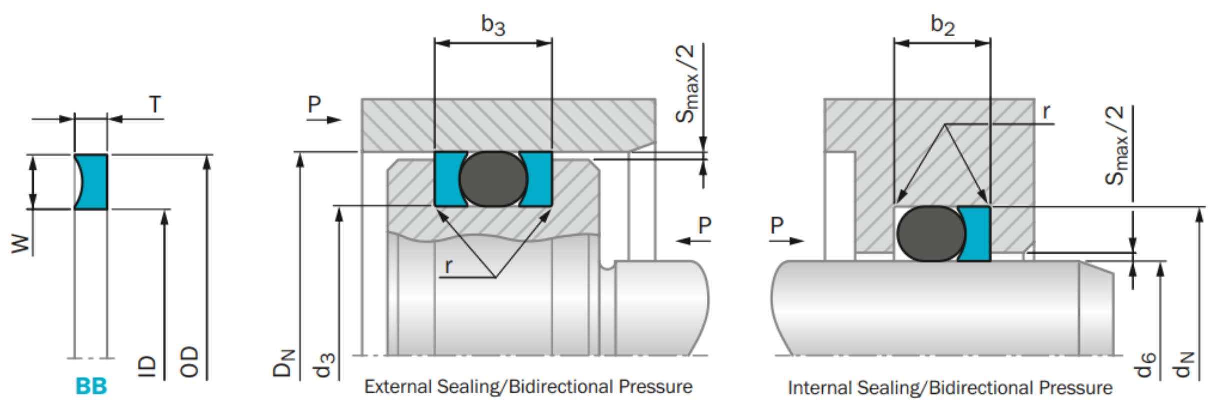

Figure 4.9. Back up concave ring (BB) and groove dimensions [98].

Table 4.8. Metric dimensions of the selected back-up ring, Trelleborg [98]

Part No.	Back-up Ring CS height (W)	thickness (T)	radius (r)	Groove diameter (d_3)	width (b_2)	Bore bore Ø (D_N)	clearance (S_{max})
BBP80B367	4.65	1.52	0.25	190.6	7.9	200.0	0.08

The stretch, reduction and compression were determined in *Table 4.9*. The recommended initial compression for a cross-section of $d_2 = 5.33$ mm was determined from the graphic in *Figure 4.8*, and it is recommended to be between 12 - 28%. Since all the thresholds are verified, the selected O-ring is validated, as well as the groove dimensions.

Table 4.9. O-ring operating conditions for the selected components - SCC

Stretch	Reduction	Compression
$S_O = \frac{190.6 - 183.52}{183.52}$ [%]	$R_O = 0.01 + 1.06 \cdot 3.9 - 0.1 \cdot 3.9^2$ [%]	$C_O = \frac{5.33 - 4.65}{5.33}$ [%]
$S_O = 3.9\% > 2\%$	$R_O = 2.6\%$	$C_O = 12.75\ \% > 12\%$

With the dimensions of the groove set, the inner length of the cap was built. It was decided to space equally the groove distance with the cap end and flange edge, which was fixed at 6.4 mm. So, the internal length of the cap was set to be 35 mm. Finally, a lead-in chamfer to a 20º angle and with $L_Z = 2.1$ mm was considered following the recommendations for an O-ring with $d_2 = 5.33$ mm.

The diameter of the external face of the cap will be equal to the flange. It was decided to use ten equally spaced, concentric M8 bolts, since similar configurations were observed in competitive benchmarking and likely have adequate dimensions to ensure watertightness. Following the thumb rule for bolt distance to an edge, $2D_{bolt} + 1$, for $D_{bolt} = 8$, this distance equals to 17 mm. So, the flange diameter was set to 270 mm, a moderate size but large enough to allow for changes in the main body surface configuration without requiring additional flange dimensioning, which will be useful when comparing the RTV and ATV model families. The cap thickness was set at 12 mm since similar were used in benchmarking models. The cap dimensions are displayed in *Figure 4.10.*

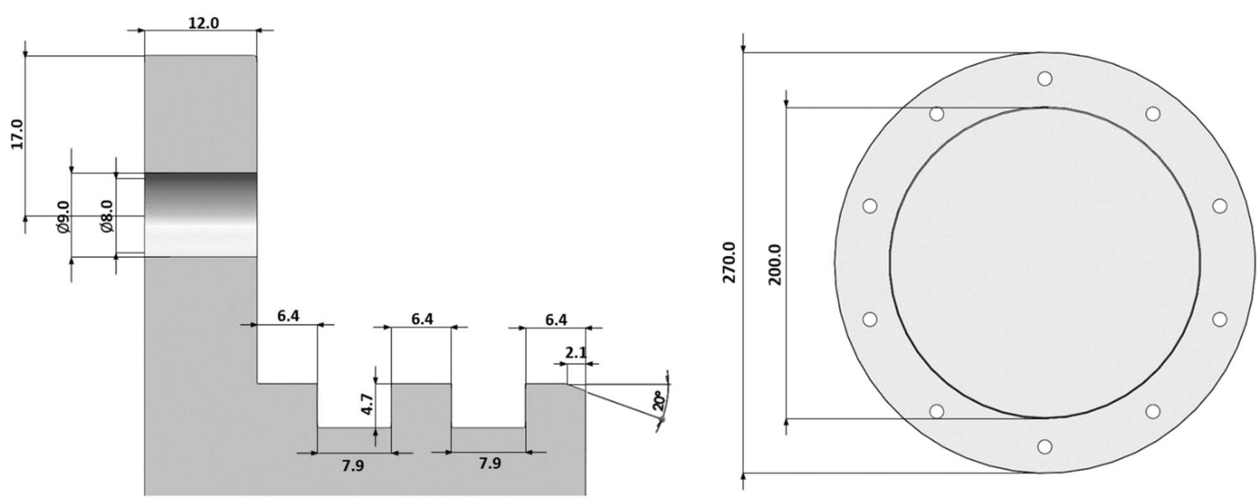

Figure 4.10. General dimensions of the SCC end cap.

All main body dimensions can now be set. The internal length, L = 500 mm, is given by the distance between the internal faces of each end cap. The axial distance from the cap face to the flange edge is 35 mm, and so, the external length of the main body is 500+2·35=570 mm. The flange thickness was set at 12 mm, the same as the cap - *Figure 4.11*.

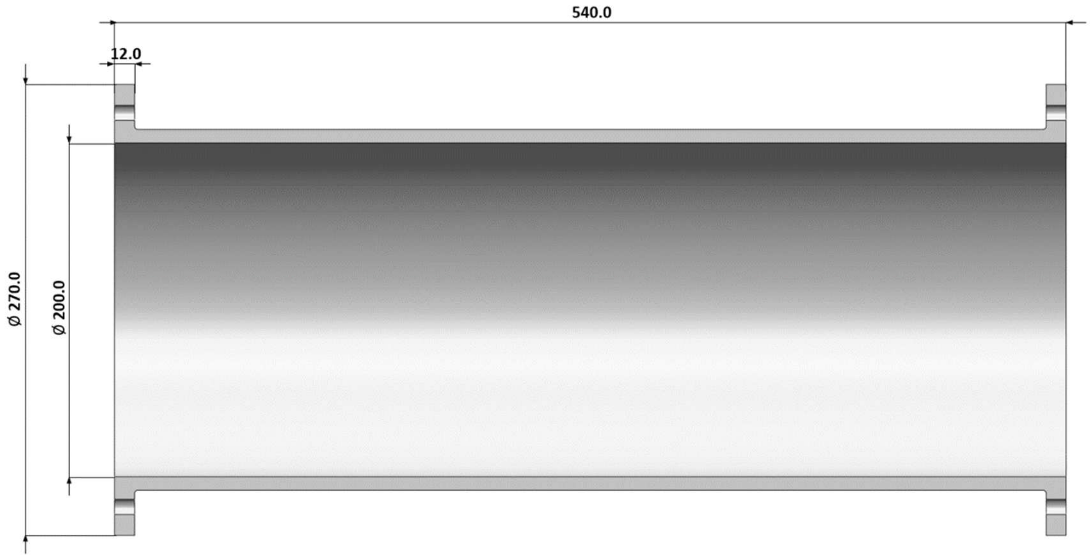

Figure 4.11. General dimensions of the SCC main body.

Finally, the normalized fastening components were selected. It was already decided that these would have an M8 internal diameter. For the bolt, a hexagonal head screw ISO 4014 was selected - *Table 4.10*. Its match is an ISO 4032 nut - *Table 4.11*, and an ISO 7089 washer - *Table 4.12*. A stainless-steel INOX A4 class 80 material was chosen to withstand the seawater corrosion.

Table 4.10. Metric dimensions of ISO 4014 bolts, Fabory [99]

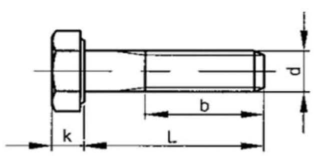

Diam.	b(min)	k	P
M6	20	4.8	1.0
M8	22	5.3	1.25

Table 4.11. Metric dimensions of ISO 4032 nuts, Fabory [99]

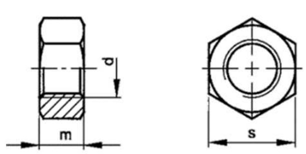

Diam.	m(max)	s	P
M6	5.2	10	1.0
M8	6.8	13	1.25

Table 4.12. Metric dimensions of ISO 7089 washers, Fabory [99]

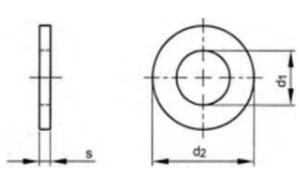

Diam.	d1	d2	s
M6	6.4	12	1.6
M8	8.4	16	1.6

Bolts are installed with preload, which ensures that the components remain clamped and in compression. Bolt preload also allow the bolt to distribute the force throughout the material surface. Preload is dependent on the tensile stress area of the fastener threads and the yield strength of the material - *Equation (4.4)*. Considering D = 8 mm, P = 1.25 mm and σ_Y = 600 MPa for an INOX A4 grade 80, and $\%_Y$=64%, the recommended multiplier for a nonpermanent bolted connection, the recommended axial preload force is 13.9 kN.

$$F_P = \%_Y \cdot \sigma_{y,b} \cdot A_S \tag{4.4}$$

Where:

$A_S = 0.7854\left[D - \dfrac{0.9743}{1/P}\right]^2$

$\%_Y$ =preload percentage of the yield

σ_y= yield strength of the bolt material

So, all the components of the SCC pressure vessel were modelled, and then assembled in *Solidworks*. This allows to better visualize what a finalized product would look like - *Figure 4.12*.

Figure 4.12. Rendered image of the SCC pressure vessel.

Some of the *Chapter 3.3.4* product specifications can be confirmed. Geometric dimensions and bolt validation are easily confirmed to be within the set and range values, but the ones referring to structural stability still require numerical analysis. With all dimensions set, it is now possible to determine the real material properties for a compatible extruded aluminium tube. Given the flange size, an extruded tube must consider a wall thickness of at least 35 mm. Referring to *Table 3.18*, the equivalent mechanical properties are given for a wall thickness of $10 < t < 50$ mm. For this range, the yield and ultimate strength are, respectively, $\sigma_y = 495$ MPa and $\sigma_u = 560$ MPa.

Now regarding weight and buoyancy balance. the pressure vessel mass and weight were determined to be 19.7 kg and 193.0 N, respectively - *Table 4.13*. Considering the density of the fluid ρ_f, $= 1.03516$ g/cm^3, and the volume of displaced fluid, $V_{disp} = 22\ 620$ cm^3, the buoyancy of the vessel is $B = 230.6$ N - *Formula (2.3)*. To which a positive net force of $230.6 - 193.0 = 37.6$ N is verified. So it is possible to load up to 3.8 kg of payload without resulting in a negative impulsion. Hence, all geometric product specifications are confirmed.

Table 4.13. Volume, mass and weight of the SCC pressure vessel

Components	Volume [cm^3]	Mass [kg]	Weight [N]
Main body	3453.7	9.7	95.1
End cap	1729.8	4.9	47.6
Fastening components	-	0.4	3.6
Total	6913.5	19.7	193.0

4.2.4 SCC detailed model FEA and validation

A finite element analysis was conducted to analyse the structural behaviour of the model. Two types of analysis were used: a nonlinear quasi-static (NLQS) analysis to determine the displacements and stress load functions; and a linear buckling analysis to estimate the critical buckling pressure. The external surfaces were firstly meshed with 2D R-TRIA elements, and then the enclosed body was meshed with 4-node tetra solid CTETRA elements using *Hypermesh* automeshing tools recommended settings [75] - *Figure 4.13*. Two types of boundary conditions were considered: the first is to apply three in-plane SPCs, similarly to what was made in *Chapter 4.2.2*. The second uses inertia relief INREL [97] as a parameter. This way, the constraint forces are eliminated by body forces, which simulation is compatible with a free-floating structure. This is only valid for models where the sum of forces is zero, which is the cause under hydrostatic pressure. However, inertia relief is not compatible with linear buckling analysis, so both boundary conditions will be considered and later compared to correlate results.

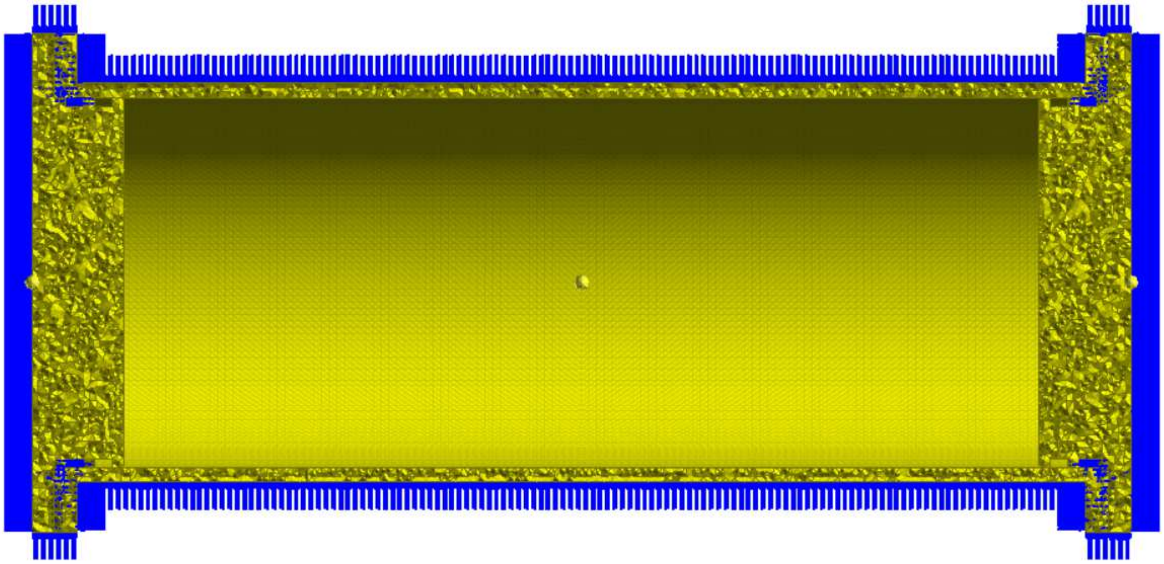

Figure 4.13. Cross-section view of the meshed SCC model.

Loading is imposed as pressure in all of the external surface elements, and unlike simplified models, rigid body elements are not required at the cylinder bases. However, rigid elements RBE2 are still used to simulate bolt behaviour. The region around bolt holes were meshed to simulate the presence of a 16 mm diameter washer. These nodes were set as dependent to an independent in-plane node, concentric to the hole. The two end nodes were then used to define a 1D CBEAM element to which bolt properties and pretension were given - *Figure 4.14*.

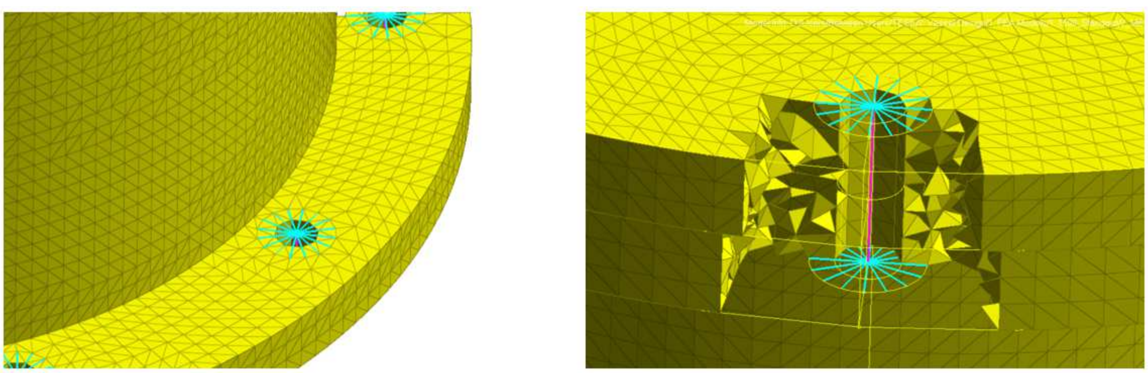

Figure 4.14. Detailed view of the connector elements: washer surface elements on the left; masked solid elements to show RBE2 elements (cyan) and CBEAM element (pink) on the right.

Contact elements were defined using *Hypermesh* master-slave algorithm - *Figure 4.15*. To prevent gap errors, the slave surface should be more finely meshed than the master surface. The two main discretization options are Node-to-Surface (N2S) and Surface-to-Surface (S2S). N2S involves the creation of contact elements linking the master surface to the slave nodes, while S2S creates contact elements linking master and slave surfaces. The S2S method was selected since it produces a smoother, more realistic contact surface, but it does require more computing power.

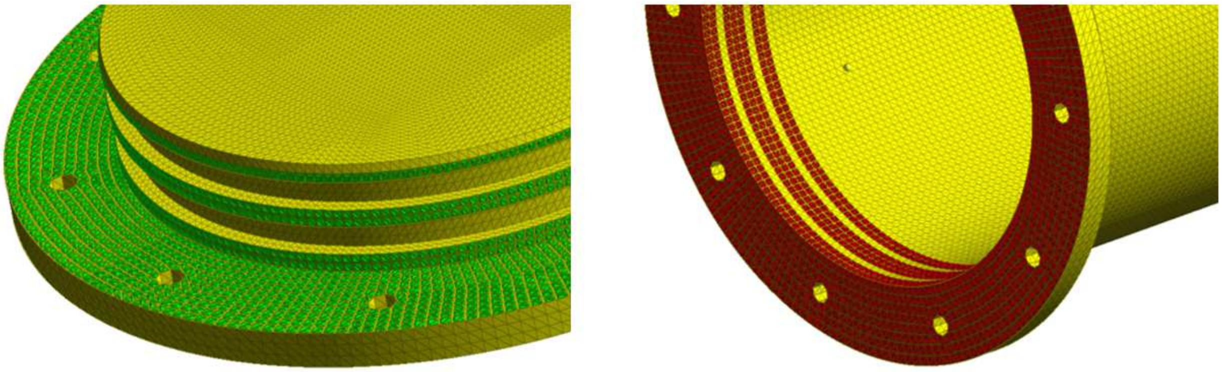

Figure 4.15. Surface elements of the contact region between the cap and the main body.

A convergence study was conducted to determine the mesh size. The model was manually meshed for consecutive smaller sizes, from 9 mm to 3 mm, increasing 82916 to 2225687 elements, a ~27x increase. Four zones were selected to study convergence in stress: Zone 1 and Zone 2 are located in the main body and are respectively the elements in the central 80 mm in the axial direction, and the elements in the main body with the contact region excluded. Zone 3 and Zone 4 are located in the left end cap and are respectively the elements in the internal face, excluding the edge contact elements, and the elements within a central radius R=130 mm, throughout the axial direction. Zones 1 and 2 started to converge at a mesh size of 4 mm - *Figure 4.17*, while Zones 3 and 4 at a mesh size of 3.5 mm - *Figure 4.18.* The contact status was also checked for convergence, and for smaller mesh sizes, the contacts were more reliable, and the vessel was confirmed to be tightly closed. The full results of all mesh convergence studies are available in full on *Appendix B.*

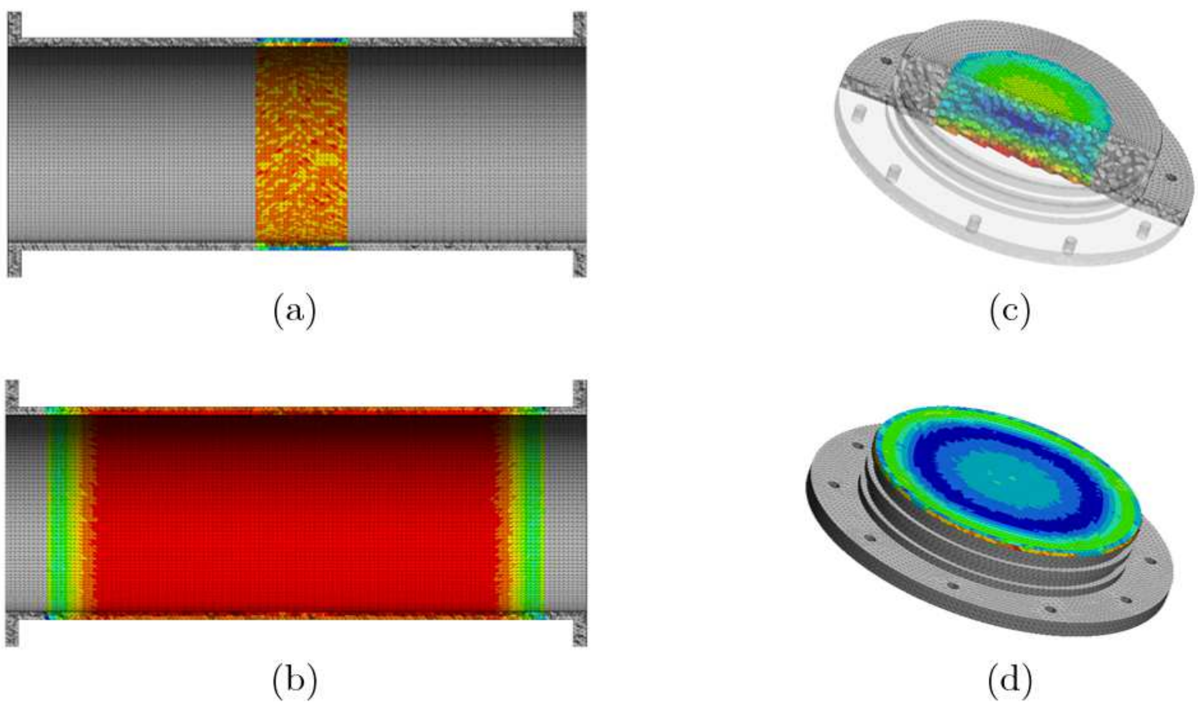

Figure 4.16. Representation of the selected zones for mesh convergence study:
(a) Zone 1; (b) Zone 2; (c) Zone 3; (d) Zone 4.

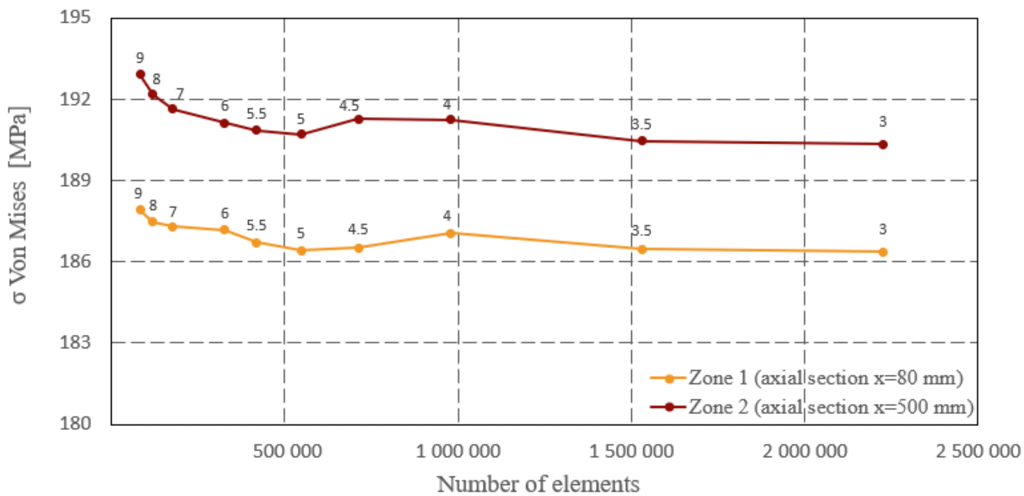

Figure 4.17. Convergence analysis for the detailed model (main body zones).

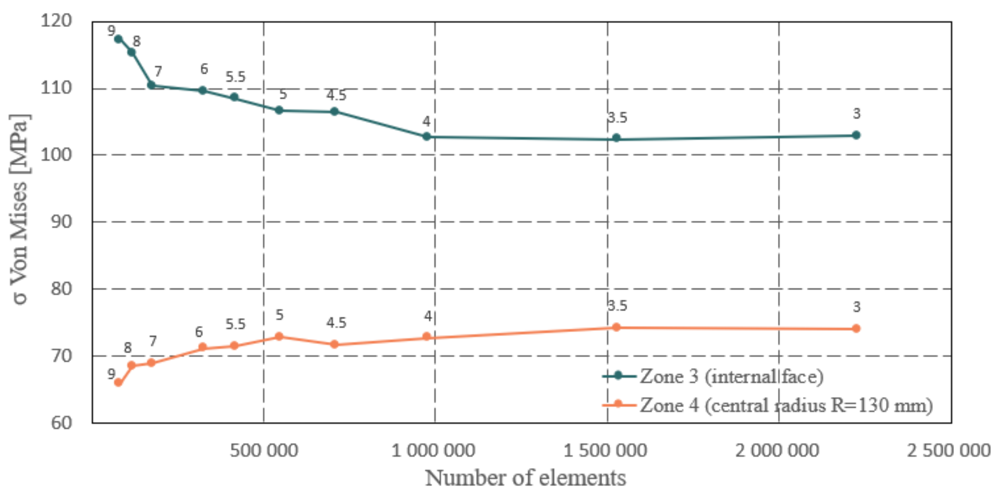

Figure 4.18. Convergence analysis for the detailed model (end cap zones).

Buckling pressure was also analysed for mesh convergence, and 3 in-plane SPCs were used since inertia relief is incompatible. P_{cr} starts to converge for a mesh size of 4.5 - *Figure 4.19*.

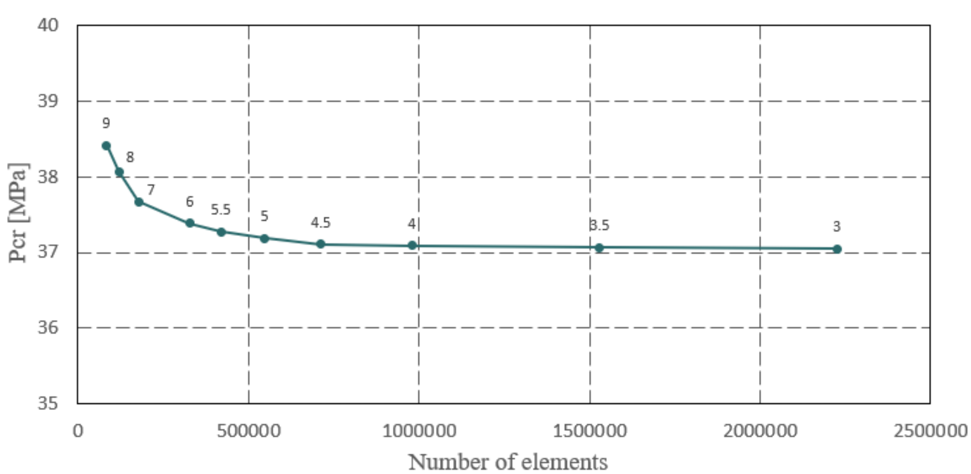

Figure 4.19. Convergence analysis of critical buckling pressure.

Both the inertia relief-based analysis and in-plane SPCs-based analysis were compared to check for congruency in results. Three analysis were considered: The first used inertia relief parameters, while the other two used SPCs applied in different nodes. The first is not compatible with linear buckling analysis but is expected to deliver accurate results for element displacement, since the lack of constraints better simulates a model purely under hydrostatic pressure. The second is restricting the movement using 3 SPCs in the XY mid-plane, similarly to the models used in mesh convergence studies discussed above - *Figure 4.20 (a)*. The third model considers 4 SPCs in the XZ mid-plane, so axial displacements can appear symmetrically to the midplane, something expected to happen in real structures under axisymmetric yielding - *Figure 4.20 (b)*.

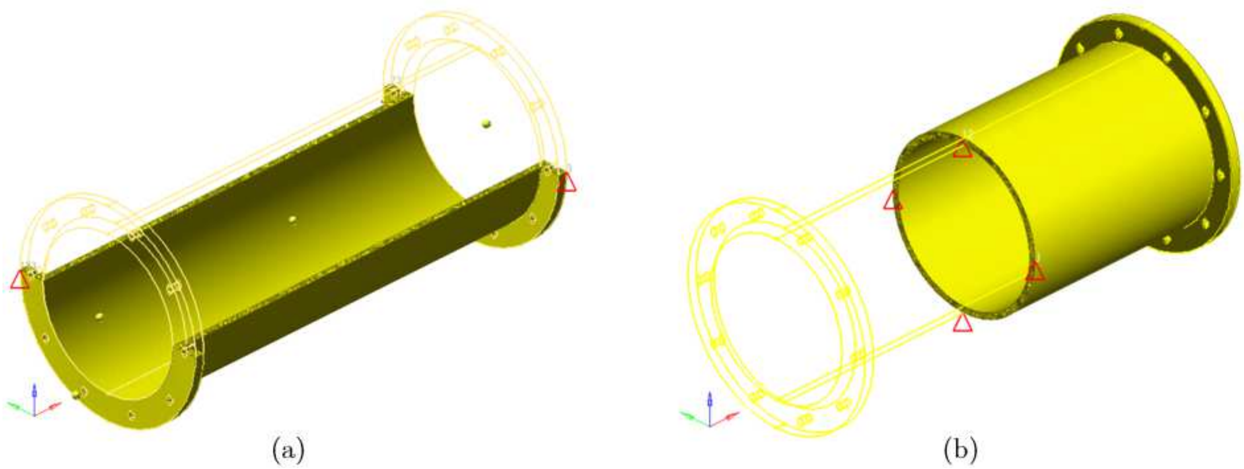

Figure 4.20. models used to compare with inertia relief analysis: (a) three SPCs in the XY mid-plane model; (b) four SPCs in the YZ mid-plane model.

This analysis, displayed in *Table 4.14* showed that the stress results were consistent across all the analysis, with an error below 0.001%. Element displacements were the same for the inertia relief and 4-node SPCs models, but 28.6% higher for the 3-node SPCs model, discarding this one for displacement study. On the other hand, the 4-node SPCs resulted in P_{cr} = 0.2 MPa, making this boundary condition unreliable for buckling analysis. So, the inertia relief analysis was validated for both displacement and stress results, and the 3-node SPCs analysis for both buckling analysis and stress results. Comparing CPU time, the inertia relief model took 15.5 minutes, while the SPC model took 35.2 minutes and a 36% higher average system load, making them more convenient.

Table 4.14. FEA results comparison between analyses using different constraints parameters

Analysis	CPU time [s]	displacement [mm]	VM Stress [MPa]	P_{cr} [MPa]
Inertia relief	930	0.353	209.543	-
XY midplane SPCs	2112	0.454	209.543	37.11
YZ midplane SPCs	2087	0.353	209.543	0.2

Mesh size was fixed at 4 mm for the main body and 3 mm for the end cap, so a more refined mesh is used in the end cap contact surface (slave surface) - *Figure 4.21 (a), (b)*. The final models were manually meshed at the surface with 2D R-tria elements - *Figure 4.21 (c), (e);* and then automeshed with 3D CTETRA elements. Tight parameters were used to make the internal mesh as regular as possible - *Figure 4.21 (d), (f)*. Making up to a total of 1 210 269 elements, this mesh size was chosen to be used in all detailed models.

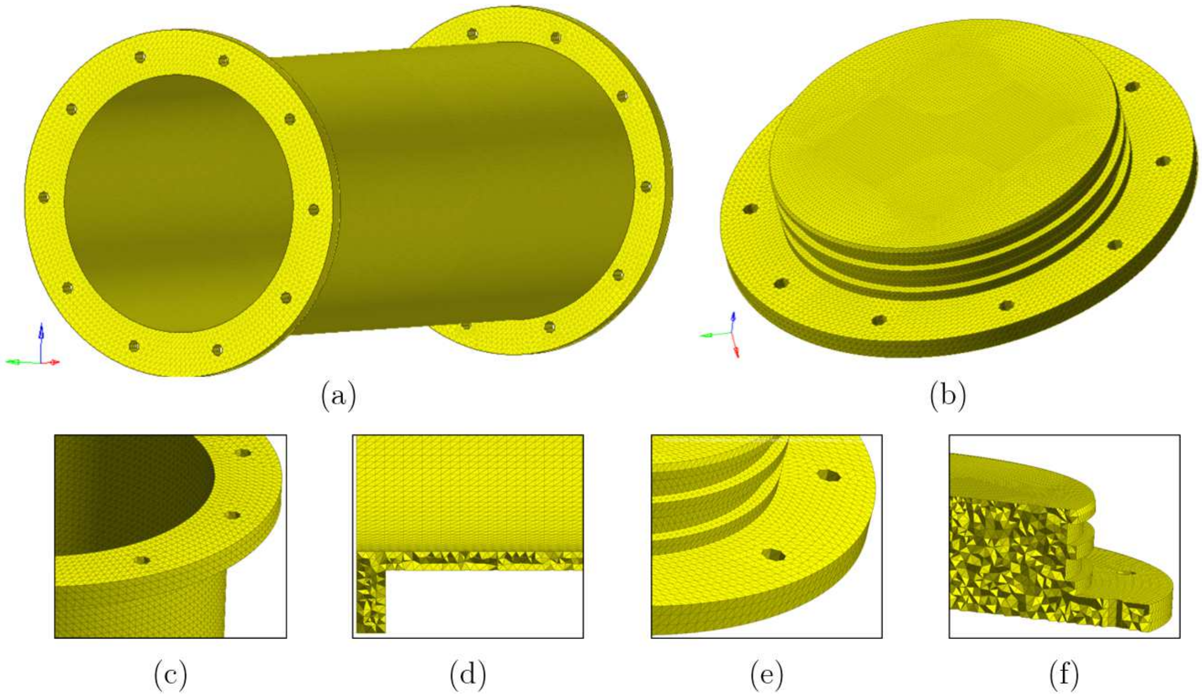

Figure 4.21. SCC model meshed to the considered parameters.

This model was submitted to the same boundary conditions described above: inertia relief for element stresses and displacements, and single point constraints for critical buckling pressure. For both of these conditions, three analysis were run, where the imposed load was updated for NDP, TDP and CDP. Stress results for Von Mises *(VM)*, tension (*P1*), compression (*P3*), critical buckling pressure (P_{cr}) and element displacements (u) are displayed in *Table 4.15*, *Figure 4.22.*

The main body behaves approximately to the simplified shell estimated results: when selecting the central zone and discarding the contact region, a maximum Von Mises stress of 190.4 MPa is observed, a 0.5% deviation when compared to the 3D-solid elements simplified shells. This confirms the validity of using simplified shells as a first step in vessel design.

The main body contact region appears to be the area more susceptible to failure. The maximum Von Mises stress is observed in this area - *Figure 4.22 (b)*. Simultaneously, the maximum displacement appears in the cap external face - *Figure 4.22 (a)*. This most likely means that the elastic deformation in the cap is pushing the contact region inward, "crushing" the edges of the main body. Maximum stresses are reported at compression - *Figure 4.22 (d)*

A critical buckling pressure of 37.07 MPa was observed, representing a 4.5% deviation from the simplified shell estimation, and the same buckling mode shape $n = 3$ was reported - *Figure 4.22 (f)*. The real buckling pressure is likely to be lower, due to beforementioned uncertainties, but since this analysis reports a safety factor of P_{cr}/NDP = 2.4, which closely doubles the previously determined PKD = 1.2 using Ross's charts, buckling is unlikely to occur at the considered nominal depth.

Table 4.15. FEA results of maximum displacement, stress and buckling pressure for the SCC vessel

Pressure [MPa]	u [mm]	VM [MPa]	P1 [MPa]	P3 [MPa]	n	P_{cr} [MPa]
NDP = 15.22	0.353	209.5	243.6	293.2		
TDP = 18.26	0.427	251.7	292.4	352.2	3	37.07
CDP = 24.35	0.574	335.9	390.0	470.1		

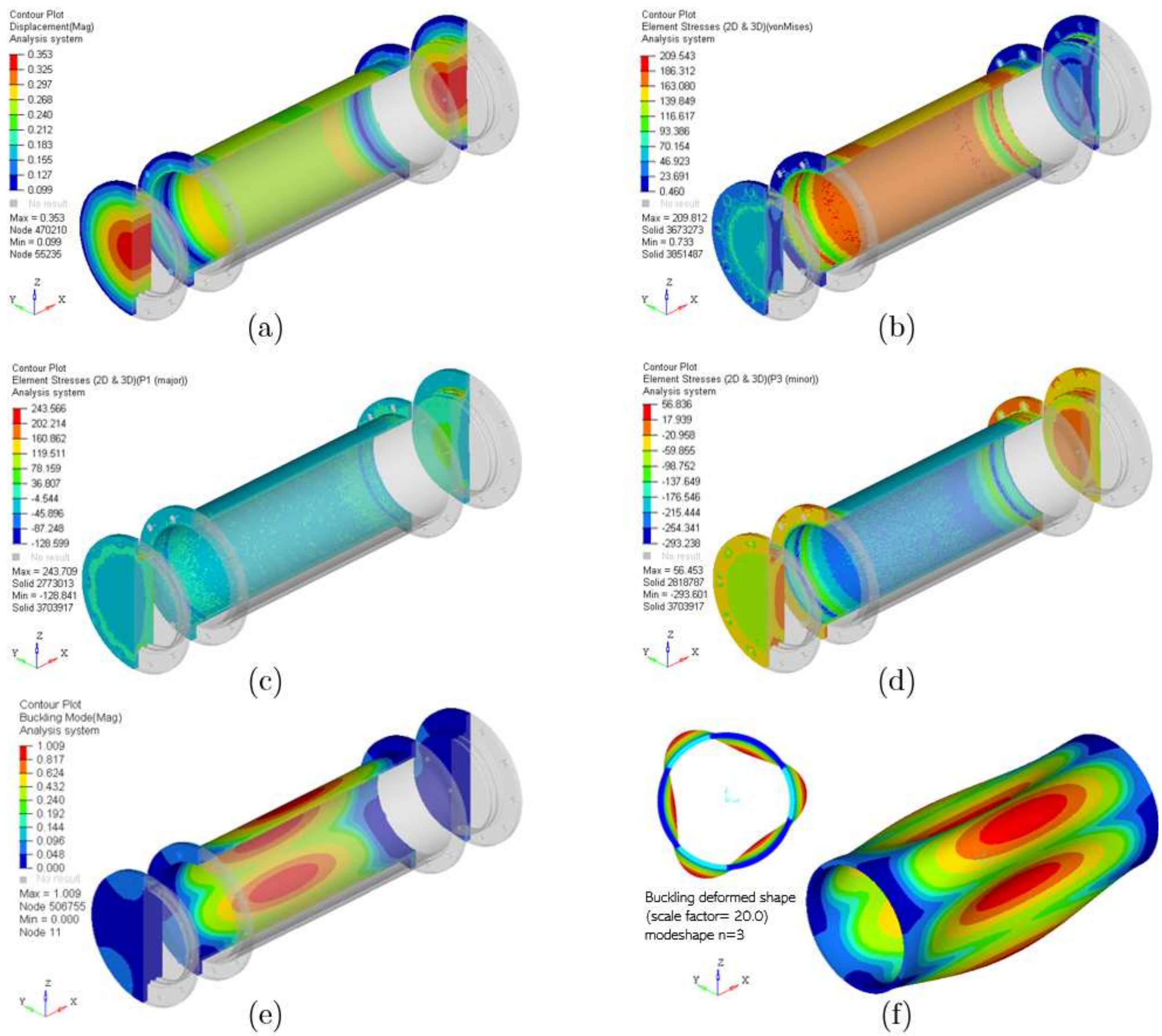

Figure 4.22. SCC vessel at NDP - FEA results: (a) displacement; (b) Von Mises stress; (c) tension stress (P1); (d) compression stress (P3); (e) buckling undeformed shape; (f) buckling mode shape (scale factor=20.0).

Now, to confirm the structural integrity. The mechanical properties for this vessel were determined in *Chapter 4.2.3*: $\sigma_y = 495$ MPa, $\sigma_u = 560$ MPa. Following DNV GL recommendations, the pressure vessel must resist at TDP without yielding, and at CDP without rupturing. In other words, the maximum stress of the vessel must be lower than the material yield strength at TDP, and lower than the material ultimate strength at CDP. The maximum stress appears at compression, with $P3_{TDP} = 352.2$ MPa and $P3_{CDP} = 470.1$ MPa. Calculating the respective Margins of Safety, the structural integrity of the model is confirmed – *Table 4.16*. As stated in *Chapter 4.2.1* the vessel appears to be over-dimensioned and reducing the shell thickness is most likely a possibility.

Table 4.16. Margins of Safety verified for the SCC pressure vessel

Pressure [MPa]	**Stress (max)** [MPa]	$MS = \dfrac{material\ strength}{\max stress \cdot SF} - 1$
NDP = 15.22	293.2	0.69
TDP = 18.26	352.2	0.41
CDP = 24.35	470.1	0.19

By checking the contact status, sealing is also confirmed. The contacts status analysis reported a continuum region across the vessel-cap contact interface, meaning that shell deformation would not affect the watertightness of the vessel - *Figure 4.23*. Due to a less refined mesh, this continuum region was not reported in the main body as well, but as previously stated, this is a visualisation disparity due to a less refined mesh in the main body. According to O-ring manufacturers [100], sealing systems can continue to operate normally until a maximum elastic deformation of 2.5% of the groove radius. The maximum model deformation is 0.353 mm, so the maximum deformation is way below this limit (0.37%) and watertightness failure is not expected to occur.

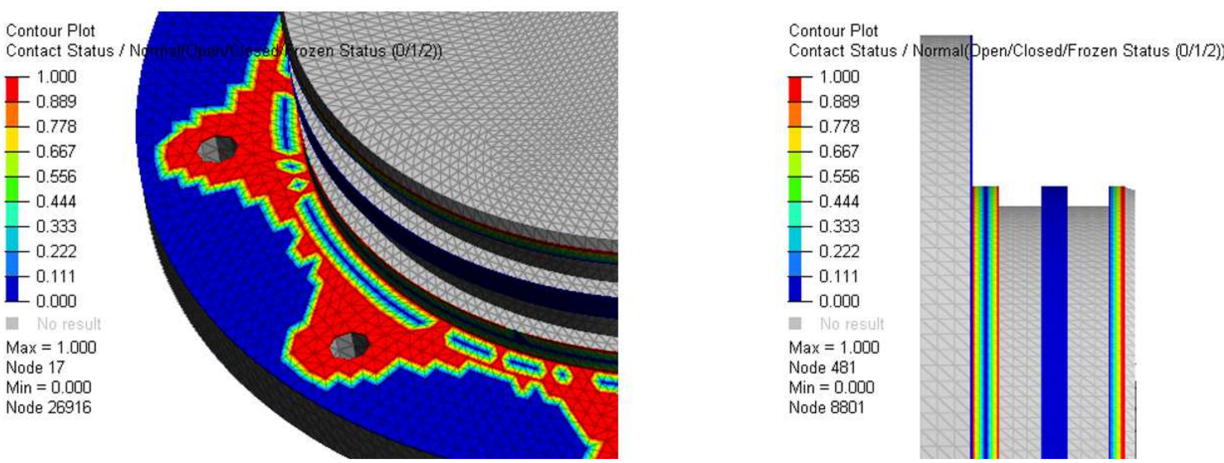

Figure 4.23. Contact status on the surface elements of the cap: a value of 0 means the contact is open, while a value of 1 means the contact is tightly closed.

4.2.5 SCC Flange influence

It was decided to design the SCC model with a flange, but other solutions must also be addressed. To determine if these are better options, two vessels with similar main body and cap configurations, but with different flange designs, were modelled. The first used a filleted flange vessel, while the second followed a no-flange design. Some changes were required, mostly on the no-flange design, which requires radially tapped bolts, so the internal length of the cap had to be increased, and so did the external vessel length, to maintain the internal volume constant. The full geometric description of both models can be found in *Appendix D*.

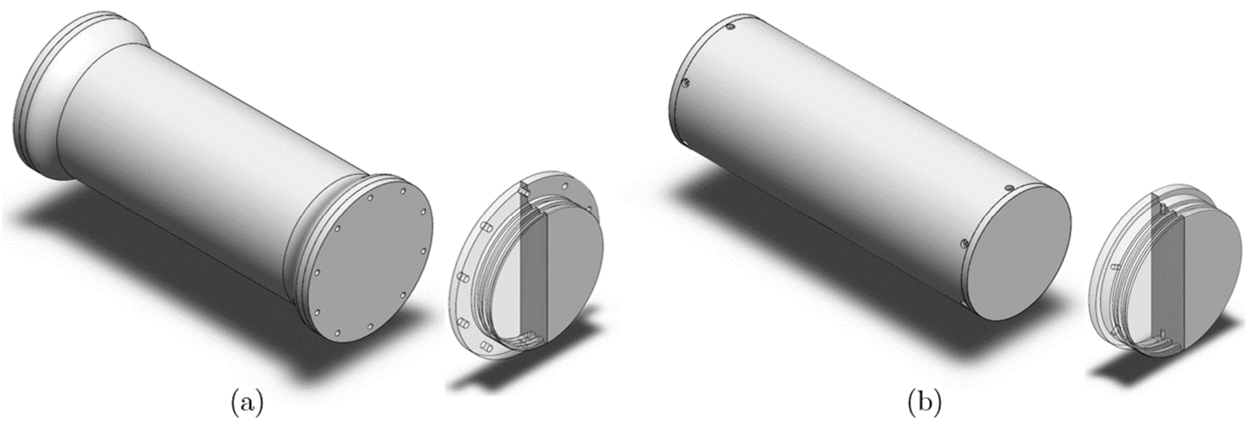

Figure 4.24. Different flange configuration models: (a) filleted flange configuration and cap; (b) no-flange configuration and cap.

Once again, two types of analysis were used: a nonlinear quasi-static (NLQS) analysis and a linear buckling analysis. The load collector is the same as well, but since the goal is to compare these vessels to the SCC model, only NDP was considered. Results of both these vessels are displayed in *Table 4.17*, together with the previously reported results for the flange vessel, and stress analysis results for both these models are also displayed below - *Figure 4.25*, with the filleted flange model on the left, and the no-flange model on the right.

Table 4.17. FEA results at NDP of maximum displacement, stress and buckling pressure for SCC models using alternative flanges

Flange configuration	**u [mm]**	**VM [MPa]**	**P1 [MPa]**	**P3 [MPa]**	**n**	**P_{cr} [MPa]**
flange	0.353	209.5	243.6	293.2		37.07
Filleted flange	0.342	209.9	232.8	258.2	3	39.40
No-flange	0.313	309.4	236.6	425.3		40.02

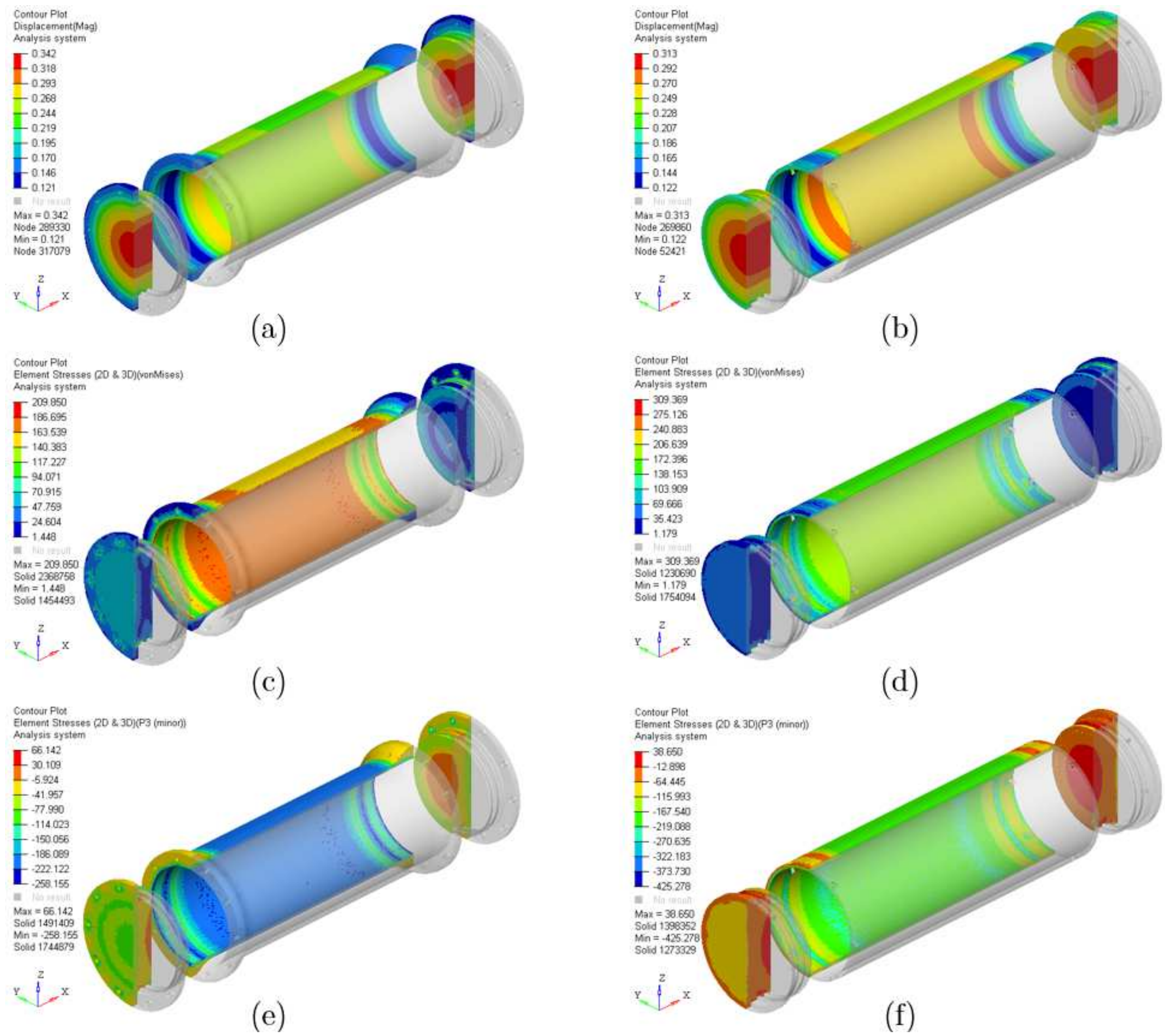

Figure 4.25. different flanged vessels at NDP - FEA results: (a) filleted flange vessel displacement; (b) no-flange vessel displacement; (c) filleted flange vessel Von Mises stress; (d) no-flange vessel Von Mises stress; (e) filleted flange vessel compression (P3) stress; (f) no-flange vessel compression (P3) stress.

Displacement is maximum in the plane face of the cap, and decreases for the models with smaller flanges, due to a more compact cap. This change is especially noticeable for the no-flange model, something to expect given the internal cap length increase – *Figure 4.25 (a), (b).* Stress is larger in the contact region, and when this region is excluded, all models present similar results, within a 1% variation, further confirming that the main body shell stress can be estimated independently of the cap and flange configuration. However, the no-flange model has large stress accumulations around the tapped hole, where the Von Mises stress is maximum and ~100 MPa higher than in the rest of the model - *Figure 4.25 (d).* It is concluded that this configuration can be prone to bolt bending due to shear stresses. The maximum stresses appear at compression - *Figure 4.25 (e), (f)*, but the filleted flange reports an 11.9% decrease compared to the flange vessel.

To check for structural integrity, the same mechanical properties of the SCC model were used, σ_y = 495 MPa, σ_u = 560 MPa. Maximum stress appears at compression for all three models, and were used to calculate the Margins of Safety (MS) in *Table 4.18.* The no-flange vessel MS is negative for both TDP and CDP, meaning this model does not fulfil the DNV GL criteria of safety. A better dimensioning of the bolt configuration is required, either by considering an additional number of bolts or increasing the wall thickness on the socket bolt groove. Regarding the filleted flange vessel, since compression stress is smaller when compared to the flange vessel, the MS increases.

Table 4.18. Margins of Safety verified for the SCC models with alternative flanges

	Filleted flange vessel		**No-flange vessel**	
Pressure [MPa]	**Stress (max) [MPa]**	**MS**	**Stress (max) [MPa]**	**MS**
NDP = 15.22	258.2	0.92	425.3	0.16
TDP = 18.26	309.8	0.60	510.3	-0.03
CDP = 24.35	413.0	0.36	680.4	-0.18

Regarding the weight and buoyancy equilibrium, the mass and weight were determined below in *Table 4.19.* The total weight of the filleted flange vessel increases, mostly due to the filleted transition added, while the weight of the no-flange vessel decreases. The buoyancy was calculated considering a fluid density ρ_f = 1.03516 g/cm^3, corresponding to B = 233.2 N and B = 228.1 N, respectively. The weight net force was determined to be, respectively, 33.7 N and 43.4 N.

Table 4.19. Mass and weight of models with alternative flanges

	Filleted flange vessel		**No-flange vessel**	
Components	**Mass [kg]**	**Weight [N]**	**Mass [kg]**	**Weight [N]**
Main body	10.8	106.0	8.7	84.9
End cap	4.6	45.3	5.0	49.1
Fastening components	0.3	2.9	0.2	1.6
Total	20.4	199.5	18.9	184.7

This study concludes that the no-flange vessel is inadequate for the mission parameters, despite being the lighter model. The use of a filleted flange increases vessel weight, but considerably increases the margin of safety. So, this model was considered adequate for the mission parameters and will be compared to all the models in development, since it offers an adequate trade-off between overall vessel weight and an increase in the mechanical properties.

4.3 RTV - Radial Thickness Variation Vessel Design

The RTV family of pressure vessels is defined as unstiffened, cylindrical shells with a sinusoidal thickness variation radially around the cross-section. This geometry was described by Tsouvalis et al. [74] in a paper previously discussed in *Chapter 2.3.3*. It was decided to further analyse this solution since if suitable for the current model, it can increase the buckling critical pressure without changing the vessel weight. Firstly, this paper was studied and characterized, and from it, a simplified 2D shell analysis similar to the one described by Tsouvalis et al. was conducted but considering a vessel with similar geometric dimensions of the shells previously developed.

4.3.1 Parametric study characterization

Tsouvalis et al. [74] analyses the effect of geometric imperfections purposefully designed to increase the structural strength of composite laminated cylinders. It was based on previous studies, which had shown that some types of initial imperfections, when deliberately introduced, increase the buckling critical pressure. The study considered a carbon/epoxy cylinder with internal radius R = 100 mm, vessel length L = 400 mm and thickness t = 10 mm. Two types of geometrical imperfections are considered: Type 1, a global shape imperfection of elliptical cross-section with constant thickness; and Type 2, a more localized thickness imperfection, with constant internal radius and sinusoidal thickness variations in the circumferential direction - *Figure 4.26*.

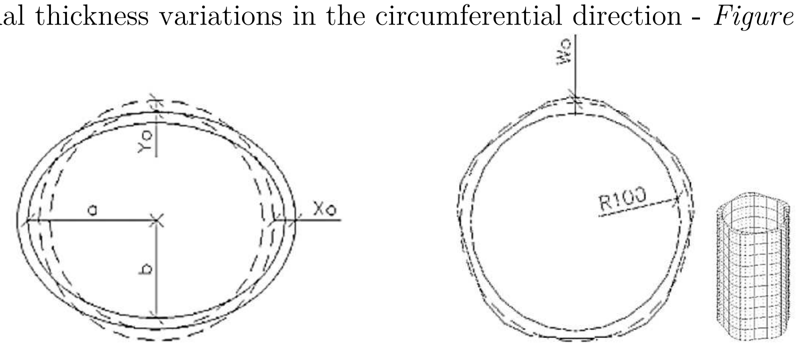

Figure 4.26. Imperfections described in Tsouvalis paper: Type 1 imperfections on the left; Type 2 imperfections on the right (N_w=5). Adapted from [74].

Type 1 imperfections are defined by X_0 and Y_0, which describe the out of circularity of this family of vessels in reference to a nominal mean radius R_m, while the wall thickness remains constant. Four cylinders were considered with a maximum imperfection X_0 equal to 0.1, 1, 5 and 10 mm, corresponding to an X_0/t ratio of 0.01, 0.1, 0.5 and 1, respectively.

Buckling loads are calculated using a non-linear analysis - *Table 4.20*. Cylinders with the smallest initial imperfections, X_0/t=0.01 and X_0/t=0.1, increase the buckling pressure. The deflected mode shape of all cylinders was n=2, so buckling deformation followed the shape of their initial imperfections, something the author concluded that contributes to increasing the buckling strength.

Table 4.20. Buckling loads of Type 1 cylinders. Adapted from [74]

X_0/t	Pcr [MPa]	Deflected shape
0	41.6	n=3
0.01	59.6	n=2
0.1	54.1	
0.5	34.7	
1.0	22.2	

Type 2 imperfections have a constant internal radius of 100 mm, and the thickness varies sinusoidally with a mean value of 105 mm. These imperfections are defined by N_w, the number of sinusoidal waves, and W_0, the maximum deviation of the external surface from the nominal external radius of the perfect cylinder, $R_{out} = 110$ mm. Three sets of cylinders were studied, with $N_w = 2$, 3 and 4, and each set considers 4 imperfections, with $W_0 = 0.1$, 1, 2.5 and 5 mm.

The results are displayed in *Table 4.21*. Starting with the N_w=2 family, buckling strength increases for W_0/t=0.01 and W_0/t=0.1, which is associated with a deflected shape of n=4. Buckling behaviour of N_w=3 family is completely different, where all cylinders present a n=3 mode shape, the same of the perfect cylinder, and P_{cr} decreases for most models. The family of N_w=4 presents similar results seen in N_w=2, but the increase of buckling strength is even greater for the first models, and the mode shape $n = 4$ tends to follow the initial imperfection as well.

Table 4.21. Buckling loads of Type 2 cylinders. Adapted from [74]

N_w	W_0	W_0/t	Pcr [MPa]	Deflected mode shape
0	**0**	**0**	41.6	n=3
2 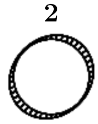	**0.1**	**0.01**	57.8	n=2
	1.0	**0.1**	50.6	
	2.5	**0.25**	37.5	
	5.0	**0.5**	19.5	
3 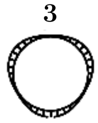	**0.1**	**0.01**	42.8	n=3
	1.0	**0.1**	38.7	
	2.5	**0.25**	33.9	
	5.0	**0.5**	23.1	
4 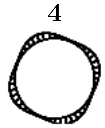	**0.1**	**0.01**	57.2	n=4
	1.0	**0.1**	53.8	
	2.5	**0.25**	46.8	
	5.0	**0.5**	34.4	

This study concludes that well-controlled geometric imperfections may result in the increase of buckling strength, and that this increase appears when these imperfections contribute to the propagation of a different buckling mode shape from the one predicted for a perfect cylinder, and this mode shape tends to follow the cross-section configuration of these imperfections [74].

4.3.2 RTV simplified shell analysis

A simplified shell FEA study was performed to analyse the influence of these small imperfections on the shell under study. Only Type 2 imperfections were analysed, since it is simpler to produce a tight-dimensioned cross-section with thickness variation than precise out-of-circularity elliptical cross-sections with constant thickness. The geometry of these models are defined by the same parametric equations given by Tsouvalis et al. – *Formula (4.5)*. The shell defined by these sinusoidal curves do not increase the cross-section area, so the weight will be the same. In a cartesian coordinate system, with x being the cylinder axis of symmetry, the external surface of the shell is given by:

$$y = \left(R + t + \frac{W_0}{2}\sin(N_w\theta)\right)\cos(\theta),\ 0 \le \theta \le 2\pi$$
$$z = \left(R + t + \frac{W_0}{2}\sin(N_w\theta)\right)\sin(\theta),\ 0 \le \theta \le 2\pi \tag{4.5}$$
$$x = x$$

Four sets of cylinders were studied, $N_w = 2, 3, 4$ and 5, and for each set, four thickness variations were selected, $W_0 = 0.5, 1.0, 2.0, 4.0$ mm, making up to 16 models - *Figure 4.27*. The SCC simplified shell acts as the reference cylinder: $R = 100$ mm, $L = 500$ mm, $t = 8.0$ mm. The deviation-thickness ratio is $W_0/t = 0.06, 0.13, 0.25, 0.5$, respectively. This ratio is higher than the one observed in Tsouvalis paper, something necessary to make the manufacture possible, since unlike that model, this one considers an aluminium alloy that must be machined.

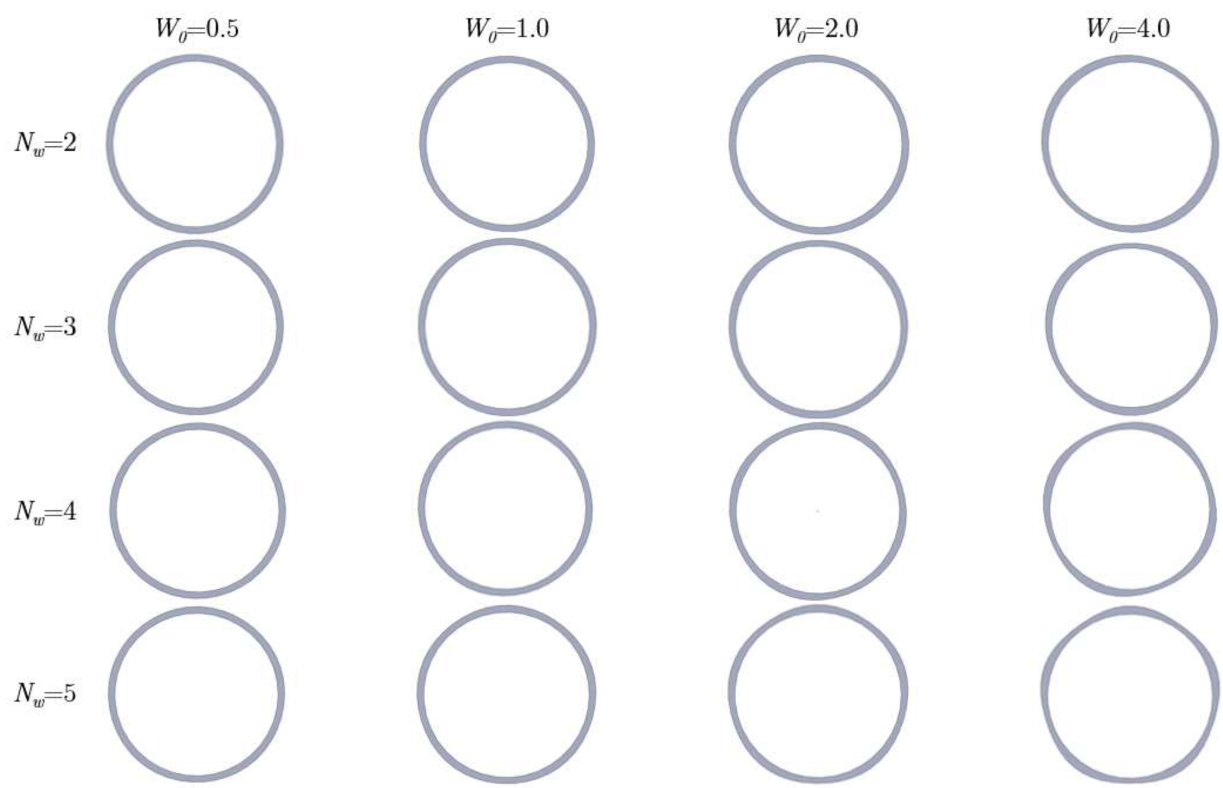

Figure 4.27. RTV family of vessels: cross-section view.

A linear static analysis at NDP was used for the element stresses, and a linear buckling analysis was used for the critical buckling pressure. Due to the irregular cross-section shell thickness, it was necessary to use 3D CTETRA elements. The model was meshed with an element size of 4 mm, and these results were compared to an equivalent meshed unstiffened shell - *Table 4.22*.

Table 4.22. FEA results at NDP of maximum stress and buckling pressure of RTV cylinder shells

N_w	W_0	W_0/t	VM Stress [MPa]	Pcr [MPa]	Deflected mode shape
0	**0**	**0.0**	190.5	35.39	n=3
2	**0.5**	**0.06**	193.6	35.81	n=3
	1.0	**0.13**	199.1	35.49	
	2.0	**0.25**	208.5	34.39	
	4.0	**0.50**	258.7	30.69	
3	**0.5**	**0.06**	232.7	37.71	n=3
	1.0	**0.13**	235.1	37.28	
	2.0	**0.25**	226.1	34.51	
	4.0	**0.50**	311.2	30.70	
4	**0.5**	**0.06**	194.5	36.01	n=3
	1.0	**0.13**	199.5	35.63	
	2.0	**0.25**	230.9	35.01	
	4.0	**0.50**	323.1	32.61	
5	**0.06**	**0.06**	194.6	35.78	n=3
	0.13	**0.13**	200.1	35.18	
	0.25	**0.25**	235.9	33.31	
	0.5	**0.50**	330.1	27.85	

This analysis does not observe the same results as the ones described by Tsouvalis et al. More importantly, the deflected mode shape does not change for different N_w values, so the described buckling pressure increase could not be inferred for these models. P_{cr} does appear to increase for smaller imperfections, but not in as a significant way. This can be due to the use of a different material, quite different of a laminar composite material, or due to a larger L/t ratio, or even from using a FEM analysis with distinct parameters.

This analysis shows an increase of buckling critical pressure only for W_0 = 0.5 mm models. However, this increase is not as significant as the one reported by Tsouvalis, and even the higher P_{cr} = 37.71 MPa seen for N_w = 3; W_0 = 0.5 mm, only increases by 6.6%. Checking for stress, it increases for all model, and the model which reported the largest P_{cr} improvement has a 22.6% shell stress increase, an unreasonable trade-off to make. Since the structural integrity does not appear to increase with the addition of small shells imperfections as expected, the RTV family of vessels was discarded from further studies and no detailed vessel was modelled.

4.4 ATV - Axial Thickness Variation Vessel Design

The ATV family of pressure vessels is defined as unstiffened cylindrical shells with a sinusoidal thickness variation in the axial direction. This proposed solution was derived from studies on stress distribution across corrugated vessels, which reports an increase of the critical buckling pressure. Firstly, the geometry is explained, and the proposed solution is characterized. Then, a simplified shell analysis was performed to check its validity. From these results, a detailed model was validated.

4.4.1 Geometric solution characterization

Ross [93] describes the use of a corrugated pressure vessel built in a pattern of 3 repetitive regions: one where the shell thickness is at its largest (the "plateau"), one where its smallest (the "valley"), and an intermediate region where it varies linearly (the "slope") - *Figure 4.28.* This contradicts the buckling mode shape in a similar way of how ring stiffeners work to prevent instability. In his study, two manned submersible hulls are built and compared with an equivalent, ring-stiffened model. These results displayed in *Table 4.23* show a 42% and 76% increase of buckling resistance, respectively. Ross concluded that this design increases buckling resistance [26].

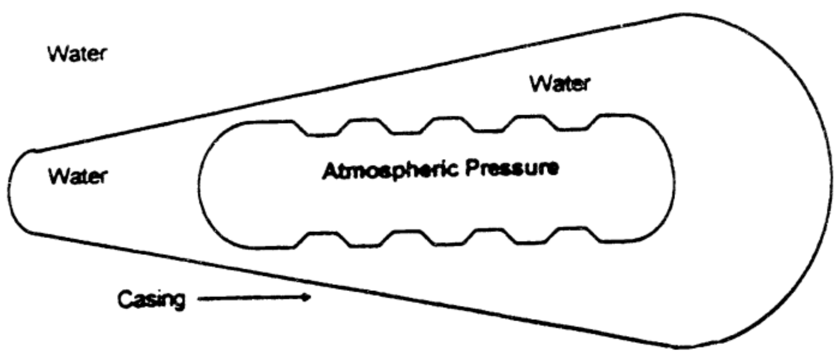

Figure 4.28. Ross corrugated circular cylinder [93].

Table 4.23. Buckling pressures of two swedged vessel design and their ring-stiffened vessel equivalents [26]

Geometry 1: L= 11m; t=3 cm; R_1=2m; R_2=2.5m		**Geometry 2:** L= 11m; t=6 cm; R_1=4.5m; R_2=5m	
Swedged Vessel	Ring-Stiffened Vessel	Swedged Vessel	Ring-Stiffened Vessel
3.6 MPa	2.5 MPa	4.3 MPa	2.4 MPa

This geometry was developed for manned submersible hulls, where the internal diameter does not have to be constant to allow for the volume to be fully used. In a small-sized pressure vessel, this solution would result in a loss of internal useful volume. So, it was taught of ways that Ross's models could be adapted for a geometry with constant internal diameter - *Figure 4.29*.

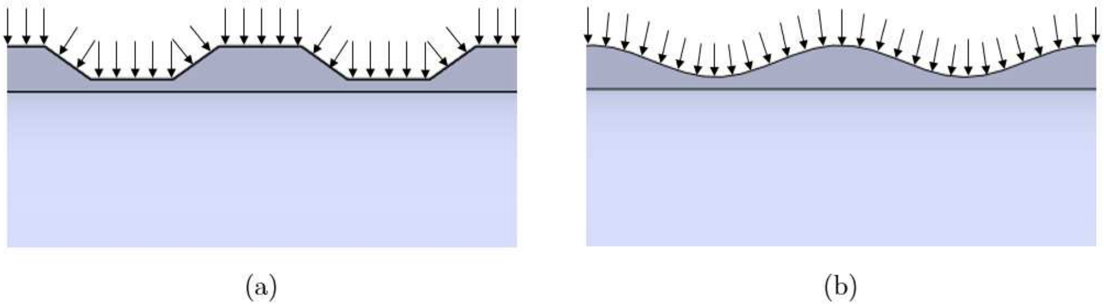

Figure 4.29. Adaptation of a corrugated shape for pressure vessels:
(a) Ross proposed geometry; (b) equivalent sinusoidal surface geometry.

A first iteration simply considered to keep the external corrugated shape for a constant internal cross-section diameter - *Figure 4.29 (a).* However, this would result in a large area where the shell thickness would be minimum, which would undoubtedly result in shell plastic failure. So, it was adapted to a repeating sinusoidal patterned surface, so a similar stress distribution to the one observed by Ross is seen, while reducing the zone with minimum thickness - *Figure 4.29 (b).*

4.4.2 ATV simplified shell analysis

As a first step, a simplified FEA analysis was performed to study for structural integrity. The surface configuration was defined using *Equation (4.6)*, which introduces 2 variables: the number of sinusoidal waves, N_w, and the sinusoidal amplitude from the external surface of the cylinder, W_A.

$$y = W_A \cos\left(\frac{Nw}{L/2}\,\pi\, x\right), \qquad 0 < x < L \tag{4.6}$$

Four different sets were studied, N_w = 15, 20, 25 and 30, and for each set, three thickness variations were selected, W_A = 1.0, 2.0 and 4.0 mm, making up to 12 models - *Figure 4.30*. Large values of W_A are expected to result in higher stress, so W_A = 4.0 mm was discarded since it would result in a "valley" region with half the shell thickness. The mean thickness is t = 8.0 mm, and the vessel length is L = 500.0 mm, the same used in SCC models. The weight of these vessels reported only a 0.27% maximum deviation from the perfect cylinder and were assumed to be the same weight.

Two types of analysis were used: a linear static analysis and a linear buckling analysis. The parameters of these analyses were the same used previously. 3D CTETRA elements were used with a mesh size of 4.0 mm. Only the NDP is presented since the goal is simply to compare stress results to the standard vessel - *Table 4.24*.

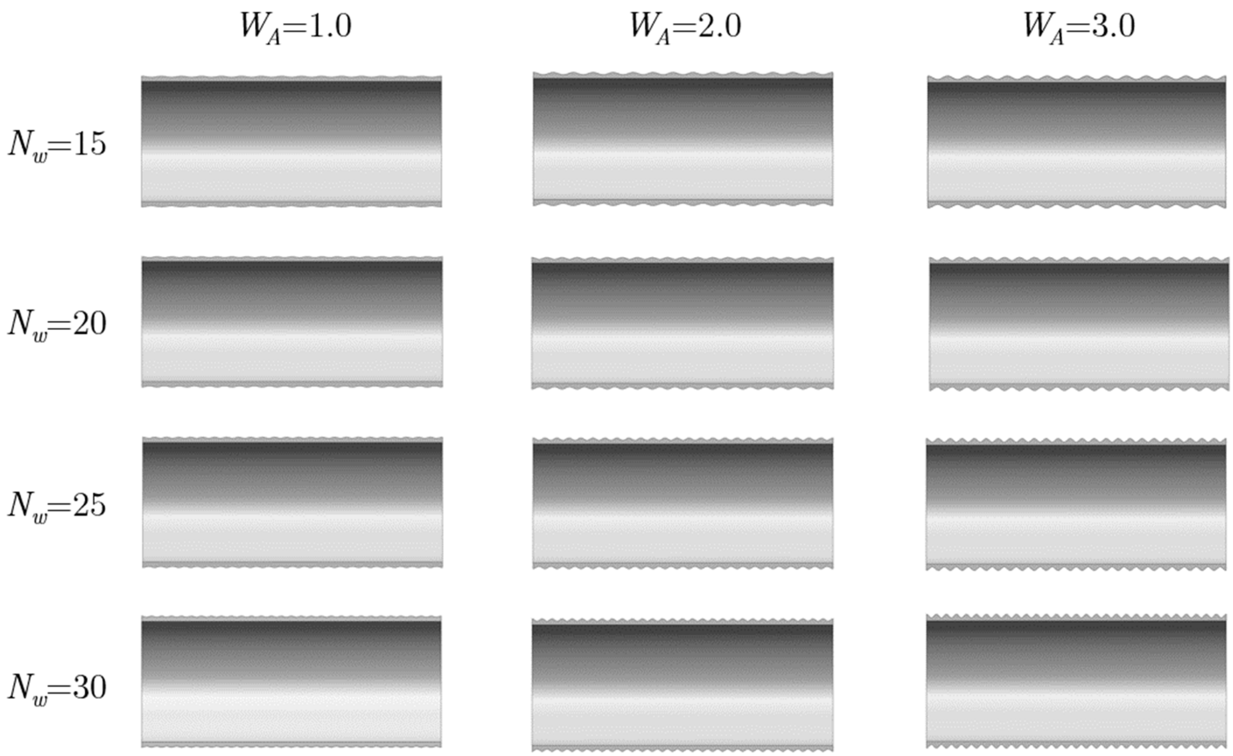

Figure 4.30. ATV family of vessels: front plane section view.

Table 4.24. FEA results at NDP of maximum stress and buckling pressure of ATV cylinder shells

N_w	W_A	W_A/t	VM stress [MPa]	Pcr [MPa]	Deflected mode shape
0	**0**	**0.0**	190.5	35.39	n=3
	1.0	**0.13**	193.9	41.58	
15	**2.0**	**0.25**	194.8	41.63	n=3
	3.0	**0.38**	252.3	44.93	
	1.0	**0.13**	192.4	41.40	
20	**2.0**	**0.25**	199.6	42.78	n=3
	3.0	**0.38**	268.8	45.37	
	1.0	**0.13**	192.5	41.35	
25	**2.0**	**0.25**	197.7	42.38	n=3
	3.0	**0.38**	218.6	44.48	
	1.0	**0.13**	192.0	41.28	
30	**2.0**	**0.25**	211.7	42.16	n=3
	3.0	**0.38**	225.3	46.18	

These results show an increase in shell stress for all models, which is maximum in the thinner thickness region - *Figure 4.31.* Stress also increases for values with a larger sinusoidal amplitude, and fairly similar results were reported for models with similar amplitudes, despite having a different total of sinusoidal waves. This is especially noticed for models with W_0 = 1.0 mm, where the same stress is reported across the different sets.

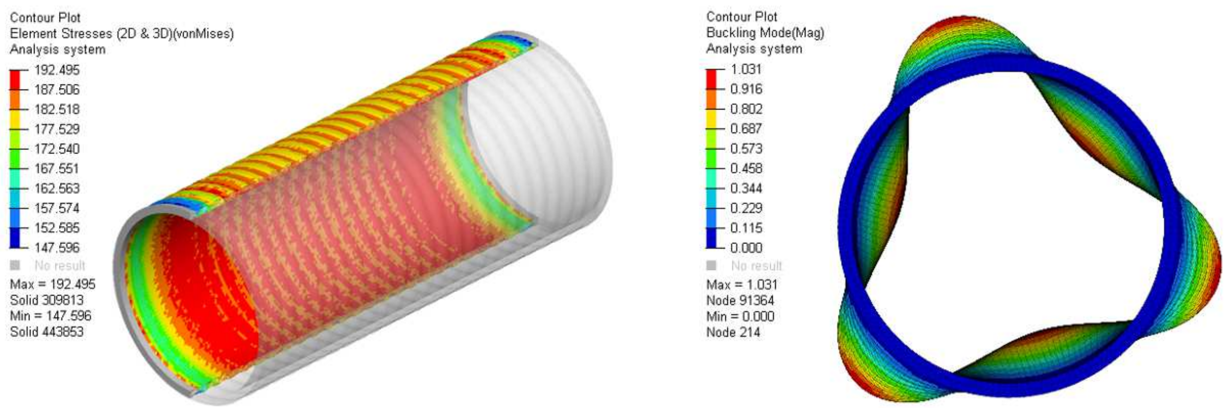

(a) (b)

Figure 4.31. ATV shell with N_w=25; W_0=1.0 – FEA results: (a) NDP Von Mises stress analysis; (b) First buckling mode, n=3 (deformation multiplier of 30.0).

Buckling stress is reported to increases for all models. The results are consistent across different sets of N_w and appear to increase with W_0. This increase is not as significant as reported by Ross. However, Ross's models considered not only a different configuration, but the dimensions were much larger. So, it is concluded that an increase of buckling pressure may be possible without increasing the overall weight of the vessel, while it does increase the element stress across the shell. This trade-off seems a valid option for certain mission parameters, and so it was decided to continue the development of this concept.

4.4.3 ATV detailed model design and analysis

It was decided to analyse the $W_0 = 2.0$ mm set for all four N_w configurations as a good balance between buckling strength and stress increase. All design variables and principal geometric dimensions were imported from the SCC vessel: $L = 500$ mm, $R = 100$ mm, $t = 8$ mm. Since the axial thickness variation does not affect the remaining geometric configurations, the same cap and fastening components were used. All the components were assembled and rendered in *Solidworks* to preview the proposed pressure vessel - *Figure 4.32*.

Two types of analysis were used: a nonlinear quasi-static (NLQS) analysis to determine the displacements and stress load functions, considering an inertia relief-based boundary conditions; and a linear buckling analysis to estimate the critical buckling pressure of the full model, considering a three in-plane SPCs boundary conditions. The vessel was modelled following the same parameters previously discussed. These analyses results are displayed in *Table 4.25*.

Figure 4.32. Rendered image of the ATV pressure vessel, $N_w = 25$.

Table 4.25. FEA results at NDP of maximum displacement, stress and buckling pressure for the ATV family of vessels

N_w	u [mm]	VM [MPa]	P1 [MPa]	P3 [MPa]	n	P_{cr} [MPa]
15	0.410	248.3	301.2	333.2	2	39.31
20	0.410	239.8	302.7	321.7		40.15
25	0.409	229.2	304.2	298.5		38.94
30	0.408	239.3	302.3	305.1		40.31

These analyses show a close correlation of stress and buckling pressure for all models, where an increase of N_w does not seem to affect extensively the maximum Von Mises stress. By analysing the main body elements excluding the contact region it is verified that stresses are close to the simplified shell estimation, averaging at 203 MPa. All models show a positive increase of buckling strength, while also reporting an increase of shell thickness. It was decided to select the $N_w = 30$ set to represent the ATV family of vessels, since it is the one displaying the highest increase of critical buckling pressure. - *Table 4.26, Figure 4.33.*

Table 4.26. FEA results of maximum displacement, stress and buckling pressure for the ATV vessel

Pressure [MPa]	**u [mm]**	**VM [MPa]**	**P1 [MPa]**	**P3 [MPa]**	**n**	**P_{cr} [MPa]**
NDP = 15.22	0.408	239.3	302.3	305.2		
TDP = 18.26	0.490	287.2	362.8	366.2	2	40.31
CDP = 24.35	0.653	382.9	483.7	488.3		

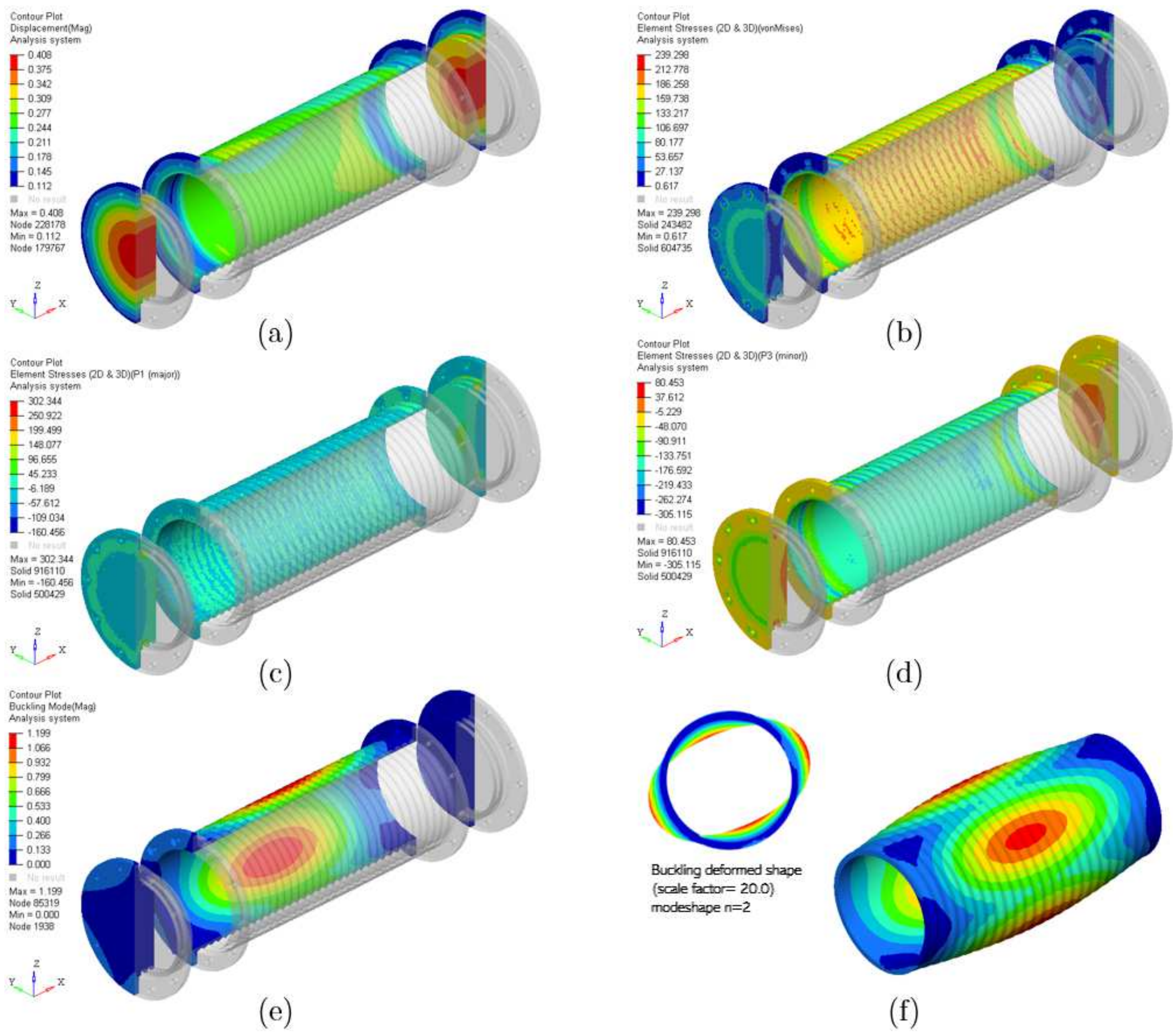

Figure 4.33. ATV vessel at NDP - FEA results: (a) displacement; (b) Von Mises stress; (c) tension stress (P1); (d) compression stress (P3); (e) Buckling undeformed shape; (f) Buckling mode shape (scale factor=20.0).

Comparing with the SCC vessel, the critical buckling pressure increases to 47.30 MPa, which represents an 8.0% increase. Associated with this increase is a different buckling mode shape, where now the deformation tends to an eigenvalue of n=2 lobes. Von Mises stress increases by 12.4%. However, the compression stress results are not as divergent, and a smaller 3.9% increase is verified.

Structural integrity safety calculations were made for $\sigma_y = 495$ MPa and $\sigma_u = 560$ MPa. The maximum stress appears at compression, $P3_{TDP} = 366.2$ MPa and $P3_{CDP} = 488.3$ MPa. The characteristic margins of safety are calculated in - *Table 4.27*. So, it is concluded that the ATV vessel configuration optimizes buckling strength without compromising the structural integrity at the considered safety factors. It is confirmed that this concept offers a trade-off between bucking strength and axisymmetric yielding strength.

Table 4.27. Margins of Safety verified for the ATV pressure vessel

Pressure [MPa]	**P3 (max) [MPa]**	$MS = \frac{material\ strength}{\max stress \cdot SF} - 1$
NDP = 15.22	305.2	0.62
TDP = 18.26	366.2	0.35
CDP = 24.35	488.3	0.15

Regarding the overall weight and buoyancy, the pressure vessel mass and weight were determined to be 19.8 kg and 193.8 N respectively - *Table 4.28*. The buoyancy was calculated considering $\rho_f = 1.03516$ g/cm^3, $V_{disp} = 22\ 763.9$ cm^3, $B = 230.9$ N - *Formula (2.3)*. This results in a positive net force of 230.9 − 193.8 = 37.1 N, so the vessel can carry up to 3.8 kg of payload, the same value calculated for the SCC vessel.

Table 4.28. Volume, mass and weight of the ATV pressure vessel

Components	**Volume [cm^3]**	**Mass [kg]**	**Weight [N]**
Main body	3482.7	9.7	95.4
End cap	1729.8	4.8	47.4
Fastening components	-	0.4	3.6
Total	6942.5	19.8	193.8

Finally, the contact status were checked. The analysis reported a continuum region across the vessel-cap contact interface, meaning watertightness is confirmed as well - *Figure 4.34*.

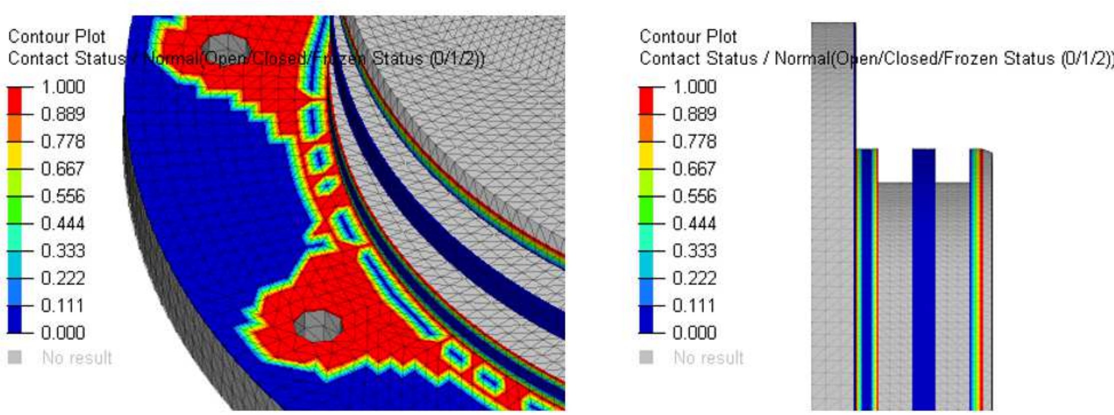

Figure 4.34. Contact status on the surface elements of the ATV cap: a value of 0 means the contact is open, while a value of 1 means the contact is tightly closed.

4.5 NCS – Noncircular Cross Section Vessel Design

The NCS family of pressure vessels is defined as stiffened cylindrical shells with a noncircular cross-section, which increases the usefulness of the internal volume for the same absolute value. Firstly, similar papers were studied to establish an understanding of this geometry based on the structural similarities. Then, a parametric study on the influence of squared cross-section shapes in shell stress was conducted to select an adequate cross-section configuration. Then, several simplified models were modelled in an iterative process to optimize the simplified shell, and following these conclusions, a detailed noncircular cross-section vessel was validated.

4.5.1 Geometric solution characterization

Adopting a noncircular cross-section in pressure vessel design has a great advantage in terms of increasing the internal useful volume: Since the inner geometric configuration is better suited for the used payload, a squared vessel would be able to fit more payload than a cylindrical vessel with the same absolute volume. This concept is the only solution found to achieve the main optimization goal of the present thesis. However, squared vessels are drastically more prone to fail under pressure conditions than their curved or spheric counterparts. To study the behaviour of noncircular pressure vessels, similar papers were consulted. Since no papers reporting prismatic vessels under external pressure conditions were found, papers referring to internal pressure conditions were used. The ASME Boiler & Pressure Vessel Code, Section VIII Appendix 13 [101] includes design rules for prismatic vessels of infinite length. Blach et al. [102] proposed new design rules based on the ASME Code, but for shells of finite length. Revani et al. [103] reported the development of a prismatic vessel with an internal plate stiffener using a finite element method approach. Lee et al. [104] proposes design principles of a finite-length prismatic vessel constructed only out of plane surfaces.

As reported by Lee et al. [104], the volume efficiency of a prismatic vessel can be as high as 30% compared to a cylindrical equivalent - *Figure 4.35*. This increase is quite relevant in the scope of the present objective, but it was concluded for fluid-carrying vessels, so a more adequate comparison will be required to determine the useful volume of payload-carrying vessels.

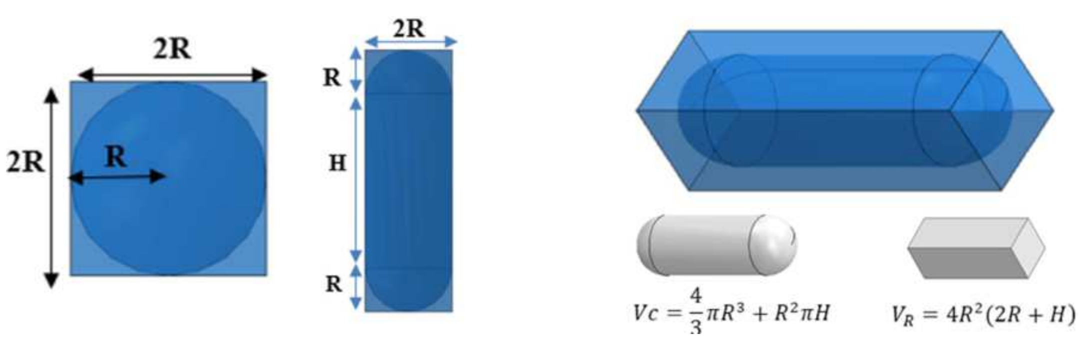

Figure 4.35. Volume efficiency comparison between cylindrical and prismatic vessels with identical dimensions. Adapted from [104].

The ASME Boiler & Pressure Vessel Code, Section VIII *"Rules for Construction of Pressure Vessels"* [85] includes in Appendix 13 design rules for several designs of infinitely long prismatic pressure vessels, which have been used widely as the main reference for vessels with this configuration [86]. It states that unlike conventional cylindrical vessels where the membrane stress is dominant and bending can be ignored, this is not the case for a noncircular pressure vessel. The total stress comes as the sum of the membrane and bending stresses, and both must be considered. In fact, it is expected for the bending stress to be way more significative than the membrane stress. Lee et al. [104] analysed the stress distribution in equivalent cylindrical and prismatic pressure vessels - *Figure 4.36*. The maximum membrane stress was the same for both models, ~10 MPa, but the maximum bending stress for the prismatic vessel was 189 MPa.

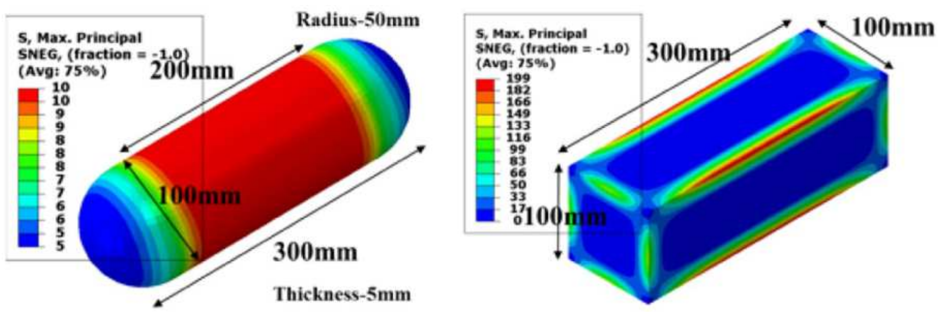

Figure 4.36. Comparison of equivalent cylindrical and prismatic vessels [104].

Lee et al. concludes that the maximum principal stress in these vessels will appear in the midpoint of the longest edge, the place where bending is at its maximum. Lee also refers that to make the model viable, stiffeners would be required to reduce the maximum bending stress, and a similar conclusion can be inferred for pressure vessels under external pressure.

Also in the ASME Code Appendix 13, several types of noncircular vessels are described. The cross-section displayed in *Figure 4.37. (c)* was promising, since it avoids creating live edges, which are zones where bending stress is likely to concentrate. In this code, several design formulas are also provided to estimate the membrane and bending stress on the shell, including situations under external pressure conditions. However, all formulas are for an infinitely long vessel only under radial pressure. Several papers report the determination of equations for finite-length vessels, Blach et al. [102], Lee et al. [104], Zeng et al. [105], but none are referent to the filleted corner cross-section.

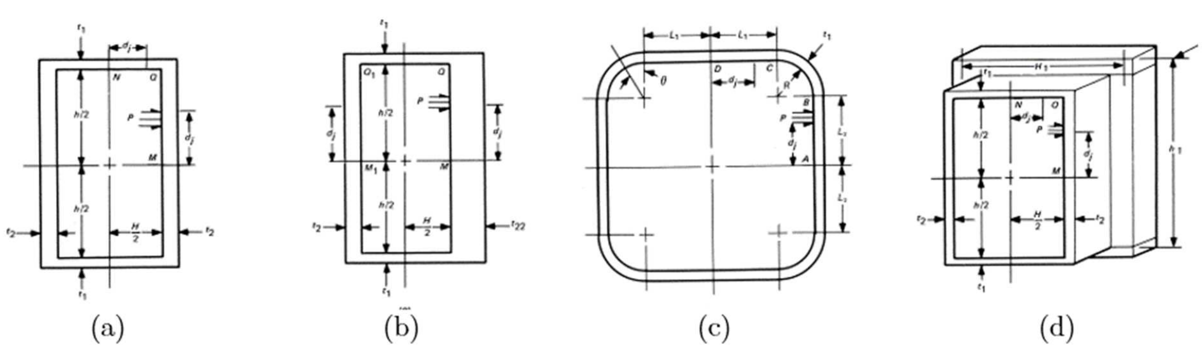

Figure 4.37. ASME Code VIII Appendix 13 vessel types: (a) equal thickness vessel; (b) different thickness vessel; (c) vessel with corners bent to a radius; (d) stiffened-reinforced vessel.

4.5.2 Simplified quadrature study

The cross-section configuration seen in *Figure 4.37 (c)* was selected as the NCS-defining geometry. The filleted corners allow for better stress distribution, and a perfectly squared vessel would need a far too thick shell. This introduces the fillet radius, R_f, as a new geometric variable. Models are to be dimensioned with the same vessel length and internal volume used in the simplified shells of the SCC family of vessels. The influence of a noncircular cross-section on the shell is to be analysed via a parametric study with consequent decrements of the fillet radius, going from the perfect cylinder to the perfect square. It is important to remember that despite the internal volume remaining unchanged, the usefulness of this space will increase. The internal cross-section area is given by R_f = fillet radius, and L_s = straight side length - *Equation (4.7)*. To have the same volume as the standard shell, their cross-section areas must be equal - *Equation (4.8)*. So, L_S can be defined as a function of R_f and R - *Equation* (4.9).

$$A_{NCS} = {L_s}^2 + 4\,R_f\,L_s + \pi\,{R_f}^2 \tag{4.7}$$

$$A_{NCS} = A_{SCC} = \pi R^2 \tag{4.8}$$

$$L_s = -2R_f + \sqrt{{R_f}^2(4-\pi) + \pi R^2}, \qquad L_s > 0 \tag{4.9}$$

To determine how adopting a squared cross-section affects structural failure, a parametric study was performed. Shells were modelled with a successively more squared configuration by reducing the fillet radius, from $R_f = R$, the shell of a perfect cylinder, up to a configuration which results in excessive structural failure. So, the study considers 6 sets of shell thickness, t_{NCS} = 8, 10, 12, 14, 16 and 18 mm, and for each set, the fillet radius decreases in 10 mm steps, R_f = 100, 90, 80, (...) mm until failure occurs -*Figure 4.38*.

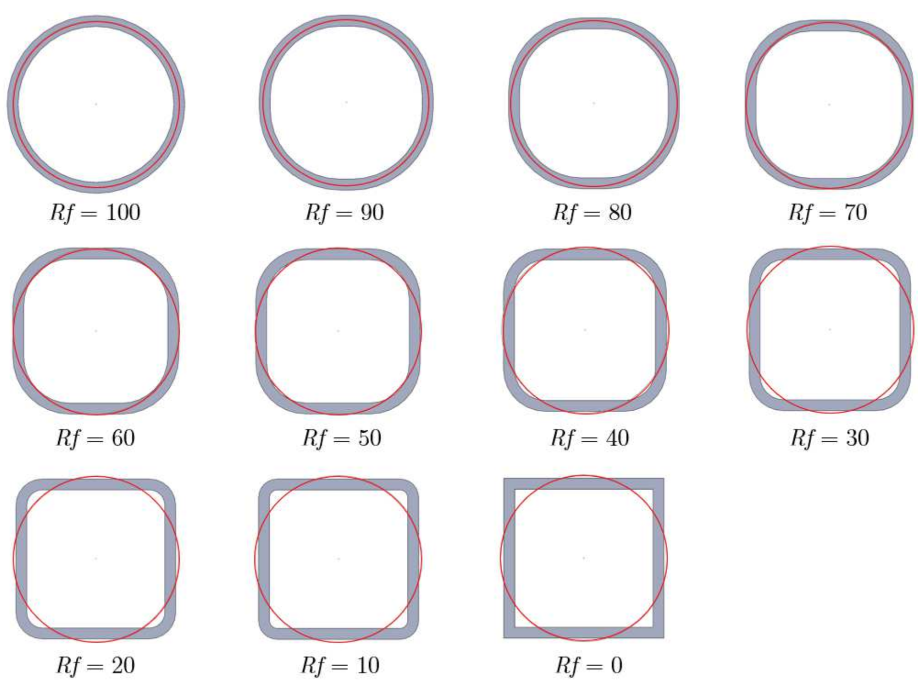

Figure 4.38. NCS family of shells – cross-section view.

Once again two types of analysis were used: a linear static analysis and a linear buckling analysis. Both 2D and 3D element types were used to check for congruence in results. It was only considered an analysis at NDP. The discrepancy of results between analyses reported an average of 4.0%, but since 2D shell element analysis are more accurate, these were the ones selected to present in the analysis below. However, both studies can be found in *Appendix C*. Shell stress appears to increase linearly with the increment of fillet radius - *Figure 4.39*. As expected, for each thickness set the vessel can withstand a more squared configuration.

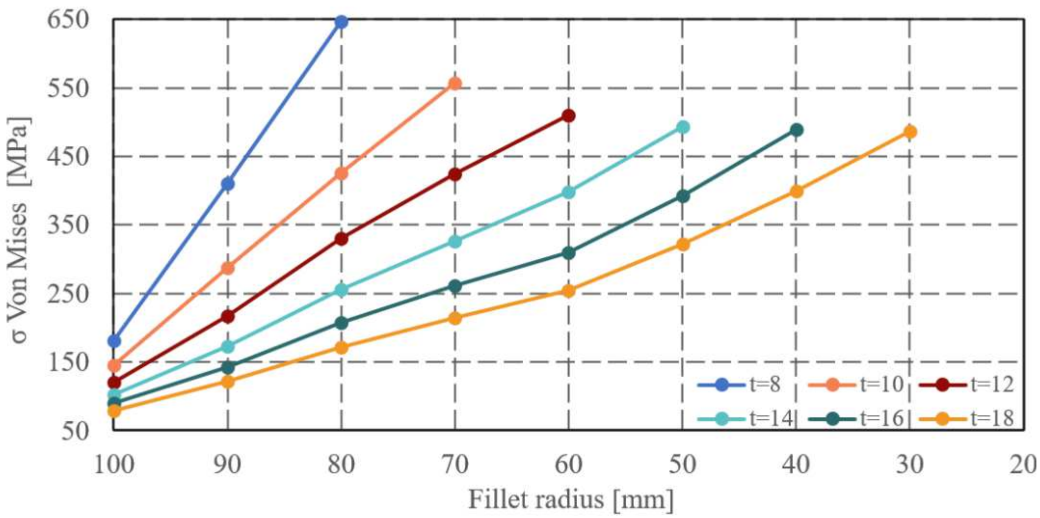

Figure 4.39. Shell stresses for different NCS vessel thickness sets.

Linear buckling analysis results show an increase of the critical buckling pressure with the increase of shell thickness, and a decrease with a more squared configuration - *Figure 4.40*. A relevant conclusion is that a more squared vessel with a thicker shell has a higher P_{cr} than the perfect cylinder with a shell thickness of 8 mm. This behaviour goes according to the expected, since buckling sensitivity is extremely sensitive to the thickness of the shell [26]. It can be concluded that axisymmetric yield failure is more likely to occur before critical buckling pressure is reached.

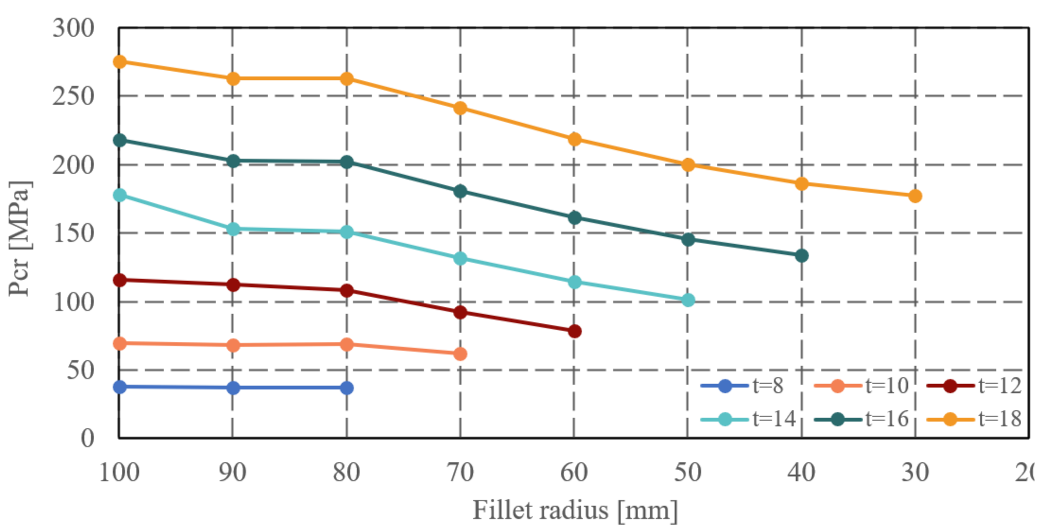

Figure 4.40. Critical buckling pressure for different NCS vessel thickness sets.

It was shown that increasing the shell thickness helps to maintain structural stability, but it also increases the weight of these models. The weight of these models was estimated in *Table 4.29.* To simplify, only the most squared vessels of which set that did no report structural failure were considered. This concludes that weight increases considerably with each consequent thickness increment, from 14 - 27%. By estimating the expected weight and buoyancy of a detailed vessel with these shells as the main body and similar end cap dimensions as the one used in the no-flange SCC model, it is concluded that the vessel becomes negatively buoyant for thickness above 14 mm.

Table 4.29. Weight and buoyancy comparison of NCS quadrature study models

t	R_f	**Volume [cm³]**	**Mass [kg]**	**Total Weight [N]**	**Buoyancy [N]**	**Δ**
8	90	2616.6	7.3	144.7	200.8	51.5
10	80	3312.7	9.3	165.9	208.6	37.7
12	70	4034.9	11.3	187.9	216.3	23.4
14	60	4788.1	13.4	210.9	224.6	8.6
16	50	5577.8	15.6	235.0	233.2	-7.0
18	40	6363.6	17.8	259.0	241.8	-22.6

From this parametric study, the fillet radius of 60 mm was selected, which was considered as a good balance between volume efficiency increase and structural stability. For R_f = 60 mm, only models with $t > 16$ mm were not reporting shell failure. However, as seen in *Table 4.29*, these models cannot withstand their own weight. So, the solution is to use a thinner shell and use structural stiffeners to increase the rigidity of the shell. In order to have a weight margin for these iterations, a shell thickness of 12 mm was selected as the starting point.

4.5.3 Stiffened models study

The two considered configurations are axial stiffeners and radial stiffeners, also called external ring stiffeners. The first is more adequate to increase the stability of the shell when submitted to axially applied loads, while the latter is better suited for radial loads. Given the nature of hydrostatic pressure load, radial stiffener rings are more suited since there is a larger radial surface area. However, axial stiffeners have an advantage from a manufacturing standpoint since these stiffeners can be defined as cross-section profile shapes in an extrusion process.

The axial stiffeners were the first considered. Since few models were found employing this solution and none provided structural analysis reports, it was decided to start with an arbitrarily set stiffener dimensioning, and keep a cycle of modelling, analysing and updating the design variables to optimize structural integrity of the vessel without overwhelmingly increasing overall weight. Some of the profiles modelled following this principle are displayed below - *Figure 4.41.*

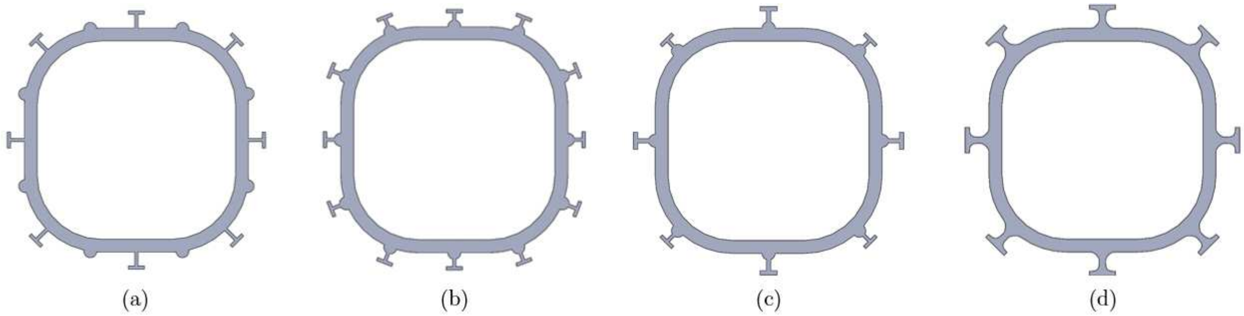

Figure 4.41. Examples of profiles modelled with axial stiffeners.

These profiles were designed with a large geometric freedom, which is the main advantage of fully extruded aluminium profiles. Models seen in *Figure 4.41 (a)*, *(b)* took advantage of this freedom to re-think how the profile could be adapted for axial tapped bolts by inserting circular boss profiles. However, results were far from promising and stress increased for all models. Other stiffener configurations were used, firstly by increasing its overall dimensions - *Figure 4.41 (c)*, and then by adopting a more filleted configuration to prevent stress accumulation in the shell-stiffener edge, *Figure 4.41 (d)*. However, no relevant optimization was registered. It concludes that axial stiffeners are not adequate in pressure vessels with these dimensions, and so their use was discarded. The full iterative study is not displayed, but can be found in *Appendix C*.

Radial stiffened models are now considered. These are defined by two geometric variables: the stiffener width, b; and height, d - *Figure 4.42*. The starting dimensions for these variables were derived from cylindrical vessels with similar dimensions. Ross [26] compiled data of several analyses of stiffened circular shells conducted by himself and various authors to create accurate design charts for general instability of equally-spaced, ring-stiffened cylinders, previously presented in *Figure 2.14*. Using stiffened shells with similar sizes as the vessel in development, the new geometric variables were set to b = 20 mm, and d = 18 mm. The number of stiffeners, n, has a large influence on the shell, and increasing n further divides the vessel in equally spaced sections, which increases stiffness of the mid-length of inter-frame spacings [54].

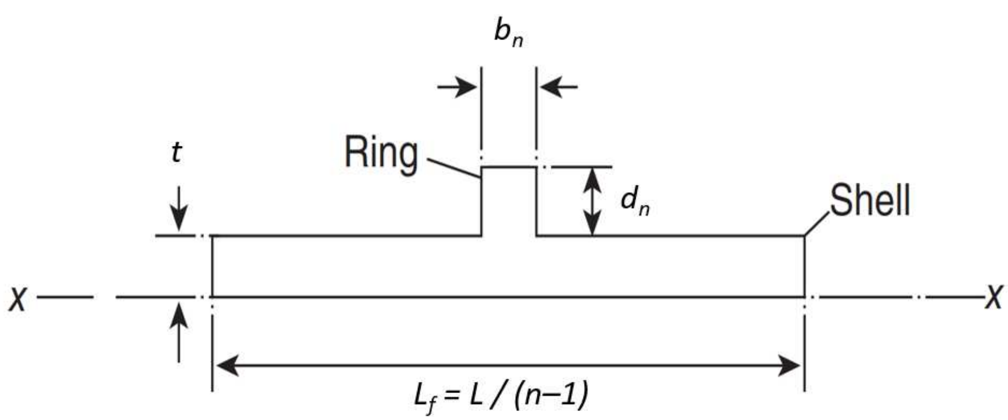

Figure 4.42. Radial stiffened shells geometric variables. Adapted from [26].

The influence of increasing the number of stiffeners in the shell was analysed to determine the appropriate number of stiffeners needed to validate this model. In this study, a noncircular shell with t = 12 mm; R_f = 60 mm; L = 500 mm was modelled with an increasing number of equally spaced radial stiffeners and analysed via a static linear FEA at NDP - *Figure 4.43*.

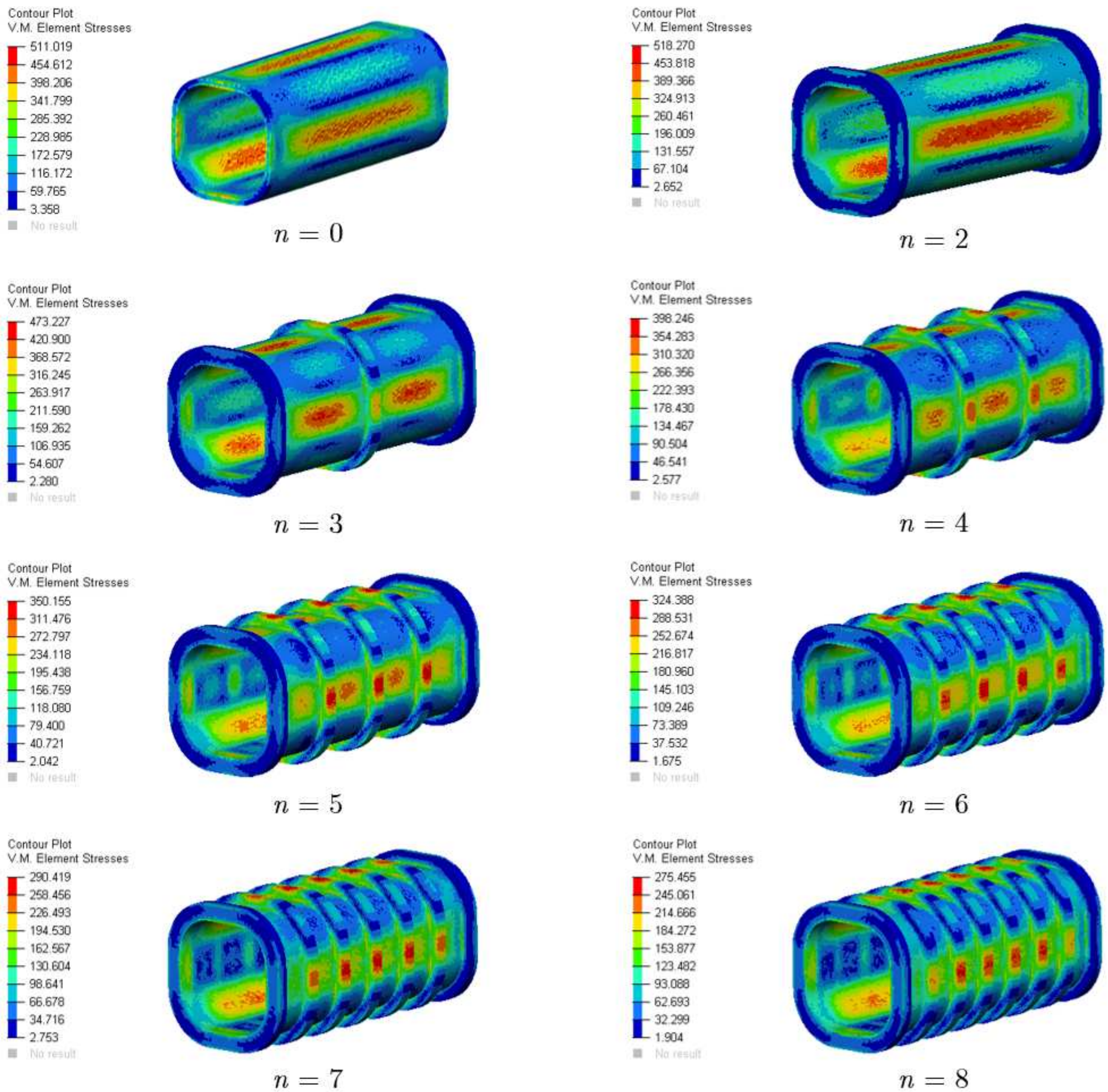

Figure 4.43. Radial stiffener influence on shell stress: Von Mises stress at NDP.

To determine when the shell is no longer bound to fail, the mechanical properties for extruded aluminium profiles were used - *Table 3.18*. Considering a profile with $25 < t < 50$ mm, the properties for an extruded 7075-T6 alloy are σ_y = 470 MPa and σ_u = 540 MPa. The results of this study can be visualized in *Figure 4.44,* together with the material yield strength. With the addition of stiffeners, failure is no longer occurring at NDP for n=5. When checking stress at TDP and CDP, it is concluded that at least 7 stiffeners are needed to fulfil all DNV GL safety requirements.

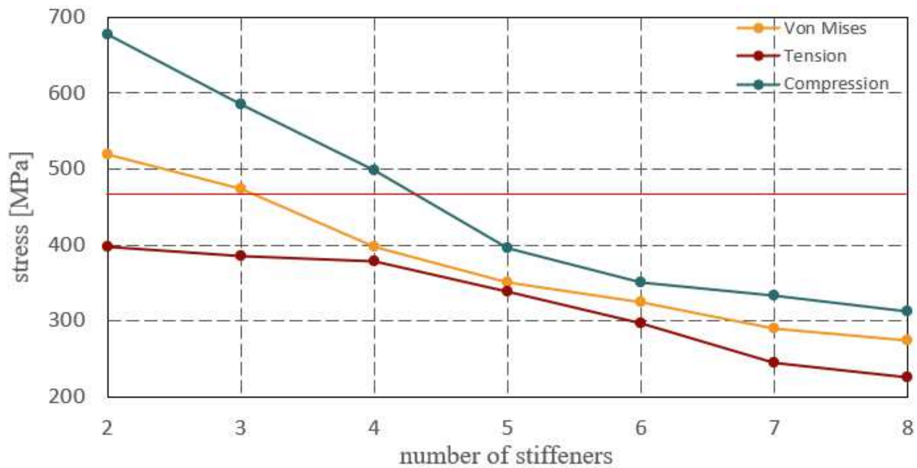

Figure 4.44. Radial stiffened shells with increasing number of stiffeners.

The vessel was further optimized for weight reduction by studying the individual influence of two geometric variables: the shell thickness, t, and the stiffener height, d. These models were built and analysed using the same FEA parameters described above. These results are compared with the yield strength adapted for the S2 safety factor in the graphs below – *Figure 4.45*.

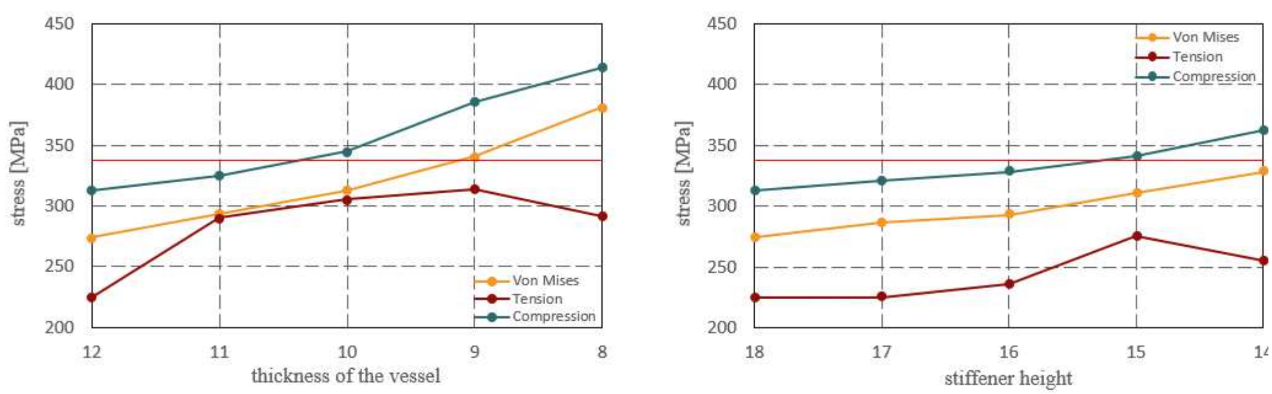

Figure 4.45. Radial stiffened shells weight optimization: shell thickness influence on the left; stiffener height influence on the right.

The models of each iteration that fulfil all safety factors are compared in *Table 4.30*. Shell thickness reduction is what more contributes to decreasing the vessel weight. So, the shell selected to be used in the main body concept has the following dimensions: $n = 8$; $b = 20$ mm; $d = 18$ mm, and the shell thickness is decreased to $t = 11$ mm.

Table 4.30. Weight comparison of structurally-safe NCS shells

n	t	d	VM Stress [MPa]	P_{cr} [MPa]	Volume [cm^3]	Mass [kg]	Weight [N]
7	**12**	**18**	290.4	186.8	6011.7	16.8	164.9
8	**12**	**16**	293.0	173.4	6026.5	16.6	162.2
8	**11**	**18**	293.6	177.9	5915.4	16.9	165.3

4.5.4 NCS detailed model design and analysis

A detailed NCS vessel following the geometric variables previously defined was assembled and studied for structural integrity. The stiffeners at the shell edge will naturally act as flanges, to which a cap is to be attached via fasteners. The internal length is to remain the same as all previous models, $L = 500$ mm. So, to determine the external vessel length, the caps must be dimensioned.

The sealing solution design must account for the noncircular profile. After consulting design recommendations from several manufacturers, it was concluded that O-rings can be used in noncircular groove patterns, as long as some guidelines are followed:

- **i.** The inner corner radius of the groove should be at least 3 times greater than the O-ring cross-section diameter [106] [107], and some recommend to be 7 to 8 times greater [108];
- **ii.** the centreline perimeter length of the groove should closely match the centreline length of the O-ring circumference [107] [106], so it is not stretched more than 5% [108];
- **iii.** The groove cross-section area should be 15-40% larger than the O-ring cross-section area;
- **iv.** It is recommended to use a face seal configuration [106] [108] [107].

It was decided to use a single face seal + single radial seal configuration, since a dual face seal would result in a large flange size. So, the main seal is secured by a face O-ring, but redundancy is still verified. It was previously defined the dimensions for a radially mounted O-ring - *Figure 4.8*. Similar groove dimensions and initial compression in proportion to O-ring cross-section for face seals are displayed in *Figure 4.46*.

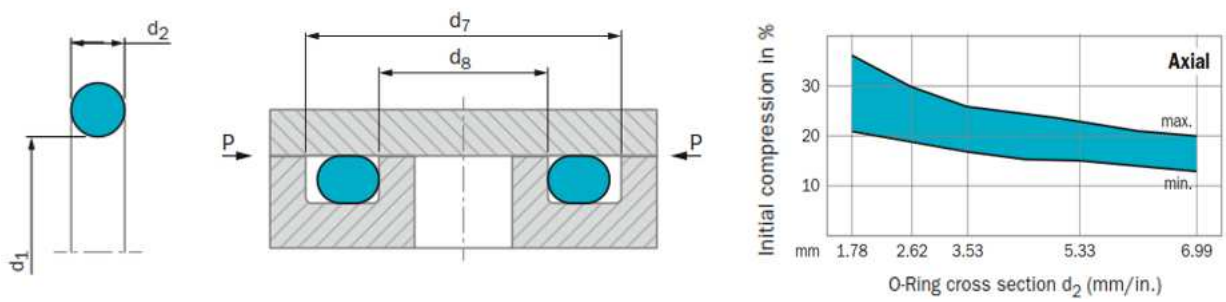

Figure 4.46. Dimensioning for a face seal application: On the left, O-ring and face groove dimensions; On the right: Permissible range of initial compression as a function of the cross-section. Adapted from [98].

Both O-rings were selected from Trelleborg Sealing Solutions 2016 catalogue [98] - *Table 4.31*.

Table 4.31. Metric dimensions of the selected O-rings, Trelleborg [98]

Application	**Part No.**	**Size code ISO 3601-1**	**d_1 [mm]**	**d_2 [mm]**
Face seal	ORAR00370	370	208.92 ± 1.42	5.33 ± 0.13
Radial seal	ORAR00368	368	196.22 ± 1.42	5.33 ± 0.13

Now checking for O-ring operating conditions. The inner corner radius is ~19 times larger than the O-ring cross-section, so the O-ring is not expected to kink in any way. The O-ring stretch, reduction and compression were calculated - *Table 4.32*. The stretch was established by considering the diameter of a circumference with the same perimeter of the groove centreline, $d_5 = 214.39$, and the radial seal, $d_5 = 201.54$. Standard back-up rings are not compatible with a noncircular groove, so the groove dimensions were determined to fulfil the compression requirements for a cross-section of 5.33 mm, which must be between 15% - 23% - *Figure 4.46*.

Table 4.32. O-ring operating conditions for the selected components - NCS

	Stretch	Reduction	Compression
Face seal	$S_O = \frac{214.39 - 208.92}{208.92}$ [%] $S_O = 2.6\% < 5\%$	$R_O = 0.01 + 1.06 \cdot 2.6 - 0.1 \cdot 2.6^2$ [%] $R_O = 3.7\%$	$C_O = \frac{5.33 - 4.20}{5.33}$ [%] $C_O = 21.2\% < 23\%$
Radial seal	$S_O = \frac{201.54 - 196.22}{196.22}$ [%] $S_O = 2.7\% < 5\%$	$R_O = 0.01 + 1.06 \cdot 2.7 - 0.1 \cdot 2.7^2$ [%] $R_O = 3.8\%$	$C_O = \frac{5.33 - 4.00}{5.33}$ [%] $C_O = 25.0\% < 28\%$

The internal cap length was set to 20 mm, which is shorter than the SCC cap, since only one radial O-ring is used. The external face of the cap equals the edge stiffener face, which doubles as flange. Since face seal O-rings are being used, a well-distributed connection is recommended to ensure a tight squeeze, so it was decided to use sixteen M6 bolts. The cap thickness cannot be defined from similar models, so a preliminary value of 12 mm was set - *Figure 4.47*.

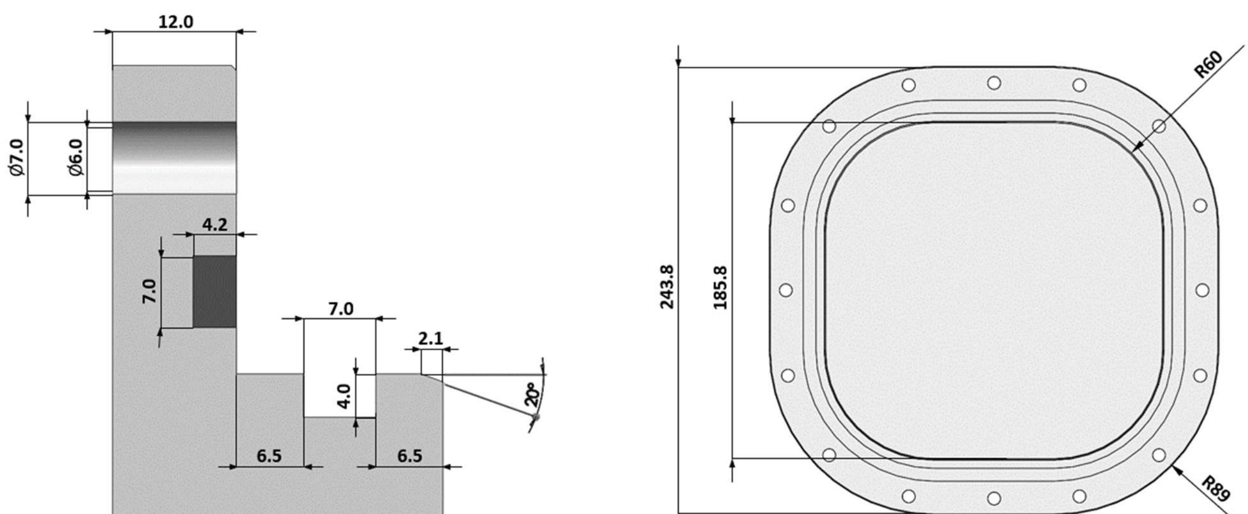

Figure 4.47. General dimensions of the NCS pressure vessel end cap.

The internal length of the main body is the distance between the internal faces of each end cap. So, the external length of the vessel is 500 + 2·20 = 540.0 mm. The remaining dimensions were already defined in the previous studies: $s = 18.0$ mm, $d = 20.0$ mm, $t = 8.0$ mm - *Figure 4.48*.

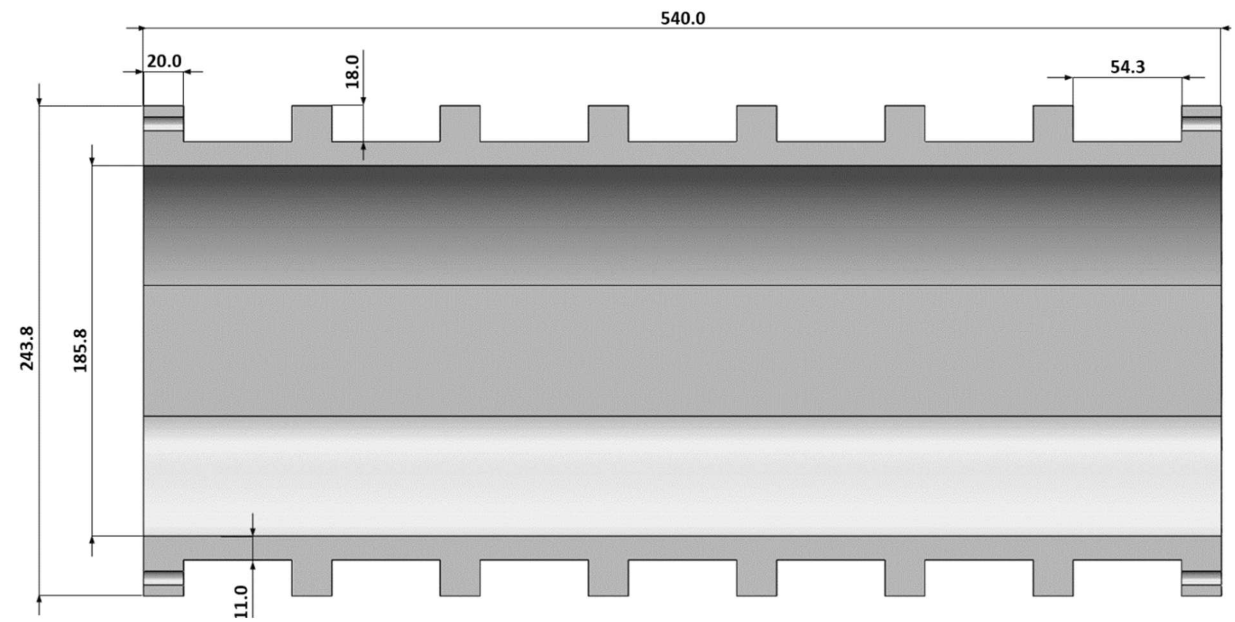

Figure 4.48. General dimensions of the NCS pressure vessel main body.

The fastening components are similar to the ones previously used, and the overall dimensions for M6 bolts were previously introduced in *Chapter 4.2.3*. The preload calculations were made considering D = 6 mm, P = 1.0 mm, $\sigma_{Y,\,b}$= 600 MPa (INOX A4 grade 80), and $\%_Y$=64%. Using *Formula (4.4)*, the recommended axial preload force is 7.6 kN. All components were assembled and rendered in *Solidworks* - *Figure 4.49*.

Figure 4.49. Rendered image of the NCS pressure vessel.

The vessel mass and weight are 24.21 kg and 239.3 N, respectively - *Table 4.33*. Considering the fluid, V_{disp} = 24 400 cm^3, and ρ_f, = 1.03516 g/cm^3 the buoyancy is B = 247.5 N, which results in a positive net force of 247.5 – 241.8 = 5.7 N, which is 0.59 kg above the neutral buoyancy threshold.

Table 4.33. Volume, mass and weight of the NCS pressure vessel iteration

Components	**Volume [cm^3]**	**Mass [kg]**	**Weight [N]**
Main body	6187.5	17.30	169.5
End cap	1213.9	3.39	33.3
Fastening components	-	0.59	5.8
Total	-	24.67	241.8

A finite element analysis was conducted for this model. Two types of analysis were used: a nonlinear quasi-static (NLQS) analysis to determine the displacements and stress load functions, considering an inertia relief-based boundary conditions; and a linear buckling analysis to estimate the critical buckling pressure of the full model, considering a three in-plane SPCs boundary conditions. The vessel was defined using the same modelling considerations previously discussed.

The results for at NDP are displayed in *Table 4.34*. Compression continues to represent the highest stress. Analyses at TDP and CDP show that the compression at CDP is higher than the material ultimate strength, meaning the safety factor S2 is not validated. Post-processing these results, stress is maximum on the contact region, 8.7% higher compression stress than the main body central shell. So, structural failure is most likely occurring due to an inadequate cap design, which causes the internal faces of the cap to "crush" the main body edges. The large displacements in the cap inner radius, which are reported to be 55.8% larger than the main body, indicate that the used cap is not thick enough to withstand the applied pressure.

Table 4.34. FEA results at NDP of maximum stress and displacements of different NCS components

Component	**u [mm]**	**VM [MPa]**	**P1 [MPa]**	**P3 [MPa]**
Detailed Vessel	0.522	321.1	277.1	364.0
Main Body (without contact)	0.335	286.9	171.7	335.1
End Cap (without contact)	0.522	247.9	248.2	241.7
Contact region	0.222	321.1	277.1	364.0

To determine a more appropriate cap thickness, 3 additional vessels with consecutive larger caps were modelled respectively with 16 mm, 20 mm and 24 mm. These were subjected to the same analysis parameters of the previous model - *Figure 4.50*. These results show a considerable decrease of element displacement on the caps, as well as a decrease in compression stress in the contact region of the main body. Re-analysing the model under the influence of TDP and CDP load conditions, it is confirmed that compression stress is no longer above the material yield strength for a cap thickness of 20 mm and 24 mm.

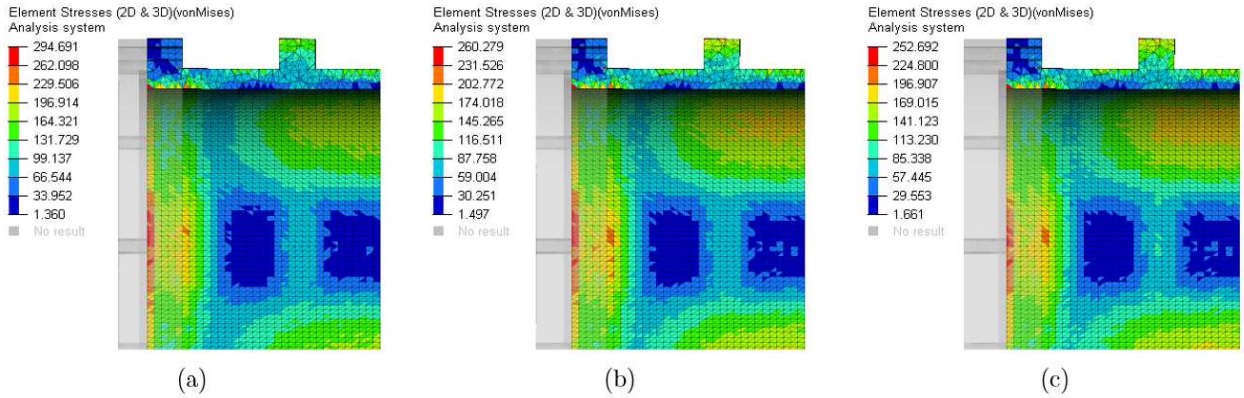

Figure 4.50. Cap thickness influence analysis, Von Mises stress at NDP:
(a) 16 mm cap thickness; (b) 20 mm cap thickness; (c) 24 mm cap thickness.

In *Figure 4.51*, the stress results at CDP were plotted together with the material ultimate strength. A shell thickness of 16 mm is slightly above the limit, and the displayed trend shows that a cap thickness of 17 mm may result in a maximum compression stress close to the ultimate strength. To have an adequate safety margin, it was instead selected a cap thickness of 18 mm.

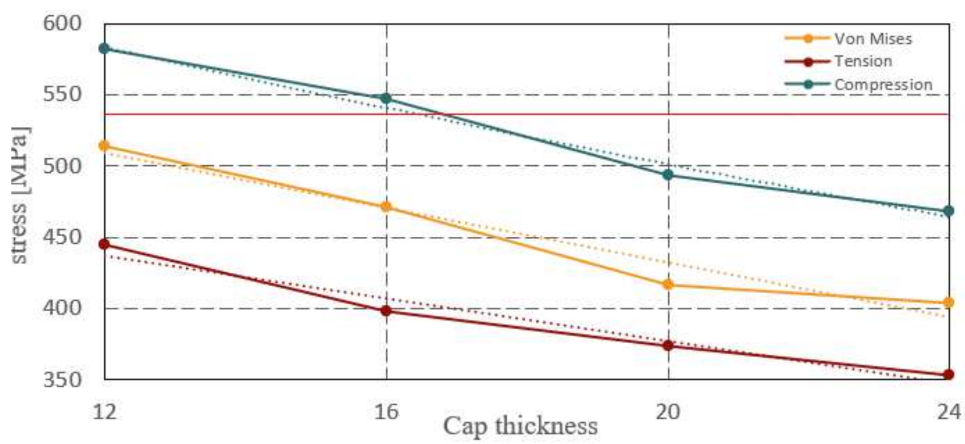

Figure 4.51. CDP stress results in cap thickness influence study.

Finally, the NCS detailed model was assembled and analysed considering the same FEA parameters described above. NDP, TDP and CDP analysis were considered, and stress results for Von Mises (VM), tension (P1), compression (P3), critical buckling pressure (P_{cr}) and element displacements (u) are displayed in *Table 4.35*, *Figure 4.52*.

The shell behaves similarly to all previous NCS models, but no longer appears to fail due to axisymmetric yield - *Figure 4.52 (a), (c)*. The buckling pressure is 80.77 MPa to which corresponds an n = 2 deformation mode shape - *Figure 4.52 (f)*. This corresponds to an extremely high safety factor of P_{cr}/NDP = 5.3. This is mostly due to the accumulative effect of a considerably thick shell used together with radial stiffeners. So, structural failure is not expected to come as the result of lobar buckling for the mission parameters.

Table 4.35. FEA results of maximum displacement, stress and buckling pressure for the NCS vessel

Pressure [MPa]	u [mm]	VM [MPa]	P1 [MPa]	P3 [MPa]	n	P_{cr} [MPa]
NDP = 15.22	0.460	289.1	277.3	330.8		
TDP = 18.26	0.552	346.9	332.8	397.0	2	80.77
CDP = 24.35	0.736	462.5	443.8	529.3		

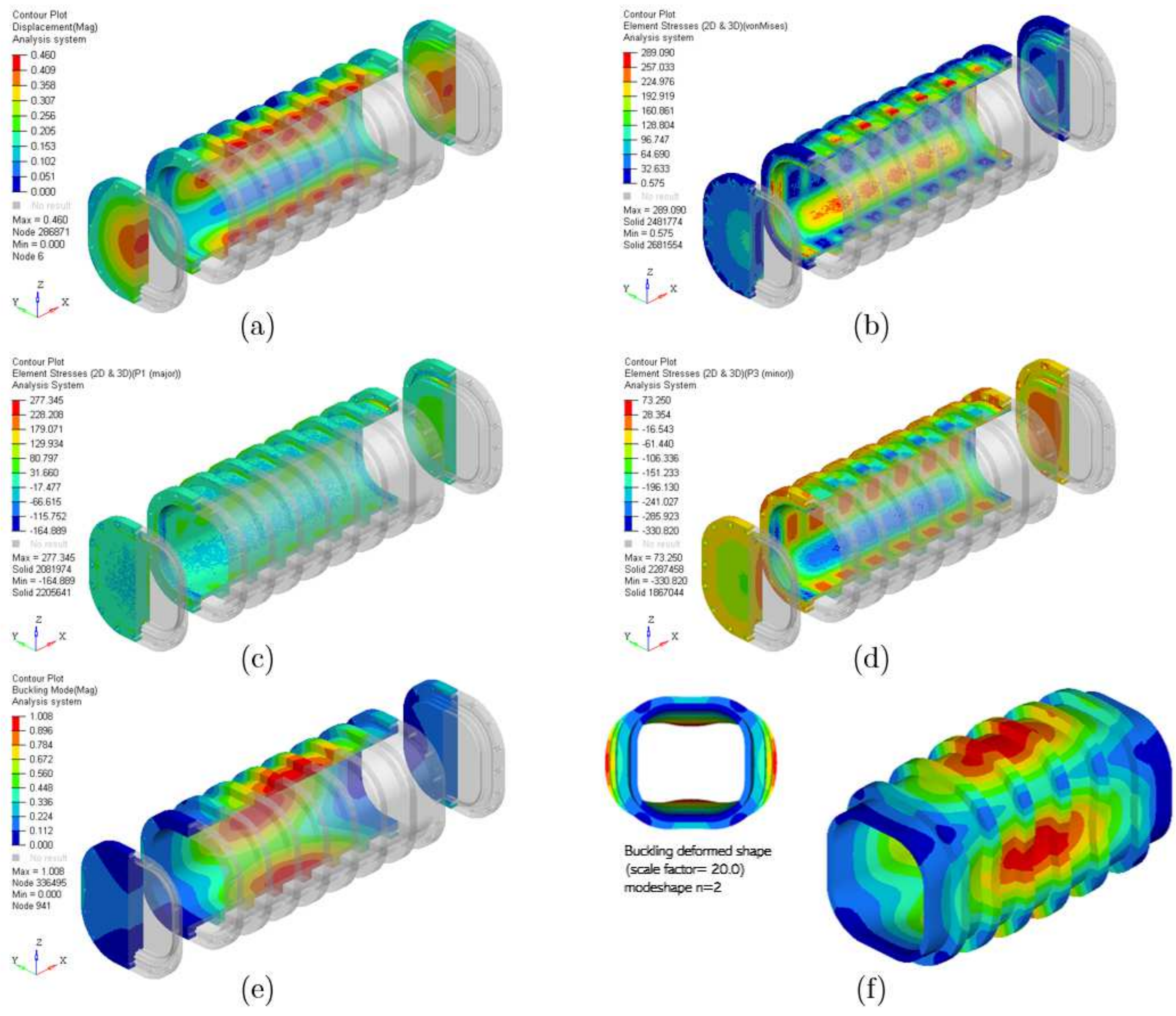

Figure 4.52. NCS pressure vessel at NDP - FEA results: (a) displacement; (b) Von Mises stress; (c) tension stress (P1); (d) compression stress (P3); (e) Buckling mode; (f) Buckling mode shape (scale factor=20.0).

The mechanical properties for this vessel are $\sigma_y = 470$ MPa and $\sigma_u = 540$ MPa. The maximum stress appears at compression, $P3_{TDP} = 397.0$ MPa and $P3_{CDP} = 529.3$ MPa, and the respective margins of safety are displayed in *Table 4.36*. It is confirmed this vessel fulfils all the considered safety factors and is validated for operation.

Table 4.36. Margins of Safety verified for the NCS pressure vessel

Pressure [MPa]	**P3 (max)** [MPa]	$MS = \dfrac{material\ strength}{\max stress \cdot SF} - 1$
NDP = 15.22	330.8	0.42
TDP = 18.26	397.0	0.18
CDP = 24.35	529.3	0.02

The mass and weight were determined to be 26.4 kg and 258.9 N respectively - *Table 4.37*. The buoyancy was calculated for $\rho_f = 1.03516$ g/cm^3, $V_{disp} = 25\,024.2$ cm^3, $B = 253.9$ N. This corresponds to a negative impulsion of 253.9 – 258.9 = -5.0 N, meaning the pressure vessel is not able to sustain its own weight. This is against the product specification previously defined, but after several iterations, this was the one with the best balance between structural integrity and weight net force.

Table 4.37. Volume, mass and weight of the NCS pressure vessel

Components	**Volume** [cm^3]	**Mass** [kg]	**Weight** [N]
Main body	6187.5	17.3	169.5
End cap	1525.9	4.3	41.8
Fastening components	-	0.6	5.8
Total	9314.6	26.4	258.9

Finally, the contact status were checked. Contact status analysis reported a continuum region across the vessel-cap contact interface, meaning watertightness is confirmed - *Figure 4.53*.

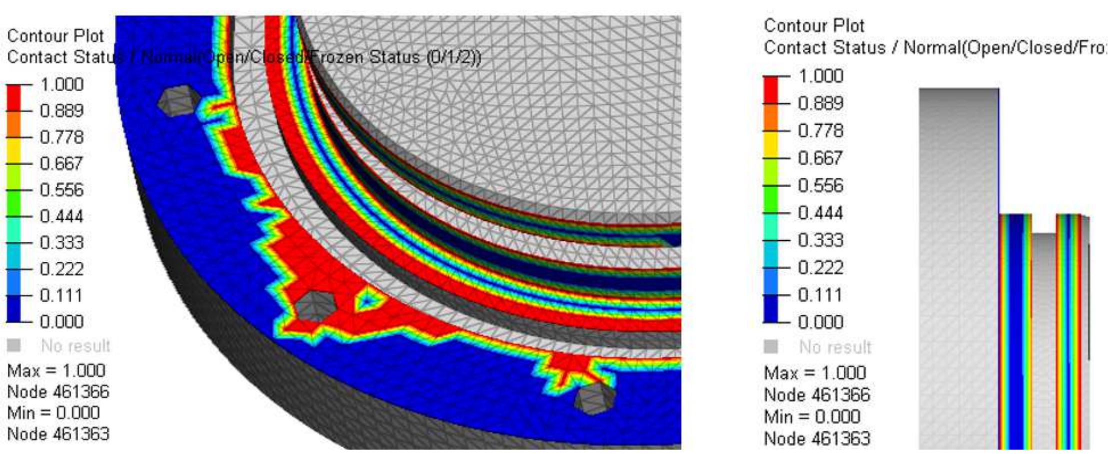

Figure 4.53. Contact status on the surface elements of the NCS cap: a value of 0 means the contact is open, while a value of 1 means the contact is tightly closed.

4.6 Concept comparison

The models previously introduced, analysed and validated are now compared side by side. These are the Standard Circular Cylinder - SCC vessel, as well as its filleted-flange variation, to be referred as SCF – Standard Circular Filleted flange vessel; the Axial Thickness Variation - ATV vessel, and the Noncircular Cross Section - NCS vessel.

To compare these models, the product specifications previously defined were revisited. However, these specifications were no longer the most relevant. Throughout product development, a better understanding of the product was progressively attained, and it was concluded that more accurate target specifications were necessary to better describe the inherent features of the different concepts, as well as apparent strength and limitations. These are the final specifications - *Table 4.38*, which were defined in reference to the same customer needs to retain their relevance from a customer perspective.

Table 4.38. Final specifications of the selected pressure vessel concepts

#	need	Metric	Imp	SCC	SCF	ATV	NCS	Units
1	1	TDP Margin of Safety	5	0.41	0.60	0.35	0.18	-
2	1	CDP Margin of Safety	5	0.19	0.36	0.15	0.02	-
3	1	Buckling Safety Factor	5	2.44	2.60	2.66	5.32	-
4	2	Watertightness	5	yes	yes	yes	yes	*binary*
12	1,4,6	Selected material	5	Al 7075	Al 7075	Al 7075	Al 7075	*list*
5	3	Internal volume	4	15708	15708	15708	15708	cm^3
6	3	Useful volume ratio	4	52.3	52.3	52.3	69.7	%
7	1,2	Nominal depth	4	1 500	1 500	1 500	1 500	m
8	3	Internal diameter	4	200	200	200	-	mm
9	3	Internal length	4	500	500	500	500	mm
10	6	Mass	3	19.7	20.4	19.8	26.4	kg
11	6	Weight net force	3	37.6	33.7	37.1	-5.0	N
17	5	Manufacture cost	2	-	=	≅	>	€
13	1,7	Stiffener configuration	1	none	none	none	radial	*list*
14	1,7,10	Cross section configuration	1	circular	circular	thick var	non-circular	*list*
15	7	Total external length	1	594	594	594	576	mm
16	7	Ext. circumscribed diameter	1	270	270	270	271	mm

The highest level of importance was given to the specifications relating to the structural integrity, indicated as margins of safety, and watertightness of the vessel. The second level of importance was used to define the internal space this vessel can provide to the user, as well as the nominal depth that the vessel was dimensioned for. The third level is referring to the weight-to-buoyancy ratio. The manufacture cost appears in the fourth level were not estimated since it was not in the scope of the present thesis to plan product manufacture, and so these were simply estimated in function of the SCC vessel. The final level regards the external configurations and dimensions of the vessel, which affects its attachability and occupied volume inside the submersible. Some of these metrics have the same set value for all concepts, which acted as design constraints in order to make a direct comparison viable.

Starting with the SCC vessel, this model ensures all product specifications that were defined in *Chapter 3.3.4*. It is the lightest of all models and has considerably high safety margins from axisymmetric yield failure, and a good safety factor from the critical buckling pressure. It stands as a valid example of how a market-standard vessel is dimensioned. Neither of the three alternative concepts to this model offer a better performance in all specifications. Instead, they present valid trade-offs which may be of interest for the specific mission parameters they were designed for.

The SCF model increased all safety measures, with a 3.4% weight increase trade-off. It contributed mostly to reduce the end cap – main body stress in the contact region, which is where stress was maximum for all concepts. So, adopting this concept can be useful if a vessel requires the use of thinner end caps. The cap attachment is made with axially tapped bolts, which can be an advantage in easiness to use since fewer fastening components are needed. This concept is expected to cost the same as the SCC vessel, since similar material and cut operations would be employed.

The ATV model achieved a trade-off of an 8% increase of the buckling pressure at the cost of a 14% Von Mises shell stress. This adaptation of Ross's manned-submersible corrugated shell prevents the propagation of the buckling deformation mode shape, thus increasing the buckling strength. The remarkable feature of this concept is achieving this increase with no considerable change in the vessel weight. As estimated with the Windenburg thinness ratio in *Chapter 4.2.2*, lobar buckling failure mode is still likely to occur for an over-dimensioned shell, making this concept a valid option for shells more prone to failure due to lobar buckling. This vessel is estimated to cost approximately the same as the SCC model. A possible inconvenience is its irregular surface configuration, which can make it difficult to attach the vessel to the submersible equipment.

The NCS model increases the internal useful volume, with a 34% weight increase trade-off. This concept followed the main optimization goal of useful volume increase, which required the use of a noncircular, stiffened shell, which margins of safety are considerably smaller than the rest of the models. The buckling SF is ~2x than the SCC model. The more negative trait is its weight net force, and the vessel buoyancy is not able to withstand its own weight. A positively buoyant vessel can be modelled if less demanding safety factors were considered, since the first iteration with a thinner shell cap was achieving both NDP and TDP safety factors. A possible inconvenience is the noncircular, stiffened configuration, which can hinder the attachment of the vessel.

The main advantage of the NCS concept is the increase in useful volume. This measurement is difficult to calculate since it depends on mission payload. Using the same approach previously described by Lee [104] in *Chapter 4.5.1*, the useful volume of this concept increases by 15.9%. However, this ratio is adequate for internal pressure vessels, which are typically designed to house fluids and gases. For a more appropriate comparison, it was developed a squared payload packaging study. This study considers a compact internal grid made of equally sized squares, which is represented on top of the pressure vessel cross-section. Then, the number of squares that can fit in each cross-section are compared - *Figure 4.54*. The volume efficiency ratio results of the relation between the area sum of all packed squares and the total area of the cross-section. Naturally, as the square length tends to zero, this ratio will tend to the unity.

Three dimensions of squares were considered: 12 mm, 37 mm and 50 mm - *Table 4.39*. These dimensions were inferred from reported in similar equipment [28] [52] and from the recommendations of the team in CEiiA. These results show that the NCS shell has a higher volume efficiency for all packed-squares lengths. For each square, the volume increase percentage was also calculated. This can be interpreted as an increase in useful volume, which was respectively of 9.0%, 33.3% and 80.0%. This study is a mere thought experiment which needs proper validation, so it should be interpreted with care. It was decided to consider the volume increase inferred from a square length of 37 mm to compare these vessels, which translates in a 33.3% increase in useful volume.

Table 4.39. Square-packing study for both cross-sections, using different square lengths

	Circular			Noncircular			
Square length	**#squares**	**Total area**	**Volume efficiency**	**#squares**	**Total area**	**Volume efficiency**	**Volume increase**
12	177	25488	81.1%	193	27792	88.5%	9.0%
37	12	16428	52.3%	16	21904	69.7%	33.3%
50	5	12500	39.8%	9	22500	71.6%	80.0%

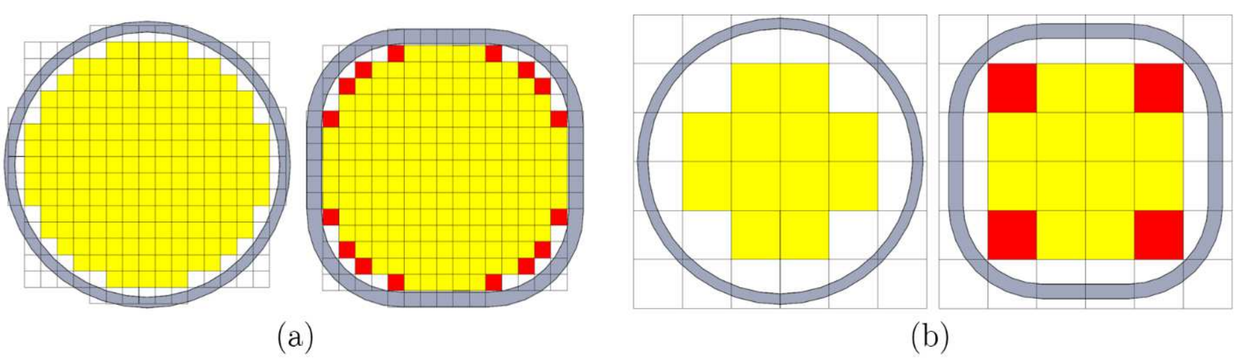

Figure 4.54. Representation of the square packing study, highlighting on red the additional squares packed to the noncircular vessel: (a) 12 mm square length; (b) 37 mm square length.

5. Conclusions & Final Remarks

Throughout this thesis, a market-standard pressure vessel was defined, and by following the concept development process, three promising concepts were compared to identify useful trade-offs in design. The market study concludes that the prevalent concept is the unstiffened cylindrical shell, and that both its material and configuration are mostly a function of the nominal depth. All vessels were divided into groups according to depth, which further allowed to establish valid relations between geometric dimensioning, vessel configuration, material selection and nominal depth.

Based on this analysis, the product specifications for a Standard Circular Cylindrical – SCC vessel were defined. This shell was the main reference to refine and validate the FEA parameters by comparing numerical results with analytical estimations. These analytical results concluded that the David Taylor Model Basin - DTMB formula was the most appropriate for a conservative shell thickness. It was also confirmed the preliminary selection of aluminium alloy 7075-T6 as the most indicated material for the considered depth. Both the simplified and detailed models' analyses report correlation in results. It concludes that the SCC vessel was over-dimensioned, as recommended by the consulted bibliography. This vessel fulfilled all the initial product specifications, however further optimization is still possible. It was also concluded that the Standard Circular Filleted flange – SCF vessel reports an 11.9% compression stress decrease, with a 3.4% weight increase trade-off.

Following the concept generation, three main body configurations were selected: The RTV and ATV families focused on the second optimization goal of increasing structural integrity, while the NCS family focused on the main goal of increasing the usefulness of the internal volume. A parametric study, best suited for the configuration and optimization goal of each concept was performed using the simplified shell analysis parameters previously validated. From these studies, the Radial Thickness Variation – RTV family was discarded since it did not report a valid optimization trade-off. The Axial Thickness Variation –ATV reported a considerable critical buckling pressure increase of 8%, with a 14% Von Mises stress increase trade-off without adding weight to the vessel. The Noncircular Cross Section – NCS vessel reported a 33.3% - 80% increase in internal useful volume, with a 34.1% weight increase trade-off.

This thesis concludes that alternative vessel configurations can be used to achieve relevant trade-offs which may be of interest for certain mission parameters. The validity of these trade-offs depends on the functionality of the pressure vessel, which is designed considering the submersible equipment it will operate on. However, these alternative concepts can prove to be of great use in future sea exploration and operation.

5.1 Future works

Regarding future works, it is proposed to analyse the ATV and NCS proposed solutions using a nonlinear buckling analysis approach for the simplified shells, considering different percentages of geometric nonlinearities to determine the sensitivity to imperfections of these solutions. A decrease in the critical buckling pressure is expected, but if this drop is within the reports of well-studied unstiffened cylindrical shells [109] [110], the realization of experimental studies for these geometries is the logical next step. It must be also stated that both geometries can still be further optimized, especially the NCS vessel, either with the goal of weight-reducing, or to further increase the quadrature of the cross-section without resulting in failure. Further development of the production and manufacturing is also required before these configurations can be adapted for the pressure vessel market. This study should analyse for material, manufacture and productions costs and establish a production outline considering profit maximization.

Another interesting approach would be to test and design these concepts for a higher nominal depth. It was decided to focus this thesis on a more accessible pressure condition, since new concepts were to be developed. Validating them for a wider range of nominal depth would increase their relevance, especially true for the NCS vessel, which shape and weight could be of great interest for benthic lander applications.

Another possibility would be to automatize the parametric studies that were considered for both the ATV and NCS vessels. Since it was proved a close correlation between the simplified shells and full models, the development of a numerical tool to automatically define and model these shells so to determine the best possible configuration for a given nominal depth would considerably accelerate the process of development using these geometries. A similar tool for unstiffened shells was developed by Siqueira [111] and proved to be a relevant asset in shell development. This tool could also be of great use to rapidly define and study the validity of these concepts for more demanding nominal depths above 3 000 m.

Following a completely different approach, the author would recommend the development of composite sandwich hull configurations. It was decided to not consider their development as concepts, since a direct comparison with a standard vessel would be difficult to achieve for a vessel with very different material properties. These are also a fairly understudied field in pressure vessel design, but preliminary results show promising possibilities for the development of lightweight, strong structures, well adapted for deep-sea missions [71] [112] [113] [114].

Bibliography

[1] US Department of Commerce, "How much of the ocean have we explored?"

[2] R. Wellborn, "USS VIRGINIA SSN 774-A NEW STEEL SHARK AT SEA - ATI Courses," *Applied Technology Institute*, 2011. Available: https://www.aticourses.com/2011/07/19/uss-virginia-ssn-774a-new-steel-shark-at-sea/. [Accessed: 10-Apr-2020].

[3] The Ocean Portal Team, "The Deep Sea | Smithsonian Ocean." [Online]. Available: https://ocean.si.edu/ecosystems/deep-sea/deep-sea. [Accessed: 10-Apr-2020].

[4] J. I. Virmani, "Ocean Vs Space: Exploration And The Quest To Inspire," 07-Jun-2017. [Online]. Available: https://www.marinetechnologynews.com/news/ocean-space-exploration-quest-549183. [Accessed: 24-Jun-2020].

[5] US Department of Commerce, "NOAA - What Is Ocean Exploration and Why Is It Important?"

[6] Parlamentary Office of Science and Technology, "NEW INDUSTRIES IN THE DEEP SEA," *Diversity*, no. 288, 2007.

[7] R. Biswas, "Deep Sea Mining Technologies , Equipment and Mineral Targets," no. June, 2019.

[8] Direção-Geral de Recursos Naturais, "Zonas Marítimas sob Jurisdição e ou Soberania Nacional - DGRM," 2020. [Online]. Available: https://www.dgrm.mm.gov.pt/am-ec-zonas-maritimas-sob-jurisdicao-ou-soberania-nacional. [Accessed: 24-Jun-2020].

[9] I. Botelho Leal and F. de Melo Gomes, "A extensão da Plataforma Continental: perspetivas e realidades | Opinião | PÚBLICO," 2017.

[10] M. C. Freire, "ONU analisou esta semana proposta de alargar fundo do mar português," *Diário de Notícias*, 2019.

[11] Germanischer Lloyd, "Rules for Classification and Construction, Naval Ship Technology, Sub-Surface Ships," *Lloydia (Cincinnati)*, pp. 1–12, 2004.

[12] M. Paschen and K. Breddermann, "Technical solutions for deep-sea vehicles that withstand enourmous pressure," in *Sustainable Development and Innovations in Marine Technologies: Proceedings of the 18th International Congress of the Maritme Association of the Mediterranean (IMAM 2019), September 9-11, 2019, Varna, Bulgaria*, 2019.

[13] CEiiA, “CEiiA - about us,” 2020. [Online]. Available: https://www.ceiia.com/about-us. [Accessed: 01-Nov-2020].

[14] CEiiA, “Relatório de Atividades e Contas 2019,” 2020. [Online]. Available: https://issuu.com/academiaceiia/docs/binder_rac_2019_03. [Accessed: 01-Nov-2020].

[15] CEiiA, “MEDUSA Faz História,” 2017. [Online]. Available: https://www.ceiia.com/single-post/2017/06/05/MEDUSA-FAZ-HISTÓRIA. [Accessed: 01-Nov-2020].

[16] Diário de Notícias, “Medusa, o Submarino autónomo que vai a três mil metros,” 2017.

[17] Seaculture, “Projecto de I&D – Avaliação do crescimento do Salmão do Atlântico em condições Offshore na Costa Oeste de Portugal],” 2018.

[18] CEiiA, “Ocean & Space - EASER,” 2018. [Online]. Available: https://www.ceiia.com/easer. [Accessed: 01-Nov-2020].

[19] CEiiA, “CEiiA | Ocean & Space - Tags,” 2017. [Online]. Available: https://www.ceiia.com/ocean-tags. [Accessed: 01-Nov-2020].

[20] Renascença, “Ranking mundial: Universidade do Porto é a melhor instituição de ensino superior em Portugal,” 2018.

[21] Encyclopædia Britannica, “Geology: definition of Continental slope,” *Encyclopædia Britannica.* [Online]. Available: https://www.britannica.com/science/continental-slope. [Accessed: 12-Apr-2020].

[22] C. Thiede *et al.*, “An overall pressure tolerant underwater vehicle: DNS Pegel,” *Ocean. ’09 IEEE Bremen Balanc. Technol. with Futur. Needs*, no. June 2009, 2009, doi: 10.1109/OCEANSE.2009.5278313.

[23] M. Lück *et al.*, “Pressure tolerant systems for deep sea applications,” *Ocean. IEEE Sydney, Ocean. 2010*, 2010, doi: 10.1109/OCEANSSYD.2010.5603538.

[24] E. E. Allmendinger, *Submersible Vehicle systems design*, no. v. 1990.

[25] M. Stewart and O. T. Lewis, *Pressure Vessels Field Manual.* 2013.

[26] C. T. F. Ross, *Pressure vessels - External Pressure Technology.* 2011.

[27] M. B. BICKELL and C. RUIZ, *Pressure Vessel Design and Analysis*, vol. 1, no. 2. 1967.

[28] A. D. Bowen *et al.*, “The Nereus Hybrid Underwater Robotic Vehicle for Global Ocean Science Operations to 11,000m Depth,” *Underw. Technol.*, vol. 28, no. 3, pp. 79–89, 2009, doi: 10.3723/ut.28.079.

[29] A. Podut, “Strength of Materials Supplement for Power Engineering,” *British Columbia Institute of Technology*, Jun 2018. Available: https://pressbooks.bccampus.ca/powr4406/

[30] OMNI Instruments, "Subsea Housings, Connectors & Accessories," 2020. [Online]. Available: https://www.omniinstruments.co.uk/subsea-offshore-systems/subsea-housings-connectors-accessories.html.

[31] Massachusetts Institute of Technology, "MIT: ATLANTIS II," *MIT*. [Online]. Available: http://web.mit.edu/12.000/www/m2005/a2/finalwebsite/equipment/transport/Hull.shtml.

[32] NOAA Ocean Exploration & Research, "What is an AUV?," 2020. [Online]. Available: https://oceanexplorer.noaa.gov/facts/auv.html. [Accessed: 01-Aug-2020].

[33] NOAA Ocean Exploration & Research, "What is an ROV?," 2020. [Online]. Available: https://oceanexplorer.noaa.gov/facts/rov.html. [Accessed: 01-Aug-2020].

[34] ROBEX - Robotic Exploration of Extreme Environments, "Deep Sea Technologies," 2020. [Online]. Available: https://www.robex-allianz.de/en/deep-sea-technologies/.

[35] NOAA Ocean Exploration & Research, "Deepwater Canyons 2012: Pathways to the Abyss," 2012.

[36] A. D. Chave, "Seeding the Seafloor with Observatories," *Woods Hole Oceoanographic Institution*, 2004. Available: https://www.whoi.edu/oceanus/feature/seeding-the-seafloor-with-observatories/

[37] Microsoft, "Project Natick," *2020*. [Online] Available: https://natick.research.microsoft.com/

[38] J. Roach, "Microsoft finds underwater datacenters are reliable, practical and use energy sustainably," *Innovation Stories*, 2020. Available: https://news.microsoft.com/innovation-stories/project-natick-underwater-datacenter/. [Accessed: 08-Jan-2021].

[39] "AUV Hugin 1000 Modelo 3D - TurboSquid 1452153." [Online]. Available: https://www.turbosquid.com/pt_br/3d-models/autonomous-vehicle-auv-hugin-model-1452153.

[40] "ROVs, The Swiss Army Knife Of The Ocean." [Online]. Available: https://www.sciencefriday.com/educational-resources/rovs-swiss-army-knife-ocean/.

[41] "DEEP SEARCH 2019 on cold-water coral reefs - NIOZ." [Online]. Available: https://www.nioz.nl/en/blog/deep-search-2019-on-cold-water-coral-reefs.

[42] "Wally ROV, Ocean Networks Canada." [Online]. Available: https://www.oceannetworks.ca /article-tags/wally.

[43] S. I. Wong, "On Lightweight Design of Submarine Pressure Hulls," 2012.

[44] Encyclopædia Britannica, "Seawater - Density of seawater and pressure," *Encyclopædia Britannica*. [Online]. Available: https://www.britannica.com/science/seawater/Density-of-seawater-and-pressure. [Accessed: 20-Apr-2020].

[45] J. R. MacKay, “Structural Analysis and Design of Pressure Hulls : the State of the Art and Future Trends,” *Def. R&D Canada – Atl.*, no. October, p. 118, 2007.

[46] K. Breddermann, P. Drescher, C. Polzin, H. Seitz, and M. Paschen, “Printed pressure housings for underwater applications,” *Ocean Eng.*, vol. 113, pp. 57–63, 2016, doi: 10.1016/j.oceaneng.2015.12.033.

[47] Laurence Brundrett, “External Pressure – Pressure Vessel Engineering,” *Pressure Vessel Engineering*. [Online]. Available: https://www.pveng.com/home/asme-code-design/external-pressure-methods/. [Accessed: 20-Apr-2020].

[48] D. Bushnell, “Buckling of Shells - Pitfall for Designers.,” *Collect. Tech. Pap. - AIAA/ASME/ASCE/AHS/ASC Struct. Struct. Dyn. Mater. Conf.*, vol. 19, no. 9, pp. 1–56, 1980.

[49] B. Prabu, A. V. Raviprakash, and A. Venkatraman, “Parametric study on buckling behaviour of dented short carbon steel cylindrical shell subjected to uniform axial compression,” *Thin-Walled Struct.*, vol. 48, no. 8, pp. 639–649, 2010, doi: 10.1016/j.tws.2010.02.009.

[50] O. Ifayefunmi and J. Błachut, “Imperfection Sensitivity: A Review of Buckling Behavior of Cones, Cylinders, and Domes,” *J. Press. Vessel Technol. Trans. ASME*, vol. 140, no. 5, 2018, doi: 10.1115/1.4039695.

[51] D. Windenburg and C. Trilling, “Collapse by Instability of thin cylindrical shells under external pressure,” *Trans. ASME*, no. 11, pp. 819–825, 1934.

[52] A. Meschini, A. Ridolfi, J. Gelli, M. Pagliai, and A. Rindi, “Pressure hull design methods for unmanned underwater vehicles,” *J. Mar. Sci. Eng.*, vol. 7, no. 11, 2019, doi: 10.3390/jmse7110382.

[53] C. T. F. Ross, P. T. Smith, and A. P. F. Little, “Collapse of composite tubes under uniform external hydrostatic pressure,” *J. Phys. Conf. Ser.*, vol. 181, no. 1, 2009, doi: 10.1088/1742-6596/181/1/012043.

[54] C. T. F. Ross, K. O. Okoto, and A. P. F. Little, “Buckling by general instability of cylindrical components of deep sea submersibles,” *Appl. Mech. Mater.*, vol. 13–14, no. January 2008, pp. 289–296, 2008, doi: 10.4028/www.scientific.net/AMM.13-14.289.

[55] Budynas-Nisbett, *Mechanical Engineering : Shigley’s Mechanical Engineering Design*, 8th ed. 2006.

[56] R. Von Mises, “Der Kritische Aussendruck für Allseits Belastete Zylindrische Rohre,” *Fest Zum 70 Geburtstag von Prof. Dr A. Stodola*, no. (also USEMB Translation Report No. 366, 1936), 1929.

[57] J. R. MacKay, “Experimental and Numerical Modeling in support of a Structural Design Framework for Submarine Pressure Hulls based on Nonlinear Finite Element Collapse

Predictions," 2012.

[58] K. Asakawa and S. Takagawa, "New Design Method of Ceramics Pressure Housings for Deep Ocean Applications," *Ocean. 2009-EUROPE*, pp. 1–3, 2009, doi: 10.1109/OCEANSE.2009.5278325.

[59] W. Flugge, *Die Stabilität der Kreiszylinderschale*. Ingenieur-Archive, 1932.

[60] L. H. Donnell, *Beams, Plates and Shells*. McGraw-Hill Companies, 1976.

[61] S. B. Kendrick, *The Buckling under External Pressure of Ring Stiffened Circular Cylinders*. 1965.

[62] A. P. F. Little, C. T. F. Ross, D. Short, and G. X. Brown, "Inelastic Buckling of Geometrically Imperfect Tubes Under External Hydrostatic Pressure," *IEE Rev.*, vol. 49, no. 2, pp. 34–37, 2003, doi: 10.1049/ir:20030203.

[63] W. A. Nash, *Hydrostatically Loaded Structures*, 1st ed. 1995.

[64] T. Tokugawa, "Model experiments on the elastic stability of closed and cross-stiffened circular cylinders under uniform external pressure," *Proc. World Eng. Congr.*, vol. 29, no. 651, pp. 249–279, 1929.

[65] A. R. Bryant, "Hydrostatic pressure buckling of a ring-stiffened tube," 1954.

[66] DNV GL, "RULES FOR CLASSIFICATION Underwater technology Part 3 Pressure hull and structures Chapter 2 Design loads," no. December, 2015.

[67] C. T. F. Ross *et al.*, "Non-linear general instability of ring-stiffened conical shells under external hydrostatic pressure," *J. Phys. Conf. Ser.*, vol. 305, no. 1, 2011, doi: 10.1088/1742-6596/305/1/012118.

[68] M. Helal, H. Huang, E. Fathallah, and D. Wang, "Numerical Analysis and Dynamic Response of Optimized Composite Cross Elliptical Pressure Hull Subject to Non-Contact Underwater Blast Loading," 2019, doi: 10.3390/app9173489.

[69] C. S. Smith, *Design of marine structures in composite materials*. Elsevier Science Publishers Ltd., 1990.

[70] C. Liang, S. Shiah, C. Jen, and H. Chen, "Optimum design of multiple intersecting spheres deep-submerged pressure hull," vol. 31, pp. 177–199, 2004, doi: 10.1016/S0029-8018(03)00120-3.

[71] J. W. Hutchinson and M. Y. He, "Buckling of cylindrical sandwich shells with metal foam cores," *Int. J. Solids Struct.*, vol. 37, no. 46, pp. 6777–6794, 2000, doi: 10.1016/S0020-7683(99)00314-5.

[72] P. Jasion and K. Magnucki, "Elastic buckling of barrelled shell under external pressure," *Thin-Walled Struct.*, vol. 45, no. 4, pp. 393–399, 2007, doi: 10.1016/j.tws.2007.04.001.

[73] A. Siqueira, A. A. Alvarez, R. R. Jr, and E. A. De Barros, “Buckling Analysis of an AUV Pressure Vessel with Sliding Stiffeners,” *J. Mar. Sci. Eng.*, vol. 8, no. 515, 2020.

[74] A. S. Petreli and N. G. Tsouvalis, “A parametric study of the effect of geometric imperfections on the buckling behaviour of composite laminated cylinders,” *Adv. Compos. Lett.*, vol. 11, no. 3, pp. 111–122, 2002, doi: 10.1177/096369350201100302.

[75] Altair Hyperworks, *Practical Aspects of Finite Element Simulation*, 3rd ed. Altair University, 2015.

[76] R. Andujar, “WHAT DOES SHAPE FUNCTION MEAN IN FINITE ELEMENT FORMULATION,” *Stochastic Simulation and Lagrangian Dynamics*, 2011. [Online]. Available: http://stochasticandlagrangian.blogspot.com/2011/07/what-does-shape-function-mean-in-finite.html. [Accessed: 01-Oct-2020].

[77] K. T. Ulrich and S. D. Eppinger, *Product Design and Development: Fifth Edition.* 2012.

[78] PREVCO, “Subsea Housings,” 2020. [Online]. Available: https://prevco.com/shop/subsea-housings. [Accessed: 29-Jan-2021].

[79] Blue Robotics, “Enclosures, Buoyancy, and Ballast for ROVs, AUVs, and marine robotics,” 2020. [Online]. Available: https://bluerobotics.com/product-category/watertight-enclosures/. [Accessed: 29-Jan-2021].

[80] Develogic, “Underwater Housing Systems,” 2020. [Online]. Available: http://www.develogic.de/products/underwater-housing-systems/. [Accessed: 29-Jan-2021].

[81] Impact Subsea, “ISP1 & ISP2 – Subsea Pressure Housings,” 2020. [Online]. Available: https://www.impactsubsea.co.uk/isp1/. [Accessed: 29-Jan-2021].

[82] Subsea Ranger, “Economic Subsea Titanium Housing,” 2020. [Online]. Available: https://subsearanger.com/. [Accessed: 29-Jan-2021].

[83] K.U.M. Umwelt, “Titanium - pressure tube and pressure housing,” 2020. [Online]. Available: https://kum-kiel.de/en/products/titan/pressure-tube/. [Accessed: 29-Jan-2021].

[84] D. George, R. Renu, and G. Mocko, “Concept Generation Through Morphological and Options Matrices,” pp. 199–210, 2013, doi: 10.1007/978-81-322-1050-4_16.

[85] Artur Siqueira Nóbrega de Freitas and Ettore A de Barros, “Mechanical Design of external pressure vessel to an AUV,” *Proc. 23rd ABCM Int. Congr. Mech. Eng.*, 2015, doi: 10.20906/cps/cob-2015-0361.

[86] N. S. Madhavan and K. P. C. Sajith, “Design of Pressure Vessel for Undersea Applications,” *IJSTE - Int. J. Sci. Technol. Eng.*, vol. 4, no. 8, p. 7, 2018, doi: DOI10.13140/RG.2.2.13145.52320.

[87] J. P. Pereira, “Desenvolvimento de Produto - Notas de Aula,” 2019.

[88] H. Singh, R. Eustice, C. Roman, and O. Pizarro, “The SeaBED AUV -- a platform for high resolution imaging The SeaBED AUV – A Platform for High Resolution Imaging,” no. January, 2010.

[89] K. Izman, A. Rahim, A. R. Othman, and M. R. Arshad, “Conceptual design of a pressure hull for an underwater pole inspection robot,” no. May, 2015.

[90] J. V Hamngton, A. M. Parker, T. M. Waligora, and A. P. Background, “DESIGN OF AN INEXPENSIVE WATERPROOF HOUSING,” pp. 2880–2887.

[91] S. Thomke and A. Nimgade, “IDEO - a case study,” *Harvard Bus. Sch.*, vol. 44, no. 0, 2017.

[92] European Committee for Standardization, “EN 755-2: Aluminium and aluminium alloys - Extruded rod/bar, tube and profiles - Part 2: Mechanical properties,” vol. 7, no. 495. pp. 72–76, 2016.

[93] C. T. F. Ross, “COLLAPSE OF CORRUGATED CIRCULAR CYLINDERS UNDER UNIFORM UNIFORM EXTERNAL PRESSURE,” no. November 2011, 2015, doi: 10.1142/S0219455405001544.

[94] R. Craven, D. Graham, and J. Dalzel-Job, “Conceptual design of a composite pressure hull,” *Ocean Eng.*, vol. 128, no. May, pp. 153–162, 2016, doi: 10.1016/j.oceaneng.2016.10.031.

[95] H. K. Jeong and P. Henry, “Optimal Design of Deep-Sea Pressure Hulls using CAE tools,” *J. Comput. Struct. Eng. Inst. Korea*, vol. 25, no. 6, pp. 477–485, 2012, doi: 10.7734/coseik.2012.25.6.477.

[96] N. G. Tsouvalis, A. A. Zafeiratou, and V. J. Papazoglou, “The effect of geometric imperfections on the buckling behaviour of composite laminated cylinders under external hydrostatic pressure,” vol. 34, pp. 217–226, 2003.

[97] Altair Hyperworks, “Hyperworks 2017 Desktop User Guides.” 2017.

[98] Trelleborg Sealing Solutions, “O-Rings and Back-up Rings - 2016 Catalog.” 2016.

[99] Fabory, “Fastener Catalog - 2020 Edition.” 2020.

[100] Parker, “O-Seals | Parker NA Online Catalog,” 2020. [Online]. Available: https://ph.parker.com/us/en/o-seals. [Accessed: 10-Jan-2021].

[101] American Society of Mechanical Engineers, *2007 ASME Boiler & Pressure Vessel Code, Section VIII, division 1.* New York, 2007.

[102] A. E. Blach, V. S. Hoa, C. K. Kwok, and A. K. W. Ahmed, “Rectangular pressure vessels of finite length,” *J. Press. Vessel Technol. Trans. ASME*, vol. 112, no. 1, pp. 50–56, 1990, doi: 10.1115/1.2928587.

[103] M. . Rezvani and H. H. Ziada, “Stress Analysis and Evaluation of Rectangular Pressure Vessel,” 1993.

[104] J. Lee, Y. Choi, C. Jo, and D. Chang, “Design of a prismatic pressure vessel: An engineering solution for non-stiffened-type vessels,” *Ocean Eng.*, vol. 142, no. August 2016, pp. 639–649, 2017, doi: 10.1016/j.oceaneng.2017.07.039.

[105] Z. J. Zeng and Y. . Guo, “The six-plate analytical method for rectangular pressure vessels of finite length,” *Int. J. Press. Vessel. Pip.*, vol. 74, 1997.

[106] Apple Rubber Products, “Seal Design Guide Manual.” 2017.

[107] D. Kern, “Racetrack Grooves: Can O-Rings be used in Non-Circular Groove Patterns?,” *Parker Community*, 2017. [Online]. Available: https://community.parker.com/technologies/sealing-and-shielding/b/blog/posts/racetrack-grooves-can-o-rings-be-used-in-non-circular-groove-patterns. [Accessed: 10-Jan-2021].

[108] HpA - Engineering & Consulting, “O-ring Seal Design: Best Practices.” pp. 5–7, 2012.

[109] C. T. F. Ross, A. Spahiu, G. X. Brown, and A. P. F. Little, “Buckling of near-perfect thick-walled circular cylinders under uniform external hydrostatic pressure,” *J. Ocean Technol.*, pp. 84–103, 2009.

[110] C. T. F. Ross, T. Bowler, and A. P. F. Little, “Collapse of geometrically imperfect stainless steel tubes under external hydrostatic pressure,” *J. Phys. Conf. Ser.*, vol. 181, no. 1, 2009, doi: 10.1088/1742-6596/181/1/012030.

[111] A. S. N. de Freitas, “Análise Estrutural e de Estabilidade do Vaso de Pressão de um AUV Análise Estrutural e de Estabilidade do Vaso de Pressão de um AUV,” 2017.

[112] G. Cha and M. Schultz, “Buckling Analysis of a Honeycomb-Core Composite Cylinder with Initial Geometric Imperfections,” *J*, no. February, 2013.

[113] C. Qiu, Z. Guan, X. Guo, and Z. Li, “Buckling of honeycomb structures under out-of-plane loads,” *J. Sandw. Struct. Mater.*, vol. 22, no. 3, pp. 797–821, 2020, doi: 10.1177/1099636218774383.

[114] M. Helal, H. Huang, D. Wang, and E. Fathallah, “Numerical analysis of sandwich composite deep submarine pressure hull considering failure criter,” *J. Mar. Sci. Eng.*, vol. 7, no. 10, 2019, doi: 10.3390/jmse7100377.

Appendix A

Complete market research tables

Table A.1. PREVCO – Polymeric Pressure Vessels

PREVCO - Polymeric Pressure Vessels	https://prevco.com/shop
"PVC housings fitted with optically clear acrylic end caps. These housings include all hardware and O-rings including spares, and our dual seal vent plug, P/N 00669-001. The end caps are supplied unmodified, ready to be machined to your requirements. These housings have been supplied to customers with various end cap materials including the stock supplied optically clear acrylic, standard PVC, Aluminium, Copper Beryllium and titanium. (…) The [aluminium] standard lengths are [defined] but we stock the raw tube material so they can quickly be made in almost any length. The housing can be fitted with a conical frustum Acrylic window for use with camera's, lasers etc. (…) The model quoted (…) would not be anodised, there would be no pressure testing and there would not be a vent plug included. If you would like us to quote for connector interfaces, brackets, pressure relief valves or chassis etc. please use the request a quote tab and let us know what you need" 	

Table A.2. BellaMare – Subsea Enclosures

BellaMare – Subsea Enclosures	https://www.subseaenclosures.com/enclosuresgallery

"Plastic, aluminium, Stainless Steel, Titanium...From shallow waters to full ocean depth. Once we have your specific requirements, we can recommend materials, enclosure shapes and sealing methods that will best suit your application. We most often provide a turn-key solution that also includes underwater connectors, viewport (glass, acrylic or sapphire), interior mounting rack, external mounting brackets, pressure release valve. When necessary we validate our designs with FEA analysis and provide pressure testing certificates."

Table A.3. Subsea Ranger

Subsea Ranger	https://subsearanger.com/

"Complementing our standard product offering is our capability to provide a custom pressure housing designed to meet your specific needs. Our experienced ocean engineering support will help you identify the specific options you need, considering the deployment carrier, operation depth and deployment and recover interval. unusual sizes and underwater bulkhead connections. Standard titanium pressure housings are single or double opened, bolted cap type pressure housing which utilized radial outer O ring seal and/or face O ring seal. Standard housing has an ID increment of 10 mm and inside depth increment of 50 mm."

PH-Ti-60-200-11000-SO

PH-Ti-60-300-6000-SO

PH-Ti-100-400-6000-SO

Table A.4. OceanTools

OceanTools	https://www.oceantools.co.uk/solutions/subsea-pressure-housings

“Several thousand OceanTools subsea pressure housings of various sizes, shapes and depth ratings have been designed, manufactured and delivered to a wide range of customers. The OceanTools design team has many years of experience, equipped with up-to-date 3D CAD and FEA software. We have delivered housings in materials including hard-anodised aluminium, stainless steel, titanium, nylon and UHMWPE. Safety factors are built into all our designs. Housings are supplied with O-rings and fasteners as appropriate, and can include underwater bulkhead connectors, mating connectors, connector assemblies, power supplies, internal brackets etc.”


Table A.5. Marine Solutions

Marine Solutions	https://marinepropulsionsolutions.com/mps-subsea/pressure-electronic-housings/

"Marine Propulsion Solutions, is a subsea engineering company who designs and manufactures affordable, harsh environment aluminium, stainless steel and Titanium enclosures for housing electrical components to full ocean depth. MPS’s enclosures are often used for thruster motor controllers, batteries, lights, camera, laser, hydrophones, data-loggers and other sensing and monitoring equipment, instrumentation housings, junction boxes, underwater camera enclosures, general subsea enclosures with internal/external mounting brackets. We offer multiple families of pressure housings which live up to their pressure rating. which can have many underwater connector interfaces and are used extensively with Remotely Operated Vehicles (ROVs), Autonomous Underwater Vehicles (AUVs) and for many other applications in the oil and gas industry, defence, research, environmental monitoring and offshore renewables.”



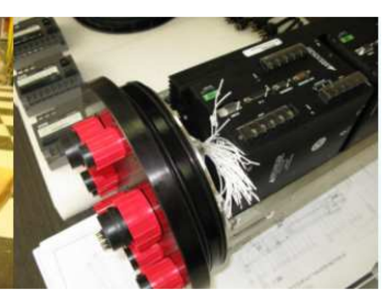

Table A.6. Robotic Ocean

Robotic Ocean	https://www.roboticocean.com/projects/

"Robotic Ocean, LLC is an OEM vendor of aluminium housings/enclosures. we have 18 tube diameters available up to 11.9. All aluminium housings are hard coat anodized for corrosion resistance. these instrumentation subsea enclosures are designed for deep ocean and harsh environments. Interface and assembly drawings are always provided for your approval of the enclosure (i.e. enclosure configuration, hole patterning, hole sizes, hole thread detail, internal bracketing, bulkhead clearances, and hole geometric dimensioning and tolerances). Composite pressure vessels are made from polyvinyl chloride, a plastic that can be utilized for subsea applications as junction boxes, electrical instrumentation housings, sensor battery enclosures, aerospace casings or chemical/biological containment. It comes in a variety of various wall thicknesses and diameters, hence the pressure limitations are different for each selection. Endcaps customization's for electrical connections, vent plugs, or other specialized hardware/apparatus is arranged."


Table A.7. OMNI Instruments

OMNI Instruments	https://www.omniinstruments.co.uk/

"Subsea aluminium housings for instrumentation and data loggers, suitable for immersion up to 300 metres of seawater, sizes 100mm and 160mm nominal bore with internal lengths from 100mm to 700mm. Options are available for one end cap to have a clear window suitable for viewing a display or a rotary switch for power on/off or other functions requiring a switch input."

"Stainless Steel subsea housings for instrumentation and data loggers with an immersion depth of up to 4000 metres of seawater. Housings can be fitted with supporting cradles for internal instrumentation, suitable numbers of subsea bulkhead connectors and can be provided with pressure testing certification. Medium and large housings also have the option of display windows."



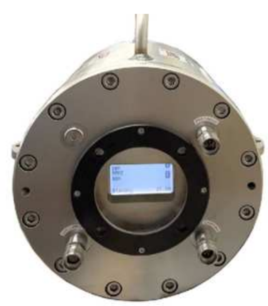

Table A.8. Blue Robotics

Blue Robotics	https://bluerobotics.com/product-category/watertight-enclosures/

“Completely configurable with a variety of tube and end cap options offering a substantial upgrade over the first generation of watertight enclosures. Precision machined O-ring interfaces, a locking cord and anti-rotation feature to secure the flange, and smooth O-ring lead-in make these enclosures a perfect fit for a wide range of applications including MATE and Robosub ROVs, subsea batteries, cameras, electronics, data loggers, environmental monitoring, instrument housings, junction boxes, and more. When used with the clear acrylic plastic tube option, it’s easy to see the components inside the enclosure, ideal for subsea development projects and research ROVs and AUVs. The aluminium tube option provides a greater depth rating, opaque appearance, and better thermal transfer for high power applications like power supply housings and battery housings. A variety of end caps are available for the ends of the enclosure including an optically clear acrylic dome, optically clear flat end cap, and aluminium end caps with 0, 4, and 7 holes, making it easy to attach any of our products with M10 threads like cable penetrators and pressure sensors. We also provide the 2d and 3d files for the end caps, allowing you to design and create custom end caps out of flat material to produce fully customized enclosures for any application.”

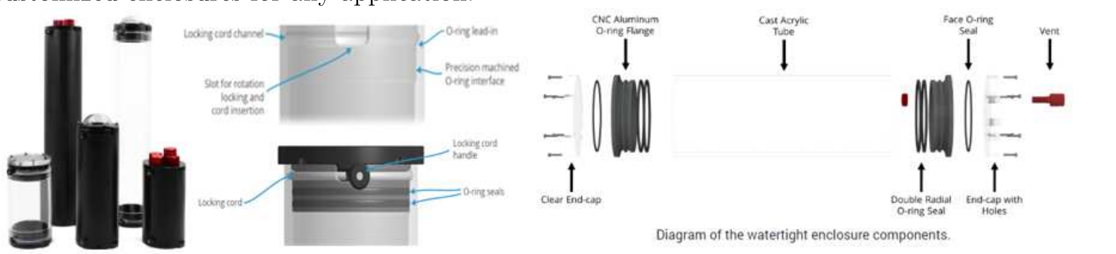

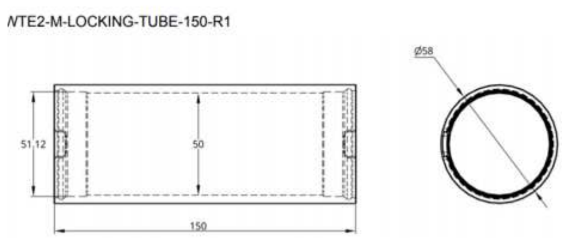

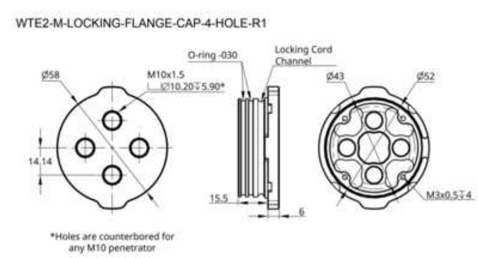

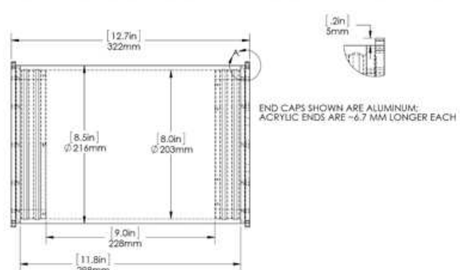

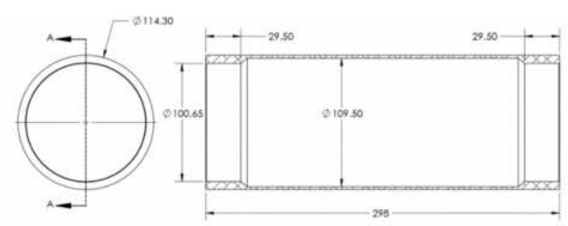

Table A.9. Impact Subsea

Impact Subsea	https://www.impactsubsea.co.uk/isp1/

"…(ISP1) is provided with a viewport which is ideal for use with a camera, subsea display or to facilitate a wireless link, (…) (while ISP2 is) provided with bespoke end caps the ISP2 is ideal for use as an instrumentation housing, control or battery pod. Lightweight and of a small diameter ensures that the ISP1 housing is suitable for a large variety of subsea applications, including installation to an AUV or ROV. Within the housing, room has been provided for inclusion of electronics and/or batteries. (Can) be provided with an integrated Depth sensor, AHRS, battery holder or a variety of other components – contact us to discuss your requirements"

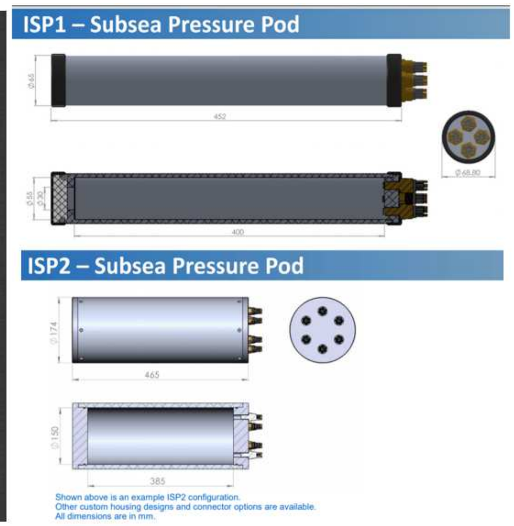

Table A.10. K.U.M. Umwelt

K.U.M. Umwelt	https://kum-kiel.de/en/products/titan/pressure-tube/

"To offer pressure housings made of titanium grade 5 (TiAl6V4) in the highest quality and at an unbeatable price makes us an internationally renowned partner in deep-sea research. Titanium is by 44% lighter than steed. By that less floatation is necessary and hence weight and costs are saved. Our pressure tubes are corrosions-free and can be deployed up to a depth of 6000m, if desired even to ultra-deep depth. Before delivery, each tube is pressure-tested in our pressure tank and certified."



Table A.11. Develogic

Develogic	http://www.develogic.de/products/underwater-housing-systems/mch-base-housing/

“The requirements for underwater housings are manifold – high depth rating, easy to handle and maintain, robust for use under rough conditions which are given on the open sea, corrosion-resistant with no limitation for the operation period and lightweight. And often we were faced with customer demands for more flexibility and the possibility to reconfigure the housings – e.g. the potential to adapt the housing to different applications with no or only very limited effort. With these requirements, we started the development of a totally new housing concept. Since 2013 Develogic offers a new range of titanium housings (DW.TH). The new range of DW.TH housings is a lightweight and easy to handle alternative to other housings. The DW.TH housings are rated to 6,000m depth. They are available with several standard diameters and lengths as well as with custom dimensions.

The Develogic modular underwater pressure housings are available in various series: Deep Water Modular Titanium Housing (DW.TW standard / compact/ large standard/ large compact). For small but very effective solutions we advise our base housing. It is also available in a shallow-water version (SW. Base) and a deep-water version (DW. Base).

Appendix B

Mesh convergence studies

B.1 Cylindrical shells convergence studies

Table B.1. 2D PSHELL models FEA results

FA Model	Mesh size	#elements	CPU time [sec]	VM Stress [MPa]	P1 Stress [MPa]	P3 Stress [MPa]	Pcr [MPa]
B11	**17**	**1 046**	6	182.0	58.8	193.9	39.29
B10	**15**	**1 388**	7	180.9	55.6	193.9	38.94
B09	**13**	**1 826**	9	180.7	56.6	193.6	38.71
B01	**10**	**3 102**	13	180.5	56.5	193.5	38.39
B02	**9**	**3 992**	17	180.4	58.4	193.5	38.29
B03	**8**	**4 916**	20	180.1	57.0	193.5	38.24
B04	**7**	**6 392**	25	180.0	58.2	193.5	38.18
B05	**6**	**8 634**	64	180.0	57.5	193.5	38.14
B06	**5**	**12 602**	58	180.0	57.9	193.5	38.15
B07	**4**	**19 752**	105	180.0	57.5	193.4	38.05
B08	**3**	**35 282**	190	180.0	57.5	193.4	38.09

Table B.2. 3D PSOLID models FEA results

FEA Model	Mesh size	#elements	CPU time [sec]	VM Stress [MPa]	P1 Stress [MPa]	P3 Stress [MPa]	Pcr [MPa]
E01	**5**	**218 765**	174	192.2	45.9	229.6	46.80
E02	**4**	**504 948**	423	190.5	45.9	226.1	39.87
E03	**3**	**1 058 002**	1095	189.8	45.9	225.2	37.11
E05	**2.5**	**1 828 274**	2633	189.5	45.9	223.4	35.65
E04	**2**	**3 661 802**	3566	189.3	45.9	223.5	35.39

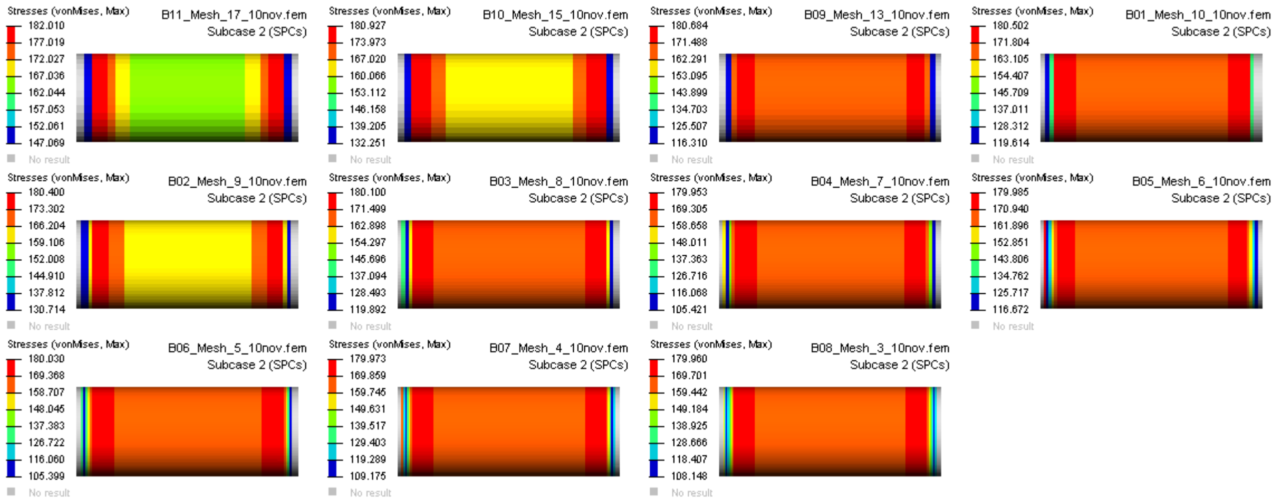

Figure B.1. 2D PSHELL – Von Mises

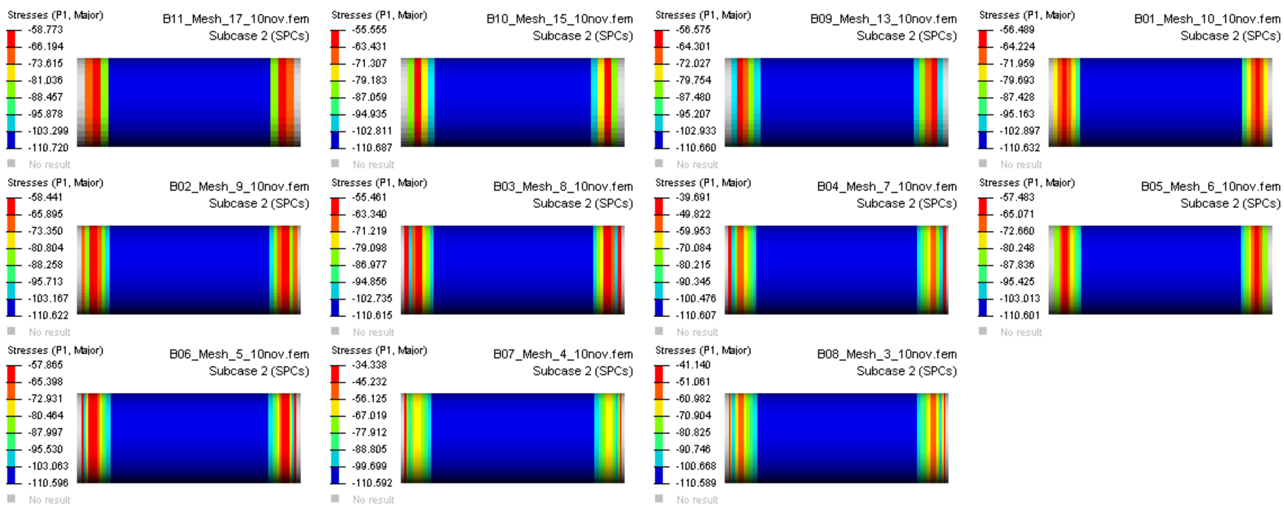

Figure B.2. 2D PSHELL – Tension (P1)

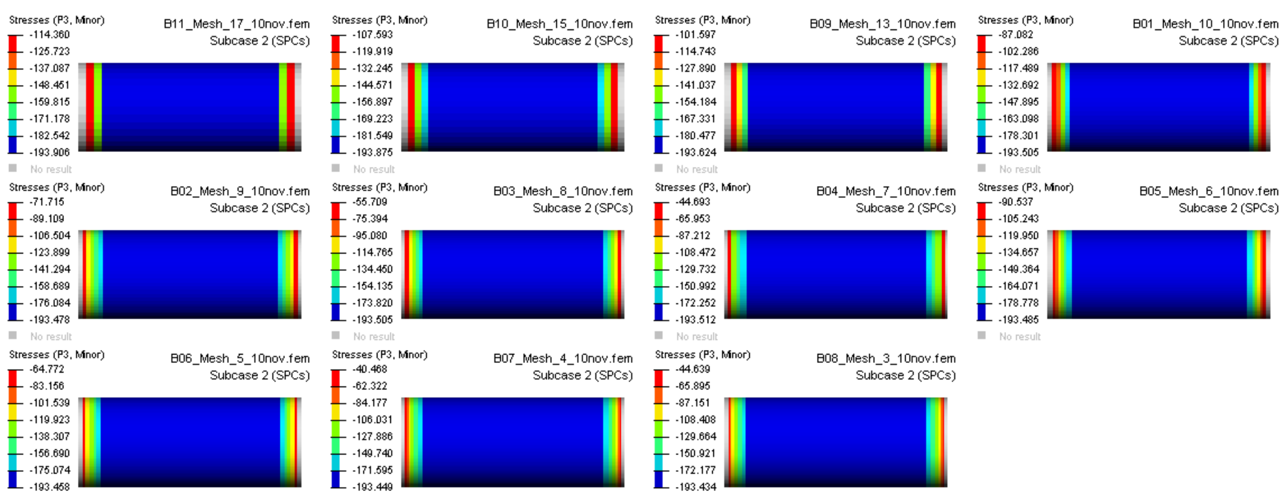

Figure B.3. 2D PSHELL – Compression (P3)

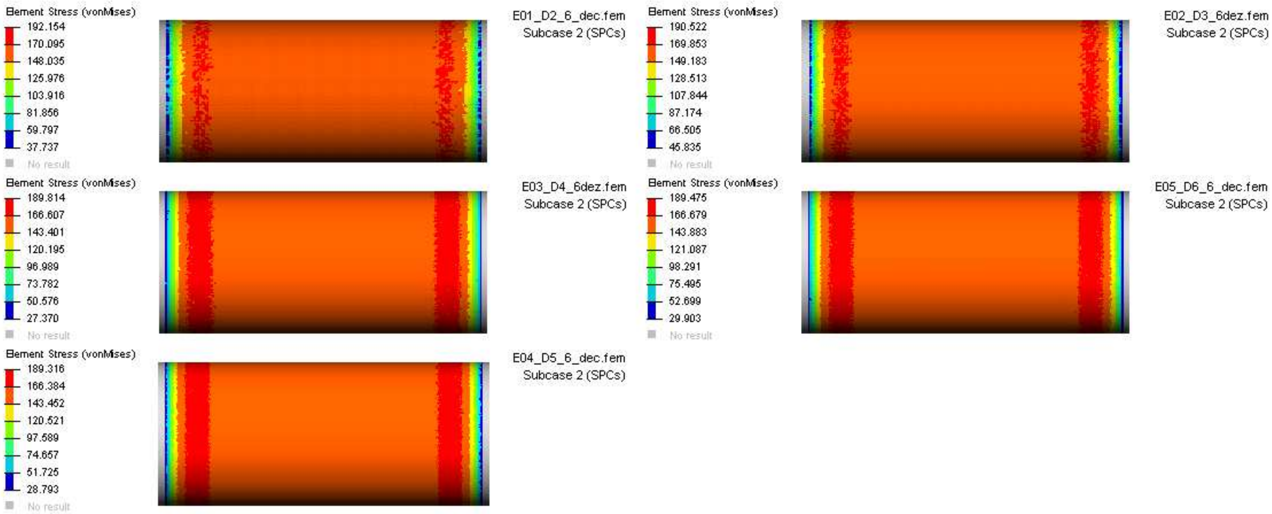

Figure B.4. 3D PSOLID –Von Mises

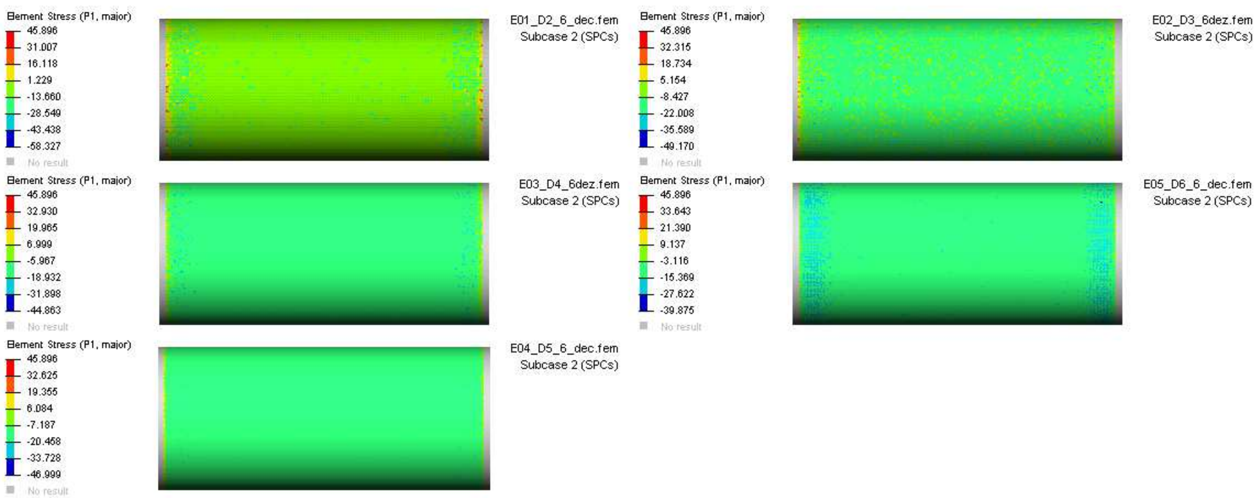

Figure B.5. 3D PSOLID –Tension (P1)

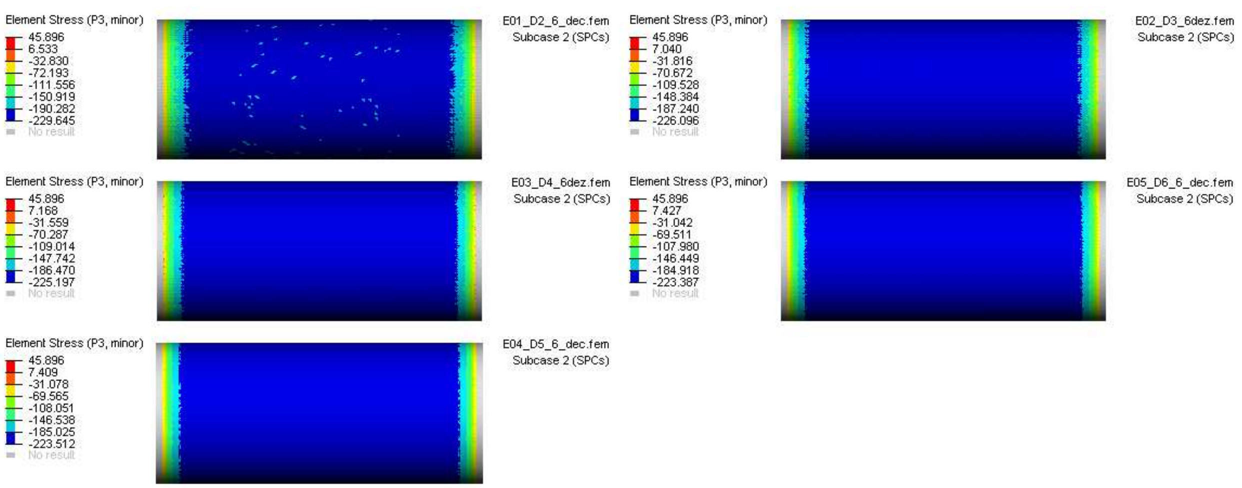

Figure B.6. 3D PSOLID –Compression (P3)

B.2 SCC detailed models convergence studies

Table B.3. detailed models FEA results at NDP – detailed vessel

FEA Model	Mesh size	#elements	CPU time [sec]	VM Stress [MPa]	P1 Stress [MPa]	P3 Stress [MPa]	Pcr [MPa]
A28	**9**	82916	51	192.9	56.3	231.6	38.42
A26	**8**	120499	66	192.2	123.0	232.1	38.07
A27	**7**	178066	87	191.6	90.2	271.4	37.67
A17	**6**	327507	165	197.8	109.4	264.6	37.39
A24	**5.5**	418898	382	203.9	93.7	289.8	37.27
A18	**5**	547101	685	202.5	112.6	299.2	37.19
A23	**4.5**	712095	1023	202.1	95.5	280.5	37.11
A19	**4**	978941	1367	212.0	139.7	287.7	37.09
A22	**3.5**	1529477	2152	212.3	101.3	294.2	37.07
A21	**3**	2225687	4964	221.3	91.3	321.3	37.05

Table B.4. detailed models FEA results at NDP – zones selected for convergence

FA Model	Mesh size	VM - Zone 1 [MPa]	VM - Zone 2 [MPa]	VM - Zone 3 [MPa]	VM - Zone 4 [MPa]
A28	**9**	187.9	192.9	117.2	65.9
A26	**8**	187.5	192.2	115.3	68.4
A27	**7**	187.3	191.6	110.3	69.0
A17	**6**	187.2	191.1	109.6	71.1
A24	**5.5**	186.7	190.8	108.4	71.4
A18	**5**	186.2	190.7	106.6	72.8
A23	**4.5**	186.5	191.3	106.5	71.8
A19	**4**	187.0	191.2	102.6	72.7
A22	**3.5**	186.5	190.4	102.4	74.3
A21	**3**	186.1	190.3	102.9	74.1

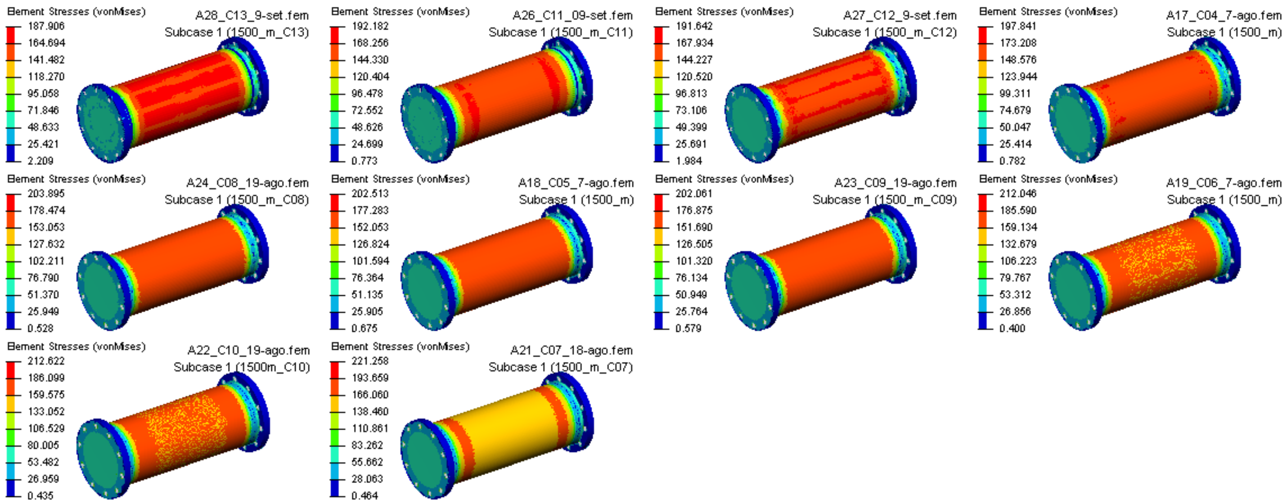

Figure B.7. 3D Full Models –Von Mises

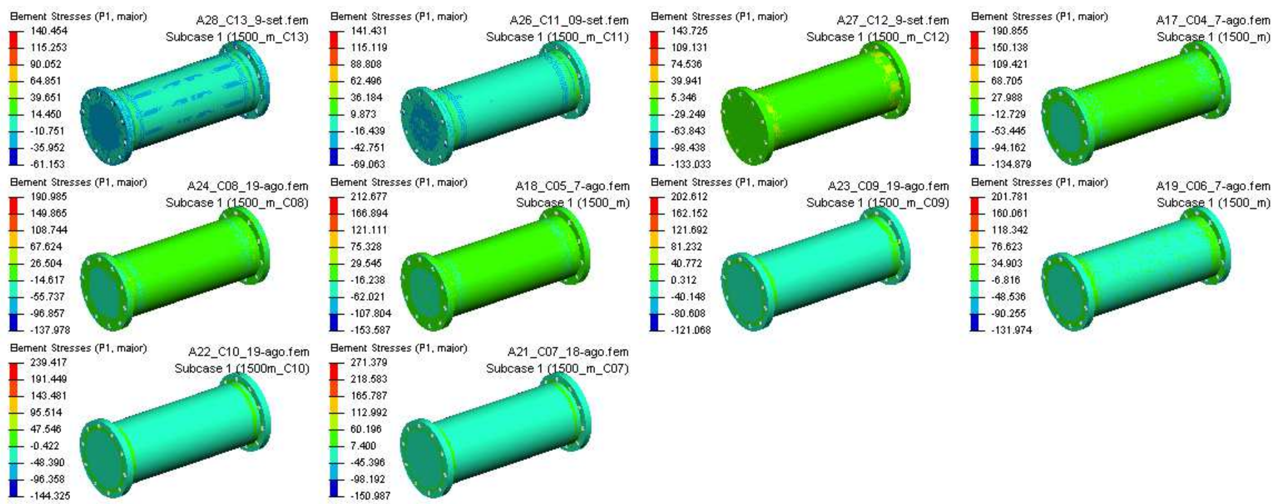

Figure B.8. 3D Full Models –Tension (P1)

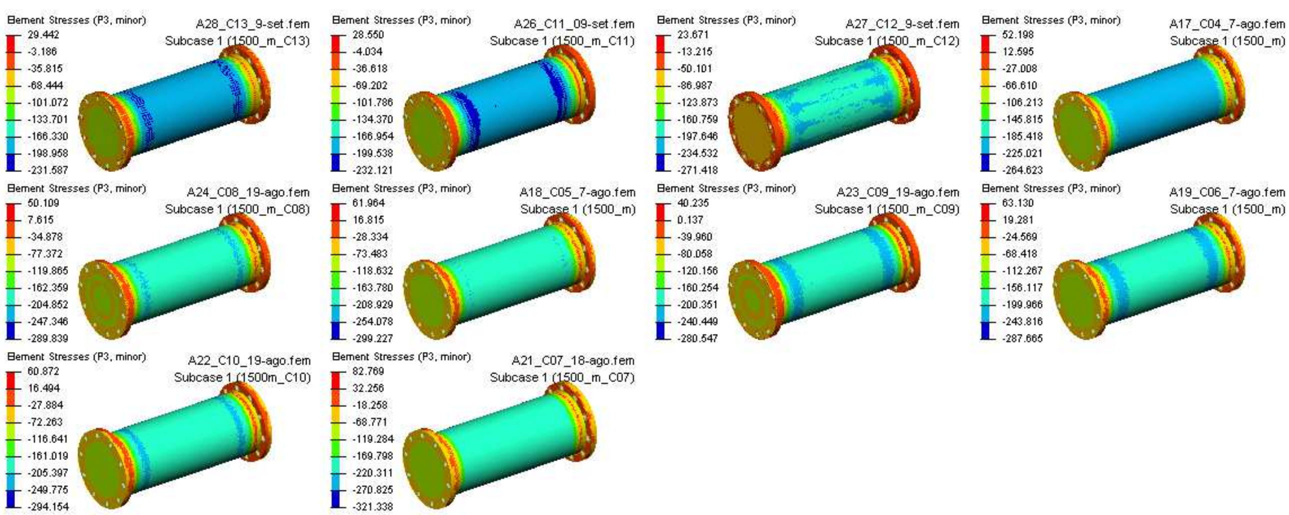

Figure B.9. 3D Full Models –Compression (P3)

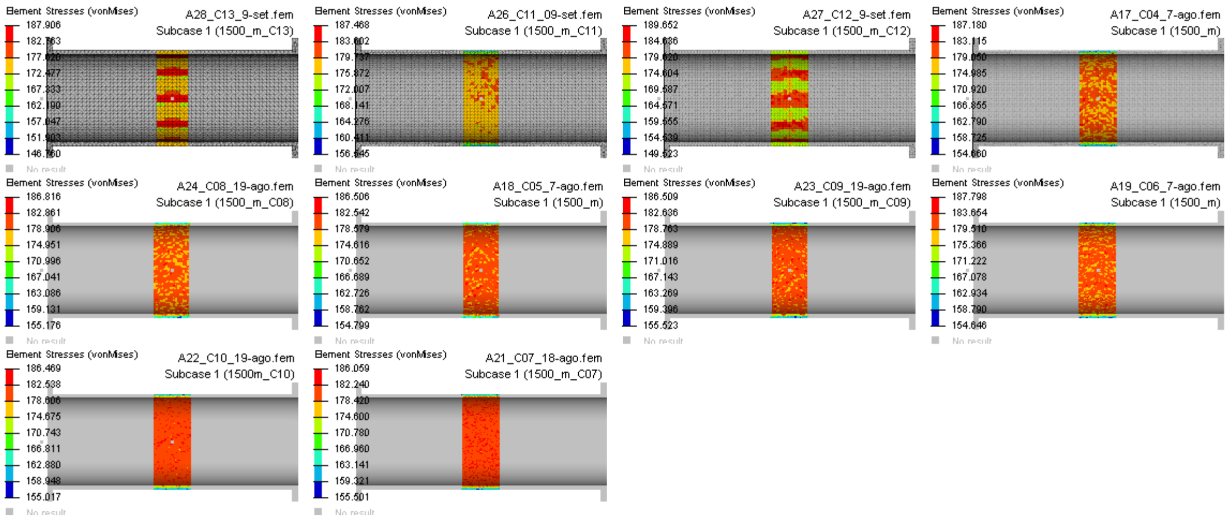

Figure B.10. Zone 1 –Von Mises

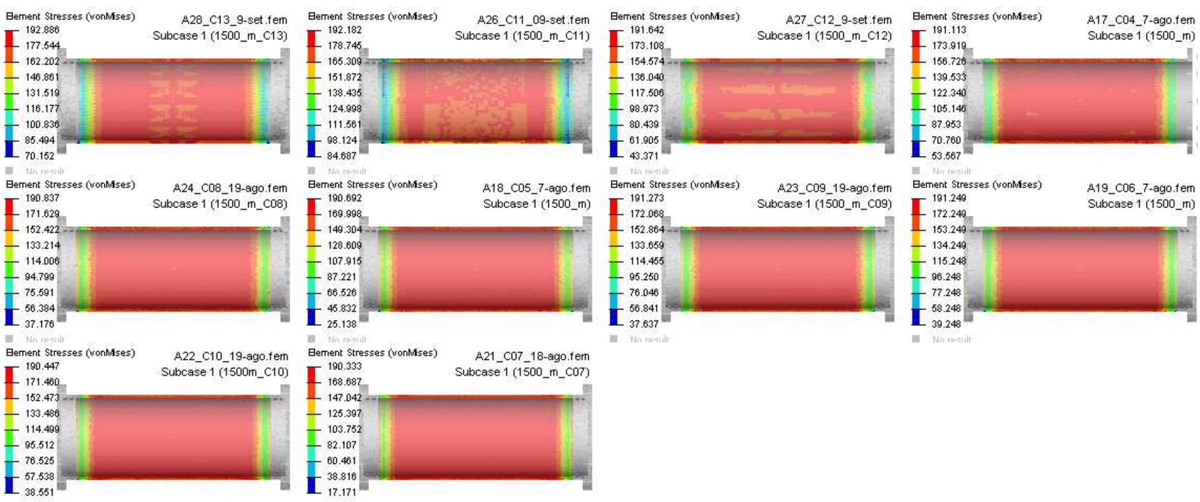

Figure B.11. Zone 2 –Von Mises

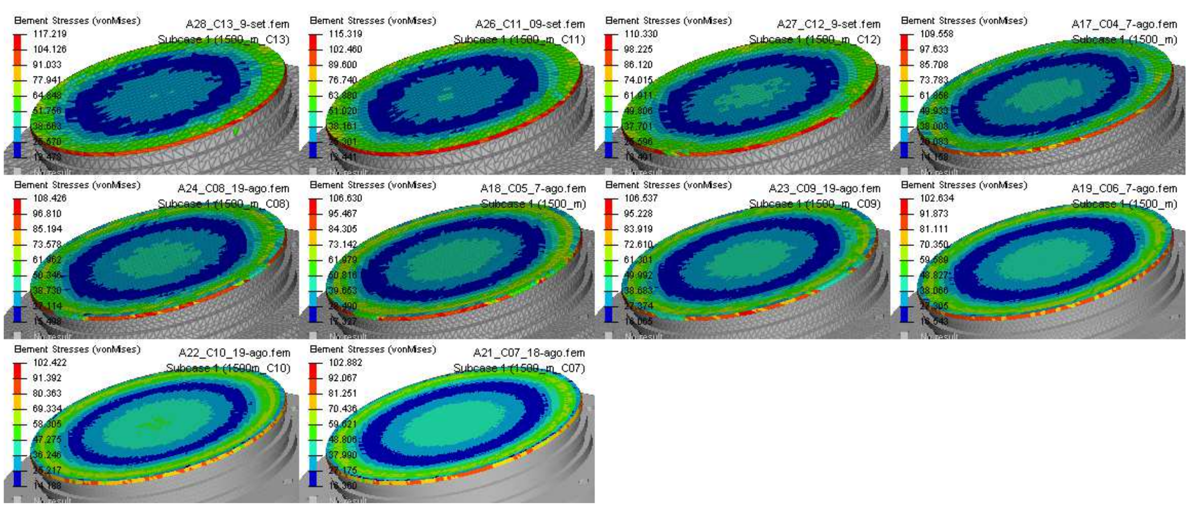

Figure B.12. Zone 3 –Von Mises

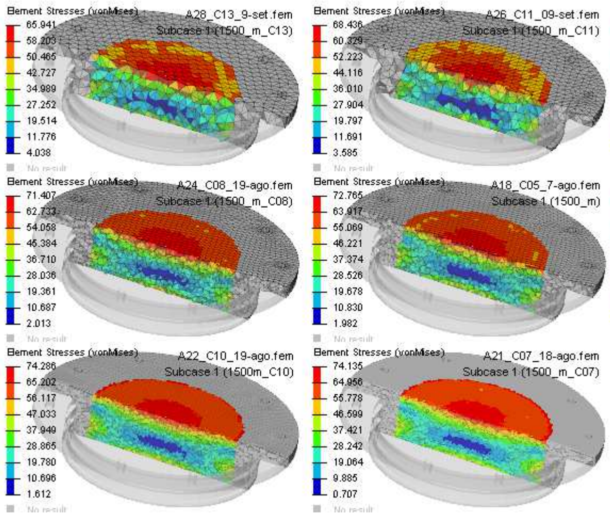

Figure B.13. Zone 4 –Von Mises

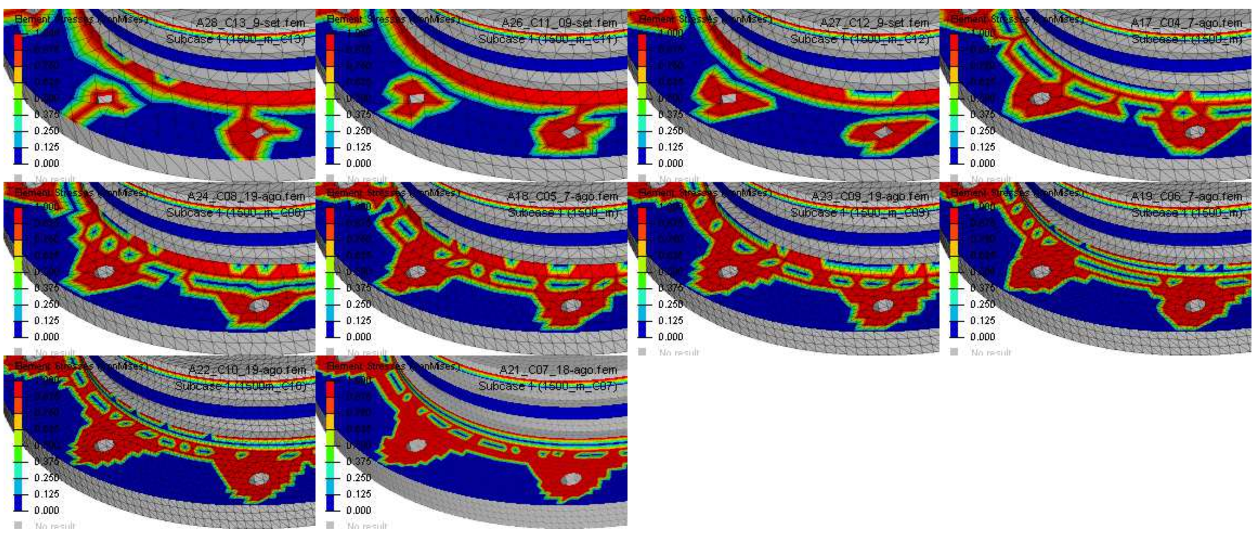

Figure B.14. Cap contact interface – contact status

Parametric studies FEA results

C.1 RTV parametric study

Table C.1. RTV parametric study FEA results at NDP

FEA Model	N_w	W_0	W_0/t	VM Stress [MPa]	P1 Stress [MPa]	P3 Stress [MPa]	Pcr [MPa]	Deflected mode shape
B00	0	**0**	**0.0**	190.5	23.3	225.2	35.39	n=3
B01	2	**0.5**	**0.06**	193.6	46.1	232.7	35.81	n=3
B02		**1.0**	**0.13**	199.1	44.0	240.0	35.49	
B03		**2.0**	**0.25**	208.5	48.9	260.0	34.39	
B04		**4.0**	**0.50**	258.7	67.6	307.6	30.69	
B05	3	**0.5**	**0.06**	232.7	109.2	235.8	37.71	n=3
B06		**1.0**	**0.13**	235.1	110.8	244.4	37.28	
B07		**2.0**	**0.25**	226.1	46.6	275.3	34.51	
B08		**4.0**	**0.50**	311.2	91.5	385.6	30.70	
B09	4	**0.5**	**0.06**	194.5	44.4	235.7	36.01	n=3
B10		**1.0**	**0.13**	199.5	41.2	243.8	35.63	
B11		**2.0**	**0.25**	230.9	45.8	280.7	35.01	
B12		**4.0**	**0.50**	323.1	69.2	383.8	32.61	
B13	5	**0.06**	**0.06**	194.6	37.6	242.2	35.78	n=3
B14		**0.13**	**0.13**	200.1	40.3	244.7	35.18	
B15		**0.25**	**0.25**	235.9	44.4	283.5	33.31	
B16		**0.5**	**0.50**	330.1	93.1	387.5	27.85	

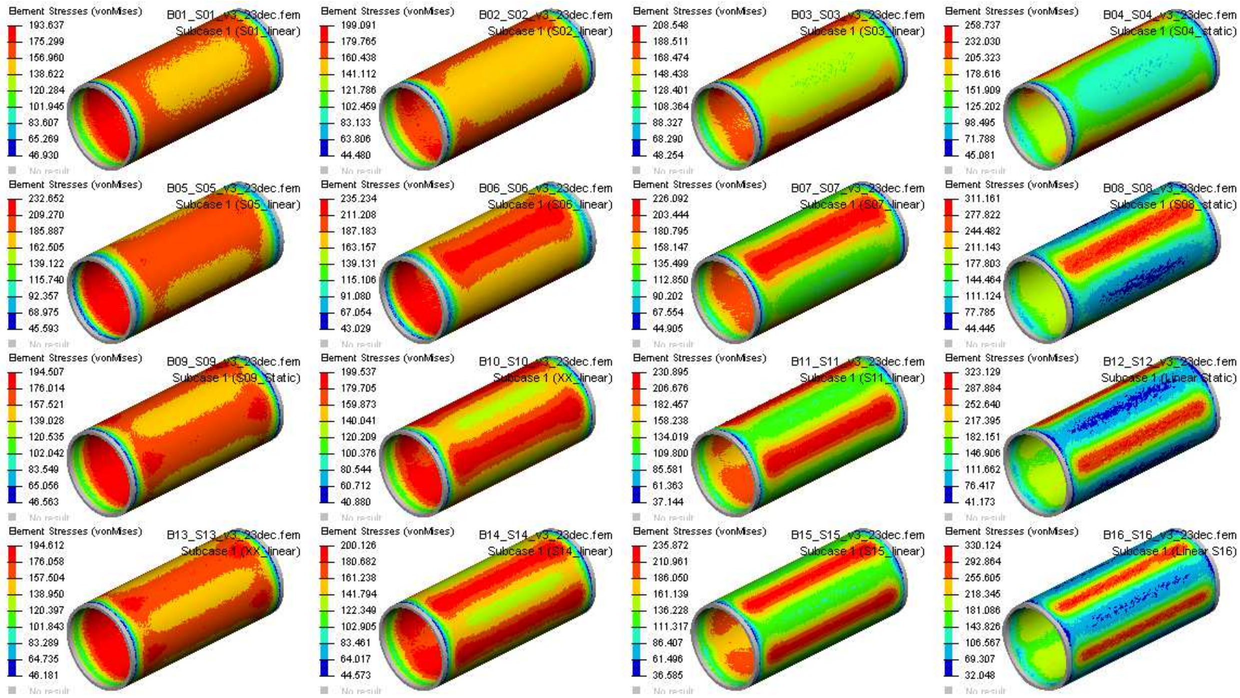

Figure C.1. RTV models – Von Mises

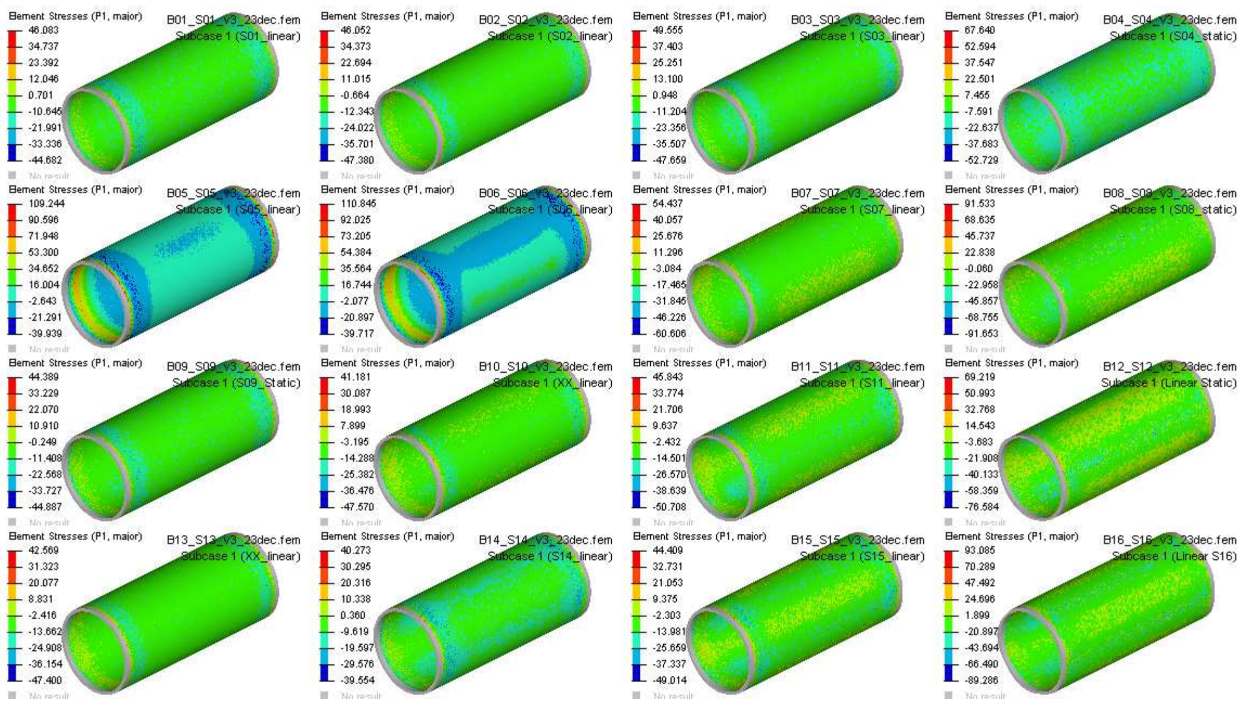

Figure C.2. RTV models – Tension (P1)

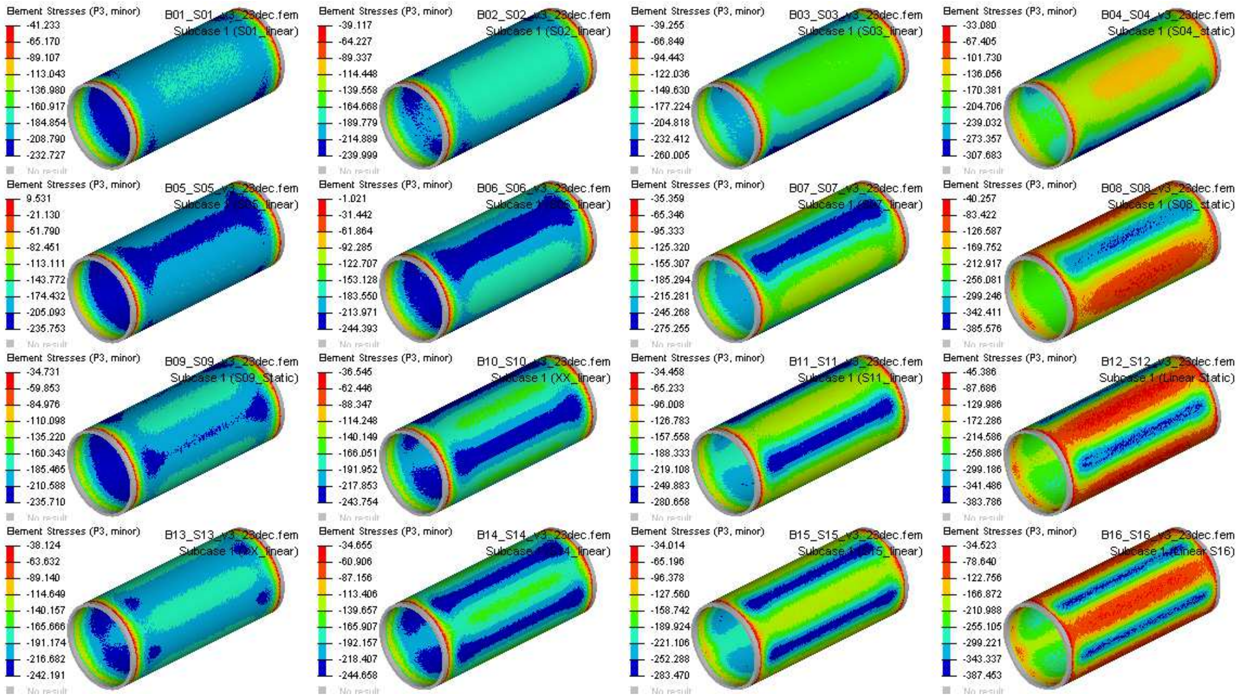

Figure C.3. RTV models – Compression (P3)

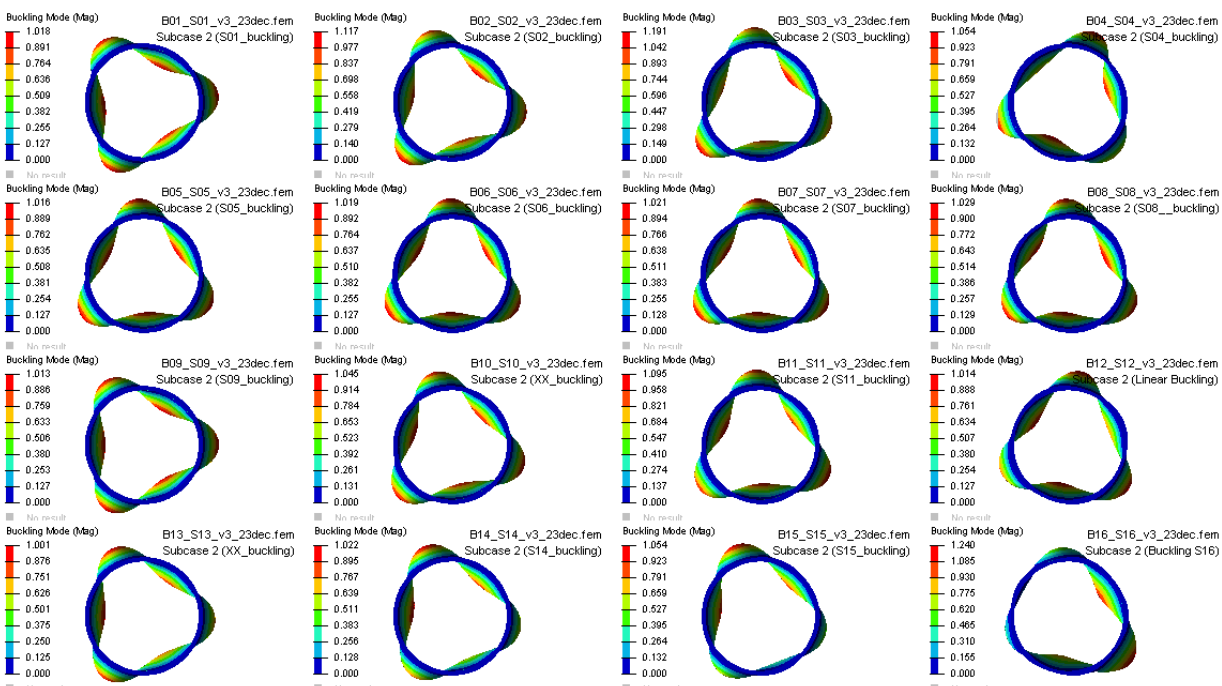

Figure C.4. RTV models –Buckling mode shape

C.2 ATV parametric study

Table C.2. ATV parametric study FEA results at NDP

FEA Model	N_w	W_A	W_A/t	VM stress [MPa]	P1 stress [MPa]	P3 stress [MPa]	Pcr [MPa]	Deflected mode shape
B00	0	**0**	**0.0**	190.5	23.3	225.2	35.39	n=3
B01		**1.0**	**0.13**	193.9	43.0	262.1	41.58	
B02	15	**2.0**	**0.25**	194.8	40.2	261.2	41.63	n=3
B03		**3.0**	**0.38**	252.3	123.4	389.0	44.93	
B04		**1.0**	**0.13**	192.4	44.3	252.8	41.40	
B05	20	**2.0**	**0.25**	199.6	59.5	298.3	42.78	n=3
B06		**3.0**	**0.38**	268.8	125.3	393.0	45.37	
B07		**1.0**	**0.13**	192.5	58.0	256.8	41.35	
B08	25	**2.0**	**0.25**	197.7	56.4	300.8	42.38	n=3
B09		**3.0**	**0.38**	218.6	68.4	388.1	44.48	
B10		**1.0**	**0.13**	192.0	62.6	252.7	41.28	
B11	30	**2.0**	**0.25**	211.7	50.2	314.4	42.16	n=3
B12		**3.0**	**0.38**	225.3	110.1	239.3	46.18	

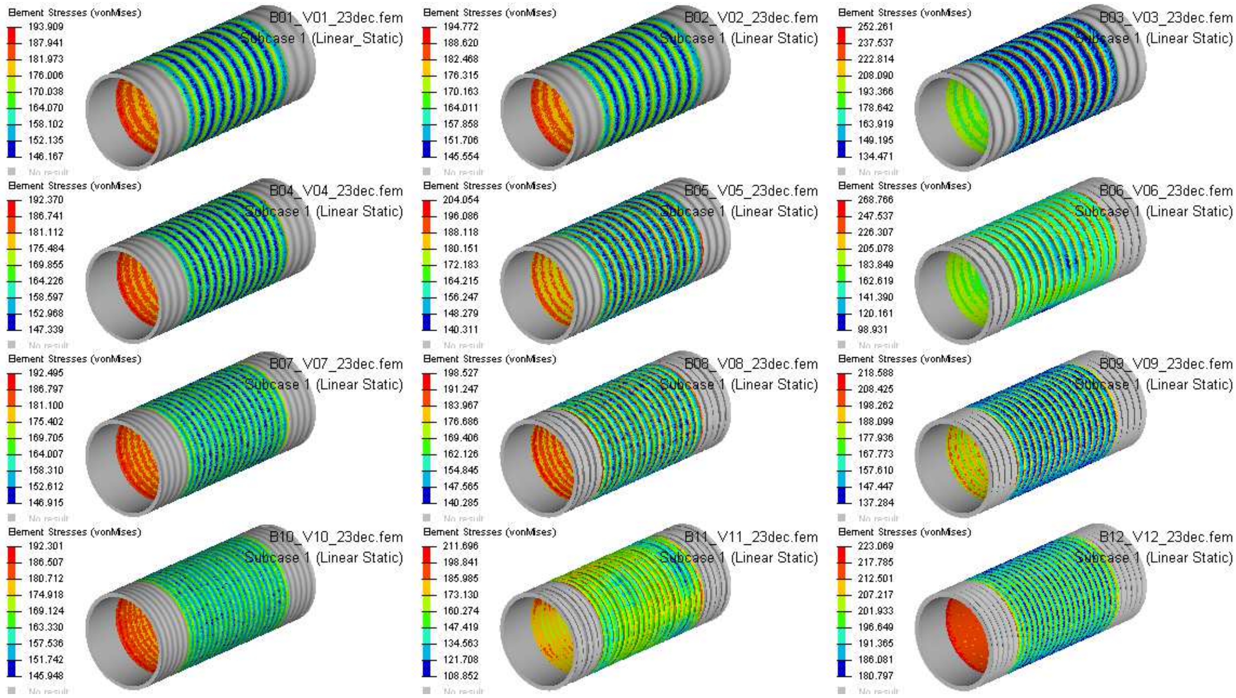

Figure C.5. ATV models – Von Mises

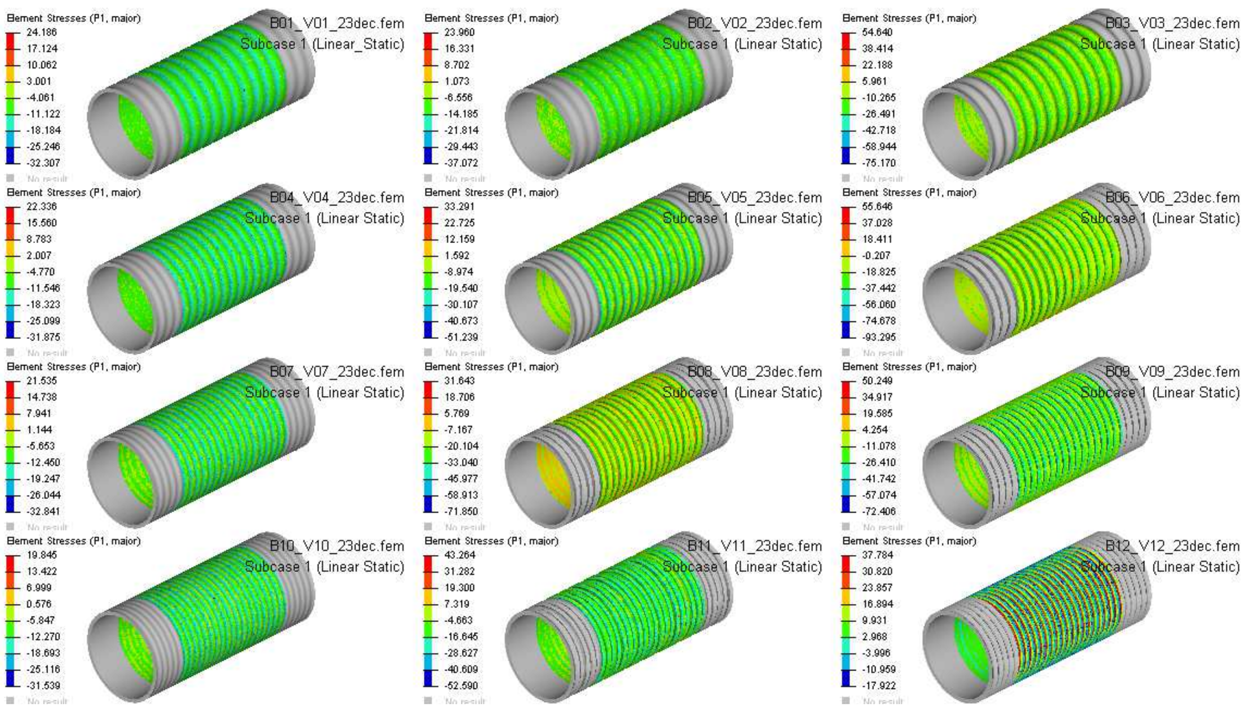

Figure C.6. ATV models – Tension (P1)

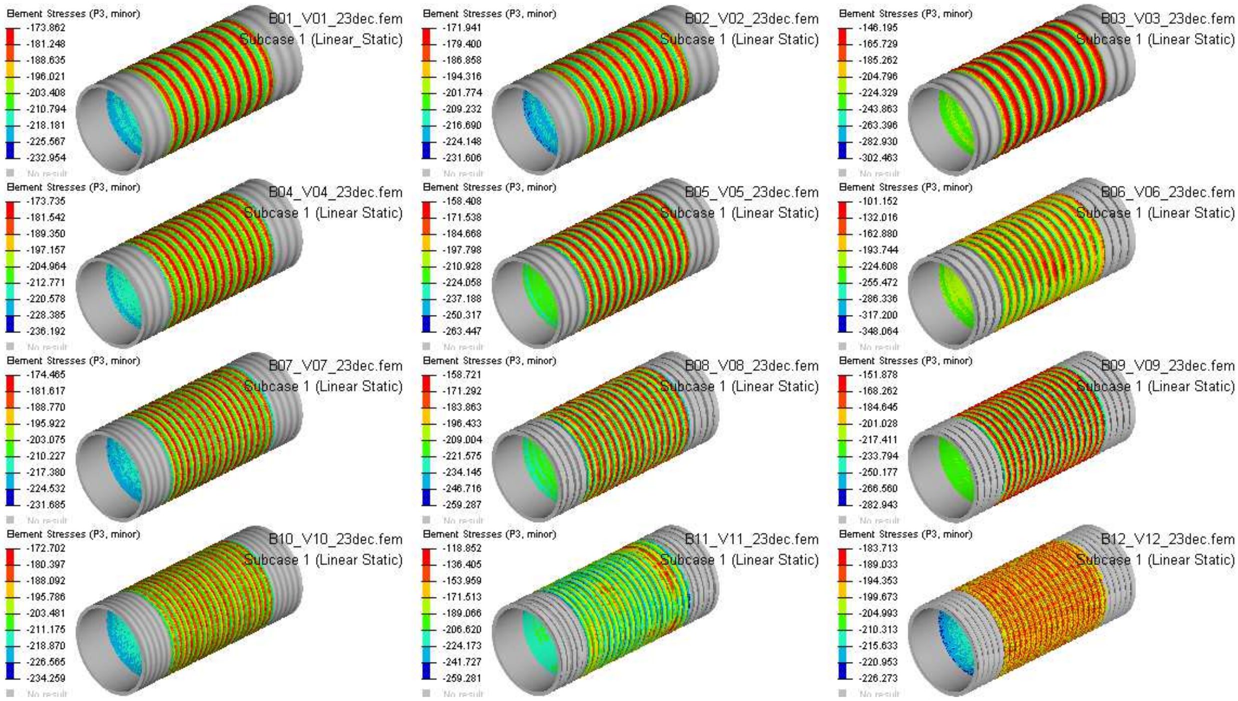

Figure C.7. ATV models – Compression (P3)

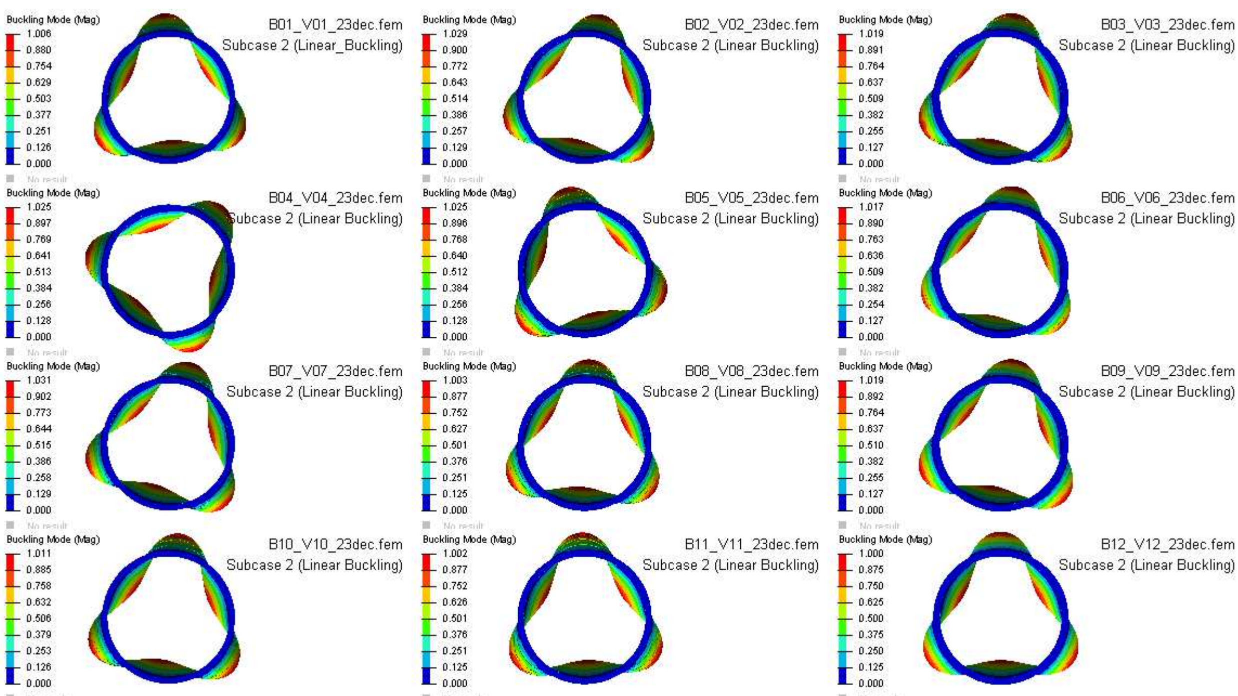

Figure C.8. ATV models – Buckling mode shape

C.3 NCS parametric quadrature study

Table C.3. NCS 2D PSHELL parametric quadrature study FEA results

t_{NCS}	R_f	FEA Model	NDP stress [MPa]	TDP stress [MPa]	TDP MS	CDP stress [MPa]	CDP MS	Pcr [MPa]
8	**100**	**B02**	181.7	218.0	0.80	290.7	0.55	38.0
	90	**B08**	410.3	492.4	-0.20	656.5	-0.31	37.1
	80	**B14**	646.6	775.9	-0.50	1034.6	-0.57	37.3
10	**100**	**B03**	144.8	173.8	1.25	231.7	0.94	69.9
	90	**B09**	287.9	345.5	0.13	460.6	-0.02	68.3
	80	**B15**	425.6	511.2	-0.23	681.6	-0.34	68.7
	70	**B21**	556.5	667.7	-0.41	890.2	-0.49	62.1
12	**100**	**B04**	121.6	144.4	1.69	192.5	1.31	115.7
	90	**B10**	217.6	261.1	0.50	348.2	0.29	112.4
	80	**B16**	329.9	395.9	-0.01	527.8	-0.15	108.4
	70	**B22**	424.9	509.9	-0.23	679.8	-0.34	92.3
	60	**B26**	509.6	611.5	-0.36	815.4	-0.45	78.5
14	**100**	**B05**	102.9	123.5	2.17	164.6	1.73	177.8
	90	**B11**	172.9	207.5	0.89	276.6	0.63	152.9
	80	**B17**	256.4	307.7	0.27	410.2	0.10	150.8
	70	**B23**	326.4	391.7	0.00	522.2	-0.14	131.5
	60	**B27**	398.8	478.6	-0.18	638.1	-0.29	114.8
	50	**B30**	493.9	592.7	-0.34	790.2	-0.43	101.5
16	**100**	**B06**	89.8	107.8	2.63	143.7	2.13	218.0
	90	**B12**	143.1	171.7	1.28	229.0	0.97	202.8
	80	**B18**	207.1	248.5	0.58	331.4	0.36	201.9
	70	**B24**	260.9	313.1	0.25	417.4	0.08	180.8
	60	**B28**	309.1	370.9	0.06	494.6	-0.09	161.1
	50	**B31**	392.9	471.5	-0.17	628.6	-0.28	145.3
	40	**B33**	489.0	586.8	-0.33	782.4	-0.42	133.8
18	**100**	**B07**	79.6	95.5	3.10	127.4	2.53	275.2
	90	**B13**	121.8	146.2	1.68	194.9	1.31	263.2
	80	**B19**	172.1	206.5	0.90	275.4	0.63	262.9
	70	**B25**	214.8	257.8	0.52	343.7	0.31	241.4
	60	**B29**	254.8	305.8	0.28	407.7	0.10	218.6
	50	**B32**	322.1	386.5	0.01	515.3	-0.13	200.1
	40	**B34**	399.3	479.2	-0.18	638.9	-0.30	186.4
	30	**B35**	486.9	584.3	-0.33	779.0	-0.42	177.5

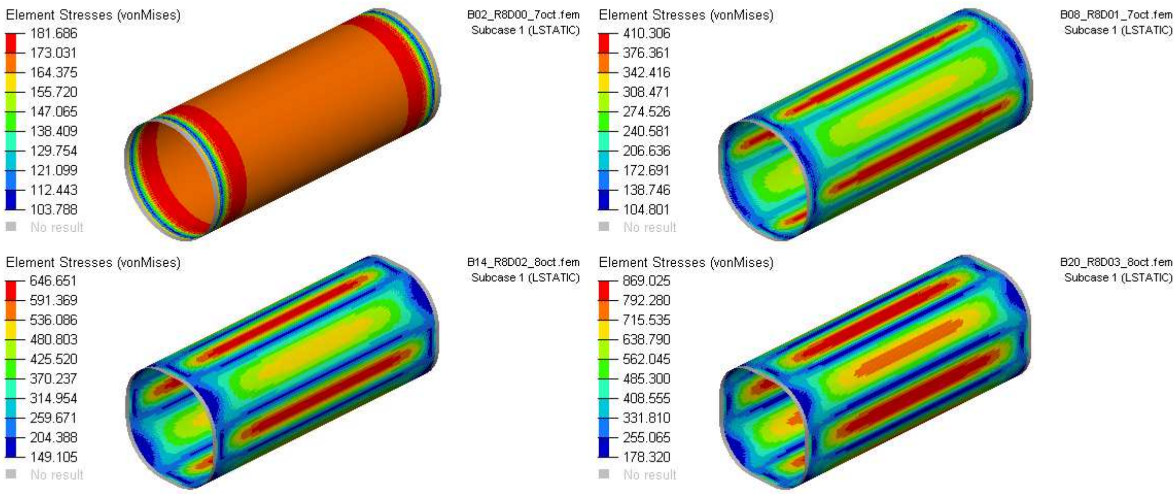

Figure C.9. NCS 2D PSHELL models (VM at NDP) – t = 8.0 mm

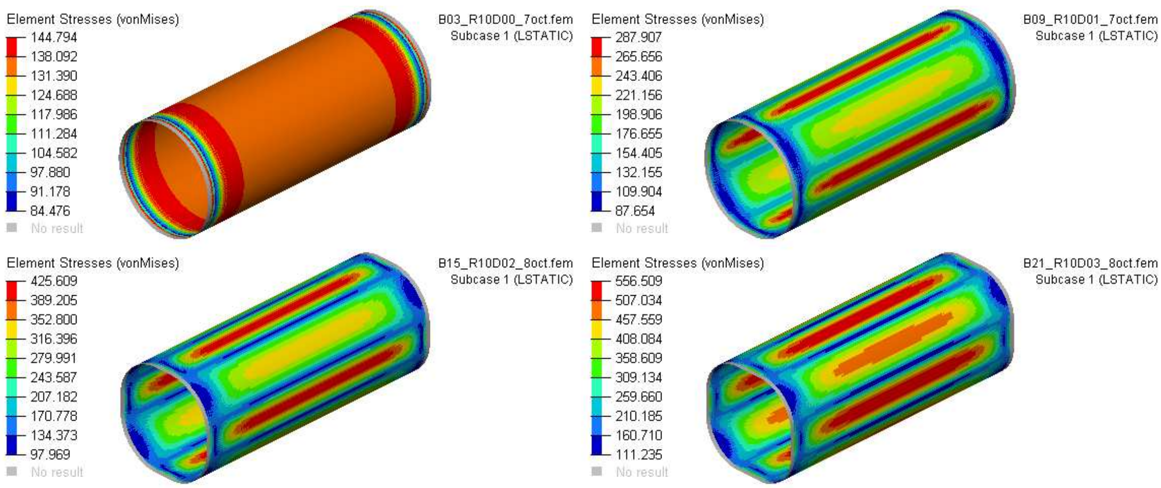

Figure C.10. NCS 2D PSHELL models (VM at NDP) – t = 10.0 mm

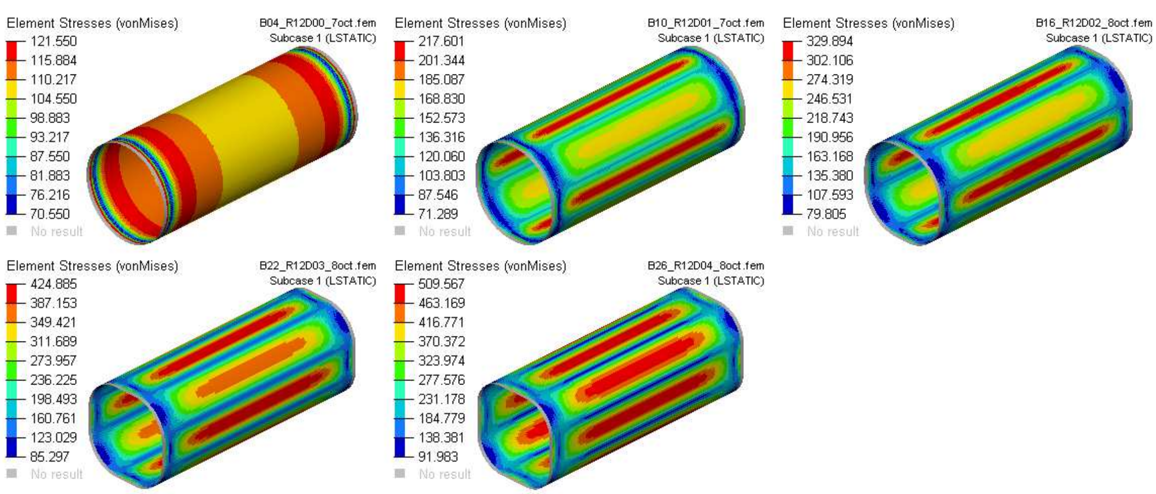

Figure C.11. NCS 2D PSHELL models (VM at NDP) – t = 12.0 mm

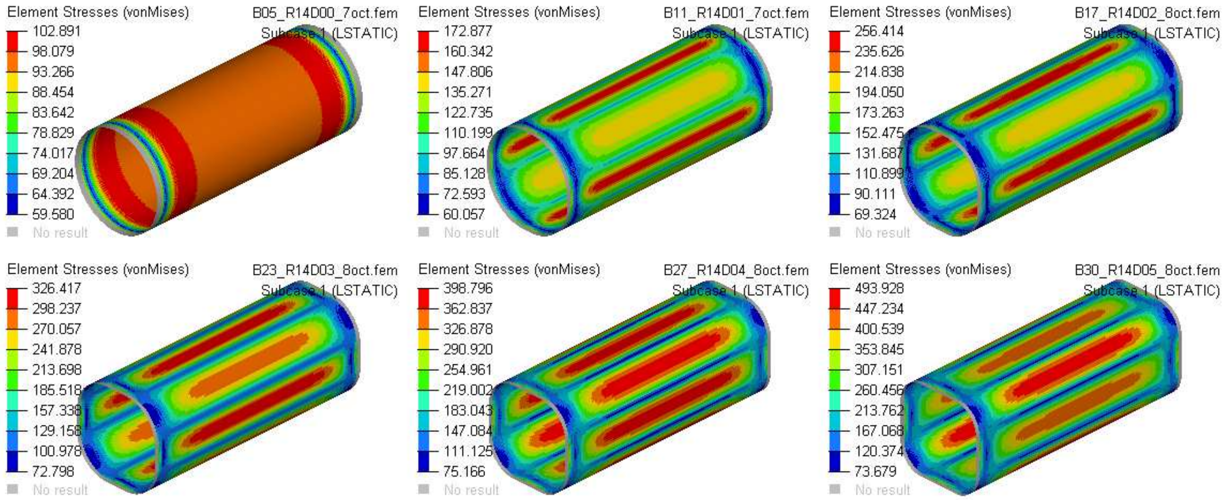

Figure C.12. NCS 2D PSHELL models (VM at NDP) – t = 14.0 mm

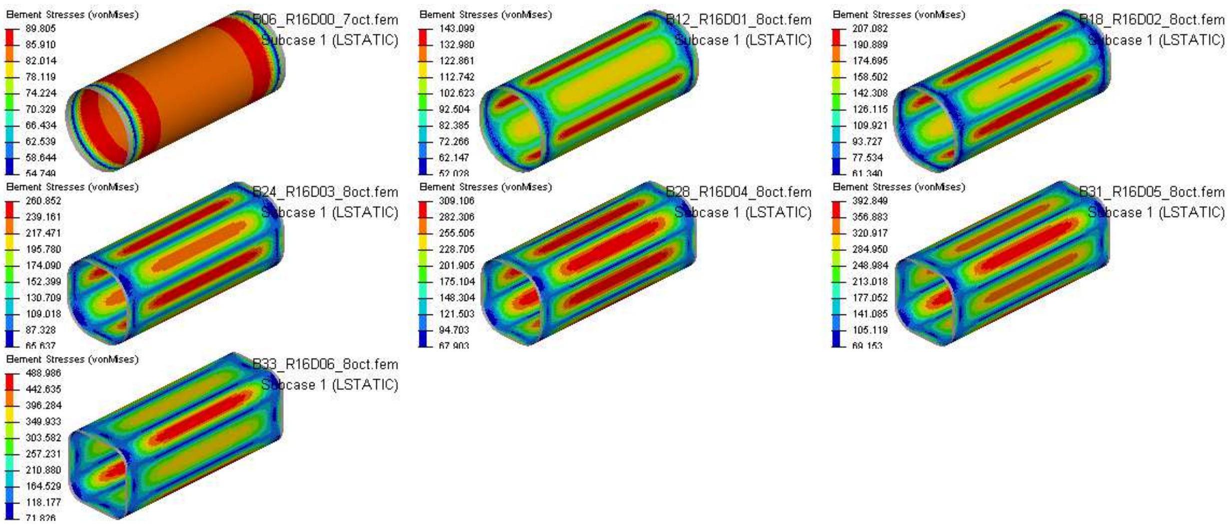

Figure C.13. NCS 2D PSHELL models (VM at NDP) – t = 16.0 mm

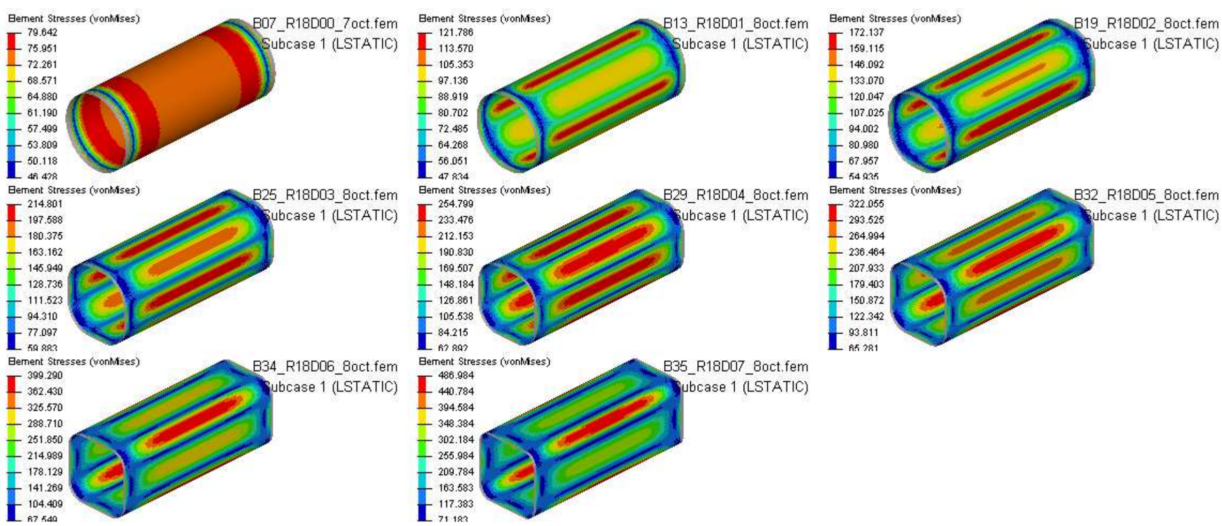

Figure C.14. NCS 2D PSHELL models (VM at NDP) – t = 14.0 mm

Table C.4. NCS 2D PSHELL parametric quadrature study FEA results

t_{NCS}	R_f	FEA Model	NDP stress [MPa]	TDP stress [MPa]	TDP MS	CDP stress [MPa]	CDP MS	Pcr [MPa]
8	**100**	**A01**	191.4	229.7	0.71	306.2	0.47	40.1
	90	**A03**	396.7	476.0	-0.18	634.7	-0.29	39.7
	80	**A04**	569.0	682.8	-0.43	910.4	-0.51	45.8
10	**100**	**A13**	155.8	187.0	1.09	249.3	0.81	67.2
	90	**A14**	271.5	325.8	0.20	434.4	0.04	75.2
	80	**A15**	426.0	511.2	-0.23	681.6	-0.34	72.5
	70	**A16**	556.4	667.7	-0.41	890.2	-0.49	62.2
12	**100**	**A17**	137.5	161.0	1.43	214.7	1.10	100.4
	90	**A18**	221.9	266.3	0.47	355.0	0.27	99.9
	80	**A19**	327.4	392.9	0.00	523.8	-0.14	93.2
	70	**A20**	419.9	503.9	-0.22	671.8	-0.33	84.1
	60	**A21**	511.0	613.2	-0.36	817.6	-0.45	72.1
14	**100**	**A22**	118.8	142.6	1.75	190.1	1.37	143.5
	90	**A23**	175.3	210.4	0.86	280.5	0.60	140.0
	80	**A24**	257.0	308.4	0.27	411.2	0.09	127.0
	70	**A25**	325.4	390.5	0.00	520.6	-0.14	111.6
	60	**A26**	422.2	506.6	-0.23	675.5	-0.33	94.2
	50	**A27**	526.1	631.3	-0.38	841.8	-0.47	83.2
16	**100**	**A28**	106.1	127.4	2.08	169.9	1.65	196.4
	90	**A29**	150.3	180.4	1.17	240.5	0.87	178.1
	80	**A30**	212.2	254.6	0.54	339.5	0.33	159.3
	70	**A31**	269.6	323.5	0.21	431.4	0.04	141.4
	60	**A32**	341.7	410.0	-0.04	546.7	-0.18	125.8
	50	**A33**	425.4	510.5	-0.23	680.6	-0.34	117.1
	40	**A34**	547.2	656.6	-0.40	875.5	-0.49	103.6
18	**100**	**A35**	96.6	115.9	2.38	154.6	1.91	241.9
	90	**A36**	131.4	157.6	1.48	210.2	1.14	221.3
	80	**A37**	174.1	208.9	0.88	278.5	0.62	200.2
	70	**A38**	225.7	270.9	0.45	361.1	0.25	184.3
	60	**A39**	285.1	342.2	0.14	456.2	-0.01	166.4
	50	**A40**	357.7	429.3	-0.09	572.4	-0.21	147.8
	40	**A41**	450.1	540.2	-0.27	720.2	-0.38	140.6
	30	**A42**	574.4	689.3	-0.43	919.1	-0.51	128.8

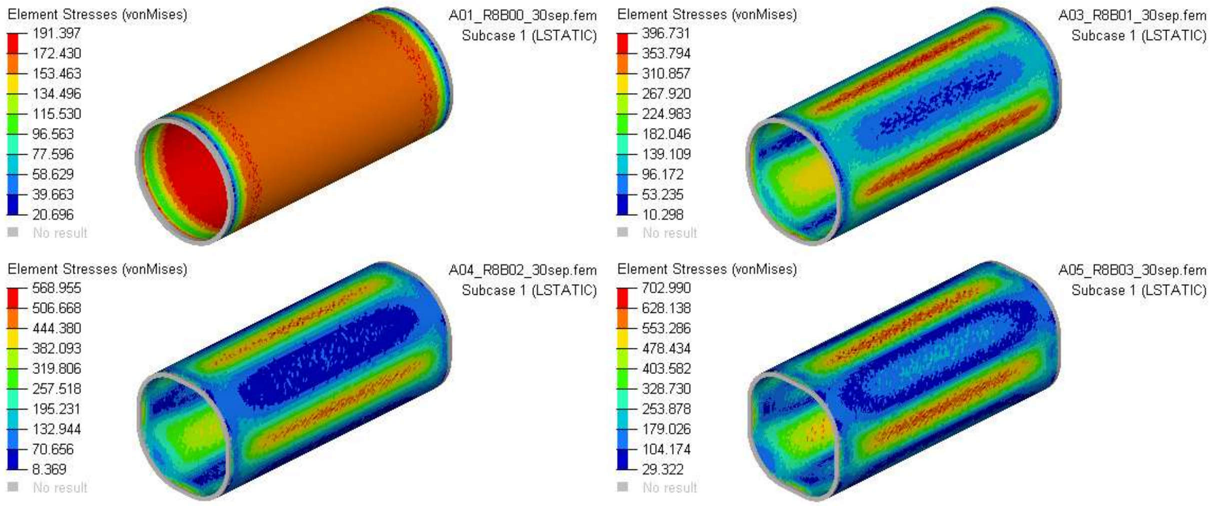

Figure C.15. NCS 3D PSOLID models (VM at NDP) – t = 8.0 mm

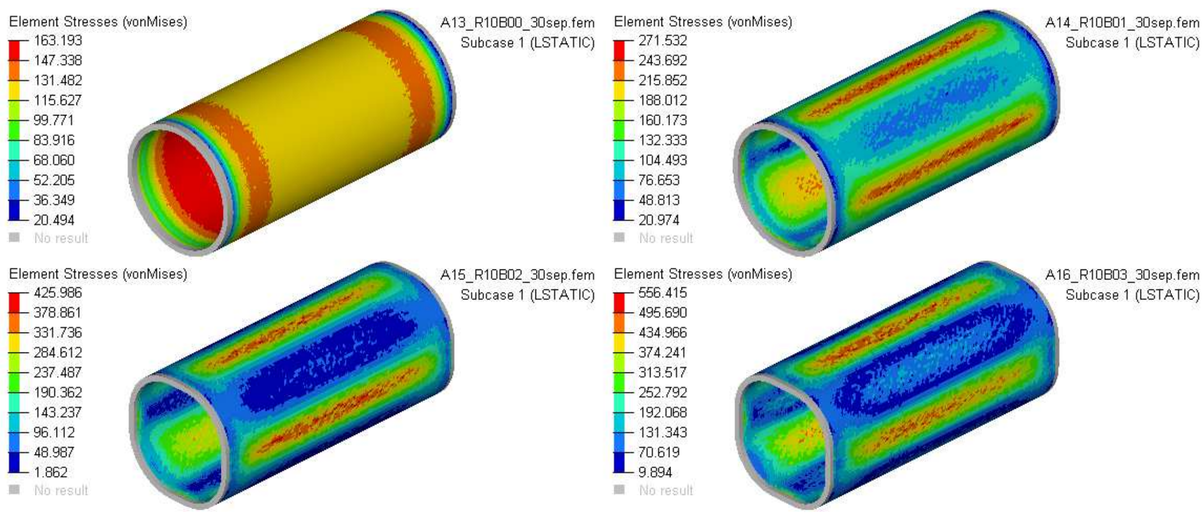

Figure C.16. NCS 3D PSOLID models (VM at NDP) – t = 10.0 mm

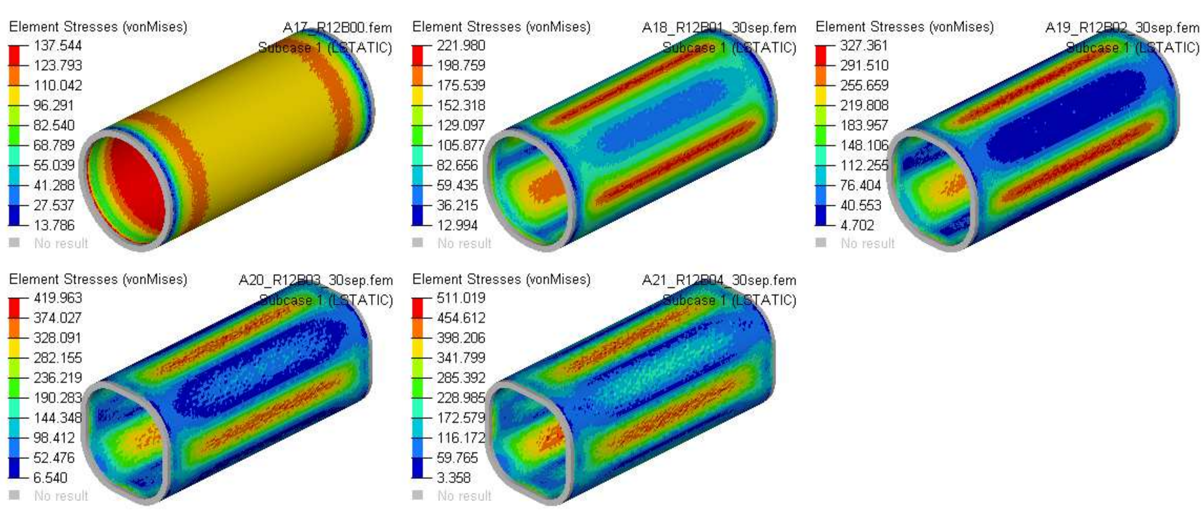

Figure C.17. NCS 3D PSOLID models (VM at NDP) – t = 12.0 mm

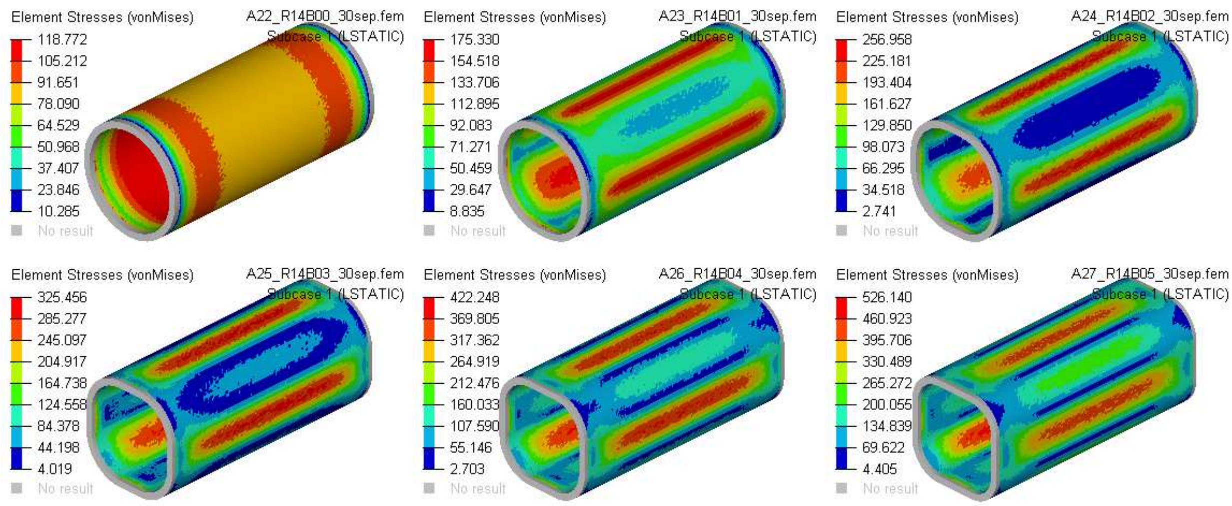

Figure C.18. NCS 3D PSOLID models (VM at NDP) – t = 14.0 mm

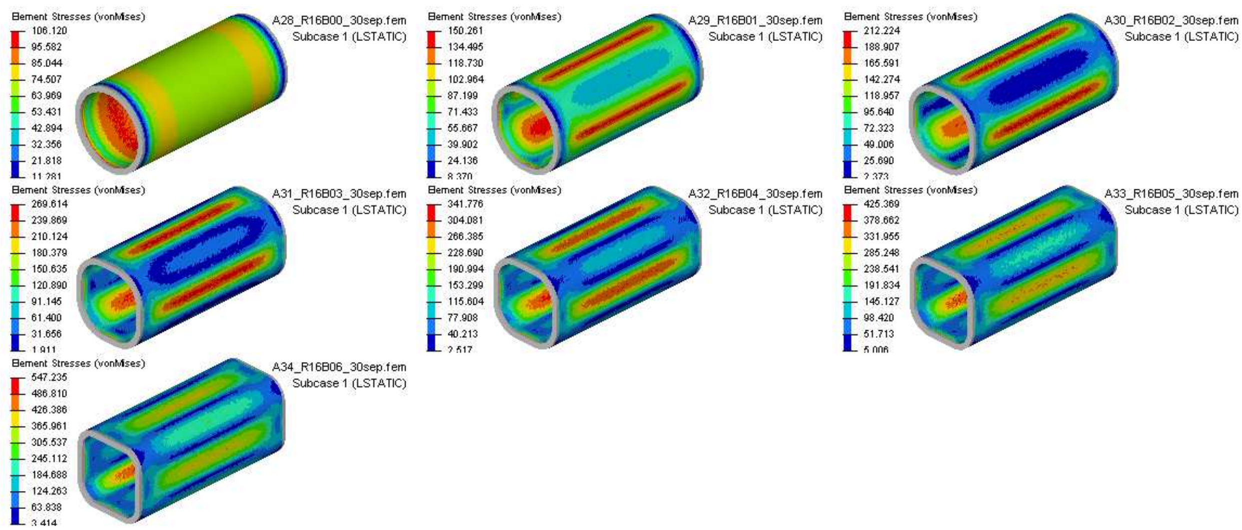

Figure C.19. NCS 3D PSOLID models (VM at NDP) – t = 16.0 mm

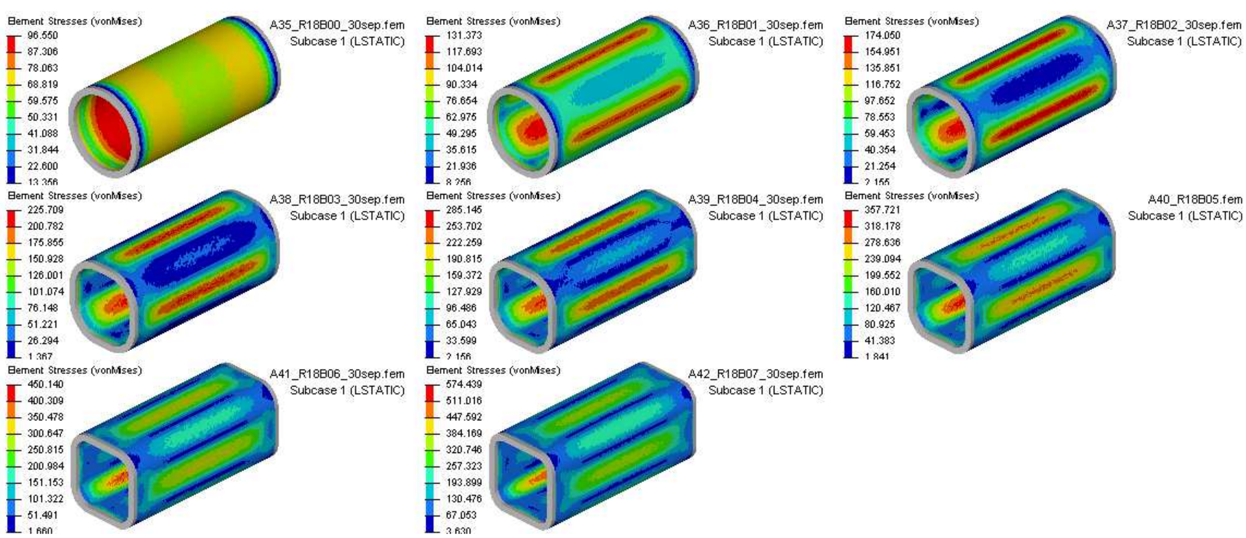

Figure C.20. NCS 3D PSOLID models (VM at NDP) – t = 18.0 mm

C.4 NCS axially stiffened models' study

Table C.5. NCS axially stiffened models' parametric study FEA results

		NDP			TDP			CDP			-
CAD Model	**FEA Model**	VM [MPa]	P1 [MPa]	P3 [MPa]	VM [MPa]	P1 [MPa]	P3 [MPa]	VM [MPa]	P1 [MPa]	P3 [MPa]	Pcr [MPa]
Q00	**C03**	511.0	361.8	654.2	613.2	434.2	785.0	817.6	578.9	1046.7	72.1
Q01	**C01**	533.1	353.4	680.5	639.7	424.0	816.6	853.0	565.4	1088.7	79.0
Q03	**C02**	560.9	429.1	650.7	673.1	515.0	780.9	897.4	686.6	1041.2	75.3
Q02	**C04**	571.7	462.4	879.1	686.0	554.9	1054.9	914.7	739.9	1406.6	75.0
Q04	**C05**	588.6	445.2	855.3	706.3	534.2	1026.4	941.7	712.3	1368.6	80.0
Q05	**C06**	592.3	488.7	852.5	710.8	586.4	1023.0	947.7	781.9	1364.0	75.1
Q06	**C10**	586.2	367.4	736.9	703.5	440.8	884.3	937.9	587.8	1179.1	102.5

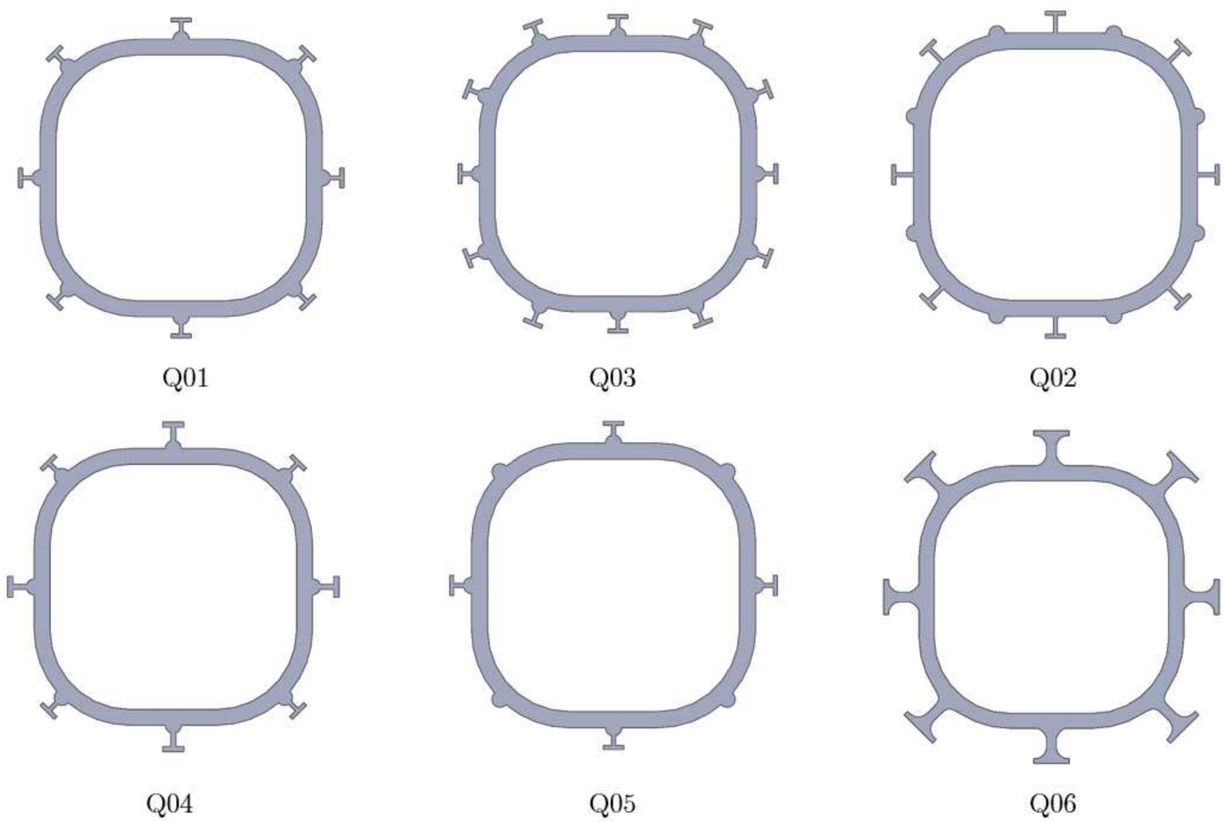

Figure C.21. NCS axial stiffened models' cross-section

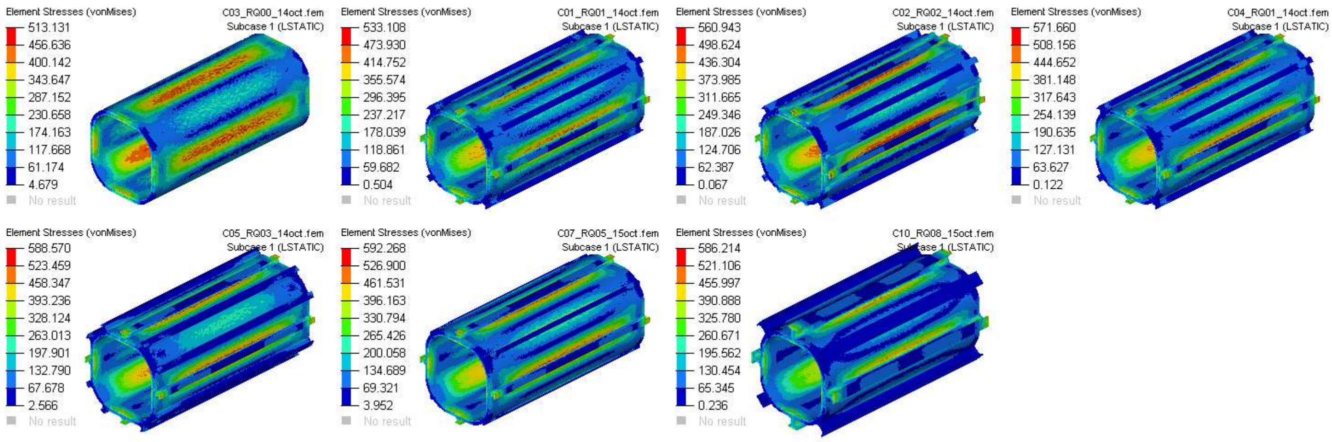

Figure C.22. NCS axial stiffened models – Von Mises

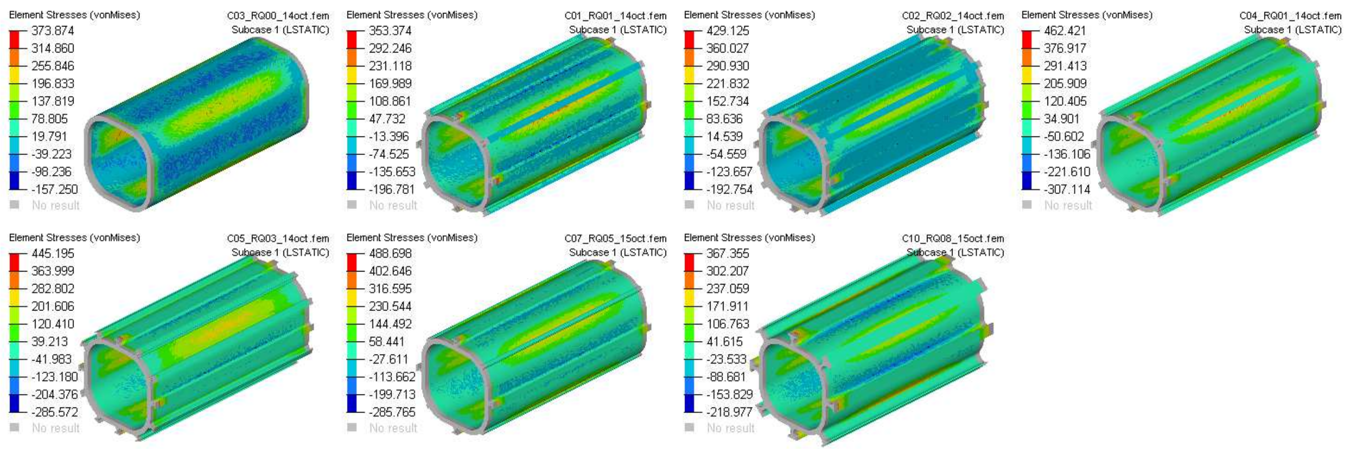

Figure C.23. NCS axial stiffened models – Tension (P1)

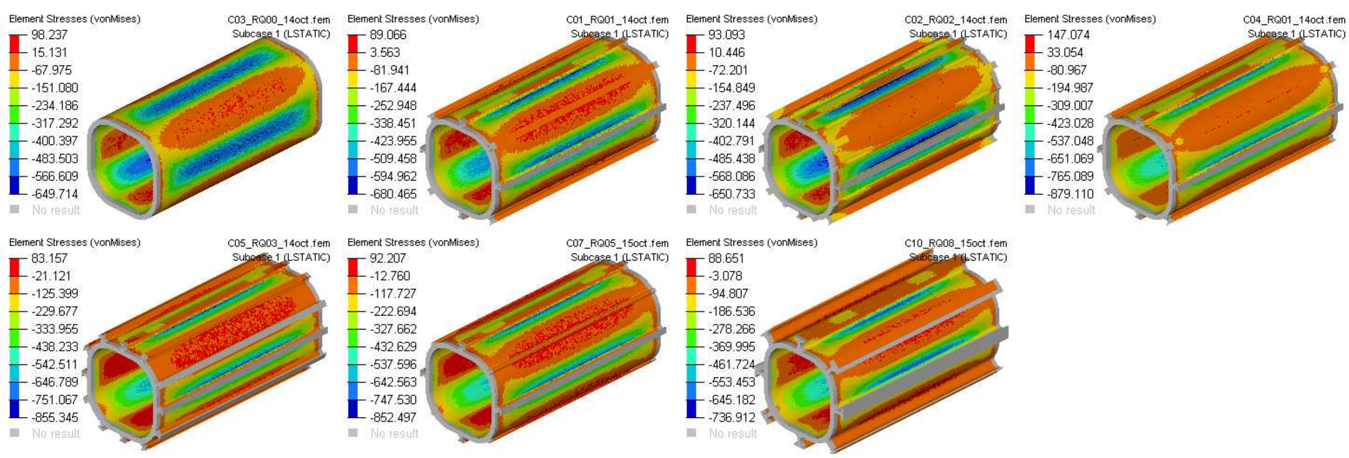

Figure C.24. NCS axial stiffened models – Compression (P3)

C.5 NCS radially stiffened models' study

Table C.6. NCS radially stiffened models' parametric study – stiffener number increase

		NDP			TDP			CDP			-
Model	**n**	VM [MPa]	P1 [MPa]	P3 [MPa]	VM [MPa]	P1 [MPa]	P3 [MPa]	VM [MPa]	P1 [MPa]	P3 [MPa]	Pcr [MPa]
D33	**2**	518.3	397.3	677.6	621.9	476.7	813.1	829.2	635.6	1084.1	75.3
D32	**3**	473.2	385.9	584.5	567.9	463.1	701.4	757.2	617.5	935.2	105.9
D31	**4**	398.3	378.8	498.4	477.9	454.5	598.1	637.2	606.0	797.4	125.8
D30	**5**	350.2	337.6	396.5	420.2	405.1	475.8	560.3	540.2	634.4	143.8
D29	**6**	324.4	296.6	351.2	389.3	355.9	421.4	519.0	474.5	561.9	162.5
D25	**7**	290.4	244.8	333.7	348.5	293.8	400.4	464.7	391.7	533.9	186.8
D19	**8**	275.5	224.7	313.1	330.5	269.7	375.8	440.7	359.6	501.0	201.5
D44	**9**	258.0	219.9	283.9	309.6	263.9	340.7	412.8	351.8	454.2	212.4

Table C.7. NCS radially stiffened models' parametric study – shell thickness decrease

		NDP			TDP			CDP			-
Model	**t [mm]**	VM [MPa]	P1 [MPa]	P3 [MPa]	VM [MPa]	P1 [MPa]	P3 [MPa]	VM [MPa]	P1 [MPa]	P3 [MPa]	Pcr [MPa]
D19	**12**	275.5	224.7	313.1	330.5	269.7	375.8	440.7	359.6	501.0	201.5
D34	**11**	294.5	290.0	324.9	353.4	348.0	389.9	471.2	464.0	519.9	177.9
D35	**10**	312.9	305.1	344.8	375.5	366.1	413.8	500.7	488.2	551.7	161.1
D40	**9**	340.6	313.6	385.7	408.8	376.3	462.8	545.0	501.7	617.1	132.8
D41	**8**	381.0	291.3	414.0	457.2	349.5	496.7	609.7	466.0	662.3	125.4

Table C.8. NCS radially stiffened models' parametric study – stiffener height decrease

		NDP			TDP			CDP			-
Model	**d [mm]**	VM [MPa]	P1 [MPa]	P3 [MPa]	VM [MPa]	P1 [MPa]	P3 [MPa]	VM [MPa]	P1 [MPa]	P3 [MPa]	Pcr [MPa]
D19	**18**	275.5	224.7	313.1	330.5	269.7	375.8	440.7	359.6	501.0	201.5
D36	**17**	286.7	225.2	320.6	344.0	270.2	384.7	458.7	360.3	512.9	183.8
D37	**16**	293.0	235.6	327.9	351.5	282.8	393.5	468.7	377.0	524.7	173.4
D38	**15**	311.1	275.3	340.7	373.3	330.3	408.9	497.8	440.4	545.2	163.8
D39	**14**	328.2	255.1	362.0	393.8	306.1	434.4	525.1	408.1	579.2	161.5

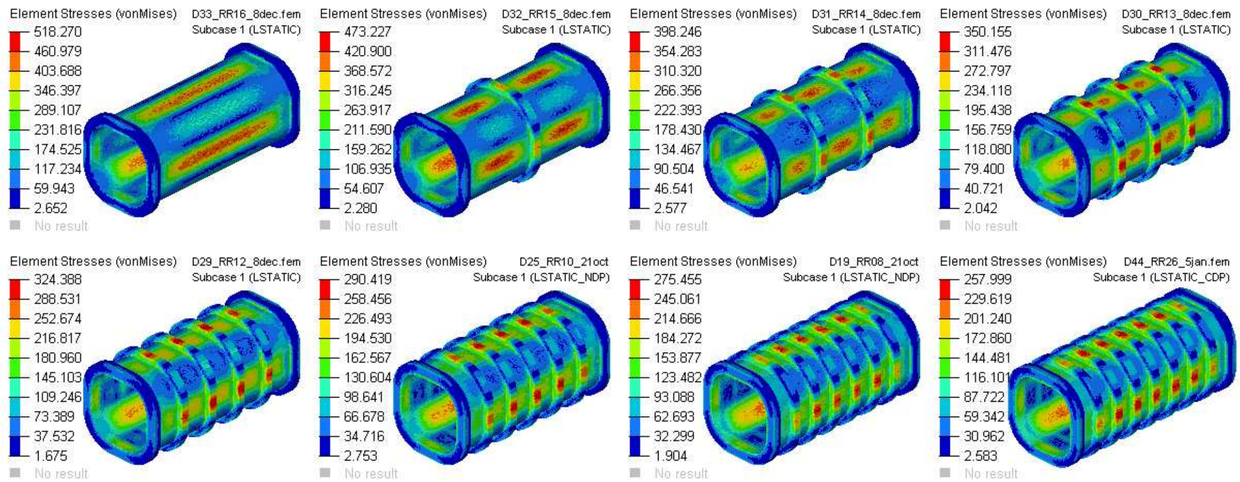

Figure C.25. NCS stiffener influence study – Von Mises

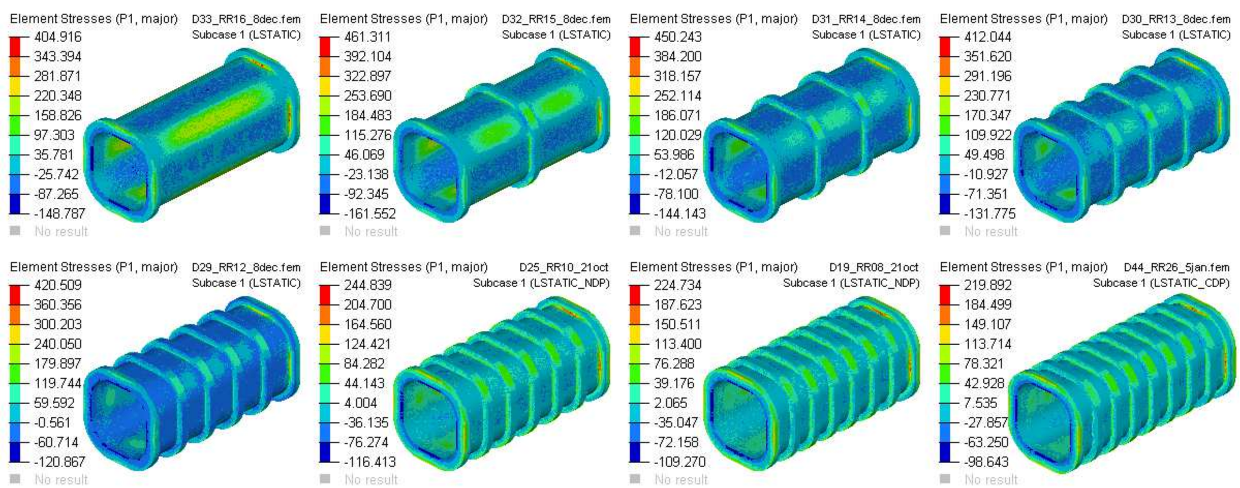

Figure C.26. NCS stiffener influence study – Tension (P1)

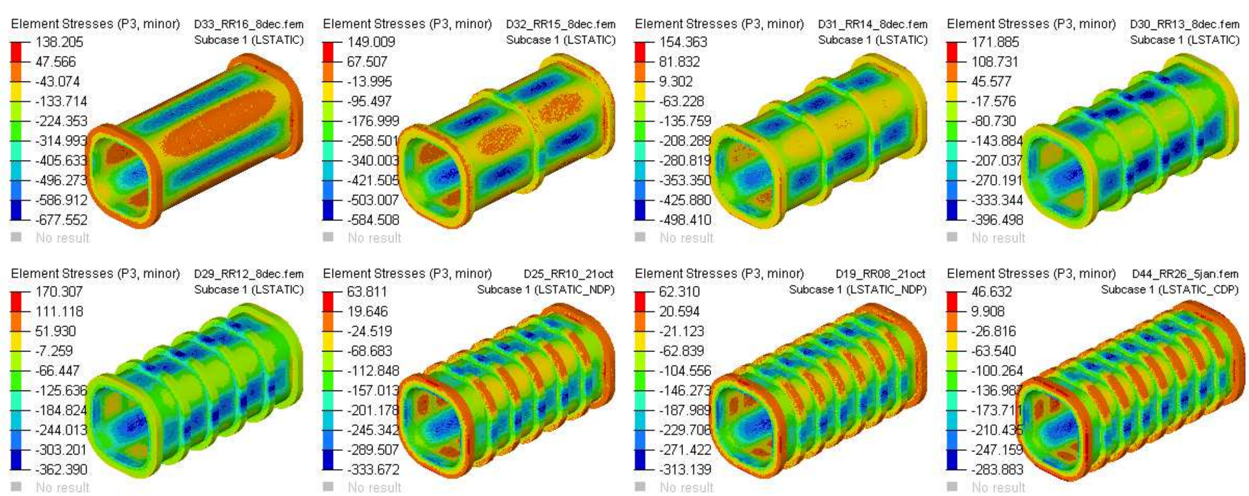

Figure C.27. NCS stiffener influence study – Compression (P3)

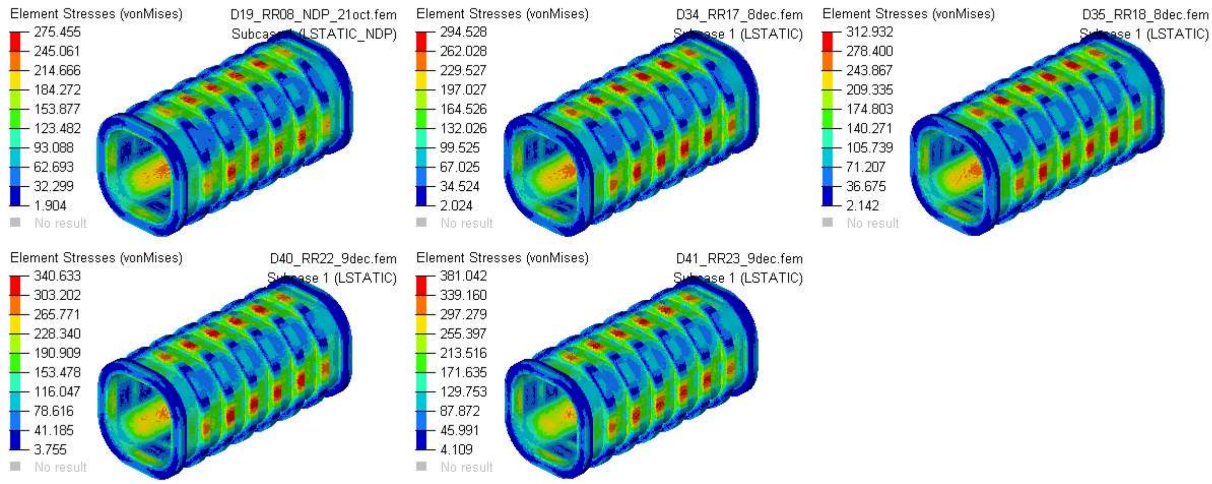

Figure C.28. NCS shell thickness study – Von Mises

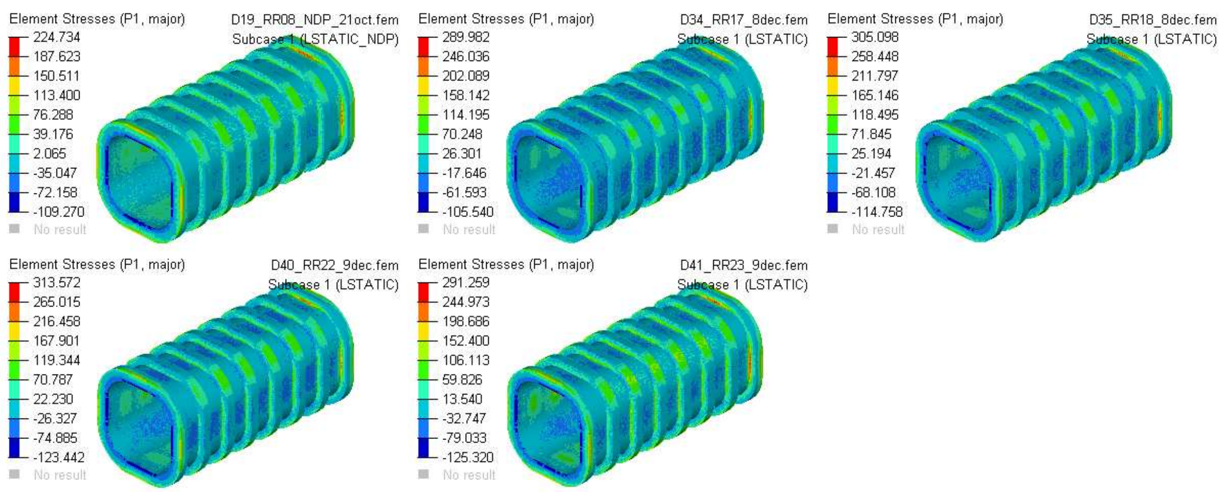

Figure C.29. NCS shell thickness study – Tension (P1)

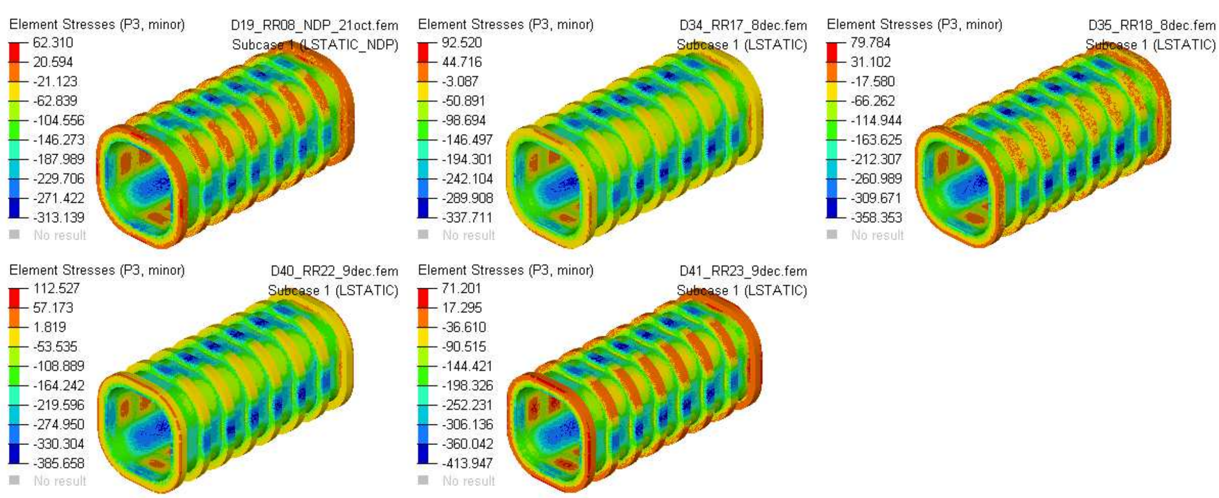

Figure C.30. NCS shell thickness study – Compression (P3)

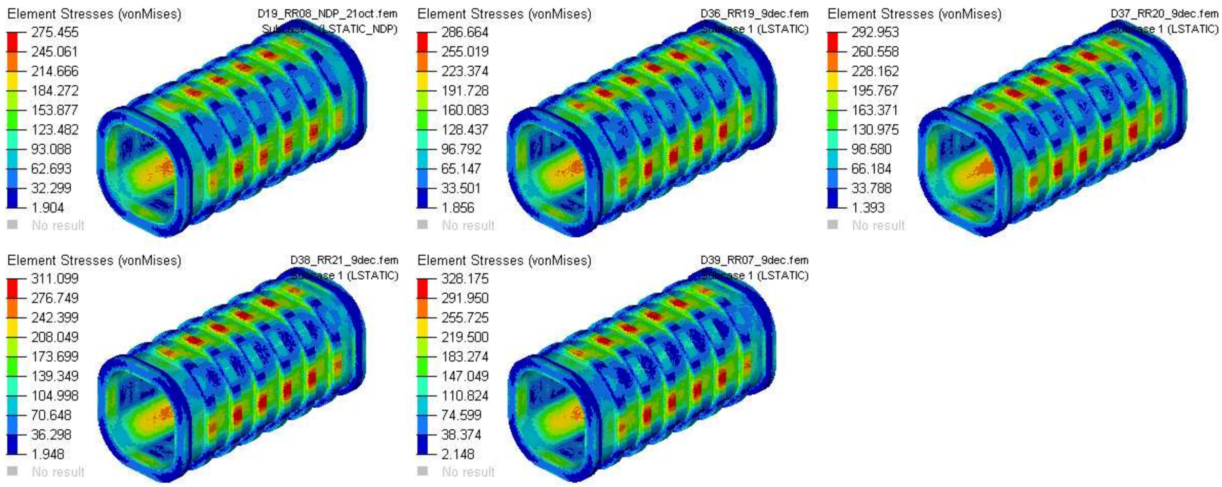

Figure C.31. NCS stiffener height study – Von Mises

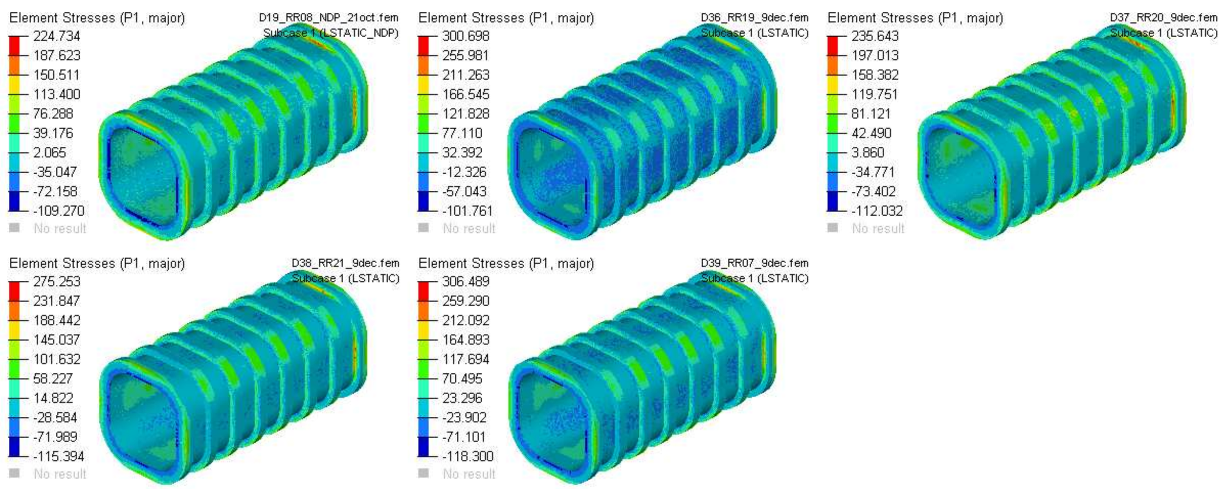

Figure C.32. NCS stiffener height study – Tension (P1)

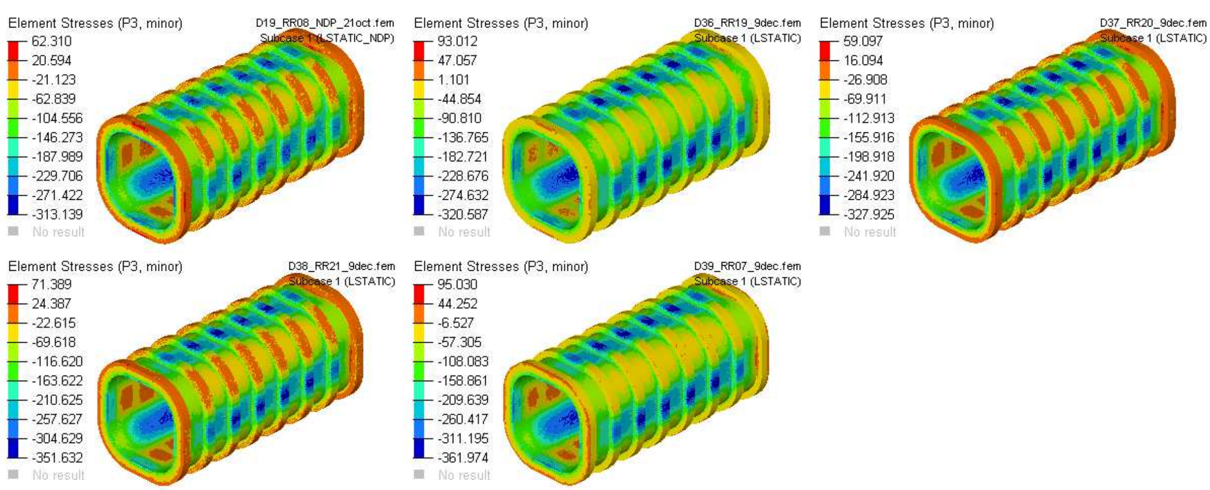

Figure C.33. NCS stiffener height study – Compression (P3)

Appendix D

Final concepts stress reports

D.1 SCC vessel

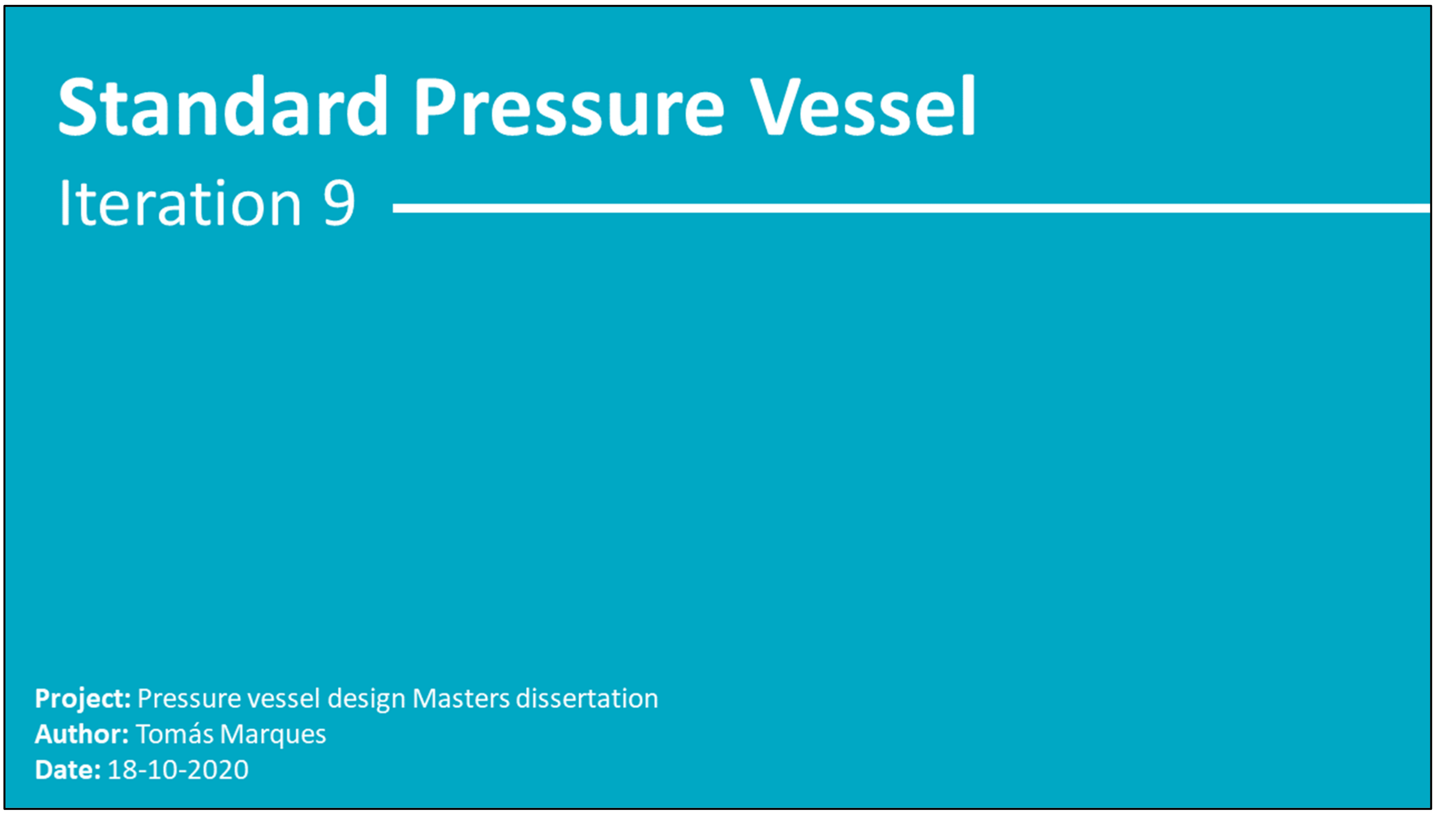

Standard Pressure Vessel

Iteration 9

Project: Pressure vessel design Masters dissertation
Author: Tomás Marques
Date: 18-10-2020

Project: Pressure vessel design Master's dissertation
Author: Tomás Marques
Date: 18-10-2020

Standard Pressure Vessel – Iteration 9

Main Design Features

Main Vessel dimensions [mm]		End Cap dimensions [mm]	
D_int =	200.0	D_ext =	270.0
L_int =	500.0	D_int =	200.0
L_total =	570.0	L_int =	35.0
t_vessel =	8.0	t_cap =	12.0
t_flange =	12.5		

Components dimensions		ISO	Material	#
O-Ring	ORAR00366-N70	3601-1	Nitrile Rubber	4
Bolt	M8 X 35	4014	INOX A4	20
Washer	M8	7089	INOX A4	40
Nut	M8	4032	INOX A4	20

Material properties

Component	Material	European Norm	Young Modulus [MPa]	Poisson coefficient	0.2% Offset Yield Strength [MPa]	Ultimate Tensile Strength [MPa]
Main Vessel	Al 7075 – T6	EN 755-2:2016	71016	0.33	495	560
Face Cap	Al 7075 – T6	EN 485-2:2016	71016	0.33	525	440

Project: Pressure vessel design Master's dissertation
Author: Tomás Marques
Date: 18-10-2020

Standard Pressure Vessel – Iteration 9

Design geometric dimensions

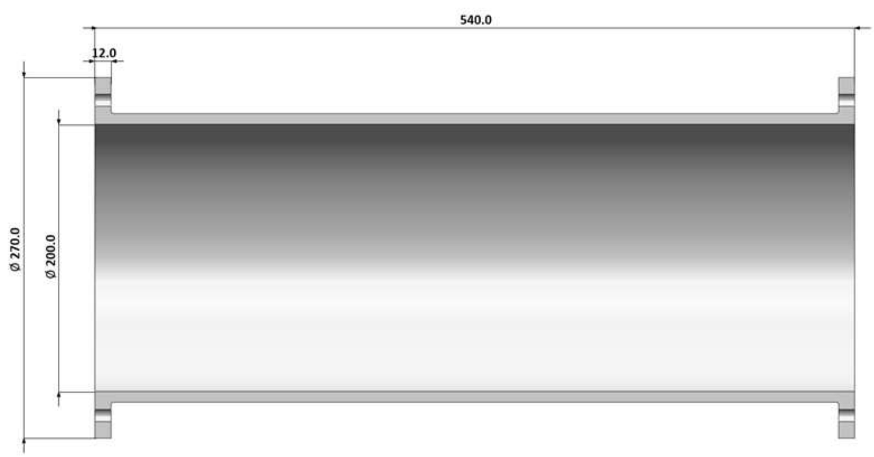

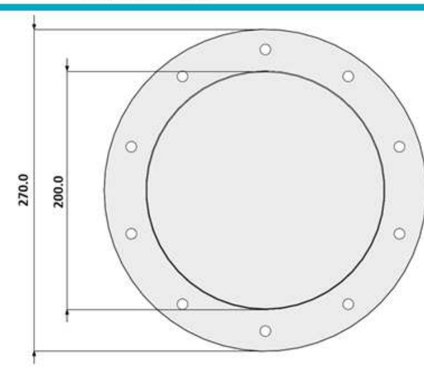

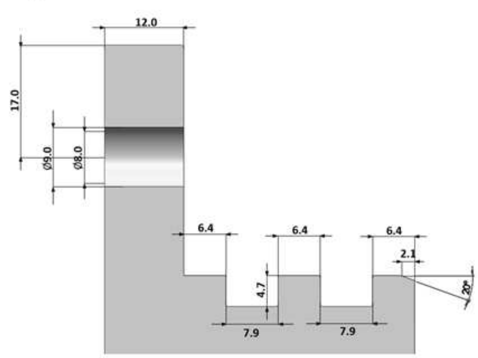

Project: Pressure vessel design Master's dissertation
Author: Tomás Marques
Date: 18-10-2020

Standard Pressure Vessel – Iteration 9

NDP Results contour plots - NLQS Analysis

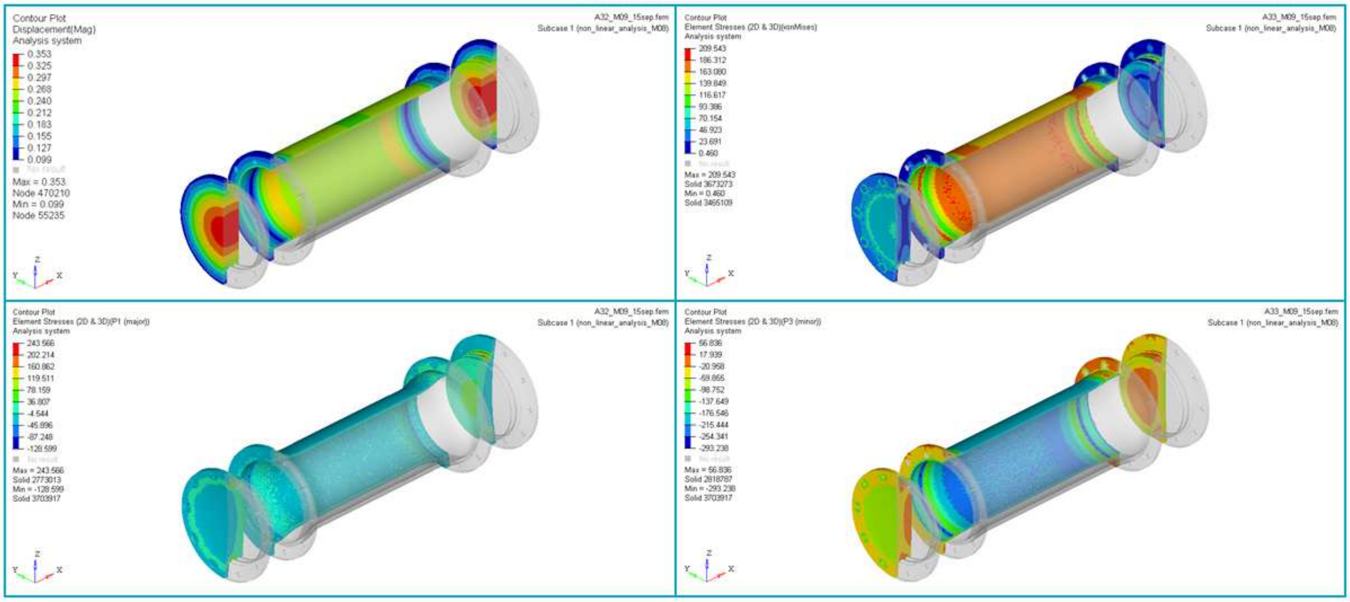

Project: Pressure vessel design Master's dissertation
Author: Tomás Marques
Date: 18-10-2020

Standard Pressure Vessel – Iteration 9

NDP Results contour plots – Linear Buckling Analysis

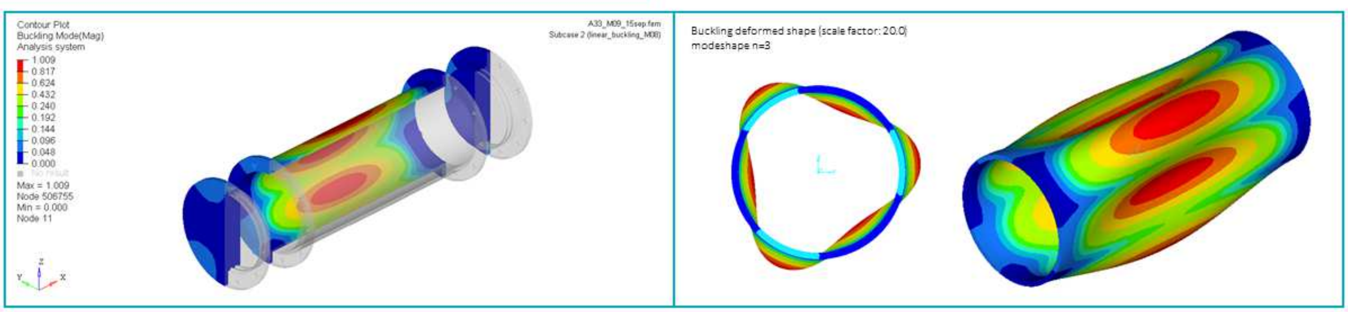

Notes

- Maximum stress at vessel-end cap contact interface (P3) of 293.3 MPa
- Maximum displacement of 0.353 mm at the external face of the cap
- Vessel appears to be over-dimensioned
- All safety factors verified

Project: Pressure vessel design Master's dissertation
Author: Tomás Marques
Date: 18-10-2020

Standard Pressure Vessel – Iteration 9

Load cases

Load case	Pressure [MPa]	Displacement [mm]	V Mises [MPa]	P1 Major [MPa]	P3 Minor [MPa]	Critical Pressure [MPa]	Buckling modeshape
NDP - Nominal Diving Pressure	NDP = 15.22	0.353	209.543	243.566	293.238	37.07	3
TDP - Test Diving Pressure	NDP x 1.2 = 18.26	0.424	251.663	292.388	352.17	-	-
CDP - Collapse Diving Pressure	NDP x 1.6 = 24.35	0.574	335.876	390.021	470.104	-	-

Safety margin calculation

Load case	Maximum stress [MPa]	Margin of Safety	Critical Pressure [MPa]	Buckling Factor
NDP - Nominal Diving Pressure	293.238	**0.69**	37.07	**2.444**
TDP - Test Diving Pressure	352.170	**0.41**	37.07	**2.037**
CDP - Collapse Diving Pressure	470.004	**0.19**	37.06	**1.527**

D.2 SCC filleted flange vessel

Filleted Flange Pressure Vessel

Iteration 3

Project: Pressure vessel design Masters dissertation
Author: Tomás Marques
Date: 21-10-2020

Filleted Flange Pressure Vessel – Iteration 3

Project: Pressure vessel design Master's dissertation
Author: Tomás Marques
Date: 21-10-2020

Main Design Features

Main Vessel dimensions [mm]		End Cap dimensions [mm]	
D_int =	200.0	D_ext =	254.0
L_int =	500.0	D_int =	200.0
L_tot =	600.0	L_int =	35.0
t_vessel =	8.0	t_cap =	12.0

Components dimensions		ISO	Material	#
O-Ring	ORAR00366-N70	3601-1	Nitrile Rubber	4
Bolt	M8 X 35	4014	INOX A4	10
Washer	M8	7089	INOX A4	10

Material properties

Component	Material	European Norm	Young Modulus [MPa]	Poisson coefficient	0.2% Offset Yield Strength [MPa]	Ultimate Tensile Strength [MPa]
Main Vessel	Al 7075 – T6	EN 755-2:2016	71016	0.33	495	560
Face Cap	Al 7075 – T6	EN 485-2:2016	71016	0.33	525	440

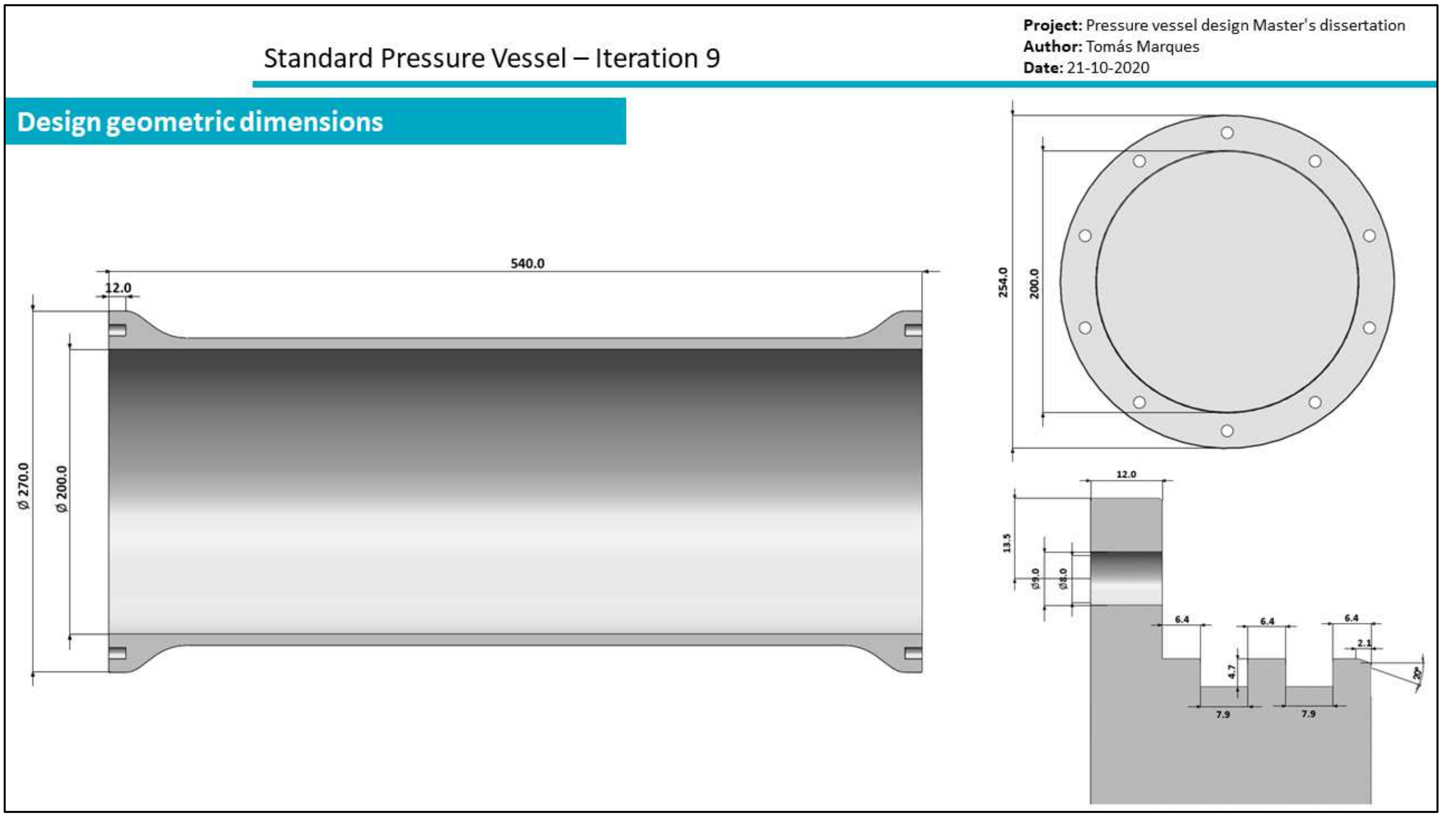
Project: Pressure vessel design Master's dissertation
Author: Tomás Marques
Date: 21-10-2020
Standard Pressure Vessel – Iteration 9
Design geometric dimensions
540.0
12.0
Ø 270.0
Ø 200.0
254.0
200.0
12.0
13.5
Ø9.0
Ø8.0
6.4
6.4
6.4
2.1
4.7
7.9
7.9
20°

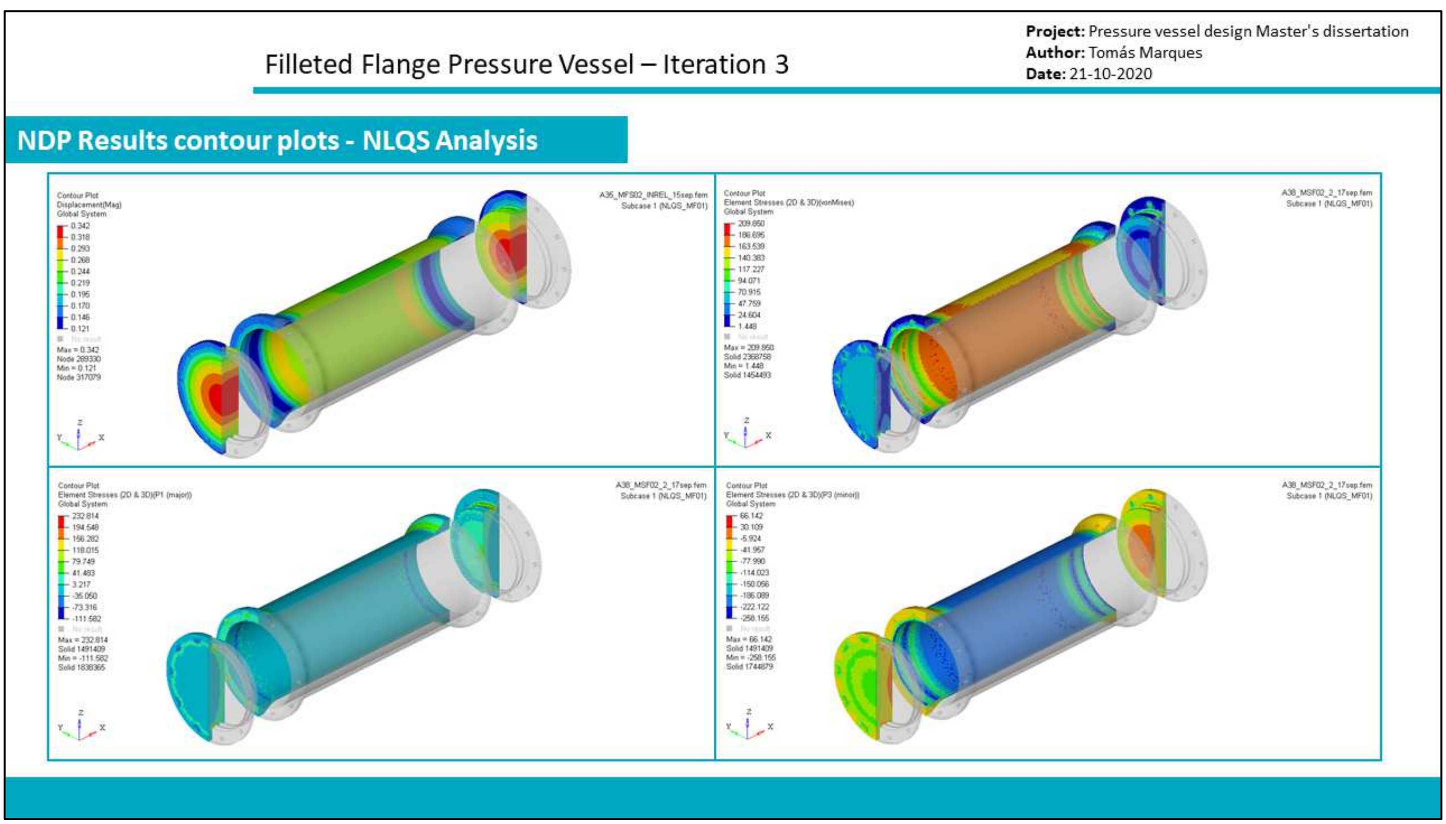
Project: Pressure vessel design Master's dissertation
Author: Tomás Marques
Date: 21-10-2020
Filleted Flange Pressure Vessel – Iteration 3
NDP Results contour plots - NLQS Analysis
Contour Plot
Displacement(Mag)
Global System
Max = 0.342
Min = 0.121
Contour Plot
Element Stresses (2D & 3D)(vonMises)
Global System
Max = 209.950
Min = 1.448
Contour Plot
Element Stresses (2D & 3D)(P1 (major))
Global System
Max = 232.814
Min = -111.582
Contour Plot
Element Stresses (2D & 3D)(P3 (minor))
Global System
Max = 66.142
Min = -258.155

Filleted Flange Pressure Vessel – Iteration 3

Project: Pressure vessel design Master's dissertation
Author: Tomás Marques
Date: 21-10-2020

NDP Results contour plots – Linear Buckling Analysis

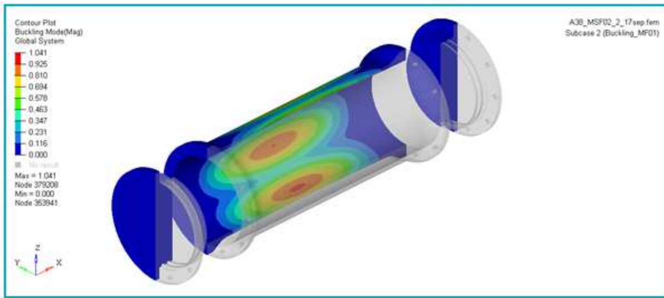

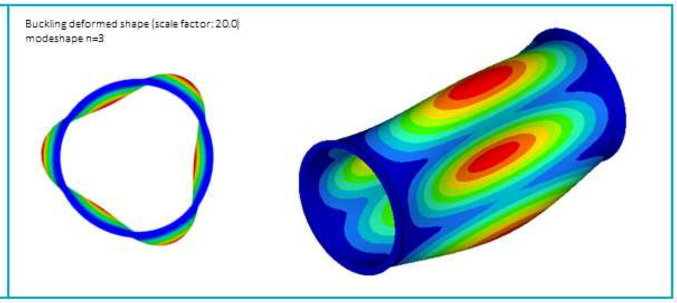

Notes

- Maximum stress at vessel-end cap contact interface (P3) of 258.2 MPa
- Maximum displacement of 0.342 mm at the external face of the cap
- Vessel appears to be over-dimensioned
- All safety factors verified

Filleted Flange Pressure Vessel – Iteration 3

Project: Pressure vessel design Master's dissertation
Author: Tomás Marques
Date: 21-10-2020

Load cases

Load case	Pressure [MPa]	Displacement [mm]	V Mises [MPa]	P1 Major [MPa]	P3 Minor [MPa]	Critical Pressure [MPa]	Buckling modeshape
NDP - Nominal Diving Pressure	NDP = 15.22	0.342	209.850	232.814	258.155	39.40	3
TDP - Test Diving Pressure	NDP x 1.2 = 18.26	0.411	252.421	279.538	309.626	-	-
CDP - Collapse Diving Pressure	NDP x 1.6 = 24.35	0.547	337.825	373.253	413.266	-	-

Safety margin calculation

Load case	Maximum stress [MPa]	Margin of Safety	Critical Pressure [MPa]	Buckling Factor
NDP - Nominal Diving Pressure	258.155	**0.92**	39.40	**2.60**
TDP - Test Diving Pressure	309.626	**0.60**	-	**2.16**
CDP - Collapse Diving Pressure	413.266	**0.36**	-	**1.62**

D.3 SCC no-flange vessel

No-Flange Pressure Vessel

Iteration 1

Project: Pressure vessel design Masters dissertation
Author: Tomás Marques
Date: 23-10-2020

No-Flange Pressure Vessel – Iteration 1

Project: Pressure vessel design Master's dissertation
Author: Tomás Marques
Date: 23-10-2020

Main Design Features

Main Vessel dimensions [mm]		End Cap dimensions [mm]	
D_int =	200.0	**D_ext =**	216.0
L_int =	500.0	**D_int =**	200.0
L_tot =	590.0	**L_int =**	44.6
t_vessel =	8.0	**t_cap =**	12.0

Components dimensions		ISO	Material	#
O-Ring	ORAR00366-N70	3601-1	Nitrile Rubber	4
Bolt	M6 X 20	4014	INOX A4	12
Washer	M8	7089	INOX A4	12

Material properties

Component	Material	European Norm	Young Modulus [MPa]	Poisson coefficient	0.2% Offset Yield Strength [MPa]	Ultimate Tensile Strength [MPa]
Main Vessel	Al 7075 – T6	EN 755-2:2016	71016	0.33	495	560
Face Cap	Al 7075 – T6	EN 485-2:2016	71016	0.33	525	440

No-Flange Pressure Vessel – Iteration 1

Project: Pressure vessel design Master's dissertation
Author: Tomás Marques
Date: 23-10-2020

Design geometric dimensions

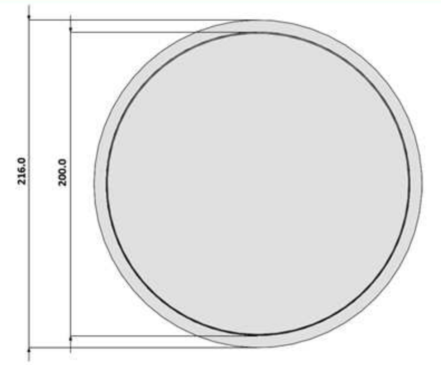

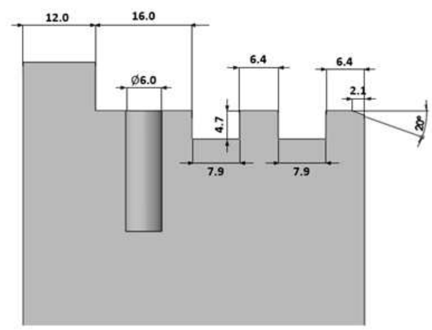

No-Flange Pressure Vessel – Iteration 1

Project: Pressure vessel design Master's dissertation
Author: Tomás Marques
Date: 23-10-2020

NDP Results contour plots - NLQS Analysis

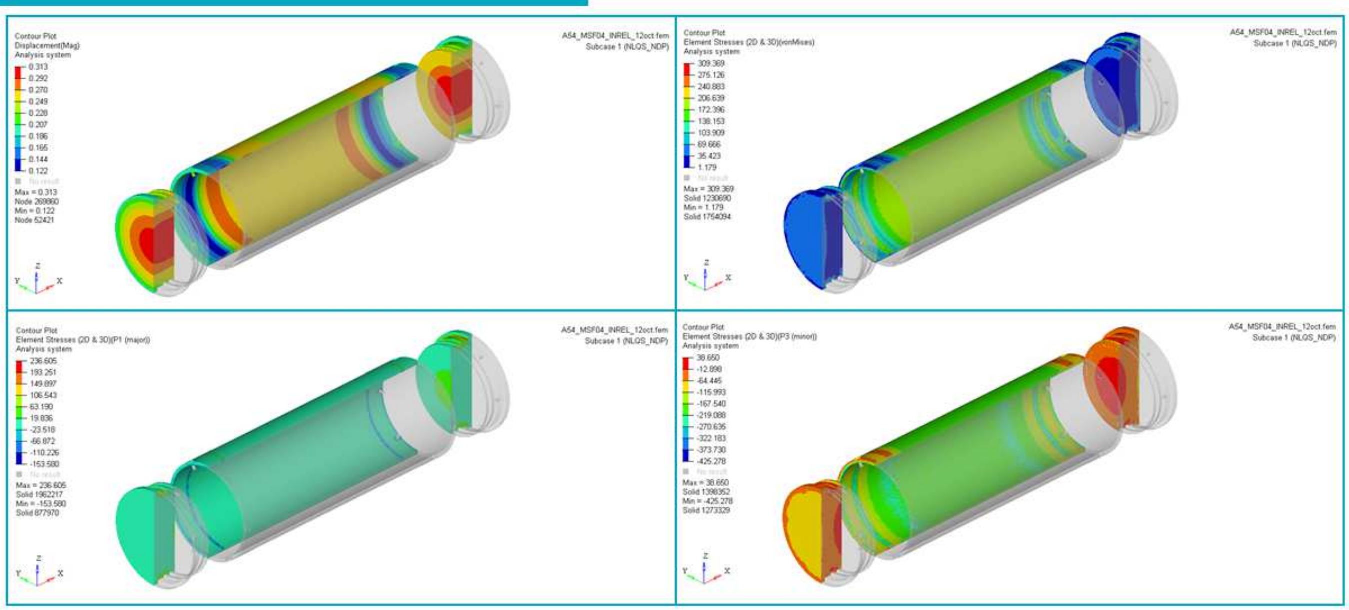

Project: Pressure vessel design Master's dissertation
Author: Tomás Marques
Date: 23-10-2020

No-Flange Pressure Vessel – Iteration 1

NDP Results contour plots – Linear Buckling Analysis

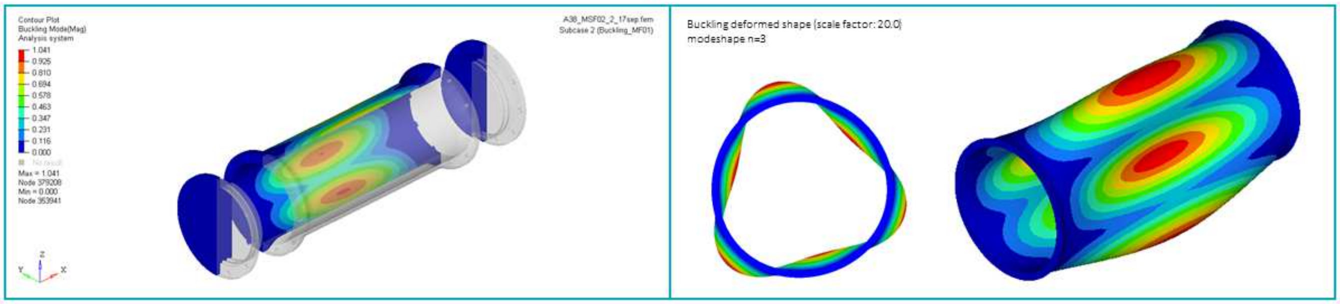

Notes

- Maximum stress at vessel-end cap contact interface (P3) of 425.3 MPa
- Maximum displacement of 0.313 mm at the external face of the cap
- S2 Safety Factor at CDP not verified

Project: Pressure vessel design Master's dissertation
Author: Tomás Marques
Date: 23-10-2020

No-Flange Pressure Vessel – Iteration 1

Load cases

Load case	Pressure [MPa]	Displacement [mm]	V Mises [MPa]	P1 Major [MPa]	P3 Minor [MPa]	Critical Pressure [MPa]	Buckling modeshape
NDP - Nominal Diving Pressure	NDP = 15.22	0.313	309.369	236.605	425.278	40.02	3
TDP - Test Diving Pressure	NDP x 1.2 = 18.26	0.376	371.243	283.926	510.334	-	-
CDP - Collapse Diving Pressure	NDP x 1.6 = 24.35	0.501	494.990	378.568	680.445	-	-

Safety margin calculation

Load case	Maximum stress [MPa]	Margin of Safety	Critical Pressure [MPa]	Buckling Factor
NDP - Nominal Diving Pressure	425.278	**0.16**	40.02	**2.64**
TDP - Test Diving Pressure	510.334	**-0.03**	-	**2.20**
CDP - Collapse Diving Pressure	680.445	**-0.18**	-	**1.65**

D.4 ATV vessel

Axial Thick Var Pressure Vessel

Iteration 4

Project: Pressure vessel design Masters dissertation
Author: Tomás Marques
Date: 23-10-2020

Axial Thickness Variation Pressure Vessel – Iteration 4

Project: Pressure vessel design Master's dissertation
Author: Tomás Marques
Date: 23-10-2020

Main Design Features

Main Vessel dimensions [mm]		End Cap dimensions [mm]	
D_int =	200.0	D_ext =	270.0
L_int =	500.0	D_int =	200.0
L_total =	570.0	L_int =	35.0
t_vessel =	8.0	t_cap =	12.0
t_flange =	12.5		

Components dimensions		ISO	Material	#
O-Ring	ORAR00366-N70	3601-1	Nitrile Rubber	4
Bolt	M8 X 35	4014	INOX A4	20
Washer	M8	7089	INOX A4	40
Nut	M8	4032	INOX A4	20

Material properties

Component	Material	European Norm	Young Modulus [MPa]	Poisson coefficient	0.2% Offset Yield Strength [MPa]	Ultimate Tensile Strength [MPa]
Main Vessel	Al 7075 – T6	EN 755-2:2016	71016	0.33	495	560
Face Cap	Al 7075 – T6	EN 485-2:2016	71016	0.33	525	440

Project: Pressure vessel design Master's dissertation
Author: Tomás Marques
Date: 23-10-2020

Axial Thickness Variation Pressure Vessel – Iteration 4

Design geometric dimensions

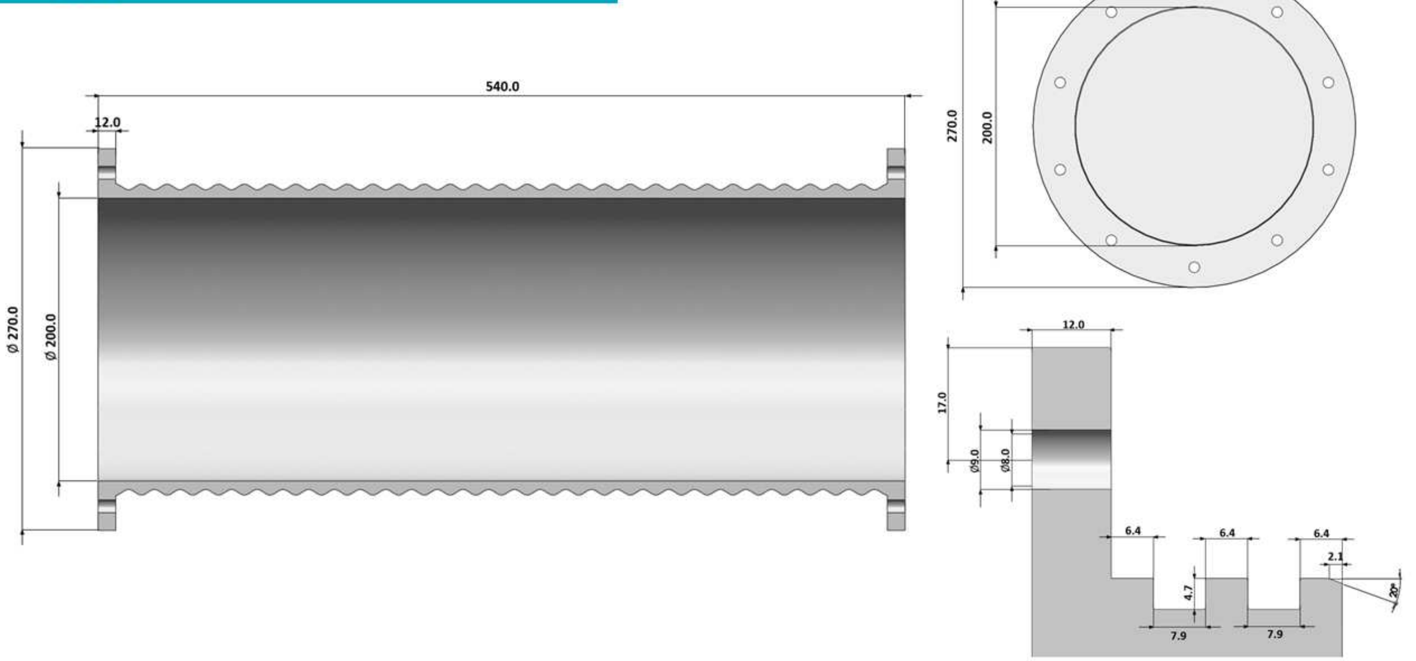

Project: Pressure vessel design Master's dissertation
Author: Tomás Marques
Date: 23-10-2020

Axial Thickness Variation Pressure Vessel – Iteration 4

NDP Results contour plots - NLQS Analysis

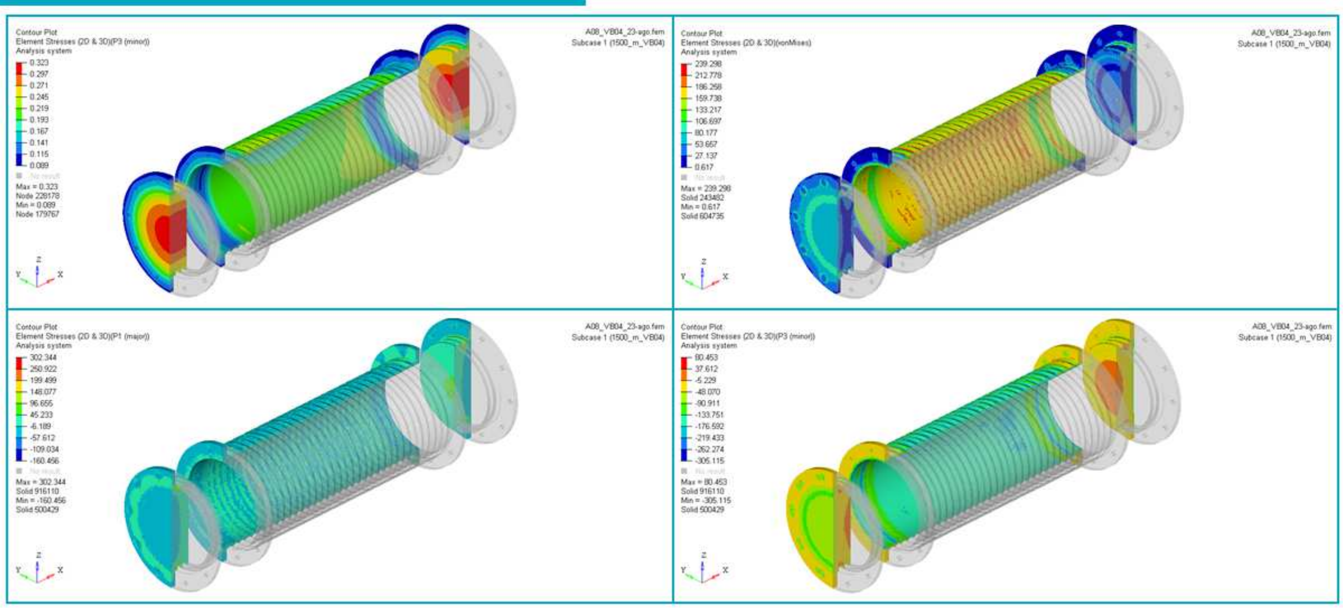

Axial Thickness Variation Pressure Vessel – Iteration 4

Project: Pressure vessel design Master's dissertation
Author: Tomás Marques
Date: 23-10-2020

NDP Results contour plots – Linear Buckling Analysis

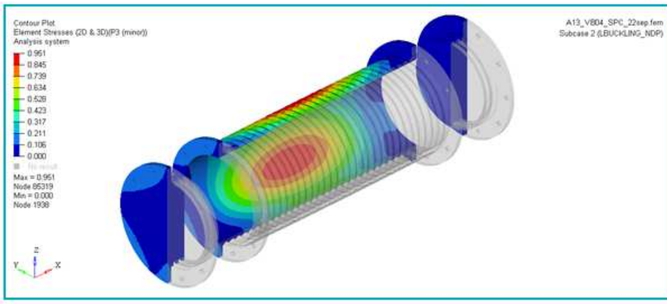

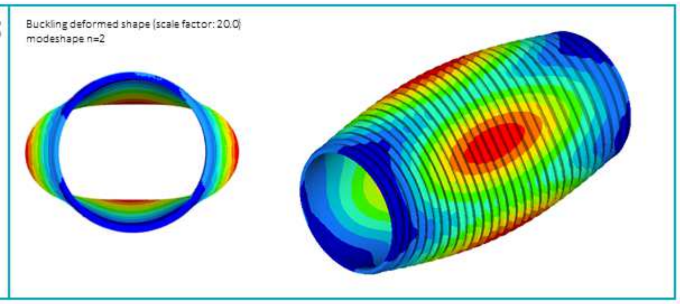

Notes

- Maximum stress at vessel-end cap contact interface (P3) of 305.2 MPa
- Maximum displacement of 0.408 mm at the external face of the cap
- Vessel appears to be over-dimensioned
- All safety factors verified

Axial Thickness Variation Pressure Vessel – Iteration 4

Project: Pressure vessel design Master's dissertation
Author: Tomás Marques
Date: 23-10-2020

Load cases

Load case	Pressure [MPa]	Displacement [mm]	V Mises [MPa]	P1 Major [MPa]	P3 Minor [MPa]	Critical Pressure [MPa]	Buckling modeshape
NDP - Nominal Diving Pressure	NDP = 15.22	0.408	239.321	302.301	305.189	40.31	2
TDP - Test Diving Pressure	NDP x 1.2 = 18.26	0.490	287.185	362.761	366.227	-	-
CDP - Collapse Diving Pressure	NDP x 1.6 = 24.35	0.653	382.914	483.682	488.302	-	-

Safety margin calculation

Load case	Maximum stress [MPa]	Margin of Safety	Critical Pressure [MPa]	Buckling Factor
NDP - Nominal Diving Pressure	305.1	**0.62**	40.31	**2.66**
TDP - Test Diving Pressure	366.1	**0.35**	-	**2.21**
CDP - Collapse Diving Pressure	488.2	**0.15**	-	**1.66**

D.5 NCS vessel

Noncircular Pressure Vessel

Iteration 5

Project: Pressure vessel design Masters dissertation
Author: Tomás Marques
Date: 14-12-2020

Noncircular cross section Pressure Vessel – Iteration 5

Project: Pressure vessel design Master's dissertation
Author: Tomás Marques
Date: 14-12-2020

Main Design Features

Main Vessel dimensions [mm]		End Cap dimensions [mm]		Stiffener dimensions [mm]	
B_int =	185.8	B_ext =	243.8	b=	20.0
R_f =	60	B_int =	185.8	d=	18.0
L_int =	500	Rf_e =	89.0	L_stiff=	54.3
L_total =	540	L_int =	20.0		
t_vessel =	11.0	t_cap =	18.0		

Components dimensions		ISO	Material	#
O-Ring (f)	ORAR00368-N70	3601-1	Nitrile Rubber	2
O-ring (r)	ORAR00370-N70	3601-1	Nitrile Rubber	2
Bolt	M6 X 35	4014	INOX A4	32
Washer	M6	7089	INOX A4	64
Nut	M6	4032	INOX A4	32

Material properties

Component	Material	European Norm	Young Modulus [MPa]	Poisson coefficient	0.2% Offset Yield Strength [MPa]	Ultimate Tensile Strength [MPa]
Main Vessel	Al 7075 – T6	EN 755-2:2016	71016	0.33	470	550
Face Cap	Al 7075 – T6	EN 485-2:2016	71016	0.33	525	440

Noncircular cross section Pressure Vessel – Iteration 5

Project: Pressure vessel design Master's dissertation
Author: Tomás Marques
Date: 14-12-2020

Design geometric dimensions

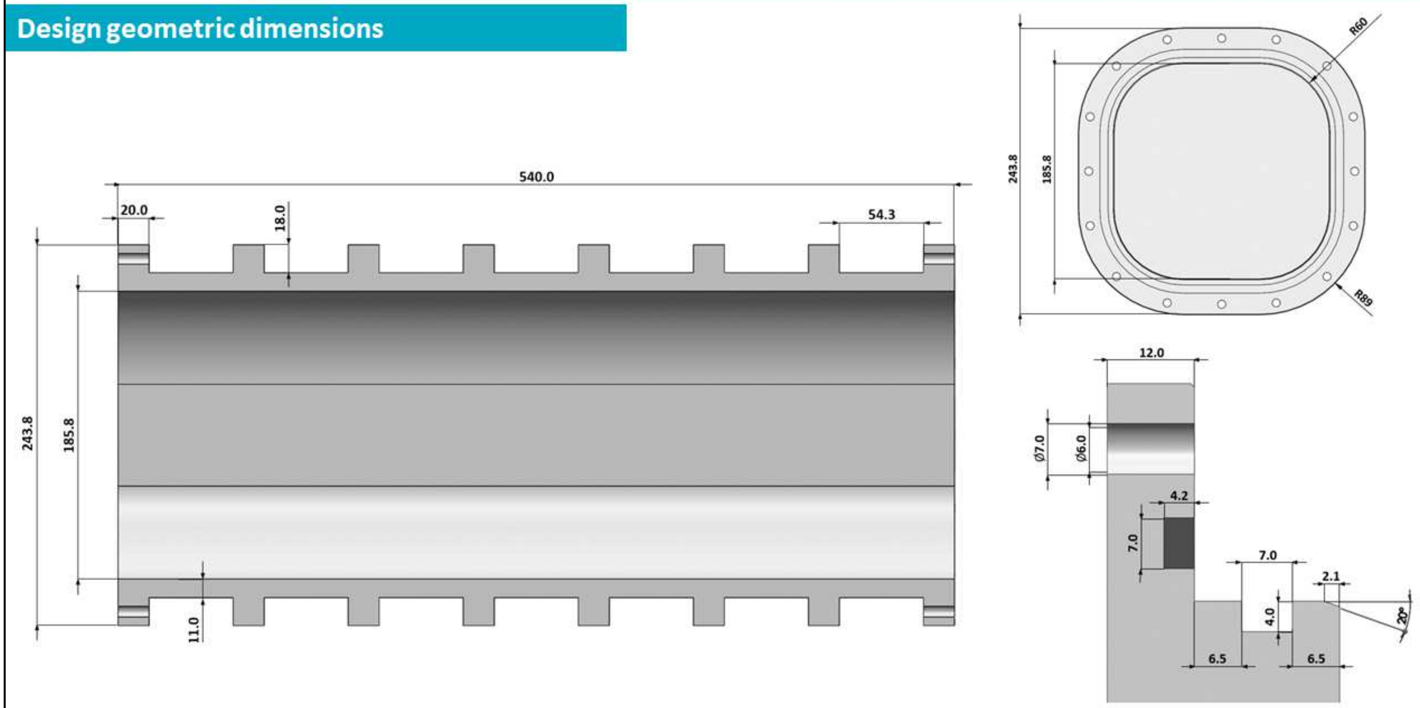

Noncircular cross section Pressure Vessel – Iteration 5

Project: Pressure vessel design Master's dissertation
Author: Tomás Marques
Date: 14-12-2020

NDP Results contour plots - NLQS Analysis

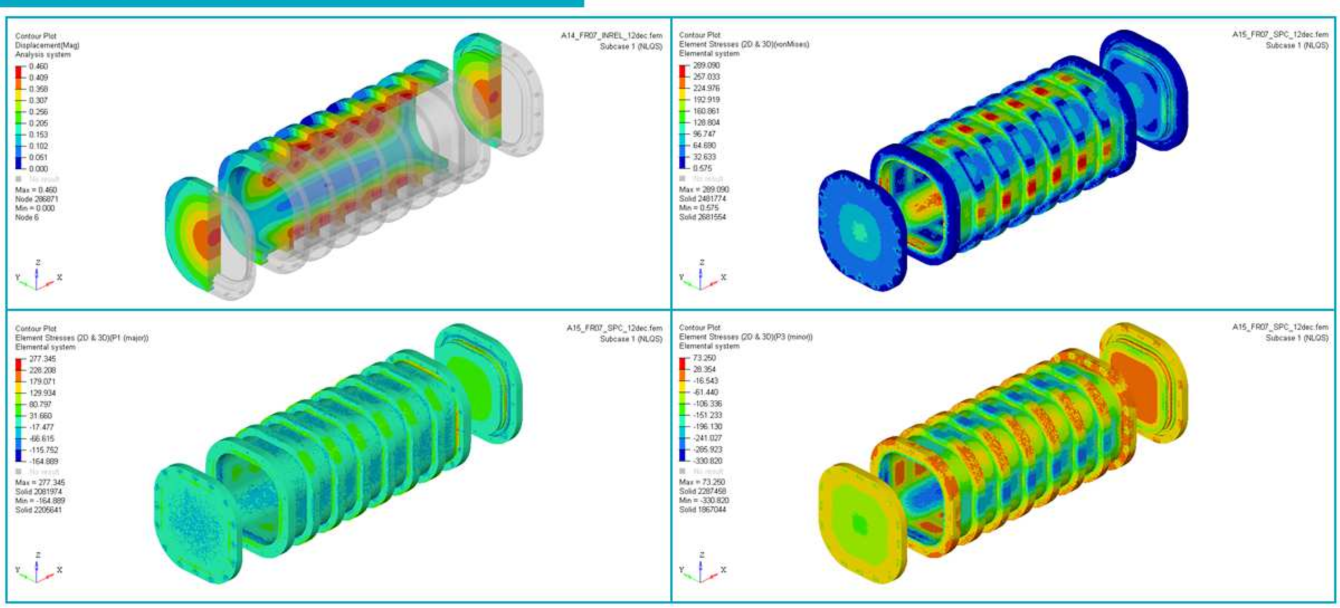

Project: Pressure vessel design Master's dissertation
Author: Tomás Marques
Date: 14-12-2020

Noncircular cross section Pressure Vessel – Iteration 5

NDP Results contour plots – Linear Buckling Analysis

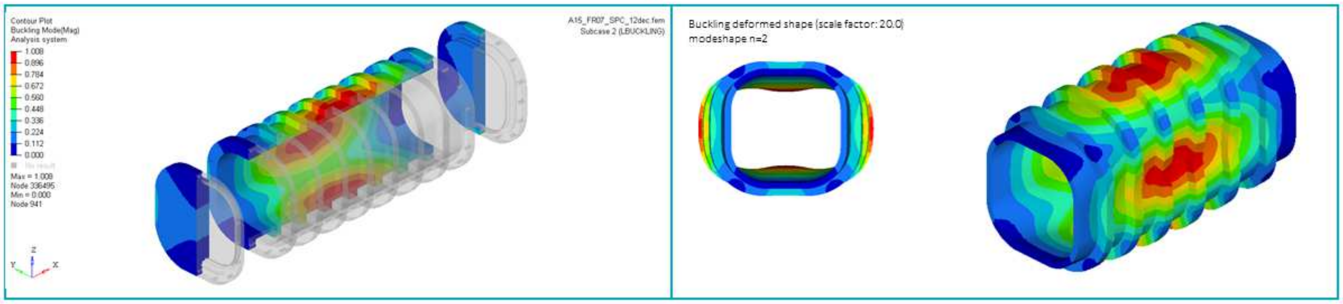

Notes

- Maximum stress at vessel-end cap contact interface (P3) of 330.8 MPa
- Maximum displacement of 0.460 mm in the axial direction of the vessel, at stiffener edge
- All safety factors verified

Project: Pressure vessel design Master's dissertation
Author: Tomás Marques
Date: 14-12-2020

Noncircular cross section Pressure Vessel – Iteration 5

Load cases

Load case	Pressure [MPa]	Displacement [mm]	V Mises [MPa]	P1 Major [MPa]	P3 Minor [MPa]	Critical Pressure [MPa]	Buckling modeshape
NDP - Nominal Diving Pressure	NDP = 15.22	0.460	289.090	277.345	330.820	80.77	2
TDP - Test Diving Pressure	NDP x 1.2 = 18.26	0.552	346.908	332.814	396.984	-	-
CDP - Collapse Diving Pressure	NDP x 1.6 = 24.35	0.736	462.544	443.752	529.312	-	-

Safety margin calculation

Load case	Maximum stress [MPa]	Margin of Safety	Critical Pressure [MPa]	Buckling Factor
NDP - Nominal Diving Pressure	330.8	**0.42**	80.77	**5.32**
TDP - Test Diving Pressure	397.0	**0.18**	-	**4.44**
CDP - Collapse Diving Pressure	529.3	**0.02**	-	**3.33**